12-4-2006

Syntheses and DNA Interactions of Acridine and Phenothiazine Based Photosensitizers

Beth Wilson

Syntheses and DNA Interactions of

Acridine and Phenothiazine Based Photosensitizers

by

Beth Wilson

Under the Direction of Dr. Kathryn B. Grant

ABSTRACT

Photosensitizing molecules and/or metal complexes that interact with DNA via intercalation and groove binding have potential applications as molecular structural probes, as footprinting reagents and in photodynamic therapeutics. To this regard, small molecules that bind to DNA and the energetics involved in these interactions, acridine-based therapeutics, photosensitization, photodynamic therapy, phenothiazine-mediated photosensitization, DNA photocleavage reaction mechanisms and photosensitizing metal complexes are introduced in Chapter I. Next, in Chapter II, the synthesis of a photonuclease consisting of a 3,6-acridinediamine chromophore attached to four metal-coordinating imidazole rings is described. The DNA photocleavage yields, emission quantum yields, and thermal denaturation studies by this acridine-imadazole conjugate in the presence of 16 metal salts are also reported. In Chapter III is the synthesis of a bisacridine covalently tethered to a copper(II)-binding pyridine linker. Additionally, DNA photocleavage studies as well as DNA binding affinity and binding mode(s) of this bisacridine incorporating the copper(II)-binding pyridine linker are examined. The syntheses, characterization, DNA photocleavage studies, DNA thermal denaturation, and

viscometric measurements of three new phenothiazinium photosensitizers are described in Chapters IV and V. Collectively, markedly enhanced DNA photocleavage yields are observed in the presence of metals (Chapters II-III) or in comparison to a parent molecule, Chapters II and IV. DNA melting isotherms show higher levels of duplex stabilization with the acridines, specifically in the presence of several metals (Chapter II-III) as well as with the phenothiazine-based ligands (Chapters IV-V). Moreover, different DNA binding modes were observed depending on metal complexation (Chapter III) and nucleic acid structure (Chapter IV). Finally, Chapter VI describes a small project implemented as a National Science Foundation pedagogical laboratory exercise in which a non-invasive procedure for DNA isolation from human cheek cells was utilized with the polymerase chain reaction to amplify alleles encoding a single nucleotide polymorphism involved in normal human color vision.

INDEX WORDS: Acridine, Allele-specific polymerase chain reaction, DNA photosensitization, Metal-assisted photocleavage, Phenothiazine, Photodynamic therapy

SYNTHESES AND DNA INTERACTIONS OF ACRIDINE AND PHENOTHIAZINE BASED PHOTOSENSITIZERS

by

Beth Wilson

A Dissertation Submitted in Partial Fulfillment of Requirements for the Degree of

Doctor of Philosophy

in the College of Arts and Sciences

Georgia State University

2006

Syntheses and DNA Interactions of

Acridine and Phenothiazine Based Photosensitizers

by

Beth Wilson

Chair:	Dr. Kathryn B. Grant
Committee:	Dr. Alfons L. Baumstark
	Dr. Lucjan Strekowski

Electronic Version Approved by:

Office of Graduate Studies
College of Arts and Sciences
Georgia State University
December 2006

Acknowledgments

First and foremost, I dedicate this dissertation to Ms. Margie Oquendo. Margie and I met as kids while growing up in Chicago. Our friendship, love and admiration for one another has spanned over three decades. Margie is my friend, sister, doppleganger and a true constant in my life. In our lives, we have shared many moments of sadness but also of great joy. Our love continues to be transcribed and our friendship will forever be translated.

Next, I would like to thank two individuals who have been the most instrumental in my doctoral work and professional life. First I thank, Professor Baumstark for discovering me (as he has said to me, "I remember when you took my 3110 class, you used to sit in the corner by the sink…") but more importantly for believing in me. He then introduced me to Professor Grant; my advisor, mentor, and friend. Professor Grant has shown me the path towards becoming a very conscientious scientist and has taught me to always play hard, even if I did not expect to win. Thank you both, I sincerely hope that I have made and continue to make you proud.

Fortuitously, I had the honor of working with Professors Lorente and Fernández (Universidad de Alcalá, Spain). They have been terrific mentors (always there to provide words of wisdom and scientific guidance), collaborators, and friends.

I gratefully acknowledge and extend my sincere thanks to Professor Strekowski for serving as a member in my defense committee, for his instruction, and for his many helpful organic discussions. Moreover, I am deeply grateful to Professors Dixon, Germann, Netzel and Wilson for their dedication, instruction, insightful discussions and for allowing me to utilize their laboratory space as well as equipment. Collectively, I

thank the Department of Chemistry staff and faculty members, in particular, Dr. Chandrasekaren for always being generous with their limited time.

Personally, I thank my best friends the beautiful Miki Kassai, the fabulous Subrata Mishra and the dashing Pete Issa for all the joy and laughter we shared. I love you guys and I will miss my everyday encounters with you very much. In addition, I thank my family, in particular, my brother Carlos for being a special and an extraordinary human being.

Also I am grateful to past and present friends in the Grant group: Dr. Tjasa Bantan-Polak, Dr. Lourdes Gude, Dr. Ghana Ravi, Dr. Xia Yang, Earl Fields and Sarah Shealy.

Finally, I would like to extend my devout appreciation to Dr. Walter T. Wilson for always loving, believing in, and caring for me even through difficult times.

Table of Content

List of Tables

List of Figures

List of Schemes

List of Abbreviations

AO	acridine orange
BSC	bathocuproinedisulfonic acid disodium salt hydrate
bp	base pair
CP DNA	*Clostridium perfringens* DNA
CT DNA	calf thymus DNA
DMF	*N*, *N*'-dimethylformamide
DMMB	1,9-dimethyl methylene blue
DMSO	dimethyl sulfoxide
EDTA	ethylenediaminetetraacetic acid
ESI	electrospray ionization
EtOH	ethanol
FDA	Food and Drug Administration
H_2O_2	hydrogen peroxide
MB	methylene blue
NMB	2,8-dimethyl methylene blue
NMR	nuclear magnetic resonance
P	proflavin
PCR	polymerase chain reaction
PDT	photodynamic therapy
SDS	sodium dodecyl sulfate
SOD	superoxide dismutase

CHAPTER I

Introduction

Small Molecules and DNA Interactions

In 1953, Watson and Crick introduced their original presentation that genetic material exists structurally as a double-helix (*1*). Subsequent discoveries on the structural features of DNA and its role in replication and transcription suggested it as a potential target for treating diseases of genetic origin, in particular cancer. Accordingly, the field of anticancer drug design over the past 40 years has focused intense research on the interaction of small molecules that bind to nucleic acids. Pioneering structural and functional studies conducted by Rauen and Reich in the 1960's on the interactions of the DNA intercalating antibiotic actinomycin D (Figure 1.1) demonstrated the utility of DNA as a powerful target for disrupting cellular metabolism (*2*, *3*).

There are two major binding modes associated with small organic molecules that interact with DNA, intercalation and groove binding. In addition, cationic molecules may externally associate with the phosphate backbone. Consequently, these binding interactions may involve changes to both DNA and ligand molecules in order to facilitate complex formation. Moreover, structural perturbations or interference by the complex with other DNA binding macromolecules such as proteins may lead to non-lethal alterations or apoptosis (*4*). The chemical structures of representative intercalating and groove binding agents are shown in Figure 1.1.

Intercalation. In 1961, Lerman conducted the seminal investigations that launched the classical intercalation model. He observed that the viscosity of a DNA solution was markedly increased while the sedimentation coefficient was decreased upon

the addition of acridine, proflavin or acridine orange. These observations led him to suggest that the acridines induced structural perturbations and that an intercalative type of binding mechanism would result in a lengthening of the DNA duplex (*5*). In addition, he conducted flow dichroism and polarized fluorescence studies that demonstrated the plane of the bound acridines was parallel to the DNA base pairs and perpendicular to the axis of the double helix (*6*). Finally, Neville and Davies reported that X-ray fiber diffraction patterns of DNA complexed with proflavin and acridine orange were consistent with intercalation (*7*).

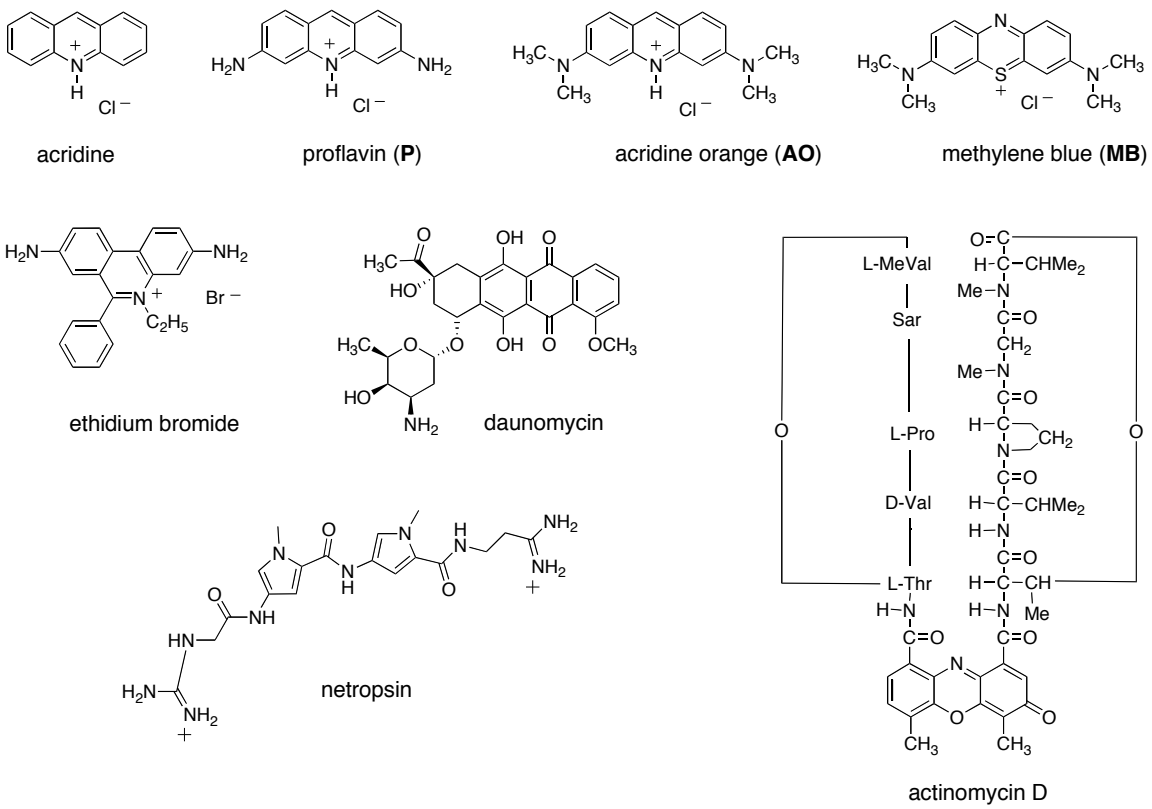

Figure 1.1. Representative classical (acridine, proflavin, acridine orange, and methylene blue) and non-classical (daunomycin and actinomycin D) intercalators and the groove binding agent netropsin.

In order for intercalation to ensue, the DNA base pairs separate by 3.4 Å to form a cavity for the incoming chromophore through localized unwinding of the duplex. The normal twist of B-form DNA is 36º (10 base pair per 360º turn). Therefore, to accommodate the ligand in the intercalation site, a reduction of this rotation occurs. However, the unwinding angle varies with the geometry of the ligand-DNA complex. For example, the insertion of the phenanthradinium ring of ethidium bromide results in a reduction of the 36º twist to 10º thereby creating an unwinding angle of 26º, while proflavin and daunomycin unwind DNA by 17º and 11º, respectively (*8*). As the duplex unwinds, the distance between the phosphate groups increases and results in the reduction of localized charge density thereby facilitating the release of condensed counterions such as sodium. The next step that occurs is the transfer of the aromatic ligand from solution to the intercalation site, a favorable hydrophobic interaction since the nonpolar intercalating aromatic ring is buried within the hydrophobic base pairs (*9*). Moreover, cationic intercalators exhibit additional counterion release through a polyelectrolyte process as described by Manning and Record (*10*, *11*). Collectively, noncovalent forces including the hydrophobic effect, a decrease in coulombic repulsion, van der Waals interactions, π-π stacking, and hydrogen bonding stabilize the energy of the newly formed complex (*9*). Furthermore, intercalators that possess substituents that form van der Waals contacts in the minor groove and/or hydrogen bond with AT base pairs (e.g., daunomycin and actionomycin D, Figure 1.1) may be influential in directing the thermodynamic binding mechanism, the geometry of the complex and sequence selectivity (*12*, *13*).

Groove Binding. The antibiotic netropsin (Figure 1.1) was the first reported AT-specific DNA groove binding agent (*14*). In contrast to intercalators, the unfused

aromatic rings of groove-binders can adopt a cresent-like shape that matches the curvature of the minor groove and bind without significant steric hinderance or pertubation of the DNA duplex. A groove binding model involves two steps in which hydrophobic transfer of the ligand from solution is then followed by noncovalent molecular interactions including hydrogen bonding to AT base pairs and van der Waals contacts within the walls of the groove (*15*). Another important feature of groove-binders is that they can be designed to cover many base pairs and consequently may exhibit high sequence-specificity recognition of nucleic acids (*8*).

Bisintercalation. Bisintercalators incorporate two covalently attached intercalating ring systems to a linking chain of variable lengths (Figure 1.2). Bisintercalating agents may offer several advantages: (i) higher binding affinity (since the binding constant of a bisintercalator, in theory, should be the square of the binding constant of the monomer), (ii) biological activity may be augmented as a function of increased binding affinity and slower dissociation rates, (iii) potential sequence selectivity, since the binding site size of a bisintercalator is increased relative to the monomer. Moreover, the linker chain may provide numerous enhancements to the structural design.

Several lines of evidence have indicated that bisintercalation is achieved when the linker chain contains structurally rigid moieties and separates the two chromophores by approximately ten angstroms (*16-19*). The former prevents self-stacking between the heterocyclic aromatic rings and the latter violation of the nearest-neighbor exclusion principle. Intramolecular interactions such as self-stacking compete with DNA binding and therefore decrease affinity (*17*). Furthermore, the linker may impart additional

stabilization to the helix by binding to the grooves. Accordingly, high-resolution structural studies of the bisintercalating drug ditercalinium have demonstrated favorable interactions by the linker localized to the major groove (*17*). These interactions have been considered an important factor in the stability and conformation of the ditercalinium-DNA complex. Similar high-resolution structural studies of the dimeric daunomycin analog WP631 have confirmed bisintercalation of the daunomycin rings and minor groove binding by the xylene linker motif (*20*). These design elements have correlated with ultra-tight binding to DNA (K_a = 3.2 x 10^{11} M^{-1}) and with enhanced cytotoxicity in MCF-7/VP-16 cell lines (*21*).

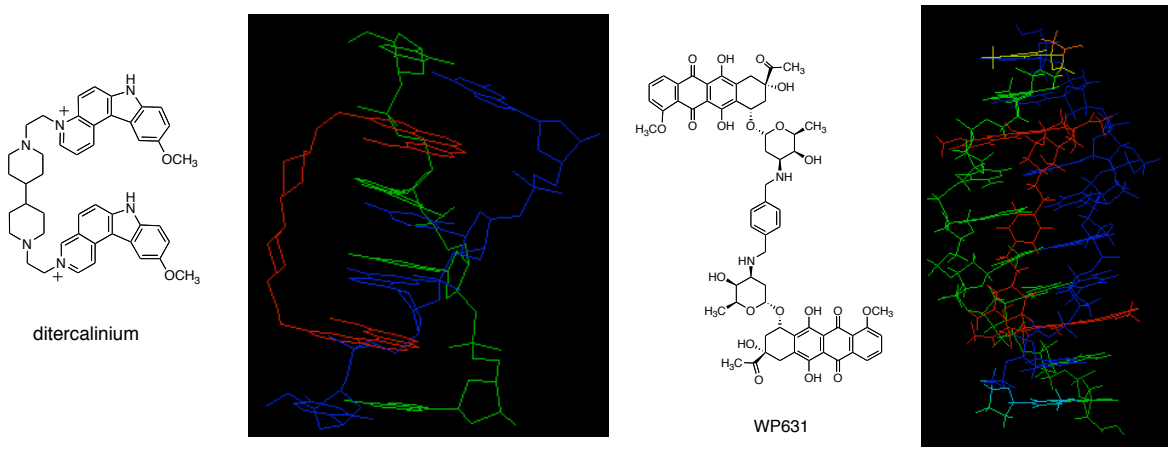

Figure 1.2. The bisintercalators ditercalinium and WP631. High resolution structures: ditercalinium (RCSB Protein Data Bank ID 1D32, reference 17); WP631 (RCSB Protein Data Bank ID 1AL9, reference 20).

Energetics of Ligand-DNA Binding. In the process of intercalation or groove binding, the overall binding free energy (eq 1.1) results from contributions of a combination of driving forces (*4*, *9*, *15*). The term ΔG_{obs} is the experimentally determined binding free energy, estimated from the association constant (*K*) by the standard Gibbs relationship (eq 1.2). Furthermore, ΔG_{conf} is the contribution from conformational changes

in the DNA and ligand while ΔG_{t+r} represents the free energy cost from the loss of translational and rotational degrees of freedom upon complex formation. The terms ΔG_{hyd} and ΔG_{pe} correspond to the hydrophobic transfer of the ligand from solution and the polyelectrolyte counterion release, respectively. Lastly, the free energy contribution arising from noncovalent molecular interactions between DNA and binding agents is ΔG_{mol}. With regards to intercalators, conformational changes and the loss of translational and rotational freedom in order to accommodate the ligand within the base pairs result in unfavorable free energy barriers for binding. Notwithstanding, such barriers are overcome by favorable free energy contributions from hydrophobic transfer of the ligand from solution, polyelectrolyte effect, and molecular noncovalent interactions within the intercalation site (*15*). In the case of groove-binders, the losses in translational and rotational freedom lead to unfavorable free energy barriers upon bimolecular complexation. Similar to intercalators, these are compensated for by hydrophobic transfer of the ligand from solution, polyelectrolyte effect, and molecular noncovalent interactions (*15*). Although the free energy contributions are similar for both binding modes, experimentally determined thermodynamic parameters suggest that intercalation is mostly favored by enthalpic contributions while groove binding is an entropically driven process (*22*). A larger entropic cost for distortion of the DNA structure by intercalation and higher favorable entropy for groove binding due to the release of water molecules from the minor groove have been proposed to account for this discrepancy (*22*).

$$\Delta G_{obs} = \Delta G_{conf} + \Delta G_{t+r} + \Delta G_{hyd} + \Delta G_{pe} + \Delta G_{mol} \quad (1.1)$$

$$\Delta G_{obs} = -RT \ln K \quad (1.2)$$

Acridines

The acridines were first developed as dyes and during the early 20th century their pharmacological properties were evaluated. At this time, proflavin was used as a topical antibacterial and antifungal agent (*23*). In the 1940's and to the present day (e.g., chloroquine, mepacrine, and pyronaridine; Figure 1.3), the acridines have been used as antimalarial drugs (*24*). The first acridine-based therapeutic agents specifically designed for cancer treatment were developed during the 1970's. These efforts led to the development of *m*-amsacrine (Figure 1.3), an 9-anilinoacridine introduced into clinical use in 1976 (*25*). Accordingly, this acridine has been clinically utilized as a single agent or in combination with other antineoplastic drugs in the treatment of acute nonlymphocytic, lymphocytic (*26, 27*), and acute myeloid (*28*, *29*) leukemias. However, *m*-amsacrine has not generally been effective in the treatment of solid tumors (*30*). Recent work on the anticancer activity of acridine derivatives (Figure 1.3) is focused on the synthetically derived pyrazoloacridines (*31*) and on pyridoacridine alkaloids isolated from marine organisms (*32*).

While the intercalative interactions and DNA binding affinity of acridines have in general been correlated with cytotoxicity, new evidence has indicated that these agents form ternary DNA-topoisomerase II enzyme complexes that disrupt cellular processes, culminating in cellular death. Eukaryotic DNA topoisomerases (I and II) are enzymes involved in topological processes that occur during transcription, recombination, chromatin assembly, and chromosome partitioning at cell division (*33*, *34*). Specifically, type I topoisomerases catalyze the cleavage of a phosphate diester bond in one strand of duplex DNA and then reseal the nick by allowing free rotation of the other strand. In

contrast, type II topoisomerases effect the cleavage of both strands and catalyze the transport of DNA segments through the break. The mechanism for both types is ATP driven and result in removing DNA supercoils (*35*). DNA binding agents are thought to "poison" the DNA-enzyme association by forming ternary complexes, which are then detected by the cell as damaged species. The interaction then triggers a cascade of events that lead to the activation of p53 protein and to the induction of apoptosis (*36*).

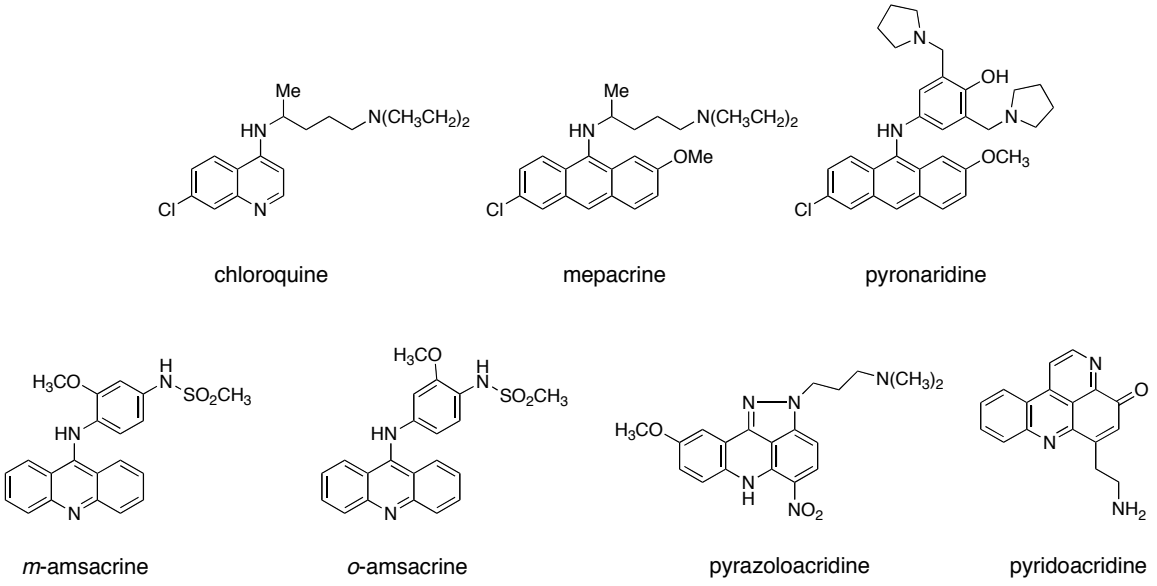

Figure 1.3. Structures of medically important acridines.

To illustrate the previous discussion, *m*-amsacrine and its structural isomer *o*-amsacrine (Figure 1.3) both bind to DNA via intercalation with an approximate 4-fold increase in the binding affinity of *o*-amsacrine (K_{obs} = 4.0 x 10^4 M^{-1}) as compared to *m*-amsacrine (K_{obs} = 1.6 x 10^4 M^{-1}) (*37*). However, *m*-amsacrine possesses higher levels of cytotoxicity in cell cultures than *o*-amsacrine and has exhibited double-strand topoisomerase II mediated DNA cleavage while *o*-amsacrine has not (*38, 39*). Studies conducted by Zwelling and colleagues have demonstrated that *m*-amsacrine exerts its

cytotoxicity through the formation of a ternary complex between ligand, DNA and topoisomerase II (*39*).

Phenothiazines

Methylene blue (**MB**), a DNA intercalating chromophore and the most extensively studied phenothiazine (Figure 1.1) was developed as dyestuff during the late 1800's. In 1891, Ehrlich successfully used methylene blue (**MB**) in patients infected with malaria (*40*). However application of **MB** as an antimalarial agent was abandoned due to the blue staining of the skin and to the development of acridine-based antimalarial agents (*41*). Notwithstanding, a recent resurgence in investigating **MB** as a potential antimalarial agent has been reported (*42*). Clinically, **MB** has been administered as an antidote for nitrate poisoning, as well as employed in the treatment of methemoglobinemia and ifosfamide-induced encephalopathy due to its low toxicity in human cells (*41*, *43*). Moreover, the phenothiazine molecule has been the basis for the development of antihistamines and antipsychotic drugs such as promethazine and chlorpromazine, respectively (*43*). Perhaps the most important and evolving application of **MB** and its derivatives has been as photosensitizing agents in photodynamic therapy.

Photosensitization

While the effects of light had been known throughout ancient civilizations, the first experimental account of photosensitization was reported by Oscar Raab in 1900. He serendipitously observed that low concentrations of acridine were lethal to paramecium during daylight experiments but not during nighttime experiments (*44*). These findings were significant in proving the connection between light activation and therapeutic outcome. Shortly thereafter, studies by von Tappeiner demonstrated the role of oxygen in

the light-dependent "photodynamic reaction" (*45*). In attempt to utilize photosensitization for potential antitumor activity, Jesionek and von Tappeiner treated skin tumors with visible light in the presence of eosin (*46*). The modern interest in photosensitization began in the 1960's with investigations by Lipson and Baldes that revealed the localization of a mixture of porphyrins (known as hematoporphyrin derivative) in tumor cells (*47*). The breakthrough however occurred in the 1970's when Dougherty reported that irradiation of murine mammary tumors with hematoporphyrin derivative resulted in significant cell death (*48*).

Photodynamic Therapy. These pioneering studies led to present day photodynamic therapy (PDT), an alternative approach to conventional chemotherapy that involves the use of a photosensitizing drug and visible light. In the presence of oxygen, the photoactivated drug generates reactive oxygen species that initiate a series of events resulting in cell death. An advantage of PDT is the localization of the photosensitizer in and selective irradiation of target tissue, thereby minimizing damage to surrounding healthy cells. Accordingly, clinical protocols for systemic applications in the treatment of numerous malignancies have been developed, including cancers of the lung, gastrointestinal tract, head and neck regions, and bladder (*49*). Moreover, the successful treatment of non-melanoma skin cancers (basal cell carcinoma and actinic keratosis) has been documented with Levulan™-mediated PDT (*50*). While the main focus of PDT has been in oncology, its most triumphant application has been in the Visudyne™-mediated treatment of wet-macular degeneration, a non-malignant ophthalmic condition that is the leading cause of blindness in the Western world (*51*). Currently, there are three photosensitizing drugs approved for PDT by the U.S.A. Food and Drug Administration:

Photofrin,™ Visudyne,™ and Levulan™ (*52*). While currently utilized PDT agents (Figure 1.4) are based on the porphyrin nucleus or mediate the *in situ* generation of endogenous porphyrins (e.g., Levulan™), other chromophores such as the phenothiazines are gaining attention as potential PDT agents.

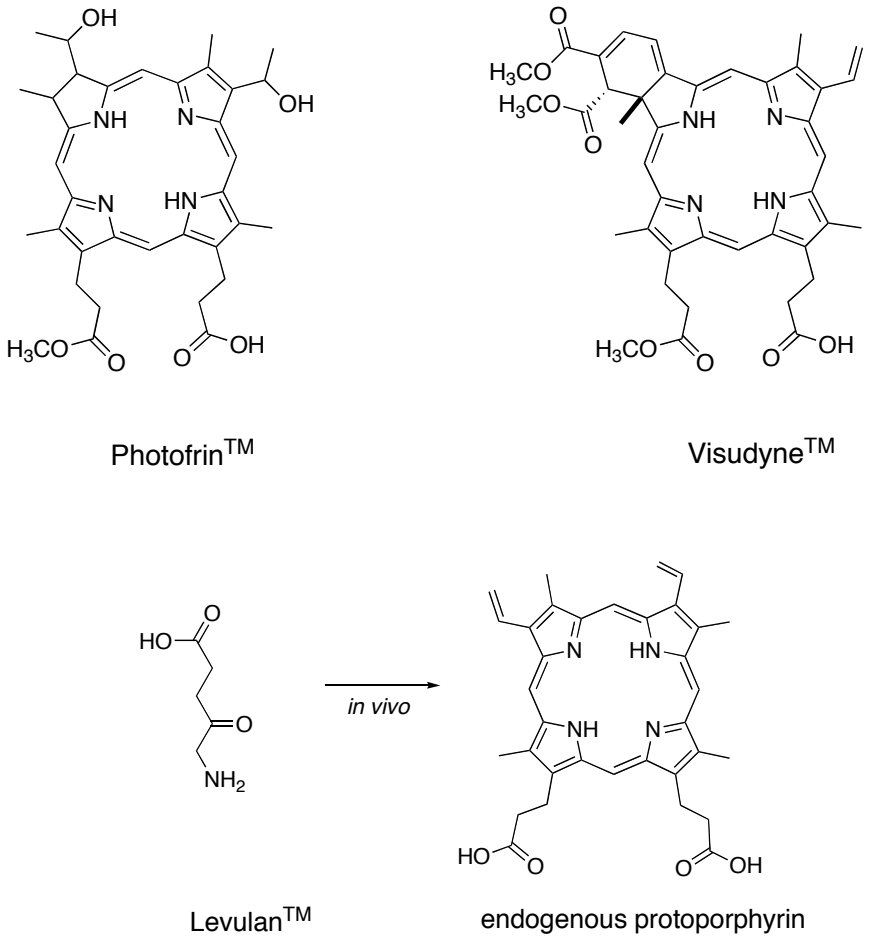

Figure 1.4. Structures of FDA approved PDT drugs.

Phenothiazines as PDT Agents. While the acridines have demonstrated PDT-mediated *in vivo* destruction of animal tumor models (Chapter II), they are generally not considered appropriate chromophores for PDT due to their light absorption properties. Acridines absorb maximal wavelengths of light ranging from approximately 350-450 nm. In contrast, **MB** and phenothiazine derivatives possessing electron-donating substituents

maximally absorb light within the therapeutic window for PDT (600-800 nm). Absorption within the therapeutic window is a desired feature, since the penetration of light into tissues is limited by: 1) light scattering, which decreases at longer wavelengths, and 2) absorption by pigmented biomolecules (*49*). With regards to PDT, **MB** and derivatives (Figure 1.5) have demonstrated phototoxicity in several malignant cell lines and colon tumors in mice. Specifically, Boehncke and co-workers demonstrated that irradiation of human immortalized keratinocytes, mouse fibroblasts, human transformed T-, and B-lymphoctes with polychromatic red light in the presence of **MB** exhibited better ED_{50} values in all cell lines and in comparison to hematoporphyrin derivative or aminolevulinic acid (*53*). Moreover, Wainwright and colleagues reported enhanced cytotoxicity in multidrug resistant mammary tumor cells irradiated in the presence of **MB** (*54*). Studies by Rice et al. revealed that photo-induced apoptosis of murine and human melanoma cell lines occurred with **MB** but that the more lipophilic derivatives dimethyl methylene blue (**DMMB**) and new methylene blue (**NMB**) were more phototoxic (*55*). Additionally, the more lipophilic derivatives (**DMMB** and **NMB**) exhibited higher levels of cellular uptake and retention. Similarly, Wainwright and co-workers correlated increased phototoxicity in murine mammary tumor cell lines with higher levels of cellular uptake and retention when employing **DMMB** or **NMB** as compared to **MB** (*56*). Additionally, these authors observed lower rates of reduction with the more lipophilic dyes and suggested that the electron donating effects of the methyl groups in the 1 and 9 or 2 and 8 positions of **DMMB** and **NMB**, respectively, accounted for this observation (*56*).

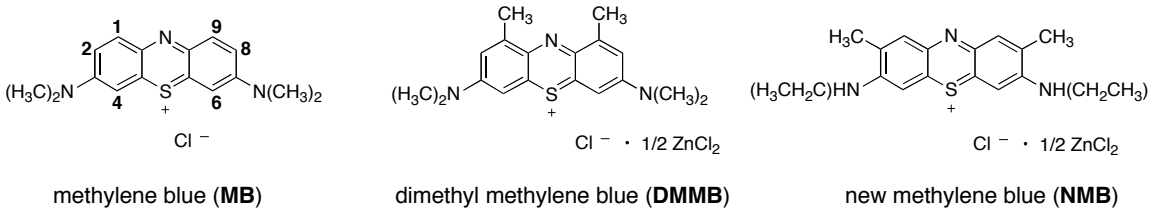

Figure 1.5. Structure of photoactive phenothiazinium salts.

With regards to *in vivo* applications, enhanced reduction of colon tumors in mice with photoactivated **MB** has been reported (*57)*. In addition, Orth et al. demonstrated that irradiation of intratumorally applied **MB** resulted in the palliative treatment of human esophageal cancers (*58*). However, clinical application of **MB** has not been successful due to its poor tumor localization and retention following intravenous or intravesical administration. This limitation has been attributed to the hydrophilic nature and the biological reduction of the chromophore into its photo-inactive leuco form (*43*). Although hydrophilicity and biological reduction have been reported as caveats for **MB**-PDT applications, Tardivo and co-workers have recently reported complete and partial responses with **MB**-PDT in patients with cancerous skin lesions, including basal cell carcinoma, Kaposi's sarcoma, and melanoma (*59*). Interestingly, these are accessible lesions that can be intradermally injected and easily irradiated.

Other applications of phenothiazine-mediated PDT include the photoinactivation of bacteria (in an attempt to ameliorate the rise in multidrug resistance to conventional antibiotics and viruses) with an emphasis on the sterilization of donated blood products. In the case of PDT-mediated antimicrobial chemotherapy, success has been limited mostly to *in vitro* assays and to surface wounds since there are no established methods of delivery (e.g., photosensitizer localization and light delivery) for systemic applications (*41*). Early studies conducted by Jacob and Menezes et al. demonstrated the abilitity of

MB to effect DNA photodamage in *Escherichia coli* and *Proteus mirabilis*, respectively (*60*, *61*). More recently, the Phoenix group has reported enhanced cell death by photoactivated **DMMB** in *Escherichia coli* and *Staphylococcus aureus* cultures with minimal lethal concentrations of 0.5 μM and 0.8 μM, respectively (*62*). Furthermore, **DMMB** has shown high levels of photo-induced bactericidal activity against the vancomycin-resistant *Enterococcus faecalis* and *faecium* strains (*63*).

Another important application of **MB**-PDT has been in the photoinacivation of viral pathogens in blood products. The photodecontamination of plasma has been utilized with **MB** in Germany since 1993 and more recently in other European communities (*64*). Floyd and colleagues have recently reported that **MB** has shown efficacy in the photoinactivation of human immunodeficiency virus (HIV). In their assays, HIV-1 infected cells that were treated with **MB** followed by irradiation with visible light (400-700 nm) resulted in the attenuation of viral infectivity in a concentration dependent manner (*65*).

DNA Damage and Photosensitization

DNA damage induced by chemical photosensitization has been extensively investigated with endogenous porphyrins, xenobiotic dyes and metal complexes. Collectively, these studies have led to a better understanding of phototoxicity and phototherapy either to prevent cell damage or to enhance the cytotoxicity of anticancer drugs. Moreover, DNA and RNA interacting photosensitizers may serve as structural and molecular probes to further elucidate nucleic acids and other biomolecules interactions.

When a sensitizing molecule absorbs a photon of light, an electronic transition results in the promotion of an electron from a ground state orbital to an unoccupied orbital and the molecule is said to be in an excited state. This excited singlet has a relatively short lifetime and can be de-activated back to the ground state with the emission of a photon (fluorescence). Alternatively, the excited singlet can be de-activated by an intersystem crossing (ISC) transition that populates the triplet excited state. Because the triplet state has a longer lifetime, it tends to be important in many photochemical reactions (*66*). Accordingly, the triplet excited state sensitiser (not directly involved in DNA damage) can react with molecular oxygen to produce reactive oxygen species (type I and II mechanisms) or accepts an electron from a biological substrate to generate oxidized species (type I mechanism). These mechanisms are schematically illustrated in Figure 1.6.

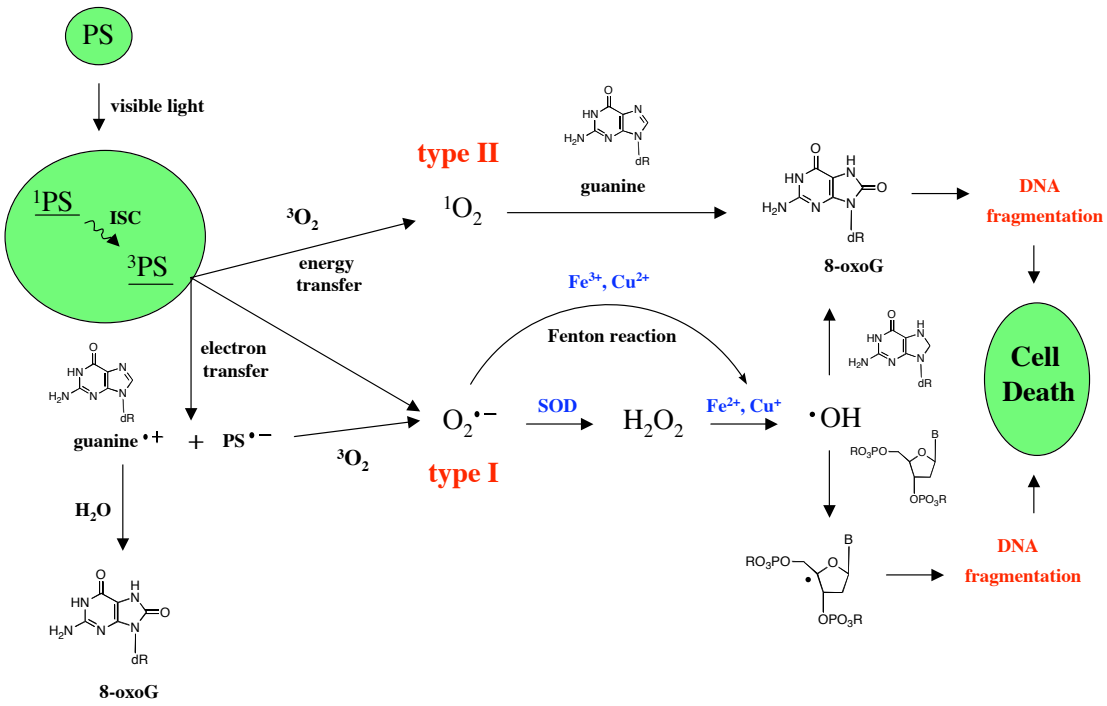

Figure 1.6. Mechanisms involved in DNA photosensitization.

Hydroxyl Radical Mediated Deoxyribose Damage. The hydroxyl radical (•OH) is chemically generated (also can be generated through the homolysis of water by ionizing radiation) via superoxide anions (type I mechanism) that can spontaneously (in aqueous media) or catalytically (*in vivo* by superoxide dismutase, SOD) dismutate to produce hydrogen peroxide. In the presence of redox active metals, hydrogen peroxide is reduced thereby generating diffusible hydroxyl radicals through Fenton reactions (Figure 1.6). This electrophilic and highly reactive radical can efficiently abstract hydrogen atoms from the deoxyribose units in DNA culminating in direct strand cleavage (frank strand breaks; *67*) and the production of alkaline-labile lesions. While single strand breaks are usually not lethal, multiple •OH-mediated lesions result in double strand breaks, which lead to permanent DNA damage (*68*). While hydrogen atom abstraction can occur from all the carbon atoms of the deoxyribose sugars (*69*, *70*), C-2' carbon-centered radicals are stabilized by the lone pair electrons of adjacent oxygen atoms which renders atom abstraction form this carbon the least favorable (*69*, *71*). The majority of hydroxyl radical chemistry involves C-4' hydrogen atom abstraction due to solvent accessibility and increased lability of the C-H bond (*69, 71*). The mechanism of Fe(II)-bleomycin mediated Frank strand cleavage via C-4' hydrogen atom abstraction (which leads to oligonucleotide 3'-phosphoglycolate, base propenal, and oligonucleotide 5'-phosphate DNA fragments) is shown in Figure 1.7.

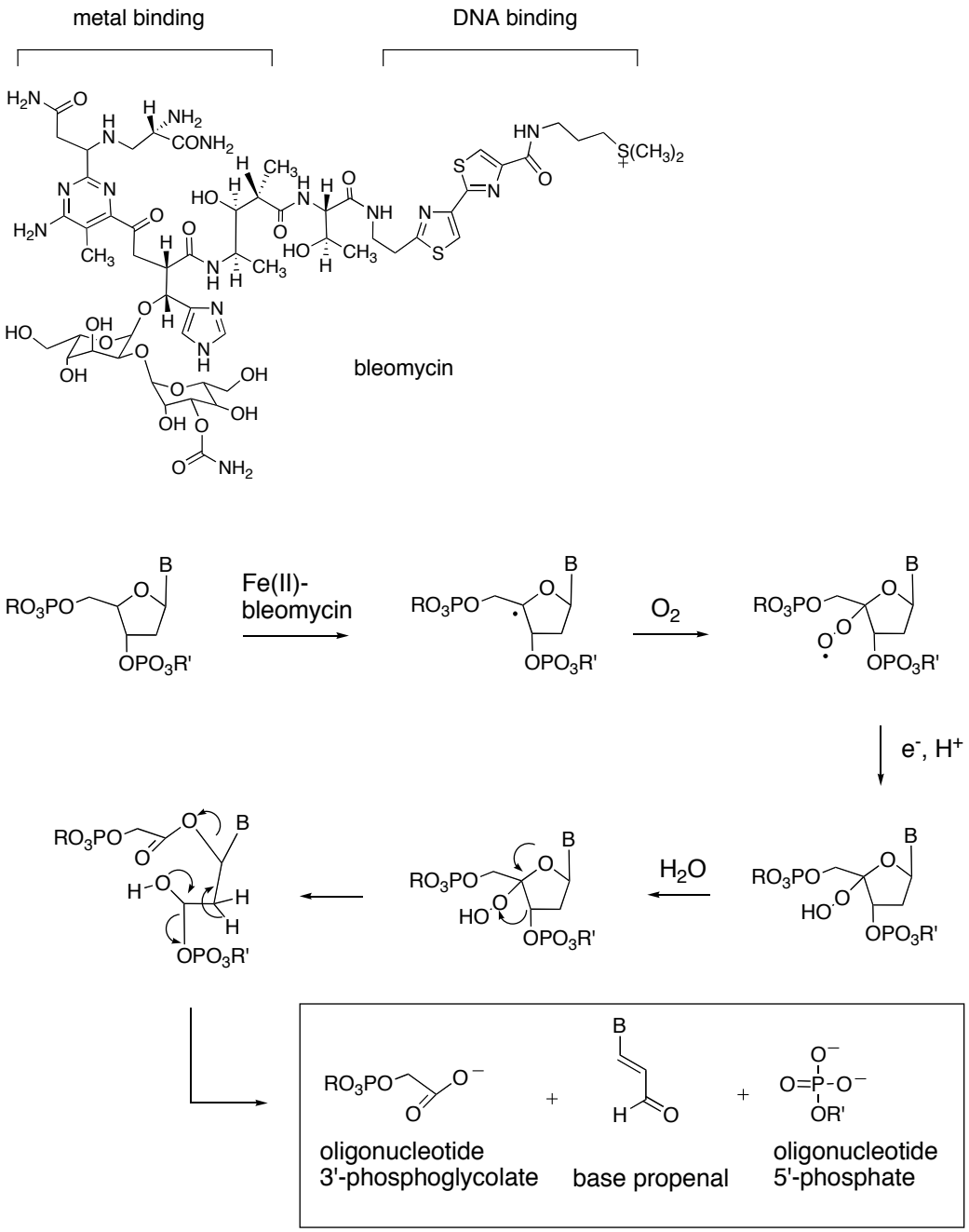

Figure 1.7. Fe(II)-bleomycin mediated C-4' hydrogen atom abstraction.

Hydroxyl Radical Mediated Base Damage. DNA oxidation by hydroxyl radicals results from the addition of the radical to double bonds (Figure 1.8). The most often targeted base is guanine since it exhibits the lowest oxidation potential in comparison to the remaining three bases. Addition of hydroxyl radicals to the C-4 and C-

5 positions of guanine result in radical adducts. However, these adducts can gain electrons from the medium or from cellular thiols *in vivo* and thus revert back to guanine (*72*). Alternatively, addition across the C-8 position generates 7,8-dihydro-8-oxoguanine (8-oxoG). These lesions do not typically result in direct strand cleavage and thus require alkali treatment for further fragmentation to occur (*73*).

Electron Transfer and Singlet Oxygen Mediated DNA Damage. In general, DNA oxidation by singlet oxygen (type II) or by electron transfer reactions (type I) leads to base modifications (predominantly 8-oxoG; Figure 1.8) and do not often result in permanent DNA damage as compared to deoxyribose chemistry. The majority of these lesions require piperidine treatment post-irradiation in order to reveal the site of damage. Notwithstanding, several accounts of direct strand cleavage at guanine bases by singlet oxygen have appeared in the literature (*74-76*). More recently, Kochevar and colleagues have reported that irradiation of HeLa cells incubated with Rose Bengal, a well known singlet oxygen generator, induced apoptosis and DNA fragmentation (*77*). Because both singlet oxygen and electron transfer mechanisms predominantly involve the formation of alkaline-labile lesions at guanine bases, it is sometimes difficult to experimentally (via nucleotide resolution assays) distinguish one mechanism from the other. However, the Barton group has reported that damage by electron transfer exhibits a signature intense cleavage at the first guanine in a '5-GG-3' step, while damage by singlet oxygen occurs equally at all guanines (*78*).

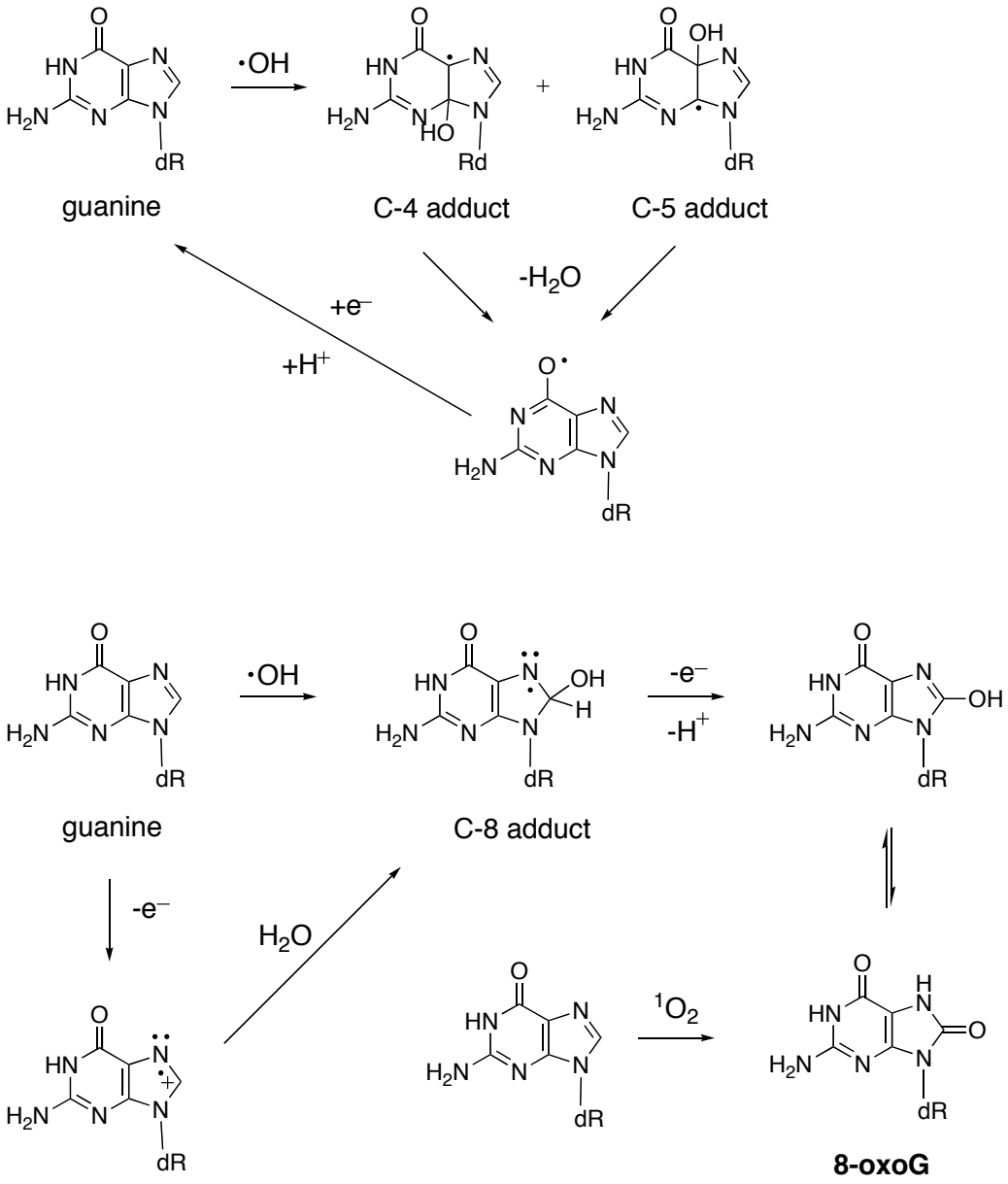

Figure 1.8. Hydroxyl radical, electron transfer and singlet oxygen guanine base modifications.

DNA Damage by Photoactive Agents. In contrast to light activated Fenton reagents which specifically generate radicals that target deoxyribose hydrogen atoms, DNA damage by many photonucleases may concomitantly involve type I and II

mechanisms. Therefore, the type of mechanism that predominates and the reactive species that lead to damage highly depend on the specific photochemistry of the photosensitiser, experimental conditions, and DNA binding interactions. For example, Shuster's group reported that DNA damage by a photoactivated intercalated anthraquinone (Figure 1.9) produced guanine base lesions consistent with an electron transfer mechanism. However, irradiated unbound molecules (excess concentration of anthraquinone relative to DNA in solution) resulted in non-specific frank strand breaks (*79*). Moreover, Bohne et al. reported two distinct mechanisms for DNA photocleavage by an acridizinium salt (*80*, Figure 1.9). In the presence of oxygen, DNA photodamage resulted from a singlet oxygen-mediated mechanism via energy transfer of the triplet excited state acridizinium salt, while anaerobic conditions implicated the involvement of hydroxyl radicals. Based on excited-state reduction potentials, the authors reasoned that under anaerobic conditions photoinduced electron transfer between the excited acridizinium and water might lead to a reduced chromophore and a water radical cation. They also suggested that hydroxyl radicals were generated by subsequent deprotonation of the water radical cation.

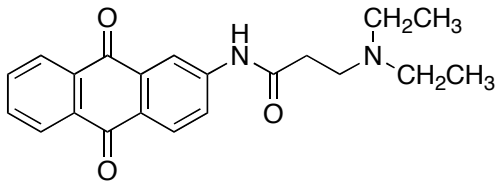

anthraquinonecarboxamide

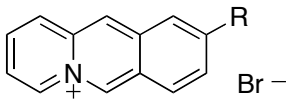

acridizinium bromide

Figure 1.9. Anthraquinone and acridizinium DNA photocleaving agents.

Metal Complexes and DNA Photocleavage. Metal ions are involved in many biological processes including hydrolysis and redox cycling reactions. Moreover, their Lewis acidic charged centers are well suited to bind negatively charged biomolecules including nucleic acids and proteins. Accordingly, the development of metal-based therapeutics has been an area of active research. One of the most successful metal complexes in medicine is cisplatin, a DNA interacting and clinically important anticancer agent. In addition, studies on DNA binding and damage by Fe(II)-bleomycin as well as by metal-porphyrin complexes have further contributed to the search for newer metal complexes with improved antitumor properties.

Numerous metal complexes by virtue of their d-orbitals and redox properties have been shown to promote photo-induced DNA damage. In this regard, representative cobalt(II), copper(II), ruthenium(II), and rhodium(III) complexes have exhibited efficient photonuclease activity (Figure 1.10). Nair and Vaidyanathan used a 2,6-bis(benziimidazol-2-yl)pyridine cobalt(II) complex to conduct aerated plasmid nicking assays that demonstrated DNA photocleavage by this cobalt(II)-complex (*81*). Based on fluorescence quenching studies, the authors postulated that DNA damage might occur through photoelectron transfer from guanine to the excited state of the complex. Zaleski's group found that copper(II) complexes of cis-1,8-bis(pyridin-3-oxy)oct-4-ene-2,6-diyne produced photolytic degradation of pUC19 plasmid DNA via C-4' hydrogen atom abstraction. This enediyne ligand was shown to undergo metal-assisted photochemical Bergman cyclization, thereby generating diradicals which efficiently abstracted C-4' hydrogens atoms (*82*). Furthermore, Turro and co-workers demonstrated that a supramolecular ruthenium(II)-viologen complex effected DNA photocleavage under

aerobic and anaerobic conditions (*83)*. The authors suggested an electron transfer mechanism involving guanine and the photooxidized ruthenium(III) center of the complex. Lastly, Barton and co-workers reported direct strand cleavage via 3'-hydrogen abstraction upon irradiation of an intercalated phenanthrenequinone diimine complex of rhodium(III). Their studies indicated that the 3'-hydrogen located in the major groove was a prime target for abstraction by a photoinduced phenanthrenequinone diimine radical owing to the spatial conformation of the rhodium complex within the major groove (*84*).

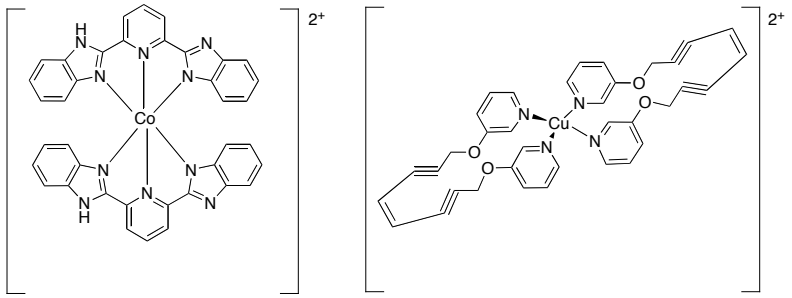

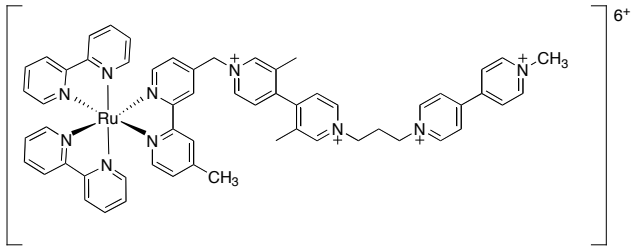

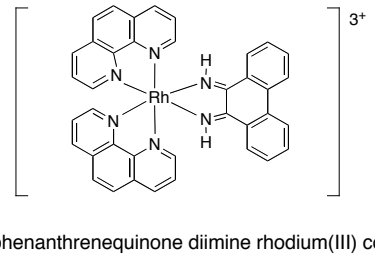

Figure 1.10. Representative DNA photocleaving metal complexes.

Photofootprinting

Footprinting is a widely utilized technique employed to map the sequence specific sites of DNA binding drugs and proteins. While many enzymatic (e.g., DNase I and II) and chemical footprinting agents (e.g., methidium-EDTA-iron(II) and 1,10-phenanthroline copper(I)) have been successfully utilized, photofootprinting reagents offer the advantage of controlling DNA cleavage with light (*85*). In this method, a radiolabeled DNA fragment is reacted with a footprinting agent in the absence and presence of DNA binding ligand. The footprinting agent then cleaves DNA at all residues except for those sites where the ligand is bound. Accordingly, the uncleaved DNA (ligand-bound sites) produce a "footprint," an electrophoretic pattern that is devoid of cleaved DNA bands. The footprinted site(s) are then compared to the electrophoretic pattern produced by the footprinting agent run in the absence of the DNA binding ligand. Typical footprinting agents cleave DNA without any sequence or base specificity, a necessary requirement to prevent binding sequence ambiguity of the ligand or protein.

Examples of photofootprinting acridine agents have been reported. Jeppesen and Nielsen described the photofootprinting capability of two acridine derivatives (DHA and MAA; Figure 1.11). Their analyses revealed comparable reactivity of the the two photoactive reagents to DNase I in identifying the binding sites of well known DNA binding agents including distamycin and echinomycin (*86*). In another study, Saito and co-workers reported efficient direct DNA strand breaks by a photoactive dibenzoyldiazomethane-acridine conjugate (Figure 1.11). Furthermore, DNA nucleotide resolution photocleavage assays by this dibenzoyldiazomethane-acridine conjugate

revealed cleavage at all residues without any sequence or base specificity, thereby demonstrating its potential application as a photofootprinting reagent (*87*).

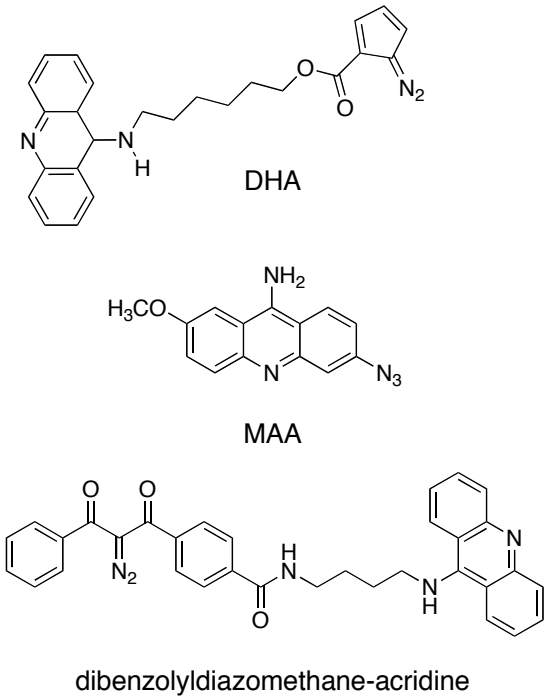

Figure 1.11. Structures of acridine based photofootprinting reagents.

Specific Aims

The objectives of the studies described in this dissertation were to synthesize acridine and phenothiazine based photosensitizers (Chapters II-V) and then to evaluate their DNA photocleavage efficiencies. The acridine and phenothiazine parent chromophores were selected due to their well-documented DNA photosensitizing capabilities and to their DNA binding interactions (predominantly via intercalation). In each case, the compounds were designed to incorporate structural features that might increase DNA binding affinity and/or effect metal complexation. Specifically,

photonuclease **7** described in Chapter II was designed to incorporate a central acridine chromophore covalently attached to four metal-binding imidazole rings. This design rationale was developed in an attempt to modulate and to enhance DNA photodamage in the presence of metal ions. Accordingly, DNA photocleavage by compound **7** was evaluated in the presence of 16 different metal salts.

The design rationale for the synthesis of compound **4** as described in Chapter III was based on utilizing two units of an acridine chromophore covalently tethered to a pyridine linker. In this case, the bisacridine element was employed to develop a putative bisintercalator. Because bisintercalators have demonstrated higher DNA binding affinities in comparison to monointercalators, DNA photodamage might be augmented as a result of the stronger association between the bisintercalator and DNA. Additionally, the pyridine linker was introduced specifically as a copper-binding motif to modulate and to enhance DNA photocleavage in the presence of copper(II) ions.

In response to the interest in developing non-porphyrin chromophores possessing suitable light properties for photodynamic therapy, three new compounds incorporating a phenothiazine nucleus were synthesized, characterized and evaluated (Chapters IV-V). The major objective involving their development was to design putative bisintercalating agents capable of effecting enhanced levels of DNA photodamage at longer wavelengths.

A salient feature of photodynamic therapy is the requirement for strong absorption of light by photosensitizing chromophores within the “therapeutic window” (600-800 nm), in order to increase the depth of light penetration in tissues. This is met by phenothiazine dyes possessing electron donating groups, a factor which motivated the design of the linkers in compounds **3**, **5**, and **6**. Moreover, the linkers are composed of six

member piperidine or piperazine and xylene ring systems to potentially provide additional duplex stability by binding within the grooves of DNA.

The major goal of this project as described in Chapters II-V was to evaluate the DNA photocleavage efficiencies produced by the compounds when irradiated in the presence of pUC19 plasmid DNA. In these assays, pUC19 plasmid DNA was utilized due to the fact that uncleaved and cleaved plasmid forms migrate through agarose gels at different rates. Upon light exposure, the DNA-bound photosensitizers are expected to generate reactive oxygen species, which then mediate direct DNA strand scission by converting uncleaved supercoiled DNA into the nicked (single strand breaks) and linear (double strand breaks) forms. The nicked, linear and supercoiled forms of pUC19 plasmid DNA are then easily visualized by staining the agarose gel with the fluorescent and DNA intercalating dye ethidium bromide. The photocleavage yields are then determined by utilizing light densitometry to quantitate each form of DNA produced during irradiation in the presence of the photosensitizing nucleases.

Corollary assays to evaluate metal complex formation, fluorescence quantum yields, DNA thermal denaturation, competitive equilibrium dialysis binding, viscosity, reactive oxygen species sequestration and DNA photocleavage at nucleotide resolution were conducted. Taken together, the projects integrated organic, biophysical, photo-, and bio-chemical methods to dissect the factors involved in the enhancement of DNA photosensitization.

Lastly, a small project was implemented as a National Science Foundation workshop laboratory exercise involving a non-invasive DNA isolation technique and the amplification of alleles encoding normal variations in human color vision (Chapter VI).

The goals of this exercise were aimed at providing the workshop participants with “hands on” experience in currently utilized protocols in molecular biology.

References

(1) Watson, J. D.; Crick, F. H. C. *Nature* **1953**, *171*, 964-967.

(2) Kersten, H.; Kersten, W.; Rauen, H. M. *Nature* **1960**, *187*, 60-61.

(3) Reich, E. *Science* **1964**, *143*, 684-689.

(4) Graves, D. E.; Velea, L. M. *Curr. Org. Chem.* **2000**, *4*, 915-929.

(5) Lerman, L. S. *J. Mol. Biol.* **1961**, *3*, 18-30.

(6) Lerman, L. S. *Proc. Natl. Acad. Sci. USA* **1964**, *49*, 94-102.

(7) Neville, D. M. Jr.; Davies, D. R. *J. Mol. Biol.* **1966**, *17*, 57-74.

(8) Wilson, W. D. In *Nucleic Acids in Chemistry and Biology*; Blackburn, G. M.; Gait, M. J., Eds.; Oxford University Press: New York, 1996; pp 331-370.

(9) Boresch, S.; Karplus, M. *J. Mol. Biol.* **1995**, *254*, 801-807.

(10) Manning, G. S. *Q. Rev. Biophys.* **1978**, *11*, 179-246.

(11) Record, M. T. Jr.; Anderson, C. F.; Lohman, T. M. *Q. Rev. Biophys.* **1978**, *11*, 103-178.

(12) Wang, A. H.-J. *Curr. Opin. Struct. Biol.* **1992**, *2*, 361-368.

(13) Krugh, T. R. *Curr. Opin. Struct. Biol.* **1994**, *4*, 351-364.

(14) Wartell, R. M.; Larson, J. E.; Wells, R. D. *J. Biol. Chem.* **1974**, *249*, 6719-6731.

(15) Chaires, J. B. *Biopolymers* **1997**, *44*, 201-215.

(16) Carpenter, M. L.; Lowe, G.; Cook, P. R. *Nucleic Acids Res.* **1996**, *24*, 1594-1601.

(17) Gao, Q.; Williams, L. D.; Egli, M.; Rabinovich, D.; Chen, S.-L.; Quigley, G. J.; Rich, A. *Proc. Natl. Acad. Sci. USA* **1991**, *88*, 2422-2426.

(18) Gaugain, B.; Barbet, J.; Oberlin, R.; Roques, B. P.; LePecq, J. B. *Biochemistry* **1978**, *17*, 5071-5078.

(19) Léon, P.; Garbay-Jaureguiberry, C.; Lambert, B.; Le Pecq, J. B.; Roques, B. P. *J. Med. Chem.* **1988**, *31*, 1021-1026.

(20) Robinson, H.; Priebe, W.; Chaires, J. B.; Wang, A. H. *Biochemistry* **1997**, *36*, 8663-8670.

(21) Chaires, J. B.; Leng, F.; Przewloka, T.; Fokt, I.; Ling, Y-H.; Perez-Soler, R.; Priebe, W. *J. Med. Chem.* **1997**, *40*, 261-266.

(22) Chaires, J. B. *Arch. Biochem. Biophys.* **2006**, *453*, 24-29.

(23) Albert, A.; *The Acridines*; St. Martin's Press: New York, 1966; pp 403-504.

(24) Greenwood, D. *J. Antimicrob. Chemother.* **1995**, *36*, 857-872.

(25) Grove, W. R.; Fortner, C. I.; Wiernik, P. H. *Clin. Pharm.* **1982**, *1*, 320-326.

(26) Van Mouwerik, T. J.; Caines, P. M.; Ballentine, R. *Drug Intell. Clin. Pharm.* **1987**, *21*, 330-334.

(27) Jehn, U. *Bone Marrow Transplant.* **1989**, *Suppl 3*, 53-58.

(28) Harousseau, J.-L.; Cahn, J.-Y.; Pignon, B.; Witz, F.; Milpied, N.; Delain, M.; Lioure, B.; Lamy, T.; Desablens, B.; Guilhot, F.; Caillot, D.; Abgrall, J.-F.; Francois, S.; Briere, J.; Guyotat, D.; Casassus, P.; Audhuy, B.; Tellier, Z.; Hurteloup, P.; Herve, P. *Blood* **1997**, *90*, 2978-2986.

(29) Brown, P.; Hoffmann, T.; Hansen, O. P.; Boesen, A. M.; Gronbaek, K.; Hippe, E.; Jensen, M. K.; Thorling, K.; Storm, H. H.; Pedersen-Bjergaard, J. *Leukemia* **1997**, *11*, 37-41.

(30) Jelic, S.; Nikolic-Tomasevic, Z.; Kovcin, V.; Milanovic, N.; Tomasevic, Z.; Jovanivic, V.; Vlajic, M. *J. Chemother.* **1997**, *9*, 364-370.

(31) Denny, W. A. *Med. Chem. Rev.* **2004**, *1*, 257-266.

(32) Demeunynck, M.; Charmantray, F.; Martelli, A. *Curr. Pharm. Design* **2001**, *7*, 1703-1724.

(33) Wang, J. C. *Annu. Rev. Biochem.* **1996**, *65*, 635-691.

(34) Pommier, Y.; Bertrand, R. In *The Causes and Consequences of Chromosomal Aberrations*; Kirsch, I. R., Ed.; CRC Press: London, 1993; pp 277-309.

(35) Stivers, J. T. *Biochemistry* **1997**, *36*, 5212-5222.

(36) Martínez, R.; Chacón-García, L. *Curr. Med. Chem.* **2005**, *12*, 127-151.

(37) Wadkins, R. M.; Graves, D. E. *Biochemistry* **1991**, 30, 4277-4283.

(38) Zwelling, L. A.; Michaels, S.; Erickson, L. C.; Ungerleider, R. S.; Nichols, M.; Kohn, K. W. *Biochemistry* **1981**, *20*, 6553-6563.

(39) Minford, J.; Pommier, Y.; Filipski, J.; Kohn, K. W.; Kerrigan, D.; Mattern, M. R.; Michaels, S.; Schwartz, R. E.; Zwelling, L. A. *Biochemistry* **1986**, *25*, 9-16.

(40) Guttmann, P.; Ehrlich, P. *Berlin Klin. Wochschr.* **1891**, *39*, 953-956.

(41) Harris, F.; Chatfield, L. K.; Phoenix, D. A. *Curr. Drug Targets* **2005**, *6*, 615-627.

(42) Wainwright, M.; Amaral, L. *Trop. Med. Int. Health* **2005**, *10*, 501-511.

(43) Wainwright, M.; Crossley, K. B. *J. Chemother.* **2002**, *14*, 431-443.

(44) Raab, O. *Z. Biol.* **1900**, *39*, 524-526.

(45) Jodlbauer, A.; von Tappeiner, H. *Münch. Med. Wochenschr.* **1904**, *52*, 1139-1141.

(46) Jesionek, A.; von Tappeiner, H. *Arch. Klin. Med.* **1905**, *82*, 223-227.

(47) Lipson, R. L.; Baldes, E. J. *Arch. Dermatol.* **1960**, *82*, 508-516.

(48) Dougherty, T. J.; Grindey, G. B.; Fiel, R.; Weishaupt, K. R.; Boyle, D. G. *J. Natl. Cancer Inst.* **1975**, *55*, 115-121.

(49) Detty, M. R.; Gibson, S. L.; Wagner, S. J. *J. Med. Chem.* **2004**, *47*, 3897-3915.

(50) Babilas, P.; Karrer, S.; Sidoroff, A.; Landthaler, M.; Szeimies, R.-M. *Photodermatol. Photoimmunol. Photomed.* **2005**, *21*, 142-149.

(51) Mellish, K. J.; Brown, S. B. *Exp. Opin. Pharmacother.* **2001**, *2*, 351-361.

(52) Brown, S. B.; Brown, E. A; Walker, I. *Lancet Oncol.* **2004**, *5*, 497-508.

(53) Boehncke, W.-H.; Rück, A.; Naumann, J.; Sterry, W.; Kaufmann, R. *Lasers Surg. Med.* **1996**, *19*, 451-457.

(54) Wainwright, M.; Phoenix, D. A.; Burrow, S. M; Waring, J. *J. Chemother.* **1999**, *11*, 61-68.

(55) Rice, L.; Wainwright, M.; Phoenix, D. A. *J. Chemother.* **2000**, *12*, 94-104.

(56) Wainwrigth, M.; Phoenix, D. A.; Rice, L.; Burrow, S. M.; Waring, J. *J. Photochem. Photobiol. B.* **1997**, *40*, 233-239.

(57) Orth, K.; Beck, G.; Genze, F.; Rück, A. *J. Photochem. Photobiol. B.* **2000**, *57*, 186-192.

(58) Orth, K.; Rück, A.; Stanescu, A.; Beger, H. G. *Lancet* **1995**, *345*, 519-520.

(59) Tardivo, J. P.; Del Giglio, A.; Santos de Oliveira, C.; Gabrielli, D. S.; Junqueira, H. C.; Tada, D. B.; Severino, D.; Turchiello, R. F.; Baptista, M. S. *Photodiag. Photodyn. Ther.* **2005**, *2*, 175-191.

(60) Jacob, H. E. *Photochem. Photobiol.* **1975**, *21*, 445-447.

(61) Menezes, S.; Capella, M. A. M.; Caldas, L. R. *J. Photochem. Photobiol. B.* **1990**, *5*, 505-517.

(62) Phoenix, D. A.; Sayed, Z.; Hussain, S.; Harris, F.; Wainwright, M. *FEMS Immunol. Med. Microbiol.* **2003**, *39*, 17-22.

(63) Wainwright, M.; Phoenix, D. A.; Gaskell, M.; Marshall, B. *J. Antimicrob. Chemother.* **1999**, *44*, 823-825.

(64) Abe, H.; Ikebuchi, K.; Hirayama, J.; Ikeda, H. *Recent Res. Devel. Photochem. Photobiol.* **2001**, *5*, 163-173.

(65) Floyd, R. A.; Schneider, J. E. Jr.; Dittmer, D. P. *Antivir. Res.* **2004**, *61*, 141-151.

(66) Ochsner, M. *J. Photochem. Photobiol. B.* **1997**, *39*, 1-18.

(67) Lloyd, D. R.; Phillips, D. H.; Carmichael, P. L. *Chem. Res. Toxicol.* **1997**, *10*, 393-400.

(68) Prise, K. M.; Davies, S.; Michael, B. D. *Radiat. Res.* **1993**, *134*, 102-106.

(69) Breen, A. P.; Murphy, J. A. *Free Radic. Biol. Med.* **1995**, *18*, 1033-1077.

(70) Cadet, J.; Delatour, T.; Douki, T.; Gasparutto, D.; Pouget, J.-P.; Ravanat, J.-L.; Sauvaigo, S. *Mutat. Res.* **1999**, *424*, 9-21.

(71) Pogozelski, W. K.; Tullius, T. D. *Chem. Rev.* **1998**, *98*, 1089-1107.

(72) Burrows, C. J.; Muller, J. G. *Chem. Rev.* **1998**, *98*, 1109-1151.

(73) Ravanat, J.-L.; Di Mascio, P.; Martinez, G. R.; Medeiros, M. H. G.; Cadet, J. *J. Biol. Chem.* **2000**, *275*, 40601-40604.

(74) Blazek, E. R.; Peak, J. G.; Peak, M. J. *Photochem. Photobiol.* **1989**, *49*, 607-613.

(75) Churchill, M. E.; Schmitz, A. M.; Peak, J. G.; Peak, M. J. *Photochem. Photobiol.* **1990**, *52*, 1017-1023.

(76) Devasagayam, T. P. A.; Steenken, S.; Obendorf, M. S. W.; Schultz, W. A.; Sies, H. *Biochemistry* **1991**, *30*, 6283-6289.

(77) Kochevar, I. E.; Lynch, M. C.; Zhuang, S.; Lambert, C. R. *Photochem. Photobiol.* **2000**, *72*, 548-553.

(78) Hall, D. B.; Kelley, S. O.; Barton, J. A. *Biochemistry* **1998**, *37*, 15933-15940.

(79) Breslin, D. T.; Schuster, G. B. *J. Am. Chem. Soc.* **1996**, *118*, 2311-2319.

(80) Bohne, C.; Faulhaber, K.; Giese, B.; Häfner, A.; Hofmann, A.; Ihmels, H.; Köhler, A.-K.; Perä, S.; Schneider, F.; Sheepwash, M. A. L. *J. Am. Chem. Soc.* **2005**, *127*, 76-85.

(81) Vaidyanathan, V. G.; Nair, B. U. *J. Inorg. Biochem.* **2003**, *94*, 121-126.

(82) Benites, P. J.; Holmberg, R. C.; Rawat, D. S.; Kraft, B. J.; Klein, L. J.; Peters, D. G.; Thorp. H. H.; Zaleski, J. M. *J. Am. Chem. Soc.* **2003**, *125*, 6434-6446.

(83) Fu, P. K.-L.; Bradley, P. M.; van Loyen, D.; Dürr, H.; Bossmann, S. H.; Turro, C. *Inorg. Chem.* **2002**, *41*, 3808-3810.

(84) Sitlani, A.; Long, E. C.; Pyle, A. M.; Barton, J. A. *J. Am. Chem. Soc.* **1992**, *114*, 2303-2312.

(85) Armitage, B. *Chem. Rev.* **1998**, *98*, 1171-1200.

(86) Jeppesen, C.; Nielsen, P. E. *Eur. J. Biochem.* **1989**, *182*, 437-444.

(87) Nakatani, K.; Shirai, J.; Sando, S.; Saito, I. *Tetrahedron Lett.* **1997**, *38*, 6047-6050.

CHAPTER II

Tunable DNA Photocleavage by an Acridine-Imadazole Conjugate

(This chapter is verbatim as it appears in Wilson, B.; Gude, L.; Fernández, M.-J.; Lorente, A.; Grant, K. B. *Inorganic Chemistry* **2005**, *44*, 6159-6173. The initial syntheses of compounds **1**-**10** were conducted by Drs. Gude, Fernández, and Lorente. Dr. Gude also conducted the characterization of the Zn(II)-complex by ^{1}H NMR spectroscopy. Mass spectra were conducted by Dr. Siming Wang at Georgia State University. The contributions to the project by the author of this dissertation were as follows: preparation of compounds **1**-**7**; conception and execution of all biological, biophysical, and photochemical experiments; and authorship of the original manuscript. The final manuscript was extensively revised by Dr. Grant.)

Abstract

We report the synthesis and characterization of photonucleases *N*,*N*'-bis[2-[bis(1*H*-imidazol-4-ylmethyl)amino]ethyl]-3,6-acridinediamine (**7**) and *N*-[2-[bis(1*H*-imidazol-4-ylmethyl)amino]ethyl]-3,6-acridinediamine (**10**), consisting of a central 3,6-acridinediamine chromophore attached to 4 and 2 metal coordinating imidazole rings, respectively. In DNA reactions employing 16 metal salts, photocleavage of pUC19 plasmid is markedly enhanced when compound **7** is irradiated in the presence of either Hg(II), Fe(III), Cd(II), Zn(II), V(V), or Pb(II) (low intensity visible light, pH 7.0, 22 ºC, 8 μM **7** to 50 μM **7**). We also show that DNA photocleavage by **7** can be modulated by modifying buffer type and pH. Evidence of metal complex formation is provided by EDTA experiments and by NMR and electrospray ionization mass spectral data. Sodium azide, sodium benzoate, superoxide dismutase, and catalase indicate the involvement of Type I and Type II photochemical processes in the metal-assisted DNA photocleavage reactions. Thermal melting studies show that compound **7** increases the T_m of calf thymus DNA by 10 $\pm$ 1 °C at pH 7.0 and that the T_m is further increased upon the addition of either Hg(II), Cd(II), Zn(II), or Pb(II). In the case of Fe(III) and V(V), a colorimetric

assay demonstrates that compound **7** sensitizes one electron photoreduction of these metals to Fe(II) and V(IV), likely accelerating the production of Type I reactive oxygen species. Our data collectively indicate that buffer, pH, Hg(II), Fe(III), Cd(II), Zn(II), V(V), Pb(II), and light can be used to "tune" DNA cleavage by compound **7** under physiologically relevant conditions. The 3,6-acridinediamine acridine orange has demonstrated great promise for use as a photosensitizer in photodynamic therapy. In view of the distribution of iron in living cells, compound **7** and other metal-binding acridine-based photonucleases should be expected to demonstrate excellent photodynamic action in vivo.

Introduction

Photodynamic therapy (PDT) has been proven to be an effective treatment option for age-related macular degeneration, actinic keratoses, as well as for neoplastic diseases such as lung, bladder, and esophageal cancers.[1] PDT is also being explored for its potential application in the photoinactivation of viruses (e.g., in blood disinfection) and of multi-drug resistant bacteria.[2] The procedure involves the administration of a photoactive drug (photosensitizer) either systemically or topically followed by irradiation of target tissue with light wavelengths specifically absorbed by the photosensitizer. Damage to surrounding healthy tissue is mitigated by the preferential accumulation and activation of the photosensitizer in diseased tissue. In this regard, PDT represents a very attractive alternative to conventional chemotherapy. Nevertheless, only a few drugs, mostly first and second generation porphyrin derivatives, have been approved for clinical use in PDT.[1a,3] The most extensively researched and utilized is Photofrin.® Yet, large doses of this porphyrin are required to achieve therapeutic efficacy, the identity of the

active component(s) has not been determined, and the drug causes prolonged periods of skin photosensitivity.[4] There is now a great interest in the development of new photoactive drugs that are therapeutically more effective and less toxic.

Following the absorption of a photon of light, PDT sensitizer molecules are excited to a high energy singlet state. Subsequent intersystem crossing yields a long-lived excited triplet state which can undergo energy transfer with ground state molecular oxygen to generate cytotoxic singlet oxygen ($^1O_2$; Type II reaction). Alternatively, the photosensitizer triplet participates in one electron oxidation of a nearby substrate such as DNA (Type I reaction). In the case of molecular oxygen, Type I electron transfer from the triplet to O_2 produces superoxide ($O_2^{\bullet -}$), which reacts further to generate hydrogen peroxide and cytotoxic hydroxyl radicals ($OH^{\bullet}$). Although Type I processes play a relatively minor role in PDT compared to Type II, singlet oxygen, hydroxyl radicals, and one electron oxidation can all cause significant damage to DNA and other biomolecules, eventually effecting necrosis and/or apoptosis of targeted cells.[5] In addition, recent investigations indicate that PDT may function by triggering localized inflammatory cell and immune reaction responses.[6]

A precondition for efficacious photodynamic activity is selective and preferential retention of the photosensitizer in diseased tissue. This prerequisite is met by sensitizing chromophores that bind to nucleic acids with high affinity. The acridines are well known DNA intercalating drugs that possess photo- and cytotoxic properties. The 3,6-acridinediamines acridine orange and proflavin have been shown to photocleave DNA[7] as a function of increasing nucleic acid bound chromophore.[7a,c] Furthermore, acridine orange has demonstrated selective localization in a number of tumor types and has effected

efficient in vivo photodestruction of epithelial tumors in mice, Walker carcinosarcoma 256 stomach tumors in rats, and musculoskeletal sarcomas in mice.[8] In fact, Tatsuta et al. reported comparable PDT-mediated necrosis of rat carcinosarcoma stomach tumors by both acridine orange and hematoporphyrin.[8c] Finally, second and third generation acridines have produced cytotoxic effects in a variety of cancerous tissues and are being developed as HIV antivirals.[9]

In view of the close association of iron and other metals with genomic DNA[10] and the co-accumulation of iron and acridine orange in lysosomes and the cell nucleus,[11] acridine-based photonucleases that sequester metals are potentially of great utility in living cells. Towards this end, we report the syntheses of compounds **7** and **10**, containing a central DNA binding 3,6-acridinediamine chromophore attached to 4 and 2 metal coordinating imidazole rings, respectively. In a survey of 16 metal salts, we demonstrate that the in vitro DNA photocleaving properties of compound **7** are markedly enhanced by specific ions in the approximate order Fe(III) ≈ Hg(II) > Cd(II) > Zn(II) > V(V) ≈ Pb(II). In the presence of these metals, pUC19 plasmid DNA is readily converted into its nicked form upon exposure to low intensity, visible light (pH 7.0, 22 ºC, 8 μM **7** to 50 μM **7**).

Results and Discussion

Synthesis.[12] The tetraimidazole derivative of 3,6-acridinediamine **7** was synthesized according to the procedures depicted in Schemes 2.1 and 2.2. In the first step of the synthetic route, 2-[bis(1*H*-imidazol-4-ylmethyl)amino]ethanol (1) was obtained by reaction of 4-(chloromethyl)-1*H*-imidazole hydrochloride with 2-aminoethanol in refluxing ethanol. Afterwards, a solution of 1 in dry DMF with thionyl chloride was

stirred at room temperature for 24 h to yield *N*-(2-chloroethyl)-*N*-(1*H*-imidazol-4-ylmethyl)-1*H*-imidazole-4-methanamine trihydrochloride (**2**).

Scheme 2.1[a]

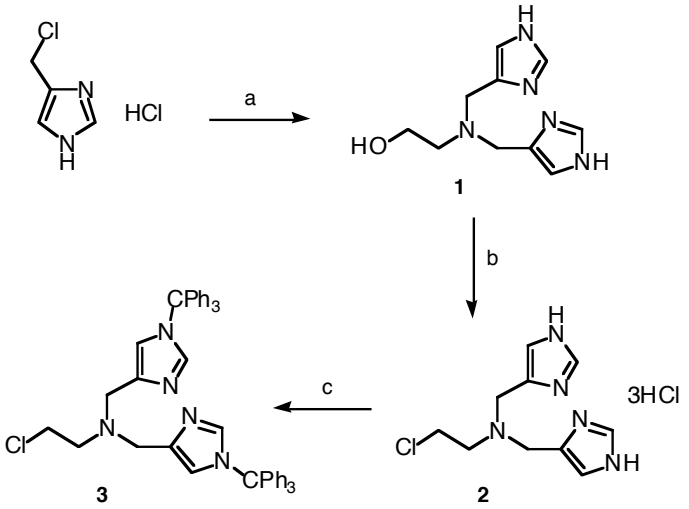

Conditions: [a]$HOCH_2CH_2NH_2$, EtOH, Et_3N, reflux, 70%; [b]$SOCl_2$, DMF, rt, 86%; [c]Ph_3CCl, Et_3N, DMF, rt, 61%.

Next, several attempts were made to accomplish the straightforward synthesis of **7** by reaction of 3,6-acridinediylbiscarbamic acid bis(1,1-dimethylethyl) ester (**4**) with **2** in the presence of different bases, but with no success. The basic conditions required for proflavin dicarbamate alkylation made previous protection of the imidazole nitrogen advisable. Therefore, we proceeded to protect it regioselectively by using the triphenylmethyl group (Scheme 2.1), a robust protecting group that under basic conditions can be easily removed by acid hydrolysis.

Scheme 2.2[a]

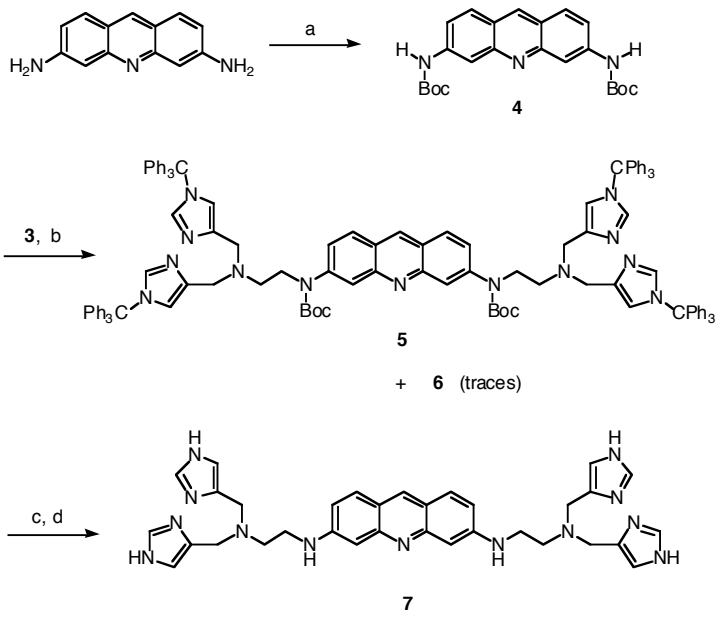

Conditions: [a] ^{t}BuOOCOCOO^{t}Bu, acetone, reflux, 72%; [b] Cs_2CO_3, DMF, rt, 89%; [c] 2 N HCl, 60 °C, [d] 2 N NaOH, 87%.

We then evaluated conditions for the reaction of protected derivative **3** with dicarbamate **4**. Although we initially employed sodium hydride in DMF, which afforded a mixture of the di- (**5**) and monoalkylated (**6**) products (in 54 and 32% yields, respectively), a more convenient approach resulted from substitution of NaH with Cs_2CO_3 (Scheme 2.2). This simplified the work-up process and increased the reaction yield. Finally, all the protecting groups were removed simultaneously by treatment of **5** at 60 °C with 2 N hydrochloric acid. After basification of the reaction mixture, *N*,*N*'-bis[2-[bis(1*H*-imidazol-4-ylmethyl)amino]ethyl]-3,6-acridinediamine (**7**) was precipitated and purified.

The synthesis of bisimidazolic proflavin derivative **10** was carried out following a similar procedure (Scheme 2.3). Compound **9** was prepared through the reaction of (6-

amino-3-acridinyl)carbamic acid 1,1-dimethylethyl ester (**8**) with **3** using cesium carbonate as base and dry DMF as solvent. Deprotection with 2 N hydrochloric acid at 60 ˚C afforded, after basification with aqueous sodium hydroxide, *N*-[2-[bis(1*H*-imidazol-4-ylmethyl)amino]ethyl]-3,6-acridinediamine (**10**).

Scheme 2.3[a]

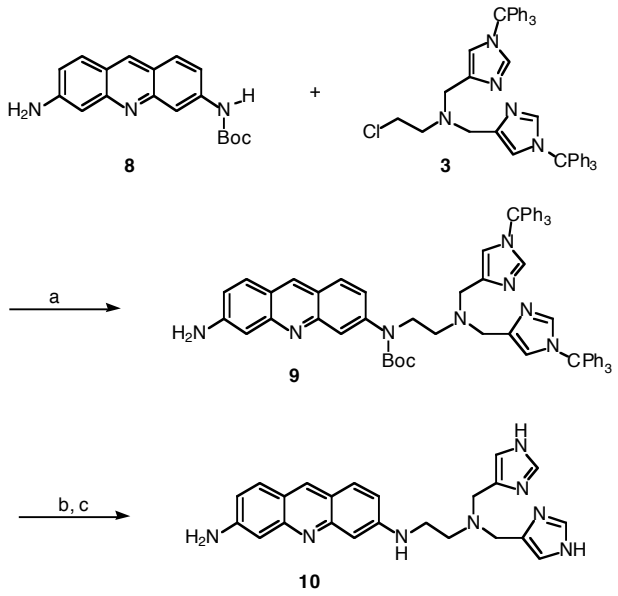

Conditions: [a]Cs_2CO_3, DMF, rt, 85%; [b] 2 N HCl, 60 ˚C, [c]2 N NaOH, 70%.

^{1}H NMR Spectroscopy. In order to obtain evidence of complex formation, NMR spectra were recorded for 5.7 mM of compound **7** as function of increasing $ZnCl_2$ concentration (300 MHz, CD_3OD). At 5.7 mM Zn(II) (1:1 metal-to-ligand ratio), integration of the H-2 and H-5 imidazole signals revealed that only two of the four protons were downfield shifted, suggesting the formation of a stoichiometric 1:1 species. (Chemical shifts were 7.58 and 6.94 ppm with no metal ion and 8.00 and 7.22 ppm with metal, respectively.) At a 2:1 metal-to-ligand ratio, the downfield shifts were observed for all the H-2 and H-5 proton signals, indicating a 2:1 metal-to-ligand complex. No

additional changes in the NMR spectra were seen at zinc(II) concentrations higher than 11.4 mM.

Mass Spectrometry. Electrospray ionization (ESI) mass spectrometry is routinely used for the detection of labile metal complexes in situ. To allow for varied stoichiometries, we prepared electrospray samples by mixing different volumes of 0.4 mM methanolic stock solutions of **7** and a metal salt (either $CdCl_2$, $FeCl_3 \bullet 6H_2O$, $HgCl_2$, Na_3VO_4, $PbCl_2$, or $ZnCl_2$) in pure HPLC grade methanol. The samples were then allowed to equilibrate at room temperature for 45 min, after which mass spectra were recorded. In the case of $ZnCl_2$ and $CdCl_2$, the major isotopic peaks were found to correspond to: 1:1 metal-to-ligand complex and unreacted **7** at a metal-to-ligand ratios of 1:2; 1:1 metal-to-ligand complex, 2:1 complex, and unreacted **7** at metal-to-ligand ratios of 1:1; and 2:1 metallic complex at metal-to-ligand ratios of 2:1. Alternatively, the major isotopic peaks of $HgCl_2$ and $PbCl_2$ indicated the formation of 1:1 metal-to-ligand complex and unreacted **7** at metal-to-ligand ratios of 1:2, and a gradual conversion of unreacted **7** to 1:1 complex as the ratios of metal-to-ligand were increased to 1:1 and then to 2:1. In the case of $FeCl_3 \bullet 6H_2O$, there was no evidence of complex formation at metal-to-ligand ratios of 1:2 and 1:1. However, at the 1:2 ratio, minor isotopic peaks corresponding to a 1:1 complex were observed. Although attempts to study vanadium(V) complex formation were unsuccessful in neat methanol, low levels of a 1:1 metal-to-ligand complex were seen at all metal-to-ligand ratios when Na_3VO_4 and compound **7** were dissolved in a 1:1 ddH_2O:methanol solution. Taken together, the ESI mass spectral data indicate that the six metals undergo complexation in the order Cd(II) ≈ Zn(II) > Hg(II) ≈ Pb(II) >> Fe(III) > V(V).

Photocleavage Experiments. To determine the effects of various metals on DNA photocleavage, compounds **7** and **10** were individually treated in the presence of $CaCl_2•2H_2O$, $CdCl_2$, $(CH_3)_2SnCl_2$, $CoCl_2•H_2O$, $CrCl_3•6H_2O$, $CuCl_2•2H_2O$, $FeCl_3•6H_2O$, $HgCl_2$, $MgCl_2•6H_2O$, $MnCl_2•4H_2O$, Na_3VO_4, $NiCl_2•6H_2O$, $PbCl_2$, $Sc(CF_3SO_3)_3$, $ZnCl_2$, and $ZrCl_4$. Photolysis reactions consisted of 20 mM sodium phosphate buffer pH 7.0 and 38 μM bp pUC19 plasmid DNA equilibrated in the absence and presence of: 25 μM metal salt, 50 μM **7** or **10**, and 25 μM metal salt with 50 μM **7** or **10**.[13] (In reactions containing $PbCl_2$ and Na_3VO_4, 20 mM sodium cacodylate buffer pH 7.0 was used to substitute for sodium phosphate.) The samples were irradiated under aerobic conditions with a low intensity, broad-spectrum 4 W T4T5/D fluorescent lamp for 50 min at 22 °C. After this, photocleavage products were resolved on a 1.0% non-denaturing agarose gel stained with ethidium bromide. ImageQuant Mac v. 1.2 software was then used to quantitate the % conversion of supercoiled plasmid DNA to its nicked form (Figure 2.1). This analysis revealed that DNA photocleavage by compound **7** was selectively enhanced in the presence of Hg(II), Fe(III), Cd(II), Zn(II), V(V), and Pb(II). In the case of compound **10**, Hg(II), Fe(III), Cd(II), and Zn(II) also increased photocleavage, but at lower levels in comparison to **7**. (The fact that **7** possesses two additional imidazole rings may confer upon this compound superior metal chelating ability.) As exemplified by the representative gel shown in Figure 2.2 (50 μM **7**, 25 μM $ZnCl_2$), minimal levels of photocleavage were always observed for DNA reactions irradiated in: the absence of compound and metal (Lane 1), the absence of compound (Lane 2), the absence of metal (Lane 3), and in a complete series of parallel reactions run in the dark (50 min, 22 °C; Lanes 5-8). We therefore concluded that Hg(II), Fe(III), Cd(II), Zn(II), V(V), and Pb(II)

ions could be used in combination with light to "tune" levels of DNA cleavage by compound **7**.

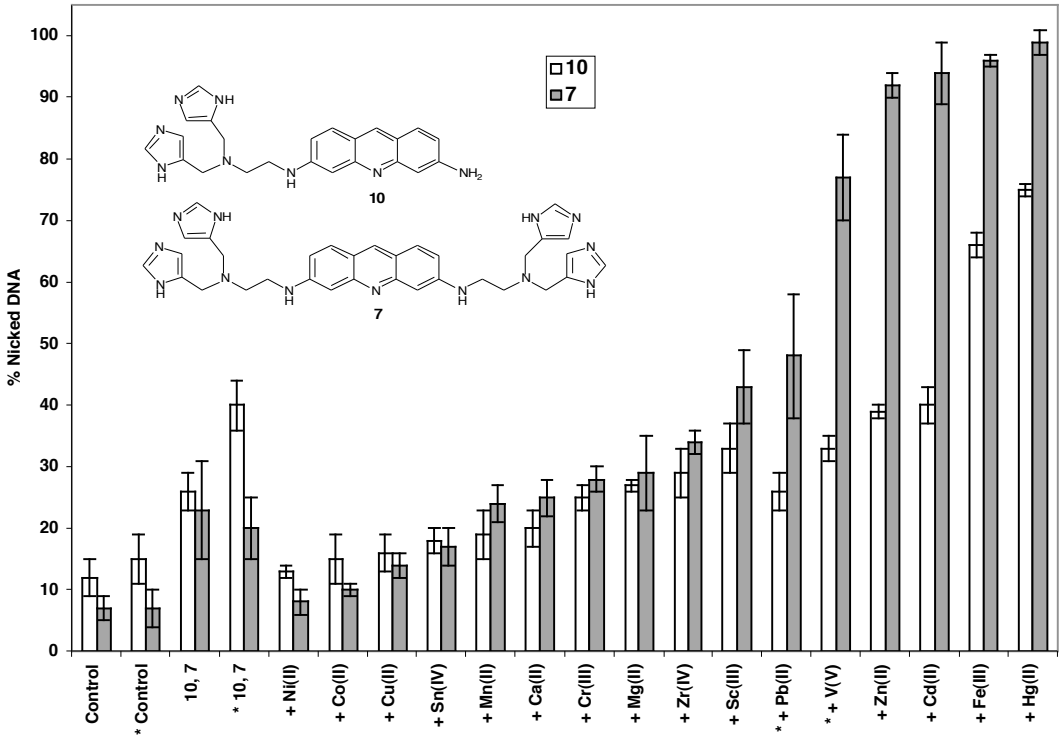

Figure 2.1. A histogram depicting metal-assisted photocleavage of pUC19 plasmid DNA in the presence of 50 μM **10** and 50 μM **7** without and with 25 μM metal salt as indicated (38 μM bp DNA, 20 mM sodium phosphate buffer pH 7.0). All reactions were irradiated with a broad-spectrum fluorescent lamp for 50 min at 22 °C. Percent cleavage (% nicked DNA) was averaged over three trials with error bars representing standard deviation. The asterisk identifies reactions in which 20 mM sodium cacodylate buffer pH 7.0 was used to substitute for sodium phosphate buffer. In the controls, DNA was irradiated in 20 mM buffer in the absence of **10**, **7**, and metal.

The central chromophore of compounds **7** and **10** is a DNA binding 3,6-acridinediamine closely related in structure to acridine orange and proflavin (Figure 2.S1 in Supporting Information). It was therefore of interest to conduct a comparative analysis of DNA photocleavage. To accomplish this, individual reactions containing 50 μM acridine orange and proflavin without and with 25 μM $ZnCl_2$, 25 μM $FeCl_3$, and 200 μM

imidazole were irradiated for 50 min with the broad- spectrum fluorescent lamp (38 μM bp pUC19 plasmid DNA, 20 mM sodium phosphate buffer pH 7.0, 22 °C). Yields were calculated and compared to data from the previous experiment (Table 2.1).

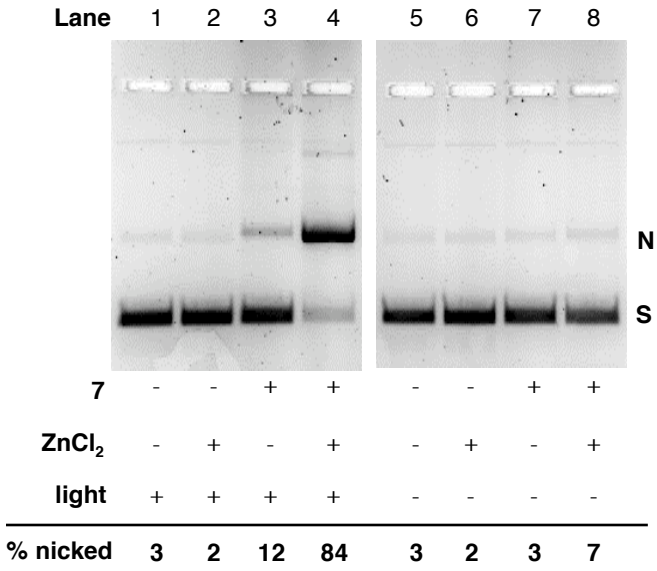

Figure 2.2. Photograph of a 1.0% non-denaturing agarose gel showing photocleavage of pUC19 plasmid DNA (50 μM **7** and 25 μM $ZnCl_2$ as indicated; 38 μM bp DNA; 20 mM sodium phosphate buffer pH 7.0; 22 °C). Lanes 1-4: reactions were irradiated with a broad-spectrum fluorescent lamp for 50 min. Lanes 5-8: parallel reactions maintained in the dark for 50 min. Abbreviations: **N** = nicked; **S** = supercoiled.

It is evident that acridine orange, proflavin, **7** and **10** all photocleave DNA at low levels in the absence of metal. However, upon the addition of either 25 μM $ZnCl_2$ or 25 μM $FeCl_3$, significant enhancements were observed for **7** and **10**, but not in the case of acridine orange and proflavin. In an attempt to "mimic" the structure of compound **7**, 4 mol equiv of imidazole were added along with each metal salt to the acridine orange and proflavin reactions, but as shown in Table 2.1, levels of photocleavage were unaffected. It is apparent that metal chelating imidazole must be covalently tethered to the DNA

binding 3,6-acridinediamine chromophore in order for Zn(II) and Fe(III) to enhance DNA photocleavage.

Table 2.1. Zn(II) and Fe(III)-Assisted Photocleavage of pUC19 DNA by Acridine Orange, Proflavin, **7** and **10**[a]

	% nicked DNA:			
reactants	**AO**	**P**	**7**	**10**
DNA	14	14	7	12
DNA + 50 μM intercalator	28	15	23	26
DNA + 50 μM intercalator + 25 μM $ZnCl_2$	30	13	92	39
DNA + 50 μM intercalator + 25 μM $ZnCl_2$, 200 μM imidazole	35	11	NA	N
DNA + 50 μM intercalator + 25 μM $FeCl_3$	29	15	96	66
DNA + 50 μM intercalator + 25 μM $FeCl_3$, 200 μM imidazole	27	17	NA	N

[a] Photocleavage reactions consisted of 38 μM bp pUC19 plasmid DNA in sodium phosphate buffer pH 7.0 equilibrated without and with $ZnCl_2$, $FeCl_3$, imidazole, and the intercalators acridine orange, proflavin, **7**, and **10**. All reactions were irradiated with a broad-spectrum fluorescent lamp for 50 min at 22 °C. Abbreviations: **AO** = acridine orange; **NA** = not applicable; **P** = proflavin.

pH Profile. The Hg(II), Fe(III), Cd(II), Zn(II), V(V), and Pb(II)-assisted photocleavage reactions were then studied by means of an extensive pH profile in which 50 μM **7**, 25 μM metal salt and 38 μM bp pUC19 plasmid DNA were irradiated in a variety of buffer systems: sodium cacodylate pH 5.0, 6.0, and 7.0; sodium phosphate pH 5.0, 6.0, 7.0, and 8.0; and sodium borate pH 8.0, and 9.0 (Table 2.2). The goal of this experiment was to access the combined effects of buffer and pH in order to gain insight into possible mechanisms underlying metal-assisted DNA photocleavage.

At pH 5.0, compound **7** was shown to efficiently photocleave DNA in the absence of metal. However, as pH was raised, the general effect was to produce a decrease in photocleavage, irrespective of the buffer system employed (Table 2.2, first row). This result can be rationalized as follows. Compound **7** would be expected to bear a relatively high net positive charge at low pH, and as a result would bind to negatively charged DNA with high affinity. However, at higher pH values, the positive charge on **7** would be reduced and as a result DNA binding affinity and photocleavage yields would decrease. Notwithstanding, it is evident that pH can be used as an additional chemical tool to "tune" the reactivity of compound **7**.

When **7** was reacted in the presence of Hg(II), Fe(III), Cd(II), Zn(II), V(V), and Pb(II), the greatest DNA photocleavage enhancement was observed at a pH value greater than 5.0 for each of the six metals (Table 2.2). It is conceivable that one or more of these metals might be compensating for the loss of positive charge experienced by compound **7** as pH is raised. (The effect of restoring electrostatic interactions between **7** and DNA would be to increase binding affinity and photocleavage yields.) The maximum cleavage enhancement was 85%, produced by Cd(II) in the presence of compound **7** and sodium phosphate buffer pH 8.0. This was followed by Zn(II), Cd(II), and Hg(II) ions, which increased DNA cleavage by 79% in sodium phosphate pH 6.0. At the near physiological pH value of 7.0, the best results were achieved by Hg(II) and Fe(III) in sodium phosphate buffer, which produced enhancements of 76% and 73%, respectively. This is significant for two reasons. The $H_2PO_4^-$ and HPO_4^{2-} conjugate pair constitutes one of the two most important buffering systems in human physiology. Second, iron, which is present in relatively high quantities in genomic DNA,[10] efficiently enhances DNA photocleavage in

the phosphate buffer system. With respect to V(V) and Pb(II), the best photocleavage results were generally obtained by using sodium cacodylate buffer.

Table 2.2. % DNA Photocleavage by Compound **7** as a Function of Buffer and pH[a]

	% nicked + %linear DNA:								
reactants	pH 5.0 phosphate	pH 5.0 cacodylate	pH 6.0 phosphate	pH 6.0 cacodylate	pH 7.0 phosphate	pH 7.0 cacodylate	pH 8.0 phosphate	pH 8.0 borate	pH 9.0 borate
7	51 ± 8	64 ± 7	21 ± 7	28 ± 7	23 ± 8	20 ± 5	13 ± 5	19 ± 4	14 ± 4
7 + Hg(II)	97 ± 2(46)	98 ± 1 (34)	100 ± 0 (79)	90 ± 1 (62)	99 ± 2 (76)	83 ± 3 (63)	81 ± 4 (68)	90 ± 3 (71)	80 ± 7 (66)
7 + Fe(III)	75 ± 3 (24)	96 ± 2 (32)	67 ± 6 (46)	95 ± 7 (67)	96 ± 1 (73)	83 ± 4 (63)	80 ± 4 (67)	64 ± 5 (45)	59 ± 11 (45)
7 + Cd(II)	96 ± 0 (45)	99 ± 1 (35)	92 ± 8 (79)	84 ± 5 (56)	94 ± 5 (71)	85 ± 4 (65)	98 ±3 (85)	86 ± 6 (67)	74 ± 6 (60)
7 + Zn(II)	89 ± 2 (38)	92 ± 3 (28)	95 ± 5 (79)	83 ± 4 (55)	92 ± 2 (69)	66 ± 6 (46)	87 ± 4 (74)	71 ± 6 (52)	57 ± 6 (43)
7 + V(V)	93 ± 1 (42)	91 ± 4 (27)	83 ± 2 (62)	97 ± 3 (69)	56 ± 10 (33)	77 ± 7 (57)	22 ± 16 (9)	29 ± 11 (10)	9 ± 2 (-5)
7 + Pb(II)	22 ± 5 (-29)	87 ± 5 (23)	33 ± 8 (12)	95 ± 9 (67)	28 ± 2 (5)	48 ± 10 (28)	20 ± 9 (7)	61 ± 5 (42)	54 ± 6 (40)

[a] % DNA photocleavage = % nicked + % linear DNA. Listed in parentheses are % DNA photocleavage enhancement values expressed as the difference: % DNA photocleavage by **7** with metal minus % photocleavage by **7** without metal. Individual reactions consisted of 38 μM bp pUC19 plasmid DNA equilibrated with 50 μM **7**, 20 mM sodium phosphate, sodium cacodylate, or sodium borate buffers, without and with 25 μM metal salt (pH 5.0-9.0). All reactions were irradiated with a broad-spectrum fluorescent lamp for 50 min at 22 °C. The data are averaged over three trials, and errors are reported as standard deviation.

Intercalators and groove binding compounds interact with double-helical DNA predominantly through π-π stacking and a combination of van der Waals and electrostatic interactions, respectively. As a consequence, double-helical DNA is stabilized, increasing the melting temperature (T_m) of the duplex as a function of the binding affinity of the intercalator or groove binder. In an attempt to explain the trends observed in the above pH profile, thermal melting curves were used to determine T_m values of 12.5 μM bp calf thymus DNA in sodium phosphate buffer pH 5.0 and pH 7.0, in the absence and presence of 8 μM **7** (Figure 2.3). While compound **7** raised the T_m of calf thymus DNA from 65 °C

to 94 °C at pH 5.0, the effect was much less pronounced at pH 7.0. In this case, the T_m was raised from 75 °C to 84 °C. In the absence of compound **7**, 4 μM $ZnCl_2$ had no effect on the melting temperature of the calf thymus DNA (T_m = 75 °C at pH 7.0). However, the addition of 4 μM $ZnCl_2$ to 8 μM **7** raised the T_m by 6 °C at pH 7.0, from 84 °C to 90 °C (Figure 2.3). Taken together, these data suggest that Zn(II) increases binding affinity and DNA photocleavage efficiency by restoring positive charge lost by **7** upon transition from pH 5.0 to pH 7.0.

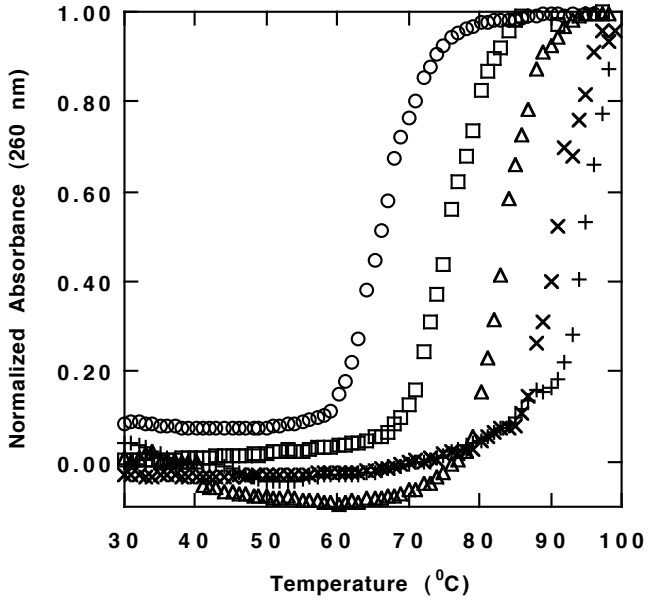

Figure 2.3. Effects of 8 μM compound **7**, 4 μM $ZnCl_2$, and 20 mM sodium phosphate buffers pH 5.0 and 7.0 on the thermal melting curve of 12.5 μM bp calf thymus DNA: ○, pH 5.0 buffer, T_m = 65 °C; □, pH 7.0 buffer, T_m = 75 °C; Δ, compound **7** in pH 7.0 buffer, T_m = 84 °C; x: $ZnCl_2$ and compound **7** in pH 7.0 buffer, T_m = 90 °C; +, compound **7** in pH 5.0 buffer, T_m = 94 °C.

Inhibition of DNA Photocleavage. Hydroxyl radical, hydrogen peroxide, singlet oxygen, and superoxide scavengers all reduce the formation of DNA strand breaks produced by the exposure of proflavin to visible light.[7b,c] A series of scavengers including

the metal chelating agent ethylenediaminetetraacetic acid (EDTA) was therefore utilized to further investigate the mechanism(s) underlying metal-assisted DNA photocleavage by compound **7**. Individual photocleavage reactions consisted of 38 μM bp plasmid DNA in pH 7.0 buffer, 50 μM **7**, and 25 μM Hg(II), Fe(III), Cd(II), Zn(II), V(V), or Pb(II) in the presence of scavenger. Sodium azide was used to trap the Type II reactive oxygen species (ROS) singlet oxygen ($^1O_2$), while superoxide dismutase (SOD), catalase, and sodium benzoate were employed for the Type I ROS superoxide ($O_2^{\bullet -}$), hydrogen peroxide (H_2O_2), and hydroxyl radicals ($OH^{\bullet}$), respectively. The data in Table 2.3 show that EDTA consistently produced strong DNA photocleavage inhibition (≥ 78% in all cases). This result indicates that complexation between compound **7** and each of the six metals is likely to be a prerequisite for efficient cleavage. In the Hg(II)/sodium benzoate, Fe(III)/sodium azide, Cd/sodium benzoate, Cd/SOD, and Pb(II)/SOD reactions, essentially no protection was observed. Otherwise, levels of photocleavage inhibition ranged from moderately low to high for all of the metal/scavenger combinations. (In the case of sodium benzoate, weak inhibitory effects cannot rule out the existence of non-diffusible hydroxyl radicals closely associated with the metal center of the complex. Second, because SOD produces H_2O_2 which itself can contribute to cleavage, weak inhibition by this enzyme cannot rule out superoxide.) In conclusion, the scavenger experiments collectively indicate that, with the exception of iron, Type I and Type II photochemical processes are involved in compound **7** metal-assisted DNA cleavage. The Fe(III) reaction appears to proceed almost exclusively through a Type I pathway.

Table 2.3. % Inhibition of Metal-Assisted DNA Photocleavage[a]

metal	azide (100 mM)	benzoate (100 mM)	SOD (50 U)	catalase (50 U)	EDTA (100 mM)
Hg(II)	35 ± 6	2 ± 2	16 ± 6	24 ± 12	78 ± 7
Fe(III)	9 ± 6	20 ± 3	23 ± 12	66 ± 4	79 ± 4
Cd(II)	18 ± 3	7 ± 9	0 ± 1	26 ± 7	79 ± 8
Zn(II)	38 ± 13	28 ± 10	18 ± 7	35 ± 3	79 ± 6
V(V)	38 ± 10	38 ± 10	18 ± 9	41 ± 11	78 ± 7
Pb(II)	28 ± 8	32 ± 19	5 ± 4	53 ± 7	79 ± 2

[a] Individual reactions consisting of 38 μM bp pUC19 plasmid DNA, 50 μM **7**, 25 μM metal salt, and one of the above reagents were irradiated with a broad-spectrum fluorescent lamp for 50 min at 22 °C. The Zn(II), Cd(II), Hg(II) and Fe(III) reactions were in 20 mM sodium phosphate buffer pH 7.0 while the V(V) and Pb(II) reactions were in sodium cacodylate buffer pH 7.0. Percent inhibition was averaged over at least three trials with error reported as standard deviation. Working reagent concentrations are in parentheses.

Photocleavage at Lower Concentrations. Metal-assisted DNA photocleavage reactions were conducted using 8 μM **7**, 4 μM metal, and 12.5 μM bp pUC19 plasmid DNA. Because distortions in UV-visible and emission spectra are typically associated with highly concentrated chromophores, it was necessary for us to examine photocleavage patterns at these lower concentrations of **7** and metal to establish the feasibility of conducting additional spectroscopic studies. Reaction samples were irradiated with the broad-spectrum fluorescent lamp for 50 min at 22 °C. After this, the % conversion of supercoiled to nicked DNA produced by **7** in the presence of the 16 metal salts was quantitated. As shown in Figure 2.4, a similar trend was observed in the DNA photocleavage cleavage studies conducted at 50 μM **7** and 25 μM metal (Figure 2.1). The metal ions Hg(II), Fe(III), Cd(II), Zn(II), V(V), and Pb(II) all enhanced photocleavage at the lower reagent concentrations (Figure 2.4).

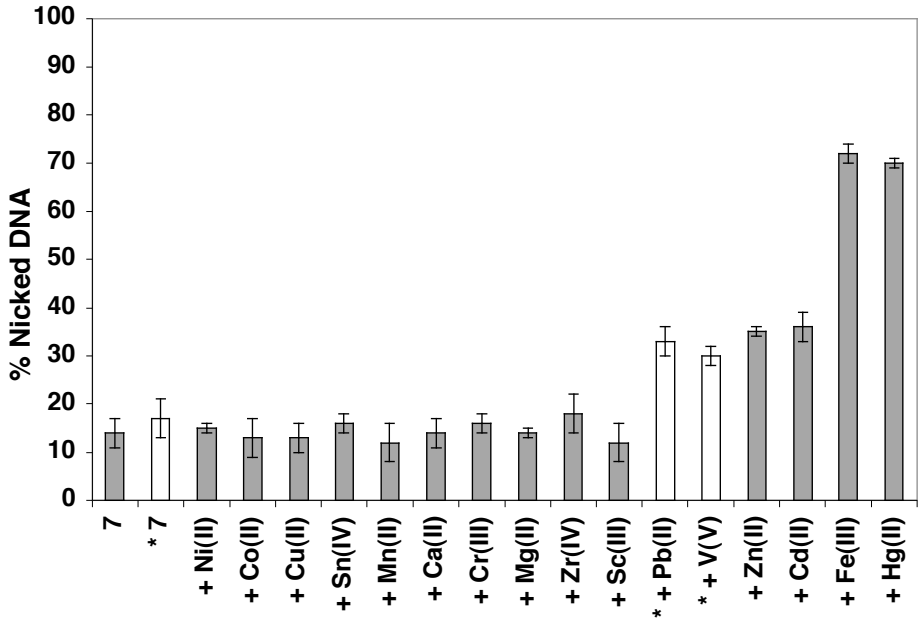

Figure 2.4. A histogram depicting metal-assisted photocleavage of pUC19 plasmid DNA in the presence of 8 μM **7** without and with 4 μM metal salt as indicated (12.5 μM bp DNA, 20 mM sodium phosphate buffer pH 7.0). All reactions were irradiated with a broad-spectrum fluorescent lamp for 50 min at 22 °C. Percent cleavage was averaged over three trials with error bars representing standard deviation. The asterisk identifies reactions in which 20 mM sodium cacodylate buffer pH 7.0 was used to substitute for sodium phosphate buffer.

Absorbance and Emission Studies. In an attempt to account for the relative influence of the 16 metal salts on the efficiency of DNA photocleavage, we recorded absorbance and fluorescence emission spectra of compound **7** equilibrated in 20 mM sodium phosphate or 20 mM sodium cacodylate pH 7.0 buffer, without and with metal salt (Table 2.4). We then calculated the % change in emission quantum yield resulting from the addition of each of the 16 metals to **7** (%Δ Φ_{em} + metal) as well as the % change in absorbance intensity (%Δ Abs + DNA) and emission quantum yield (%Δ Φ_{em} + DNA)

and the change in the wavelength of maximum absorbance ($\Delta \lambda_{max}$ + DNA) resulting from the addition of calf thymus DNA (Table 2.4).

Table 2.4. Absorbance, Emission and Thermal Melting Data[a]

	absorbance studies				emission studies			T_m studies	
reactants	abs	%Δ abs + DNA	λ_{max}(nm)	Δ λ_{max} + DNA	Φ_{em}	%Δ Φ_m + metal	%Δ Φ_m + DNA	T_m(ºC)	ΔT_m(ºC)
7	0.16	-6	459	8	0.090	NA	-26	84	NA
7 + Hg(II)	0.15	-10	451	16	0.025	-72	16	86	2
7 + Fe(III)	0.20	-21	459	8	0.068	-24	-28	84	0
7 + Cd(II)	0.18	-17	448	18	0.036	-60	-42	90	6
7 + Zn(II)	0.17	-17	458	9	0.062	-31	-42	90	6
7 + Sc(III)	0.21	-23	459	8	0.083	-8	-30	84	0
7 + Zr(IV)	0.21	-24	459	8	0.083	-8	-31	83	-1
7 + Mg(II)	0.21	-21	459	8	0.088	-2	-24	84	0
7 + Cr(III)	0.21	-18	458	9	0.085	-6	-22	83	-1
7 + Ca(II)	0.22	-29	459	8	0.087	-3	-18	84	0
7 + Mn(II)	0.20	-18	459	8	0.088	-2	-21	84	0
7 + Sn(IV)	0.22	-19	459	8	0.101	+12	-26	84	0
7 + Cu(II)	0.18	-19	452	7	0.019	-79	-74	87	3
7 + Co(II)	0.17	-15	448	11	0.023	-74	-74	88	4
7 + Ni(II)	0.12	3	448	16	0.011	-88	-46	92	8
*__7__	0.16	-10	452	17	0.083	NA	-17	85	NA
*__7__ + V(V)	0.15	-27	451	20	0.080	-4	-12	86	1
*__7__ + Pb(II)	0.17	-24	452	18	0.074	-11	-40	87	2

[a]Absorbance and T_m measurements were conducted using solutions consisting of 8 μM **7** in 20 mM sodium phosphate buffer pH 7.0 equilibrated without and with 12.5 μM bp calf thymus DNA and 4 μM metal salt (22 °C). T_m data were averaged over two trials producing an average standard deviation of ± 1 °C. Φ_{em} measurements were conducted at 25 °C with **7** in 20 mM sodium phosphate buffer pH 7.0 equilibrated without and with calf thymus DNA and metal salt. Absorbance in all Φ_{em}experiments was ~ 0.04 at the 430 nm excitation wavelength. Φ_{em} values were averaged over three trials producing an average standard deviation of ± 0.002. Abbreviations: **Abs** = absorbance intensity at λ_{max}; **NA** = not applicable; %Δ + DNA = percent change upon addition of DNA = [((**7** + metal + DNA) – (**7** + metal))/(**7** + metal)] x 100; Δ = change upon addition of DNA = (**7** + metal + DNA) – (**7** + metal); %Δ + metal = percent change upon addition of metal = [((**7** + metal) – (**7**))/(**7**)] x 100; Δ T_m = $T_{m(7 + Metal)}$ - $T_{m(7)}$. The asterisk identifies solutions in which 20 mM sodium cacodylate buffer pH 7.0 was used to substitute for 20 mM sodium phosphate buffer pH 7.0.

Bathochromic wavelength shifts and hypochromic absorption are characteristic of the electronic spectra of many DNA-bound groove binders and most if not all DNA-bound intercalators. The "%ΔAbs + DNA" and "Δ λ_{max} + DNA" data in Table 2.4 show that compound **7** demonstrates appreciable bathochromicity and hypochromicity in the presence of DNA. While the data cannot be used to account for different photocleavage levels, it is very likely that compound **7** continues to bind to DNA in the presence of each of the 16 metals: red-shifts (positive "Δ λ_{max} + DNA" values) are consistently produced upon the addition of DNA, and with the exception of Ni(II), depressed absorption (negative "%Δ Abs + DNA") is observed. In addition, none of the metal-induced changes in the electronic spectra of **7** appear to be of sufficient magnitude to markedly attenuate or enhance DNA photocleavage levels.

Upon binding to DNA, acridine orange exhibits an increase in fluorescence emission. In the case of proflavin, pronounced sequence dependent effects are observed. Fluorescence emission is increased in the presence of A•T rich DNA and but is almost completely quenched by G•C rich sequences.[14] The "%Δ Φ_{em} + DNA" values in Table 2.4 indicate that fluorescence is reduced upon the addition of DNA to (i) compound **7** and (ii) compound **7** in the presence of 15 out of 16 metals.

Table 2.4 also summarizes the effects of metal ions on compound **7** fluorescence emission in the absence of DNA. The 14 "%Δ Φ_{em} + metal" values recorded in sodium phosphate buffer show that the photoinactive metals Ni(II), Cu(II), Co(II) produce the most significant reductions in fluorescence intensity, followed by the three photoactive metals Hg(II), Cd(II), and Zn(II). The percent changes in emission quantum yield produced by the photoactive metal Fe(III) and the seven photoinactive metals Sn(IV),

Sc(III), Zr(IV), Cr(III), Ca(II), Mg(II) and Mn(II) are all lower. Overall, the 14 metals follow the order: Ni(II) > Cu(II) > Co(II) > Hg(II) > Cd(II) > Zn(II) > Fe(III) > Sn(IV) > Sc(III) = Zr(IV) > Cr(III) > Ca(II) > Mg(II) = Mn(II). The two "$\%\Delta\ \Phi_{em}$ + metal" values recorded in sodium cacodylate buffer show that Pb(II) is a more efficient quencher than V(V).

According to Hard-Soft Acid-Base (HASB) Theory, the seven metals with the largest "$\%\Delta\ \Phi_{em}$ + metal" values in their respective buffer systems are classified as either borderline or soft acids (Ni(II), Cu(II), Co(II), Hg(II), Cd(II), Zn(II), and Pb(II)), while the nine metals that have relatively minor effects on fluorescence emission (Fe(III), Sn(IV), Sc(III), Zr(IV), Cr(III), Ca(II), Mg(II), Mn(II) and V(V)), are classified as hard acids. Because imidazole is a borderline base, it is conceivable that compound **7** might display a preference for forming stable complexes with the seven borderline and soft metals. Therefore, it is possible that there is a relationship between the degree of fluorescence quenching and the degree of complex formation between compound **7** and each of the 16 metals.

Thermal Denaturation Studies. In our next set of experiments, we determined the T_m values of 12.5 μM bp calf thymus DNA at pH 7.0 in the absence and presence of 8 μM **7** and 4 μM of the 16 metal salts. The change in DNA melting temperature effected by the addition of metal to **7** was defined as $\Delta T_m = T_{m\ (7\ +\ Metal)} - T_{m\ (7)}$ (Table 2.4). Under our experimental conditions, the T_m obtained for calf thymus DNA was 74 $\pm$ 1 °C. The addition of each of the 16 metal salts to the DNA made little difference, since the resulting T_m values ranged from 73 – 75 °C. Therefore, none of the metals were able to effect the stability of double-helical calf thymus DNA on their own. Addition of **7** to the

calf thymus DNA raised the T_m to 84 °C in 20 mM sodium phosphate buffer pH 7.0. When compound **7** and metals were present in combination, additional statistically significant increases in T_m were observed for seven of the 16 metals: Ni(II), ΔT_m = 8 °C; Cd(II), ΔT_m = 6 °C; Zn(II), ΔT_m = 6 °C; Co(II), ΔT_m = 4 °C; Cu(II), ΔT_m = 3 °C; Hg(II), ΔT_m = 2 °C; and Pb(II), ΔT_m = 2 °C. (T_m values determined over several trials showed the error in measurement to be $\pm$ 1 °C.)

Taken together, the thermal denaturation and fluorescence quenching data suggest possible correlations between metal complex stability and DNA binding affinity. The seven borderline and soft acids Ni(II), Cd(II), Zn(II), Co(II), Cu(II), Hg(II), and Pb(II) produce: (i) appreciable positive ΔT_m values indicative of the formation of stable complexes that increase the binding affinity of **7** to DNA, and (ii) moderate to high "%Δ Φ_{em} + metal" values in their respective buffer systems. Alternatively, the nine hard metals Sn(IV), Mn(II), Ca(II), Cr(III), Mg(II), Zr(IV), Sc(III), V(V), and Fe(III) have no appreciable effects on T_m and have lower "%Δ Φ_{em} + metal" values. Again, because imidazole is a borderline base, it is reasonable that compound **7** should display a preference for forming complexes with the seven borderline and soft metals rather than with the nine hard metals.

The appreciable ΔT_m values associated with Cd(II), Zn(II), Hg(II), and Pb(II) are consistent with the observation that levels of DNA photocleavage are increased when each of these four metals is added to compound **7** (Figure 2.1). In contrast, Ni(II), Co(II), and Cu(II) have appreciable ΔT_m values but at 25 μM concentrations yield the lowest levels of DNA photocleavage out of the 16 metals tested (Ni(II) < Cu(II) < Co(II); Figure 2.1). In addition, Ni(II), Co(II), and Cu(II) produce the three largest "%Δ Φ_{em} + metal"

values in Table 2.4 (Ni(II) > Cu(II) > Co(II)). In the case of many photosensitizers[5c] including the 3,6-acridinediamine proflavin,[7b,c, 15] dye sensitized generation of singlet oxygen ($^1O_2$; Type II reaction) and superoxide ($O_2^{\bullet -}$; Type I reaction) are thought to arise from the triplet state. With respect to compound **7**, fluorescence quenching by any one of the following three mechanisms could reduce the triplet state population, either directly or indirectly: (i) heavy atom or paramagnetically induced spin-orbit coupling that increases the rate of $S_1 \rightarrow T_1$ and $T_1 \rightarrow S_0$ processes, (ii) electron transfer between the excited singlet state fluorophore and the metal ion, (iii) energy transfer from the excited singlet state to the metal ion.[16] The efficiency of Type I and Type II triplet state photochemical processes that contribute to DNA photocleavage would then be decreased. This hypothesis is consistent with the observation that compound **7** produces appreciably T_m but extremely low levels of DNA photocleavage in the presence of Ni(II), Co(II), and Cu(II) (Figures 2.1 and 2.4). In a study of acridine orange-DNA-metal ternary complexes, Bregadze and co-workers observed significant emission quenching by Ni(II), Co(II), and Cu(II) relative to Mn(II) and Zn(II).[10] By calculating overlapping integrals and energy transfer radii, the investigators concluded that Ni(II), Co(II), and Cu(II) had quenched the excited singlet state of acridine orange by Förster-energy transfer.[10, 17] While the photoactive metals Cd(II), Zn(II), Hg(II), and Pb(II) also produce relatively high levels of fluorescence quenching, there is no reason to assume that any of the 16 metal ions evaluated in this study quench the singlet excited state of compound **7** by the same or even a single mechanism.

The two remaining metals in the series of 16 constitute a special case. As expected, the ΔT_m and "$\%\Delta\ \Phi_{em}$ + metal" values of the hard acids V(V) and Fe(III) are

negligible. However, DNA photocleavage by compound **7** is increased in both cases. For the six photoactive metals Hg(II), Fe(III), Cd(II), Zn(II), V(V), and Pb(II), complex formation is indicated by scavenger experiments in which EDTA was shown to inhibit metal-assisted DNA photocleavage by **7** (Table 2.3). Additional evidence was provided by NMR and/or ESI mass spectra of **7** recorded in the presence of Hg(II), Fe(III), Cd(II), Zn(II), V(V), and Pb(II). While extensive 2:1 metal-to-ligand complex formation was observed only in the case of Cd(II) and Zn(II), 1:1 metallic complexes were formed by all six photoactive metals the following order: Cd(II) ≈ Zn(II) > Hg(II) ≈ Pb(II) >> Fe(III) > V(V). Thus, the extent of metal complex formation was found to be in good agreement with the magnitude of the T_m increase: Cd(II) ≈ Zn(II) > Hg(II) ≈ Pb(II) >> Fe(III) ≈ V(V). Taken together, these data indicate that V(V) and Fe(III) are likely to form weak complexes with compound **7**. There is at least one reasonable explanation to account for the observation that both metals significantly enhance DNA photocleavage. It is well known that electron transfer from the photochemically excited triplet states of acridine orange,[18a] proflavin,[18b] and other 3,6-acridinediamines[18b] effect photoreduction of Fe(III) to Fe(II). Although acridine-sensitized photoreduction of V(V) to V(IV) has not been documented, irradiation of oxoperoxovanadium(V) in acidic media has been shown to produce V(IV) with evolution of molecular oxygen.[19] A potential source of photocleavage enhancement might therefore involve compound **7**-sensitized one electron photoreduction of Fe(III) and V(V). The reduced metals would then be expected to produce highly reactive, DNA damaging hydroxyl radicals by the Fenton reaction.[20]

Spectrophotometric Determination of Fe(II) and V(IV). In order to test for photoreduction of Fe(III), we employed 1,10-phenanthroline, which forms a stable

complex with Fe(II) (λ_{max} = 510 nm).[21] Because vanadium(IV) reduces ferric to ferrous ions, we then used a modified version of this colorimetric assay to detect V(IV).[22] For determination of Fe(II), individual photolysis reactions contained 20 mM sodium phosphate buffer pH 7.0 with two or more of the following reagents: 50 μM compound **7**, 25 μM $FeCl_3 \bullet 6H_2O$, and 400 μM 1,10-phenanthroline monohydrate. The samples were then irradiated with the broad-spectrum fluorescent lamp (50 min at 22 °C), while a parallel set of reactions was kept in the dark. An irradiated reaction sample was then equilibrated in 100 mM EDTA to promote Fe(II)/1,10-phenanthroline complex disassociation. For V(IV) detection, the same procedure was employed except that: (i) 20 mM sodium cacodylate buffer pH 7.0 and 25 μM Na_3VO_4 were used during photolysis to substitute for 20 mM sodium phosphate buffer and 25 μM $FeCl_3 \bullet 6H_2O$; (ii) 25 μM $FeCl_3 \bullet 6H_2O$ was added immediately after the sample irradiation interval to enable V(IV) to reduce Fe(III) to Fe(II) and the Fe(II) product to form a complex with 1,10-phenanthroline. UV-visible spectra were immediately recorded (Figure 2.5).

The reaction irradiated in the presence of compound **7**, Fe(III), and 1,10-phenanthroline produced an orange color change and a ~ 510 nm shoulder in the absorption band of **7** (Figure 2.5A). A similar shoulder appeared upon the addition of Fe(III) to the reaction irradiated in the presence of compound **7**, V(V), and 1,10-phenanthroline (Figure 2.5D). When EDTA was added to both reactions, the 510 nm absorption became attenuated until the shoulder disappeared (Figure 2.5A and 2.5D).

The signature orange color change and absorption at ~ 510 nm were absent in all of the dark reactions and in all of the reactions in which either 1,10-phenanthroline or compound **7** were omitted (Figure 2.5). These data collectively indicate that compound **7**

sensitizes the one electron photoreduction of Fe(III) and V(V). There are numerous examples of stable Fe(II)[20c,e,g] and V(IV)[20a,b,d] complexes that participate in the Fenton reaction[20g] (Figure 2.6). The reduced metals react with hydrogen peroxide to produce

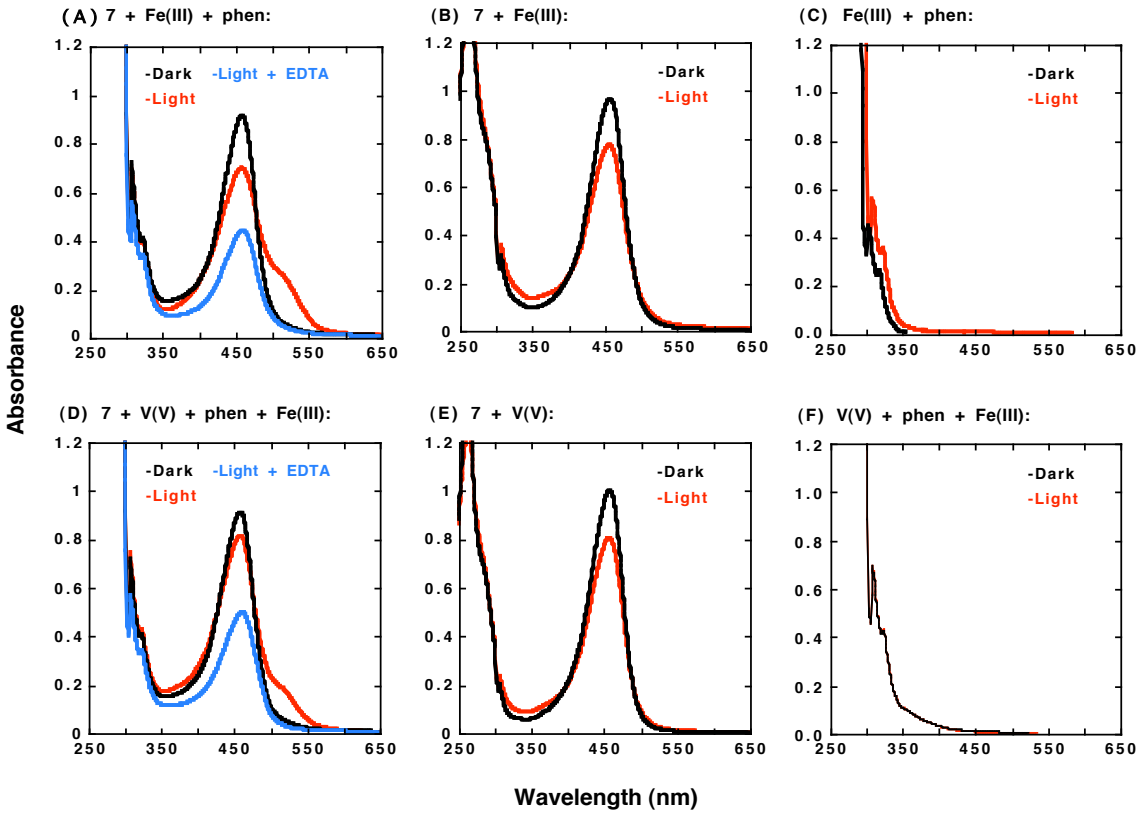

Figure 2.5. UV-visible spectra to detect Fe(II) (A-C) and V(IV) (D-F) formation in 20 mM pH 7.0 buffer. Reactions containing 25 μM $FeCl_3 \bullet 6H_2O$ or 25 μM Na_3VO_4, and 50 μM **7** and/or 400 μM 1,10-phenanthroline monohydrate were irradiated with a broad spectrum visible lamp for 50 min at 22 °C (red) or were maintained in the dark for 50 min at 22 °C (black). A final concentration of 100 mM EDTA was added after irradiation (blue). In the V(IV) assay, 25 μM $FeCl_3 \bullet 6H_2O$ was added after irradiation (D, F).

short lived, diffusible hydroxyl radicals ($OH^{\bullet}$) that cleave DNA with an extremely high rate constant. (In the case of iron, a few studies have suggested that a non-diffusible iron-oxygen (ferryl) radical is the active species formed.[20c,f]) Through the use of catalase, sodium benzoate, and superoxide dismutase, we showed that hydrogen peroxide (H_2O_2),

hydroxyl radicals, superoxide anion radicals ($O_2^{\bullet -}$) contribute to Fe(III) and V(V)-assisted DNA photocleavage by compound **7** (Table 2.3). The H_2O_2 detected in these experiments was most likely formed through dismutation of superoxide anion radicals ($O_2^{\bullet -}$)[20f] produced by Type I electron transfer from the excited triplet state of compound **7** to O_2. The fact that the H_2O_2 was generated in the presence of Fe(II) and V(IV) suggests that the hydroxyl radicals originated from the Fenton reaction (Figure 2.6).

$$M^{n-1} + H_2O_2 \longrightarrow M^n + OH^{\bullet} + OH^-$$

Figure 2.6. Fenton reaction. Abbreviation: M = metal.

According to Rehm and Weller theory, excited state redox potentials can be calculated from corresponding ground state redox potentials and exited state energies.[23] Thus, for acridine orange, the excited singlet state oxidation potential was estimated to be –1.71 V in 0.18 M phosphate buffer pH 6.5.[24] This value was obtained by Kittler and co-workers using eq 1, in which $U(^*D/D^{\bullet +})$ stands for excited state oxidation potential, $U(D/D^{\bullet +})$ is the ground state oxidation potential, and E_∞ is excited state energy.

$$U(^*D/D^{\bullet +}) = U(D/D^{\bullet +}) - E_\infty \qquad (2.1)$$

By substituting Kittler's value for the ground state oxidation potential of acridine orange in 0.18 M phosphate buffer pH 6.5 (0.70 V)[24] and the excited triplet state energy of acridine orange (2.13 eV) [25] into equation 1, we obtained an estimated value of –1.43 V for the excited triplet state oxidation potential of acridine orange. Standard reduction potentials at pH 7.0 are 0.991 V[26] and 0.330 V[27] for the V(V)/V(IV) and $O_2/O_2^{\bullet -}$ couples, respectively. In the case of iron, the reduction potential of the LFe(III)/LFe(II) couple

shows extreme variability based on the nature of the ligand L: at pH 7.0, standard values range from –0.750 V to 1.15 V. [28] Notwithstanding, the estimated excited singlet and excited triplet state oxidation potentials of acridine orange are more negative than all of the above ground state reduction potentials, indicating that it should be possible for acridine orange to sensitize one electron reduction of V(V), Fe(III), and O_2. In the case of Fe(III) and O_2, this assertion is supported by the following experimental data. Acridine orange photosensitized cell inactivation [29] and proflavin triplet state photosensitized DNA cleavage [7b, 15b] have both been associated with superoxide production, while the excited triplet states of acridine orange,[18a] proflavin,[18b] and other 3,6-acridinediamines[18b] have been shown to effect photoreduction of Fe(III) to Fe(II). Because the central core of compound **7** is a 3,6-acridinediamine nearly identical in structure to acridine orange (Figure 2.S1 in Supporting Information), the two chromophores are likely to have similar excited singlet and triplet state oxidation potentials. Electron transfer from the excited states of compound **7** to V(V), Fe(III), and O_2 should also be feasible. This hypothesis is consistent with the following lines of evidence reported in this paper. (i) In a series of scavenger experiments, SOD was shown to inhibit Hg(II), Fe(III), Zn(II), and V(V)-assisted DNA photocleavage, indicating that compound **7** is capable of photosensitizing one electron reduction of O_2 to $O_2^{\bullet -}$ (Table 2.3). (ii) In a spectrophotometric assay based on 1,10-phenanthroline, compound **7** was shown to photosensitize one electron reduction of Fe(III) and V(V) (Figure 2.5).

In summary, this report describes the synthesis and characterization of compounds **7** and **10**, which contain a central DNA binding 3,6-acridinediamine chromophore attached to 4 and 2 metal coordinating imidazole rings, respectively. In a

survey of 16 metal salts, we have demonstrated that the highest levels of DNA photocleavage are attained by **7** in the presence of either Hg(II), Fe(III), Cd(II), Zn(II), V(V), or Pb(II) (pH 7.0, 22 ºC, 8 μM **7** to 50 μM **7**). Scavenger experiments conducted with sodium azide, superoxide dismutase, catalase, and sodium benzoate indicated the involvement of Type I and Type II photochemical processes in these metal-assisted DNA photocleavage reactions. Compound **7** afforded relatively low amounts of photocleavage both in the absence of metal and in the presence of either Ni(II), Co(II), Cu(II), Sn(IV), Mn(II), Ca(II), Cr(III), Mg(II), Zr(IV), or Sc(III). We also showed that photocleavage could be modulated by modifying buffer type and pH.

Metallic complex formation between compound **7** and the six photoactive metals Hg(II), Fe(III), Cd(II), Zn(II), V(V), and Pb(II) was implied by scavenger experiments in which EDTA was shown to inhibit metal-assisted DNA photocleavage. Direct evidence was provided by NMR and/or ESI mass spectral data.

On the basis of thermal melting and spectroscopic studies, we concluded that several phenomena were likely to influence DNA photocleavage. When the 16 metals were added to **7**, significant changes in emission quantum yield and significant increases in T_m were observed only for the seven borderline and soft metals in the series. The ΔT_m values of 8 °C for Ni(II), 6 °C for Cd(II), 6 °C for Zn(II), 4 °C for Co(II), 3 °C for Cu(II), 2 °C for Hg(II), and 2 °C for Pb(II) indicate that the seven borderline and soft metals form complexes that increase the binding affinity of **7** to DNA. Alternatively, the minimal "%Δ Φ_{em} + metal" and ΔT_m values associated with Fe(III), Sn(IV), Sc(III), Zr(IV), Cr(III), Ca(II), Mg(II), Mn(II) and V(V) suggest that that these nine hard metals are unable to form strong complexes with the borderline imidazole rings of compound **7**.

Regarding the six photoactive metals for which ESI mass spectra were recorded, the extent of metal complex formation (Cd(II) ≈ Zn(II) > Hg(II) ≈ Pb(II) >> Fe(III) > V(V)) was found to be in good agreement with the above melting temperature trends. It is likely that complex formation with positively charged metal enhanced electrostatic interactions between compound **7** and the negatively charged DNA phosphate backbone. This may in fact account for the increase in DNA photocleavage by compound **7** produced in the presence of Hg(II), Cd(II), Zn(II), and Pb(II). Although Ni(II), Co(II), and Cu(II) also raised T_m when added to compound **7**, they were shown to efficiently quench fluorescence and in turn to inhibit photocleavage. Melting temperature values were unchanged upon addition of Fe(III) and V(V) to **7**, in agreement with fluorescence quenching data and with ESI spectra that showed weak complexation between the two metals and **7**. To account for the fact that DNA photocleavage was enhanced, we employed a colorimetric assay to demonstrate that compound **7** sensitized the one electron photoreduction of Fe(III) and V(V). The reduced metals would then accelerate the production of highly reactive, DNA damaging hydroxyl radicals by the Fenton reaction.[20]

Perhaps our most significant finding was the notable increase in compound **7** DNA photocleavage produced by Fe(III) in sodium phosphate buffer pH 7.0 (Figure 2.1, Figure 2.4, Table 2.2). This is important in light of the fact that the $H_2PO_4^-$ and HPO_4^{2-} conjugate pair constitutes one of the two most important buffering systems in human physiology. Second, iron is widely distributed throughout the human body and as a result, has the potential to play an important role in the photodynamic action of compound **7** in vivo. Several lines of experimental evidence have established that cellular lysosomes

contain low molecular weight pools of weakly chelated, redox active iron capable of catalyzing the Fenton reaction.[11, 30] (This iron pool is thought to arise from lysosomal degradation of ferritin and other metalloproteins.) Upon entry into the cell, acridine orange accumulates mainly in the lysosomes and to the lesser degree in the cytoplasm and nucleus.[11, 30a,c, 31] After this, iron catalyzed rupture of the lysosomal membranes is triggered by reactive oxygen species generated upon exposure to H_2O_2.[11, 30a,c, 32] Irradiation of acridine orange with intense blue light also produces reactive oxygen species that rupture the membranes.[31b, 33] In both cases, the acridine orange is relocated from the lysosomes to the cytoplasm and nucleus.[11, 30a, 31b] It has recently been suggested that membrane rupture also triggers the diffusion of the weakly chelated iron from the lysosomes into the nucleus, resulting in significant damage to genomic DNA by the Fenton reaction.[11]

Acridine orange has demonstrated promise for use as a photosensitizer in photodynamic therapy. It is selectively localized in a number of tumor types and has been used to effect efficient in vivo photodestruction of epithelial tumors, Walker carcinosarcoma 256 stomach tumors, and musculoskeletal sarcomas in animal models.[8] Furthermore, the reactive oxygen species produced by irradiation of DNA bound acridine orange are thought to play a role in triggering tumor cell death.[8a,c, 31a, 34] The 3,6-acridinediamine **7** possesses four iron chelating imidazole rings attached to a central "acridine orange" core. In this paper, we have shown that iron markedly enhances DNA photocleavage by compound **7** in vitro, while having little if any effect on photocleavage produced by acridine orange (Table 2.1). We expect that it should also be possible for compound **7** to demonstrate superior photodynamic action in vivo. It is conceivable that

compound **7** might chelate iron in lysosomes, facilitating the relocation of this metal to the nucleus upon irradiation-induced membrane rupture. Subsequent binding of **7** to nucleic acids would enable iron to catalyze the production of hydroxyl radicals within angstroms of genomic DNA.

Conclusions

Our data indicate that buffer, pH, Hg(II), Fe(III), Cd(II), Zn(II), V(V), Pb(II) and light can be used to "tune" DNA cleavage by compound **7** under physiologically relevant conditions. In addition to its potential use as a photosensitizer in photodynamic therapy, **7** has serendipitously demonstrated metal chemosensing capabilities as indicated by our spectrofluorometric experiments. Our immediate goal will be to explore the anti-tumor properties of compound **7** in vivo. The use of metal coordinating imidazole rings may represent an attractive chemical tool to enhance the photodynamic action of acridine orange for chemotherapeutic purposes.

Experimental Section

General Methods. Melting points were determined in an Electrothermal IA9100 apparatus. Infrared spectra were taken on an FT-IR Perkin-Elmer 1725X spectrophotometer. All ^{1}H and ^{13}C NMR spectra were recorded at 300 and 75 MHz, respectively, on a Varian Mercury spectrometer. EI and CI mass spectra were generated on a Hewlett-Packard HP-5988a spectrometer at 70 eV, while ESI and APCI mass spectra were done either on an Automass Multi GC/API/MS Finnigan spectrometer or on a Micromass Q-Tof hybrid mass spectrometer. FAB mass spectra were recorded using a V.G. Autoexpec spectrometer with 3-nitrobenzyl alcohol as matrix. Elemental analyses were performed with a Heraeus CHN analyzer. Merck silica gel 60 (230-400 ASTM

mesh) was employed for flash column chromatography. UV-visible spectra were recorded with a Shimadzu UV-1601 spectrophotometer, while a Cary Bio100 UV-vis spectrophotometer (Varian) was used to plot thermal melting curves.

Distilled, de-ionized water was utilized in the preparation of all buffers and aqueous reactions. Chemicals were of the highest available purity and were used without further purification. The metal salts $CaCl_2 \bullet 2H_2O$, $CdCl_2$, $(CH_3)_2SnCl_2$, $CoCl_2 \bullet H_2O$, $CrCl_3 \bullet 6H_2O$, $CuCl_2 \bullet 2H_2O$, $FeCl_3 \bullet 6H_2O$, $HgCl_2$, $MgCl_2 \bullet 6H_2O$, $MnCl_2 \bullet 4H_2O$, Na_3VO_4, $NiCl_2 \bullet 6H_2O$, $PbCl_2$, $Sc(CF_3SO_3)_3$, $ZnCl_2$, and $ZrCl_4$ were purchased from the Aldrich Chemical Company (purity > 99%). Superoxide dismutase and catalase were from Sigma. All other reagents, including cacodylic acid, ethidium bromide, 1,10-phenanthroline monohydrate, sodium azide, sodium benzoate, sodium borate, sodium cacodylate, sodium phosphate dibasic, and sodium phosphate monobasic, were from Aldrich. Both 1*H*-imidazole-4-methanol hydrochloride,[35] 4-(chloromethyl)-1*H*-imidazole hydrochloride[36] were synthesized according to reported procedures. Transformation of *E. coli* competent cells (Stratagene, XL-1 blue) with pUC19 plasmid DNA (Sigma) and growth of bacterial cultures in Lauria-Bertani broth were performed using standard laboratory protocols.[37] The plasmid DNA was purified with a Qiagen Plasmid Mega Kit. Calf thymus DNA (average size of ≤ 2000 bp, Invitrogen Catalog # 15633-019) was utilized without further purification.

To promote complex formation, aqueous stock solutions containing 250 μM of **7** or **10** and 125 μM of each respective metal salt were equilibrated in the dark for 24 h at 22 °C. Subsequent photocleavage experiments and absorbance, emission and thermal

melting studies were conducted using the equilibrated solutions diluted to the appropriate concentration.

2-[Bis(1*H*-imidazol-4-ylmethyl)amino]ethanol (1). To a solution of 2-aminoethanol (0.6 mL, 9.8 mmol) in dry ethanol (20 mL) was added triethylamine (5.5 mL, 39.2 mmol). The reaction mixture was heated at reflux after which a solution of 4-(chloromethyl)-1*H*-imidazole hydrochloride (3 g, 19.6 mmol) in dry ethanol (30 mL) was added dropwise over 20 min. The mixture was heated at reflux for 3 h and the solvent evaporated under reduced pressure. The resulting residue was stirred with dichloromethane (100 mL) for 2 h, from which an oil was separated. The dichloromethane was decanted and the oily product purified by flash column chromatography using silica gel as adsorbent and methanol-ethyl acetate (1:1) as eluent. This afforded **2** as a colorless oil in 70% yield. IR (KBr): 3108, 2879, 1628, 1571, 1450, 1085 cm^{-1}. ^{1}H NMR (CD_3OD): δ 7.76 (d, J = 1.1 Hz, 2H, H-2), 7.16 (d, J = 1.1 Hz, 2H, H-5), 3.88 (s, 4H, CH_2Im), 3.70 (t, J = 5.5 Hz, 2H, CH_2OH), 2.81 (t, J = 5.5 Hz, 2H, CH_2N). ^{13}C NMR (CD_3OD): δ 136.80 (C-2), 133.79 (C-4), 120.47 (C-5), 59.47 (CH_2OH), 55.70 (CH_2N), 50.23 (CH_2Im). MS (CI): m/z 222 ($[M + H]^+$, 32%), 170 (8), 161 (41), 142 (100), 109 (13), 90 (11), 81 (33). Anal. Calcd for $C_{10}H_{15}N_5O$: C, 54.28; H, 6.83; N, 31.65. Found: C, 54.04; H, 6.90; N, 31.91.

***N*-(2-Chloroethyl)-*N*-(1*H*-imidazol-4-ylmethyl)-1*H*-imidazole-4-methanamine Trihydrochloride (2).** To a solution of 2-[bis(1*H*-imidazol-4-ylmethyl)amino]ethanol (**1**) (259 mg, 1.17 mmol) in dry DMF (5 mL) was added thionyl chloride (170 mL, 2.34 mmol). The reaction mixture was stirred at room temperature for 24 h and then concentrated to dryness. The oily product thus obtained was dissolved in methanol,

precipitated with cold ethyl acetate, filtered out, and washed thoroughly with cold ethyl acetate. The hygroscopic solid was dried and kept under vacuum. Yield: 352 mg (86%); Mp: 173-174 °C. IR (KBr): 3412, 3118, 1701, 1621, 1439, 1277, 1169, 1087 cm^{-1}. ^{1}H NMR (CD_3OD): δ 8.92 (d, J = 1.0 Hz, 2H, H-2), 7.59 (d, J = 1.0 Hz, 2H, H-5), 3.96 (s, 4H, CH_2Im), 3.65 (t, J = 6.5 Hz, 2H, CH_2Cl), 2.93 (t, J = 6.5 Hz, 2H, CH_2N). ^{13}C NMR (CD_3OD): δ 135.63 (C-2), 131.43 (C-4), 119.22 (C-5), 55.80 (CH_2N), 48.45 (CH_2Im), 42.12 (CH_2Cl). MS (ESI): m/z 240 $[(M - 3HCl) + H]^+$ (Calcd for $C_{10}H_{17}Cl_4N_5$ 347). Anal. Calcd for $C_{10}H_{17}Cl_4N_5$: C, 34.58; H, 4.94; Cl, 40.31; N, 20.18. Found: C, 34.72; H, 4.91; N, 19.83.

***N*-(2-Chloroethyl)-*N*-[1-(triphenylmethyl)-1*H*-imidazol-4-ylmethyl]-1-(triphenylmethyl)-1*H*-imidazole-4-methanamine (3).** To a solution of *N*-(2-chloroethyl)-*N*-(1*H*-imidazol-4-ylmethyl)-1*H*-imidazole-4-methanamine trihydrochloride (**2**) (492 mg, 1.42 mmol) in dry DMF (8 mL) was added triethylamine (2 mL, 14.75 mmol). The reaction mixture was stirred at room temperature for 20 min and then a solution of triphenylmethylchloride (2.10 g, 7.36 mmol) in anhydrous DMF (20 mL) was added dropwise. After 2 h stirring, the reaction mixture was poured onto crushed ice. The precipitate was filtered and purified by flash column chromatography using silica gel (0.1% Ca enriched) as adsorbent and ethyl acetate as eluent to give **3** in 61% yield; Mp: 125-127 °C. IR (KBr): 3059, 3031, 2927, 1596, 1492, 1444, 1324, 1237 cm^{-1}. ^{1}H NMR ($CDCl_3$): δ 7.36 (d, J = 1.5 Hz, 2H, H-2 Im), 7.30-7.26 (m, 18H, Ph), 7.13-7.08 (m, 12H, Ph), 6.60 (br s, 2H, H-5 Im), 3.64 (s, 4H, CH_2Im), 3.41 (t, J = 7.4 Hz, 2H, CH_2Cl), 2.84 (t, J = 7.4 Hz, 2H, CH_2N). ^{13}C NMR ($CDCl_3$): δ 142.36 (Cipso Ph), 138.48 (C-2 Im), 138.25 (C-4 Im), 129.65, 127.98, 127.92 (Ph), 120.43 (C-5 Im), 75.10 (CPh_3), 54.65

(CH_2N), 51.90 (CH_2Im), 42.13 (CH_2Cl). MS (APCI): *m/z* 724 ([M + H]+) (Calcd for $C_{48}H_{42}ClN_5$ 723). Anal. Calcd for $C_{48}H_{42}ClN_5$: C, 79.63; H, 5.85; Cl, 4.83; N, 9.68. Found: C, 79.92; H, 5.62; N, 9.45.

3,6-Acridinediylbiscarbamic Acid Bis(1,1-dimethylethyl) Ester (4). To a solution of di-*tert*-butyl dicarbonate (26.4 mL, 115 mmol) in dry acetone (250 mL) was added 3,6-acridinediamine (2 g, 9.56 mmol). The reaction mixture was heated at reflux for 72 h and then concentrated to dryness. The crude product thus obtained was purified by flash column chromatography on silica gel using hexane-ethyl acetate (1:1) as eluent. The 3,6-acridinediylbiscarbamic acid bis(1,1-dimethylethyl) ester (**4**) was obtained in 72% yield; Mp: > 280 ˚C. IR (KBr): 3282, 2976, 1703, 1618, 1523, 1461, 1367, 1336, 1235, 1156 cm^{-1}. ^1H NMR (DMSO-d_6): δ 9.81 (s, 2H, N-H), 8.75 (s, 1H, H-9), 8.19 (d, *J* = 2.2 Hz, 2H, H-4, H-5), 7.96 (d, *J* = 9.1 Hz, 2H, H-1, H-8), 7.58 (dd, *J* = 9.1, 2.2 Hz, 2H, H-2, H-7), 1.52 (s, 18H, CMe_3). ^{13}C NMR (DMSO-d_6): δ 152.90 (CO), 149.95 (C-4a, C-10a), 141.39 (C-3, C-6), 135.26 (C-9), 129.18 (C-1, C-8), 122.01 (C-8a, C-9a), 119.67 (C-2, C-7), 112.40 (C-4, C-5), 79.88 (CMe_3), 28.29 (CMe_3). MS (EI): *m/z* 409 (M^+, 17%), 353 (8), 309 (18), 297 (93), 254 (13), 253 (83), 235 (3), 210 (11), 209 (72), 208 (25), 182 (31), 181 (37), 179 (11), 154 (13), 153 (11), 127 (9). Anal Calcd for $C_{23}H_{27}N_3O_4$: C, 67.46; H, 6.65; N, 10.26. Found: C, 67.59; H, 6.53; N, 10.02. Continued elution with ethyl acetate and then with ethyl acetate-acetone-triethylamine (5:5:1) afforded the (6-amino-3-acridinyl)carbamic acid 1,1-dimethylethyl ester (**8**) in 10% yield.

Synthesis of 3,6-Acridinediylbis[2-[bis[[1-(triphenylmethyl)-1*H*-imidazol-4-yl]methyl]-amino]ethyl]carbamic Acid Bis(1,1-dimethylethyl) Ester (5). A mixture of 3,6-acridinediylbiscarbamic acid bis(1,1-dimethylethyl) ester (**4**) (61 mg, 0.15 mmol) and

Cs_2CO_3 (635 mg, 1.95 mmol) in dry DMF (5 mL) was stirred at room temperature for 30 min, after which *N*-(2-chloroethyl)-*N*-[1-(triphenylmethyl)-1*H*-imidazol-4-ylmethyl]-1-(triphenylmethyl)-1*H*-imidazole-4-methanamine (**3**) (225 mg, 0.31 mmol) in 5 mL DMF was added. After 24 h of stirring at room temperature, **3** (225 mg, 0.31 mmol) in 6 mL DMF was added. The reaction was stirred for another 24 h and then poured onto crushed ice. The resulting precipitate was collected, washed thoroughly with cold water, dried and purified by flash column chromatography on silica gel using ethyl acetate-methanol (9:1) as eluent, yielding pure 3,6-acridinediyl-bis[2-[bis[[1-(triphenylmethyl)-1*H*-imidazol-4-yl]methyl]-amino]ethyl]carbamic acid bis(1,1-dimethylethyl) ester (**5**) (239 mg, 89%); Mp: 125-127 ˚C. IR (KBr): 3423, 3059, 2926, 2849, 1698, 1615, 1492, 1448, 1367, 1300, 1239, 1152, 1037 cm^{-1}. ^1H NMR ($CDCl_3$): δ 8.37 (s, 1H, H-9 Acr), 7.87 (d, J = 1.8 Hz, 2H, H-4, H-5 Acr), 7.62 (d, J = 9.1 Hz, 2H, H-1, H-8 Acr), 7.43 (dd, J = 9.1, 1.8 Hz, 2H, H-2, H-7 Acr), 7.31 (d, J = 1.1 Hz, 4H, H-2 Im), 7.23-7.15 (m, 36 H, Ph), 7.06-7.01 (m, 24 H, Ph), 6.49 (d, J = 1.1 Hz, 4H, H-5 Im), 3.92 (t, J = 7.3 Hz, 4H, CH_2N-Acr), 3.58 (s, 8H, CH_2Im), 2.84 (t, J = 7.3 Hz, 4H, CH_2N), 1.39 (s, 18H, CMe_3). ^{13}C NMR ($CDCl_3$): δ 154.15 (CO), 149.41 (C-4a, C-10a Acr), 144.81 (C-3, C-6 Acr), 142.41 (C_{ipso} Ph), 138.35 (C-2, C-4 Im), 134.62 (C-9 Acr), 129.63, 127.90, 127.83 (Ph), 127.49, (C-1, C-8 Acr), 126.97 (C-2, C-7 Acr), 124.31 (C-8a, C-9a Acr), 123.53 (C-4, C-5 Acr), 120.38 (C-5 Im), 80.56 (CMe$_3$), 74.97 (CPh$_3$) 51.87 (CH_2N), 50.78 (CH$_2$Im), 48.53 (CH$_2$N-Acr), 28.35 (CMe_3). MS (FAB): m/z 1785 $[M + H]^+$ (Calcd for $C_{119}H_{109}N_{13}O_4$ 1784). Anal. Calcd for $C_{119}H_{109}N_{13}O_4$: C, 80.06; H, 6.15; N, 10.20. Found: C, 80.27; H, 6.22; N, 9.97.

3,6-Acridinediyl-[2-[bis[[1-(triphenylmethyl)-1*H*-imidazol-4-yl]methyl]-amino]ethyl]carbamic Acid Bis(1,1-dimethylethyl) Ester (**6**)**:** Mp: 117-118 ˚C. IR

(KBr): 3415, 3058, 2975, 1698, 1617, 1569, 1544, 1492, 1450, 1367, 1240, 1152, 1037 cm^{-1}. ^1H NMR ($CDCl_3$): δ 8.46 (s, 1H, H-9 Acr), 7.92 (d, J = 1.7 Hz, 1H, H-4 Acr), 7.87 (br s 2H, H-7, H-8 Acr), 7.76 (br s, H-5 Acr), 7.64 (d, J = 8.9 Hz, 1H, H-1 Acr), 7.41 (dd, J = 8.9, 1.7 Hz, H-2 Acr), 7.31 (d, J = 1.3 Hz, 2H, H-2 Im), 7.23-7.20 (m, 18H Ph), 7.05-7.02 (m, 12H, Ph), 6.52 (d, J = 1.3 Hz, 2H, H-5 Im), 3.90 (t, J = 7.0 Hz, 4H, CH_2N-Acr), 3.59 (s, 4H, CH_2Im), 2.84 (t, J = 7.0 Hz, 2H, CH_2N), 1.58 (s, 9H, CMe_3), 1.39 (s, 9H, CMe_3). ^{13}C NMR ($CDCl_3$): δ 154.12, 152.40 (CO) 149.55 (C-4a, C-10a Acr), 144.97 (C-3, C-6 Acr), 142.42 (C_{ipso} Ph), 138.35 (C-2, C-4 Im), 135.01 (C-9 Acr), 129.64 (C-8 Acr and Ph), 127.88 (Ph), 127.80 (Ph and C-1 Acr), 126.57 (C-2 Acr), 123.78 (C-8a Acr), 123.25 (C-9a, C-4a Acr), 120.42 (C-5 Im), 119.78 (C-7 Acr), 113.70 (C-5 Acr), 81.12, 80.60 (CMe$_3$), 75.01 (CPh$_3$), 51.78 (CH_2N), 50.94 (CH$_2$Im), 48.42 (CH$_2$N-Acr), 28.32 (CMe_3). MS (FAB): m/z 1097 $[M+H]^+$ (Calcd for $C_{71}H_{68}N_8O_4$ 1096). Anal. Calcd for $C_{71}H_{68}N_8O_4$: C, 77.71; H, 6.25; N, 10.21. Found: C, 77.51; H, 6.34; N, 10.47.

***N,N'*-Bis[2-[bis(1*H*-imidazol-4-ylmethyl)amino]ethyl]-3,6-acridinediamine (7).** A suspension of **5** (591 mg, 0.33 mmol) in 2 N HCl (20 mL) was heated at 50-60 ˚C for 3.5 h. The resulting precipitate of triphenylmethanol was filtered off and the filtrate basified to pH 8-9 with 2 N NaOH. The precipitate thus obtained was filtered, washed with cold water, and dried in a vacuum dessicator to give 177 mg (87%) of pure product; Mp: 146-148 ˚C. IR (KBr): 3118, 2923, 2834, 2834, 1642, 1610, 1450, 1375, 1279, 1168, 1105 cm^{-1}. ^1H NMR (CD_3OD): δ 8.30 (s, 1H, H-9 Acr), 7.62-7.58 (m, 6H, H-1, H-8 Acr and H-2 Im), 6.97 (d, 4H, J = 0.7 Hz, 4H, H-5 Im), 6.90 (dd, J = 9.2, 2.2 Hz, 2H, H-2, H-7 Acr), 6.58 (d, J = 2.2 Hz, 2H, H-4, H-5 Acr), 3.69 (s, 8H, CH_2Im), 3.28 (t, J = 5.9 Hz, 4H, CH_2N-Acr), 2.76 (t, J = 5.9 Hz, 4H, CH_2N). ^{13}C NMR (CD_3OD): δ 153.13 (C-4a, C-

10a Acr), 150.36 (C-3, C-6 Acr), 138.54 (C-9 Acr), 136.49 (C-2 Im), 134.90 (C-4 Im), 130.64 (C-1, C-8 Acr), 120.65 (C-5 Im), 120.10 (C-8a, C-9a Acr), 119.22 (C-2, C-7 Acr), 97.91 (C-4, C-5 Acr), 52.13 (CH_2N), 50.74 (CH_2Im), 41.72 (CH_2N-Acr). MS (FAB) *m/z* 616 $[M + H]^+$ (Calcd for $C_{33}H_{37}N_{13}$ 615). Anal. Calcd for $C_{33}H_{37}N_{13}$: C, 64.37; H, 6.06; N, 29.57. Found: C, 64.24; H, 6.11; N, 29.71.

(6-Amino-3-acridinyl)carbamic Acid 1,1-Dimethylethyl Ester (8). To a solution of di-tert-butyldicarbonate (4.4 mL, 19.12 mmol) in dry acetone (150 mL) was added 3,6-acridinediamine (2 g, 9.56 mmol). The reaction mixture was heated at reflux for 8 h and then concentrated to dryness. The crude product thus obtained was purified by flash column chromatography using silica gel as adsorbent. With hexane-ethyl acetate (1:1) as eluent, 3,6-acridinediylbiscarbamic acid bis(1,1-dimethylethyl) ester (**4**) (746 mg, 25%) was obtained. Continued elution with ethyl acetate and then ethyl acetate-acetone-triethylamine (5:5:1) afforded 2.3 g (59%) of the (6-amino-3-acridinyl)carbamic acid 1,1-dimethylethyl ester (**8**); Mp: > 280 °C. IR (KBr): 3363, 2976, 1709, 1624, 1572 cm-1. ^{1}H NMR (DMSO-d_6): δ 9.69 (s, 1H, N-H), 8.50 (s, 1H, H-9), 8.05 (d, J = 2.1 Hz, 1H, H-4), 7.81 (d, J = 9.1 Hz, 1H, H-1), 7.73 (d, J = 9.1 Hz, 1H, H-8), 7.43 (dd, J = 9.1, 2.1 Hz, 1H, H-2), 6.99 (dd, J = 9.1, 2.1 Hz, 1H, H-7), 6.85 (d, J = 2.1 Hz, 1H, H-5), 6.04 (s, 2H, NH_2), 1.51 (s, 9H, CMe_3). ^{13}C NMR (DMSO-d_6): δ 152.93 (CO), 151.49 (C-10a), 151.06 (C-6), 49.75 (C-4a), 140.93 (C-3), 134.96 (C-9), 129.61 (C-8), 129.12 (C-1), 120.54 (C-9a), 120.11 (C-8a), 120.00 (C-7), 117.68 (C-2), 112.16 (C-4), 102.93 (C-5), 79.68 (CMe_3), 28.32 (CMe_3). MS (EI): *m/z* 309 (M^+, 8%), 253 (33), 235 (23), 209 (100), 182 (31), 181 (25), 127 (5), 104 (7), 57 (10). Anal. Calcd for $C_{18}H_{19}N_3O_2$: C, 69.88; H, 6.19; N, 13.58. Found: C, 69.61; H, 6.13; N, 13.84.

(6-Amino-3-acridinyl)-[2-[bis[[1-(triphenylmethyl)-1*H*-imidazol-4-yl]methyl]amino]ethyl]carbamic Acid 1,1-Dimethylethyl Ester (**9**)**.** To a mixture of 6-amino-3-acridinyl)carbamic acid 1,1-dimethylethyl ester (**8**) (156 mg, 0.51 mmol) and cesium carbonate (900 mg, 2.76 mmol) in dry DMF (40 mL) was added *N*-(2-chloroethyl)-*N*-[1-(triphenylmethyl)-1*H*-imidazol-4-ylmethyl]-1-(triphenylmethyl)-1*H*-imidazole-4-methanamine (**3**) (400 mg, 0.55 mmol). The reaction mixture was stirred at room temperature under argon. After 24 and 48 h, an additional amount (100 mg, 0.14 mmol) of **3** was added. Finally, the reaction was stirred for another 24 h and then poured onto crushed ice. The precipitate was filtered and washed with cold water. The solid thus obtained was purified by column chromatography on silica gel (0.1% Ca enriched) using ethyl acetate-triethylamine (10:1) and acetone-ethyl acetate-triethylamine (5:5:1) as eluents, yielding pure **9** (428 mg, 85 %); Mp: 115-117 ˚C. IR (KBr): 3353, 3058, 2925, 1694, 1641, 1612, 1492, 1463, 1445 cm^{-1}. ^{1}H NMR (CD_3OD): δ 8.46 (s, 1H, H-9 Acr), 7.77 (d, J = 9.0, 1H, H-8 Acr), 7.71 (d, J = 2.0, 1H, H-4 Acr), 7.61 (d, J = 9.0 Hz, 1H, H-1 Acr), 7.29 (d, J = 1.5 Hz, 2H, H-2 Im), 7.21-7.18 (m, 19H, H-2 Acr and Ph), 7.12 (dd, J = 9.0, 2.0 Hz, 1H, H-7 Acr), 7.01-6.96 (m, 13H, H-5 Acr and Ph), 6.55 (d, J = 1.5 Hz, $_2$H, H-5 Im), 3.82 (t, J = 7.0 Hz, 2H, CH_2N-Acr), 3.52 (s, 4H, CH_2Im), 2.74 (t, J = 7.0 Hz, 2H, CH_2N), 1.36 (s, 9H, CMe_3). ^{13}C NMR (CD_3OD): δ 155.52 (CO), 153.43 (C-10a Acr), 151.69 (C-4a Acr), 148.94 (C-6 Acr), 146.14 (C-3 Acr), 143.28 (C_{ipso} Ph), 139.01, 138.88 (C-2, C-4 Im), 137.84 (C-9 Acr), 130.89 (C-8 Acr), 130.49 (Ph), 129.62 (C-1 Acr), 129.02 (Ph), 125.31 (C-2 Acr), 123.35, 122.89, (C-8a, C-9a Acr), 122.28 (C-4 Acr), 121.89, 121.82 (C-5 Im, C-7 Acr), 102.54 (C-5 Acr), 82.00 (CMe$_3$), 76.64 (CPh$_3$), 54.79 (CH_2N), 52.72 (CH$_2$Im), 52.18 (CH$_2$N-Acr), 28.71 (CMe_3). MS (FAB): m/z 997 $[M + H]^+$

(Calcd for $C_{66}H_{60}N_8O_2$ 996). Anal. Calcd for $C_{66}H_{60}N_8O_2$: C, 79.49; H, 6.06; N, 11.24. Found: C, 79.63; H, 6.21; N, 10.96.

***N*-[2-[Bis(1*H*-imidazol-4-ylmethyl)amino]ethyl]-3,6-acridinediamine (10).** A suspension of **9** (377 mg, 0.38 mmol) in 2 N HCl (20 mL) was heated at 50-60 ˚C for 3.5 h. The resulting white precipitate of triphenylmethanol was filtered off and the filtrate basified to pH 8-9 with 2 N NaOH. The precipitate thus obtained was filtered and dried in a vacuum dessicator, affording 109 mg (70%) of pure product that decomposed above 198 ˚C. IR (KBr): 3328, 3115, 2827, 1610, 1521, 1464, 1418, 1390, 1274, 1223, 1159, 1104 cm-1. ^{1}H NMR (CD_3OD): δ 8.36 (s, 1H, H-9 Acr), 7.67-7.60 (m, 2H, H-1, H-8 Acr), 7.63 (s, 2H, H-2 Im), 7.25 (s, 1H, NH-Acr), 6.97 (s, 2H, H-5 Im), 6.91 (m, 2H, H-2, H-7 Acr), 6.85 (br s, 1H, H-5 Acr), 6.58 (br s, 1H, H-4 Acr), 3.68 (s, 4H, CH_2Im), 3.27 (t, *J* = 6.0 Hz, 2H, CH_2N-Acr), 2.74 (t, *J* = 6.0 Hz, 2H, CH_2N). ^{13}C NMR (CD_3OD): δ 153.80, 153.33, (C-4a, C-10a Acr), 150.24, 149.76, (C-3, C-6 Acr), 139.02 (C-9 Acr), 136.49 (C-2 Im), 134.99 (C-4 Im), 131.30, 130.78, (C-1, C-8 Acr), 120.60 (C-5 Im), 120.11, 119.94, (C-8a, C-9a Acr), 119.44, 118.87 (C-2, C-7 Acr), 101.50 (C-5 Acr), 97.46 (C-4 Acr), 52.09 (CH_2N), 50.74 (*C*H_2Im), 41.69 (*C*H_2N-Acr). MS (FAB): *m/z* 413 $[M+H]^+$ (Calcd for $C_{23}H_{24}N_8$ 412). Anal. Calcd for $C_{23}H_{24}N_8$: C, 66.97; H, 5.86; N, 27.16. Found: C, 66.84; H, 5.61; N, 27.56.

Photocleavage Experiments. In a total volume of 20 μL, individual reactions contained 38 μM bp pUC19 plasmid DNA in (i) 20 mM buffer or in (ii) 20 mM buffer, 50 μM **7** and/or 25 μM of one of the following metal salts: $CaCl_2$•$2H_2O$, $CdCl_2$, $(CH_3)_2SnCl_2$, $CoCl_2$•H_2O, $CrCl_3$•$6H_2O$, $CuCl_2$•$2H_2O$, $FeCl_3$•$6H_2O$, $HgCl_2$, $MgCl_2$•$6H_2O$, $MnCl_2$•$4H_2O$, Na_3VO_4, $NiCl_2$•$6H_2O$, $PbCl_2$, $Sc(CF_3SO_3)_3$, $ZnCl_2$, or $ZrCl_4$. The buffer

systems employed were: 20 mM sodium cacodylate pH 5.0, 6.0, and 7.0; 20 mM sodium phosphate pH 5.0, 6.0, 7.0, and 8.0; and sodium borate pH 8.0, and 9.0. Reactions were kept in the dark or were irradiated for 50 min at 22 °C in 1.7 mL microcentrifuge tubes with a broad-spectrum 4 W T4T5/D fluorescent lamp (EIKO Ltd.) located 6 cm above the opened tubes. Aerobic ventilation was achieved by placing a table fan directly adjacent to the lamp. Cleavage products were then electrophoresed on a 1.0 % non-denaturing agarose gel stained with ethidium bromide (0.5 μg/mL), visualized on a transilluminator set at 302 nm, photographed, and scanned. Amounts of supercoiled, nicked and linear plasmid DNA were then quantitated using ImageQuant Mac v.1.2 software (Amersham Biosciences). In calculating photocleavage yields, the density of the supercoiled DNA band was multiplied by a correction factor of 1.22 to compensate for the relatively low ethidium bromide staining efficiency of supercoiled DNA compared to nicked and linear plasmid.

Thermal Melting Studies. Individual 3 mL solutions containing 12.5 mM bp calf thymus DNA in (i) 20 mM sodium phosphate buffer pH 7.0 or in (ii) 20 mM sodium phosphate buffer pH 7.0, 8 μM **7** and/or 4 μM of each of the 16 metal salts were placed in 3 mL (1 cm) quartz cuvettes (Starna). For V(V) and Pb(II), 20 mM sodium cacodylate buffer was used to substitute for the sodium phosphate buffer. While absorbance was monitored at 260 nm, DNA was denatured by using a Peltier heat block to increase the temperature from 25 ºC to 100 ºC at a rate of 0.5 °C min^{-1}. KaleidaGraph™ Version 3.5 was then utilized to approximate the first derivative of $\Delta A_{260}/\Delta T$ vs temperature, where the T_m value at the inflection point of each sigmoidal melting transition was marked by the maximum of its corresponding first derivative plot.

Scavenger Experiments. Individual 20 μL reactions containing 20 mM sodium phosphate buffer pH 7.0, 38 μM bp pUC19 plasmid DNA, 50 μM **7**, and 25 μM of the metals salts $CdCl_2$, $FeCl_3 \bullet 6H_2O$, $HgCl_2$, Na_3VO_4, $PbCl_2$, and $ZnCl_2$ were irradiated with a broad-spectrum 4 W T4T5/D fluorescent lamp (EIKO Ltd.) in the presence of either 100 mM sodium azide, 100 mM sodium benzoate, 50 U superoxide dismutase, 50 U catalase, or 100 mM EDTA (50 min at 22 °C). For V(V) and Pb(II), 20 mM sodium cacodylate buffer was used to substitute for the sodium phosphate buffer. Reaction products were then resolved on a 1.0% non-denaturing agarose gel and quantitated as described above. The percent inhibition of DNA photocleavage was calculated based on cleavage yields obtained in parallel reactions run without scavenger: [((% cleavage in the presence of **7** and metal) – (% cleavage in the presence of scavenger, **7**, and metal))/(% cleavage in the presence of **7** and metal)] x 100.

Quantum Yield Measurements. Emission spectra were recorded from 440 to 630 nm at 25 °C in 1 cm quartz cuvettes (Starna) using an Olis SLM-8000 spectrofluorimeter equipped with Olis Spectral Works v. 3.0.12 software. A 2 μM solution of proflavin in 50 μM potassium acetate buffer pH 4.0 (Φ = 0.27, [38] λ_{max} = 444 nm, ε = 30 800 M^{-1} cm^{-1}) was used as the reference to calculate the quantum yields of 5 μM **7** in 20 mM sodium phosphate buffer pH 7.0 (λ_{max} = 459 nm, ε = 20 000 M^{-1} cm^{-1}) and in 20 mM sodium cacodylate buffer pH 7.0. Compound **7**, calf thymus DNA, and metal salt were adjusted to the following concentrations in order to give an absorbance of ~0.04 at the 430 nm excitation wavelength: 4-7 μM **7** and 2-3.5 μM metal salt in solutions containing compound **7** and metals salt; 7-10 μM **7**, 3.5-5 μM and 10.9-15.6 μM bp DNA in solutions containing compound **7**, metal salt, and calf thymus DNA.

Additional emission spectra were then recorded 20 mM sodium phosphate buffer pH 7.0 and in 20 mM sodium cacodylate buffer pH 7.0 after which emission quantum yields were relative to **7** in the appropriate buffer. The excitation and emission monochromator slit widths of the spectrofluorimeter were set at 1 nm and 8 nm, receptively. An excitation polarizer set at 0° and an emission polarizer set at the "magic angle" (54.7°) were used in order to eliminate possible effects from non-isotropic fluorescence. Lamp spectral intensity output was monitored by recording the Raman peak of water (λ_{ex} = 350 nm, λ_{em} 397 nm) and the emission of **7** (λ_{ex} = 430 nm, λ_{em} 500 nm). The emission spectra were corrected for wavelength-dependent response of the spectrofluorimeter, converted to quanta units, and integrated. Relative emission quantum yields were then calculated by the comparative method.[39] All data were averaged over three trials with errors reported as standard deviation.

Colorimetric Detection of Fe(II).[21] A series of 500 μL reactions was prepared containing 20 mM sodium phosphate buffer pH 7.0 and two or more of the following reagents: 50 μM **7**, 25 μM $FeCl_3 \bullet 6H_2O$, and 400 μM 1,10-phenanthroline monohydrate. The samples were irradiated with the 4W F4T5/D fluorescent lamp, while a parallel set of reactions was kept in the dark. After 50 min, the solutions were visually examined for color change, placed in 500 μL quartz cuvettes, and monitored between 250 nm and 650 nm for evidence of Fe(II)–1,10-phenanthroline complex formation. To dissociate the 510 nm complex, an irradiated reaction sample containing 50 μM **7**, 25 μM $FeCl_3 \bullet 6H_2O$, and 400 μM 1,10-phenanthroline was equilibrated in 100 mM EDTA for 6 h in the dark.

Colorimetric Detection of V(IV).[22] In order to detect V(IV), the following modifications were made to the colorimetric assay described above: (i) 20 mM sodium

cacodylate buffer pH 7.0 and 25 μM Na_3VO_4 were used during photolysis to substitute for 20 mM sodium phosphate buffer and 25 μM $FeCl_3 \cdot 6H_2O$; (ii) after 50 min of irradiation, 12.5 μL of 1 mM $FeCl_3 \cdot 6H_2O$ were added to the reactions containing **7**, V(V), 1,10-phenanthroline, and V(V), 1,10-phenanthroline. The solutions were equilibrated in the dark for 45 min, visually examined for color change, and monitored between 200 nm and 650 nm for evidence of Fe(II)–1,10-phenanthroline complex formation.

Acknowledgment. We thank Professors Thomas L. Netzel and Marcus W. Germann (Georgia State University) for assistance with emission quantum yield measurements and thermal melting studies, respectively. We also thank Professor Christoph J. Fahrni (Georgia Institute of Technology) and Professor Jerry C. Smith (Georgia State University) for helpful discussions. Support of this research by the CICYT (Project BQU 2002-02576; A.L.), the National Science Foundation (CHE-9984772; K.B.G.), the American Chemical Society Petroleum Research Fund (32897-G3; K.B.G.), and the Consejería de Educación de la Comunidad de Madrid (L.G.) is gratefully acknowledged.

Note Added after ASAP Pbublication. The heading of column 9 in Table 4 was corrected and other minor changes in the text were made to the version posted ASAP August 11, 2005; the corrected version was posted August 12, 2005.

References

(1) (a) Dolmans, D. E. J. G. J.; Fukumura, D.; Jain, R. K. *Nat. Rev. Cancer* 2003, *3*, 380-387. (b) Stapleton, M.; Rhodes, L. E. *J. Dermatolog. Treat.* 2003, *2*, 107-112. (c) Vrouenraets, M. B.; Visser, G. W. M.; Snow, G. B.; van Dongen, G. A. M. S. *Anticancer Res.* 2003, *23*, 505-522. (d) Zeitouni, N. C.; Oseroff, A. R.; Shieh, S. *Mol. Immunol.* 2003, *39*, 1133-1136. (e) Dougherty, T. J. *J. Clin. Laser. Med. Surg.* 2002, *20,* 3-7. (f) Fong, D. S. *Ophthalmology* 2000, *107*, 2314-2317.

(2) (a) Ashkenazi, H.; Nitzan, Y.; Gál, D. *Photochem. Photobiol.* 2003, *77*, 186-191. (b) Wainwright, M. *Int. J. Antimicro. Agents* 2003, *21*, 510-520. (c) Ramaiah, D.; Eckert, I.; Arun, K. T.; Weidenfeller, L.; Epe, B. *Photochem. Photobiol.* 2002, *76*, 672-677. (d) Wagner, S. J.; Skripchenko, A.; Thompson-Montgomery, D. *Photochem. Photobiol.* 2002, *76*, 514-517. (e) Smetana, Z.; Ben-Hur, E.; Mendelson, E.; Salzberg, S.; Wagner, P.; Malik, Z. *J. Photochem. Photobiol. B: Biol.* 1998, *44*, 77-83.

(3) Bonnet, R. In *Chemical Aspects of Photodynamic Therapy*; Phillips, D., Ed., Gordon and Breach Science: The Netherlands, 2000; Vol. I, pp 70-87.

(4) (a) Konan, Y. N.; Gurny, R.; Allémann, E. *J. Photochem. Photobiol. B: Biol.* 2002, *66*, 89-106. (b) Zovinka, E. P.; Sunseri, D.R. *J. Chem. Ed.* 2002, *79*, 1331-1335. (c) Schuitmaker, J. J.; Baas, P.; van Leegoed, H. L. L. M.; van der Meulen, F. W.; Star, W. M.; van Zandwijk, N. *J. Photochem. Photobiol. B: Biol.* 1996, *34*, 3-12.

(5) (a) Quédraogo, G. D.; Redmond, R. W. *Photochem. Photobiol.* 2003, *77*, 192-203. (b) Choi Kim, H. R.; Luo, Y.; Li, G.; Kessel, D. *Cancer Res.* 1999, *59*, 3429-3432. (c) Ochsner, M. *J. Photochem. Photobiol. B: Biol.* 1997, *39*, 1-18.

(6) (a) Gollnick, S. O.; Evans, S. S.; Baumann, H.; Owczarczak, B.; Maier, P.; Vaughan, L.; Wang, W. C.; Unger, E.; Henderson, B. W. *Br. J. Cancer* 2003, *88*, 1772-1779. (b) Korbelik, M.; Dougherty, G. J. *Cancer Res.* 1996, *59*, 1941-1946.

(7) (a) Bowler, B. E.; Hollis, S.; Lippard, S. J. *J. Am. Chem. Soc.* 1984, *106,* 6102-6104. (b) Piette, J.; Lopez, M.; Calberg-Bacq, C. M.; Van de Vorst, A. *Int. J. Radiat. Biol.* 1981, *40*, 427-433. (c) Piette, J.; Calberg-Bacq, C.M.; Van de Vorst, A. *Photochem. Photobiol.* 1979, *30*, 369-378. (d) Freifelder, D.; Davison, P. F.; Geiduschek, E. P. *Biophys. J.* 1961, *1,* 389-400.

(8) (a) Kusuzaki, K.; Aomori, K.; Suginoshita, T.; Minami, G.; Takeshita, H.; Murata, H.; Hashiguchi, S.; Ashihara, T.; Hirasawa, Y. *Oncology* 2000, *59,* 174-180. (b) Kusuzaki, K.; Suginoshita, T.; Minami, G.; Aomori, K.; Takeshita, H.; Murata, H.; Hashiguchi, S.; Ashihara, T.; Hirasawa, Y. *Anticancer Res.* 2000, *20,* 3019-3024. (c) Tatsuta, M.; Iishi, H.; Yamamura, H.; Yamamoto, R.; Okuda, S. *Oncology* 1988, *45*, 35-40. (d) Tatsuta, M.; Yamamura, H.; Yamamoto, R.; Ichii, M.; Noguchi, S.; Iishi, H.; Mishima, H.; Hattori, T.; Okuda, S. *Eur. J. Cancer Clin. Oncol.* 1984, *20,* 543-552. (e) Tomson, S. H.; Emmett, E. A.; Fox, S. H. *Cancer Res.* 1974, *34*, 3124-3127.

(9) (a) Malinina, L.; Soler-López, M.; Aymamí, J.; Subirana, J. A. *Biochemistry* 2002, *41*, 9341-9348. (b) Mazerska, Z.; Dziegielewski, J.; Konopa, J. *Biochem.*

Pharmacol. 2001, *61*, 685-694. (c) Giménez-Arnau, E.; Missailidis, S.; Stevens, M. F. G. *Anti-Cancer Drug Des.* 1998, *13*, 431-451.

(10) Bregadze, V.; Khutsishvili, I.; Chkhaberidze, J.; Sologhashvili, K. *Inorg. Chim. Acta* 2002, *339,* 145-159.

(11) Kurz, T.; Leake, A.; von Zglinicki, T.; Brunk, U. T. *Ann. N.Y. Acad. Sci.* 2004, *1019,* 285-288.

(12) Lorente, A.; Espinosa, J. F.; Fernández-Saiz, M.; Lehn, J.-M.; Wilson, W. D.; Zhong, Y. Y. *Tetrahedron Lett.* 1996, *37*, 4417-4420.

(13) Optimal levels of DNA photocleavage were produced at a metal-to-ligand ratio of 1:2 for Hg(II), Cd(II), Zn(II), and Pb(II), and at a metal-to-ligand ratio of 2:1 for Fe(III) and V(V) (38 μM bp pUC19 plasmid DNA, 50 μM **7**). To facilitate comparison of the 16 metals, the experiments described in this paper were conducted using the 1:2 metal-to-ligand ratio.

(14) (a) Kubota, Y.; Steiner, R. F. *Biophys. Chem.* 1977, *6,* 279-289. (b) Schreiber, J. P.; Daune, M. P. *J. Mol. Biol.* 1974, *83,* 487-501.

(15) (a) van de Vorst, A.; Lion, Y. *Z. Naturforsch.* 1976, *31,* 203-204. (b) van de Vorst, A.; Lion, Y.; Saucin, M. *Biochim. Biophys. Acta* 1976, *430,* 467-477.

(16) (a) Prusik, T.; Kolubayev, T.; Morelli, M. J.; Brenner, H. C. *Photochem. Photobiol.* 1980, *31,* 315-321. (b) Kemlo, J. A.; Shepherd, T. M. *Chem. Phys. Lett.* 1977, *47,* 158-62. (c) Varnes, A. W.; Dodson, R. B.; Wehry, E. L. *J. Am. Chem. Soc.* 1972, *94,* 946-950. (d) Lower, S. K.; El-Sayed, M. A. *Chem. Rev.* 1966, *66,* 199-241. (e) McClure, D. S. *J. Chem. Phys.* 1952, *20,* 682-686.

(17) Bregadze, V. G.; Chkhaberidze, J. G.; Khutsishvili, I. G. *Met. Ions Biol. Syst.* 1996, *33,* 253-267.

(18) (a) Kellmann, A. *Photochem. Photobiol.* 1974, *20*, 103-108. (b) Oster, G. K.; Oster, G. *J. Am. Chem. Soc.* 1959 *81*, 5543-5545.

(19) Shinohara, N.; Nakamura, Y. *Bull. Chem. Soc. Jpn.* 1989, *62,* 734-737.

(20) (a) Bandwar, R. P.; Rao, C. P. *J. Inorg. Biochem.* 1997, *68,* 1-6. (b) Sakurai, H.; Tamura, H.; Okatani, K. *Biochem. Biophys. Res. Commun.* 1995, *206,* 133-137. (c) Stohs, S. J.; Bagchi, D. *Free Radical Biol. Med.* 1995, *18,* 321-336. (d) Shi, X.; Dalal, N. S. *Arch. Biochem. Biophys.* 1993, *307,* 336-341. (e) Tullius, T. D.; Dombroski, B. A. *Proc. Natl. Acad. Sci. U.S.A.* 1986, *83,* 5469-5473. (f) Halliwell, B; Gutteridge, J. M. C. *Biochem. J.* 1984, *219,* 1-14. (g) Fenton, H. J. H *J. Chem. Soc. Trans.* 1894, *65,* 899-905.

(21) Bhat, R.; Hadi, S. M. *Mutagenesis* 1992, *7,* 119-124.

(22) (a) Rao, G. N.; Prakash, R. *Curr. Sci.* 1974, *43,* 279. (b) Vinkovetskaya, S. Y. *Nauchno. Tr. Nauchno.-Issled. Proekt. Inst. Redkometall. Prom.* 1973, *42,* 202-204.

(23) Rehm, D.; Weller, A. *Ber. Bunsenges. Phys. Chem.* 1969, *73,* 834-839.

(24) Kittler, L.; Loeber, G.; Gollmick, F. A.; Berg, H. *Bioelectrochem. Bioenerg.* 1980, *7,* 503-511.

(25) Chambers, R. W.; Kearns, D. R. *Photochem. Photobiol.* 1969, *10,* 215-219.

(26) Isreal, Y.; Meites, L. In *Standard Potentials in Aqueous Solution;* Bard, A.J.; Parsons, R.; Jordan, J., Eds., Marcel Dekker, Inc.: New York, 1985; pp 507-525.

(27) Sawada, Y.; Iyanagi,T.; Yamazaki, I. *Biochemistry* 1975, *14,* 3761-3764.

(28) Pierre, J. L.; Fontecave, M.; Crichton, R. R. *BioMetals* 2002, *15,* 341-346.

(29) Martin J. P.; Logsdon, N. *Photochem. Photobiol.* 1987, *46,* 45-53.

(30) (a) Persson, H. L.; Yu, Z.; Tirosh, O.; Eaton, J. W.; Brunk, U. T. *Free Radical Biol. Med.* 2003, *34,* 1295-1305. (b) Yu, Z.; Persson, H. L.; Eaton, J. W.; Brunk, U. T. *Free Radical Biol. Med.* 2003, *34,* 1243-1252. (c) Antunes, F.; Cadenas, E.; Brunk, U. T. *Biochem. J.* 2001, *356,* 549-555. (d) Petrat, F.; De Groot, H.; Rauen, U. *Biochem. J.* 2001, *356,* 61-69.

(31) (a) Kusuzaki, K.; Minami, G.; Takeshita, H.; Murata, H.; Hashiguchi, S.; Nozaki, T.; Ashihara, T.; Hirasawa, Y. *Jpn. J. Cancer Res.* 2000, *91,* 439-445. (b) Brunk, U. T.; Dalen, H.; Roberg, K.; Hellquist, H. B. *Free Radical Biol. Med.* 1997, *23,* 616-626.

(32) Hellquist, H. B.; Svensson, I.; Brunk, U. T. *Redox Rep.* 1997, *3,* 65-70.

(33) (a) Zdolsek, J. M.; Olsson, G. M.; Brunk, U. T. *Photochem. Photobiol.* 1990, *51,* 67-76. (b) Williams, D. S.; Slater, T. F. *Biochem. Soc. Trans.* 1973, *1,* 200-202.

(34) Minami, G. *Kyoto-furitsu Ika Daigaku Zasshi* 1999, *108,* 587-602.

(35) Totter, J. R.; Darby, W. J. *Org. Synth. Coll. Vol. III,* 1955, 460-462.

(36) Turner, R. A.; Huebner, C. F; Scholz, C. R. *J. Am. Chem. Soc.* 1949, *71*, 2801-2803.

(37) Sambrook, J.; Fritsch, E. F.; Maniatis, T. In *Molecular Cloning A Laboratory Manual,* 2nd ed.; Cold Spring Harbor Press: New York, 1989.

(38) Melhuish, W. H. *J. Opt. Soc. Am.* 1964, *54*, 183-186.

(39) (a) Fery-Forgues, S.; Lavabre, D. *J. Chem. Ed.* 1999, *76*, 1260-1264. (b) Demas, J. N.; Crosby, G. A. *J. Phys. Chem.* 1971, *75*, 991-1024. (c) Parker, C. A.; Rees, W. T. *Analyst* 1960, *85*, 587-600.

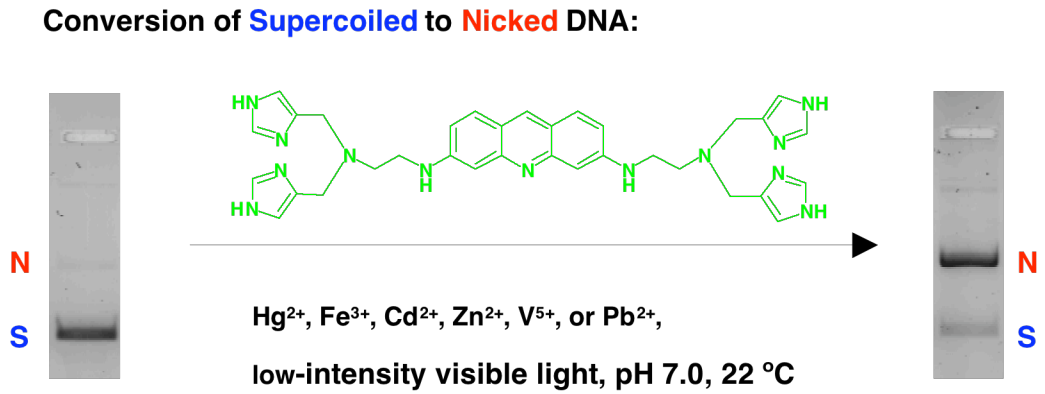

Figure 2.7. Synopsis Graphic. The synthesis and DNA photocleaving properties of a 3,6-acridinediamine chromophore centrally attached to four metal coordinating imidazoles are reported. Nicking assays of pUC19 plasmid DNA reacted with this acridine-imidazole conjugate reveal that the presence of either Hg(II), Fe(III), Cd(II), Zn(II), V(V), or Pb(II) serves to markedly enhance DNA cleavage produced by irradiation with low intensity, visible light. Moreover, photocleavage efficiency can be regulated by modifying buffer type and pH.

Supporting Information

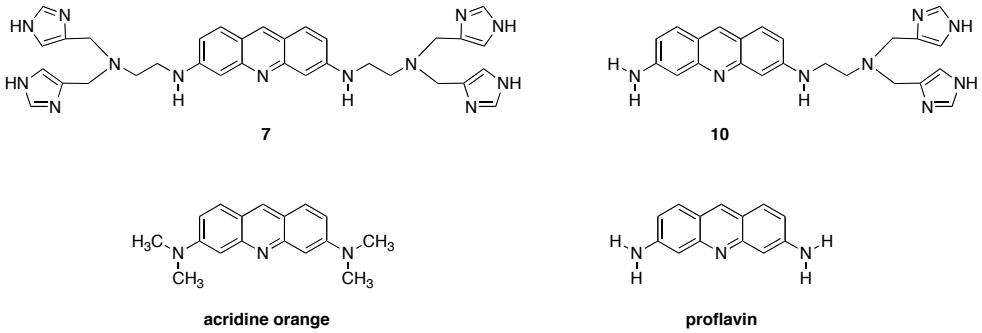

Figure 2.S1. The 3,6-acridinediamines **7**, **10**, **acridine orange**, and **proflavin**.

CHAPTER III

Copper-Activated DNA Photocleavage by a Pyridine-Linked Bis-Acridine Intercalator

(This chapter is verbatim as it will appear in Fernández, M.-J.; Wilson, B.; Palacios, M.; Rodrigo, M.-M.; Grant, K. B.; Lorente, A. *Bioconjugate Chemistry*. The synthesis of compound **4** was conducted by Ms. Palacios and Dr. Fernández. Additionally, competition dialysis experiments and electrospray spectrometry were conducted by Dr. Fernández. The original manuscript was written by Drs. Fernández, Lorente, and Grant. The contributions to the project by the author of this dissertation were as follows: thermal denaturation and DNA photocleavage experiments, viscometric titrations, colorimetric assays and minor revisions to the manuscript. The final manuscript was extensively revised by Dr. Grant.)

Abstract

We report the synthesis of new photonuclease **4** consisting of two acridine rings joined by a pyridine-based copper binding linker. We have shown that photocleavage of plasmid DNA is markedly enhanced when this ligand is irradiated in the presence of copper(II) (419 nm, 22 °C, pH 7.0). Viscometric data indicate that **4** binds to DNA by monofunctional intercalation, and equilibrium dialysis provides an estimated binding constant of 1.13 x 10^5 M^{-1} for its association with calf thymus DNA. In competition dialysis experiments, **4** exhibits preferential binding to GC-rich DNA sequences. When Cu(II) is added at a ligand to metal ratio of 1:1, electrospray ionization mass spectrometry demonstrates that compound **4** undergoes complex formation, while thermal melting studies show a 10 °C increase in the T_m of calf thymus DNA. Groove binding and intercalation are suggested by viscometric data. Finally, colorimetric and scavenger experiments indicate that the generation of Cu(I), H_2O_2, and superoxide contributes to the production of DNA frank strand breaks by the Cu(II) complex of **4**. Whereas the strand breaks are distributed in a relatively uniform fashion over the four DNA bases,

subsequent piperidine treatment of the photolysis reactions shows that alkaline labile lesions occur predominantly at guanine.

Introduction

The design and synthesis of small molecules that bind to and cleave nucleic acids are still major challenges. These artificial nucleases have important applications as tools in molecular biology and as potential therapeutic agents for the treatment of cancer and viral diseases. DNA cleavage is often associated with redox active or photoactivated transition metal complexes *(1-3)*. To date, a number of metal complexes capable of inducing double-stranded DNA lesions have been developed *(4-7)*.

Photosensitization of intercalating units can promote DNA damage by three main mechanisms: a) electron transfer from DNA nucleobases, specially guanine, to a photochemically excited state of the intercalator, b) photogeneration of hydroxyl radicals, an intermediate reactive species which can abstract hydrogen atoms from the DNA sugar backbone, and c) preferential oxidation of guanines by singlet molecular oxygen generated through energy transfer from an electronically excited photosensitizer *(8-11)*. In some cases, photoreduction of metal complexes is an important step in DNA cleavage reactions *(12-16)*.

Photochemical DNA-cleaving molecules can be used as photonucleases, as photo-footprinting agents, and as drugs in photodynamic therapy. Copper exists at micromolar levels in serum and other biological fluids (*17*), and is closely associated with nucleic acids and chromosomes *(18-20)*, where it is thought to play a role in regulating gene expression *(21, 22)*. Taking this into account, photonucleases which bind to copper may be of greater utility at the cellular level in comparison to photonucleases containing other

transition metals or to chemical nucleases which require an external reducing agent. Accordingly, a number of references on copper binding complexes with photolytic activity have appeared in the literature *(14-15, 23-35)*. While *in vivo* levels of free copper are tightly controlled by proteins *(36-38)*, the kinetically labile nature of this metal allows ion exchange between small ligands and proteins to take place *(38, 39)*.

Herein we present the synthesis, characterization, and DNA photocleaving properties of a pyridine-linked bis-acridine intercalator (**4**). We have found that **4** is a good DNA photocleaver, but that cleavage efficiency is markedly enhanced in the presence of Cu(II), converting pUC19 plasmid DNA into its nicked and linear forms upon exposure to visible light (419 nm, pH 7.0, 22 °C). Use of the colorimetric reagent bathocuproinedisulfonic acid disodium salt hydrate (BCS) indicates that the DNA photocleavage reaction involves acridine sensitized photoreduction of Cu(II) to Cu(I).

Materials and Methods

General Procedures. Merck silica gel 60 (230-400 ASTM mesh) was employed for flash column chromatography. TLC was performed on precoated aluminum silica gel plates (Merck or Macherey-Nagel 60F254 0.25 mm). Melting points were determined in an Electrothermal digital IA9100 apparatus. Infrared spectra were taken on an FT-IR Perkin-Elmer 1725X spectrophotometer. All ^{1}H and ^{13}C NMR spectra were recorded at 300 and 75 MHz, respectively, on a Varian Mercury-VX-300 spectrometer. Chemical shifts are reported in ppm using the residual peaks of either chloroform (δ 7.26 and 77.0 ppm) or methanol (δ 3.30 and 49.0 ppm) as an internal reference. Carbon and proton assignments were based on HSQC and HMBC experiments. CI mass spectra were generated on a Hewlett-Packard HP-5988a spectrometer at 70 eV. An Automass Multi

GC/API/MS Finnigan spectrometer was used for ESI mass spectra. Elemental analyses were performed with a Heraeus CHN analyzer. A Cary Bio100 UV-visible spectrophotometer (Varian) was used to plot thermal melting curves, while all other UV-visible spectra were recorded with a Shimadzu UV-1601 or a Lambda 18 Perkin-Elmer spectrophotometer. DNA photolysis reactions were run in an aerobically ventilated Rayonet Photochemical Reactor fitted with eight RPR–4190 Å lamps (The Southern New England Ultraviolet Company).

Reagents were of the highest available purity and were used without further purification. L-ascorbic acid, catalase, copper(II) chloride dihydrate, sodium phosphate monobasic and dibasic salts, and superoxide dismutase were purchased from Sigma. Glycogen and G-50 Sephadex columns were from Roche Applied Science. Sequenase™ Version 2.0, Sequenase™ Stop Solution, and [^{35}S]dATPaS were supplied by Amersham Biosciences. *Eco*RI and *Fsp*I restriction endonucleases were from New England Biolabs. All other chemicals including bathocuproinedisulfonic acid disodium salt hydrate, dimethyl sulfoxide, ethanol, ethidium bromide, D-mannitol, piperidine, and sodium azide were obtained from the Aldrich Chemical Company. Both 2,6-bis[(2-hydroxyethyl)methylaminomethyl]pyridine (**1**) *(40)* and (6-amino-3-acridinyl)carbamic acid methyl ester (**3**) *(41)* were prepared according to reported procedures.

Transformation of *E. coli* competent cells (Stratagene, XL-1 blue) with pUC19 plasmid DNA (Sigma) and growth of bacterial cultures were performed according to established methods *(42)*. Purification of the plasmid DNA was accomplished using a Qiagen Plasmid Mega Kit. All enzymes were used according to manufacturer's instructions in the buffers supplied.

2,6-Bis[(2-chloroethyl)methylaminomethyl]pyridine (2). Thionyl chloride (10 mL) was added to 348 mg (1.32 mmol) of 2,6-bis[(2 hydroxyethyl)methylaminomethyl]pyridine (**1**). The reaction mixture was stirred at room temperature for 24 h and then was concentrated at reduced pressure affording a syrup characterized as **2** • 3HCl. IR (film): υ 3393, 2968, 2666, 1598, 1463, 1407, 1217, 1160, 756 cm^{-1}. ^{1}H-NMR (CD_3OD): δ 8.04 (t, J = 7.7 Hz, H4), 7.56 (d, J = 7.7 Hz, 2H, H3, H5), 4.62 and 4.80 (AB, 4H, J = 14 Hz, CH_2-pyr), 4.12 (t, J = 6.4 Hz, 4H, CH_2Cl), 3.69 (m, 4H, CH_2N), 3.01 (s, 6H, CH_3). ^{13}C-NMR (CD_3OD): δ 151.44 (C2, C6), 140.92 (C4), 125.41 (C3, C5), 60.54 (CH_2-pyr), 58.33 (CH_2N), 42.21 (CH_3), 38.04 (CH_2Cl). To a solution of 1.23 g (3.08 mmol) of **2** • 3HCl in methanol (20 mL), 1.14 g (10.78 mmol) of Na_2CO_3 were added. The mixture was stirred for 3 h and then concentrated to dryness. The residue was treated with dichloromethane (25 mL) and the mixture was washed three times with water (10 mL). The organic layer was dried over $MgSO_4$, filtered and concentrated at reduced pressure to yield **2** as a brown oil (580 mg, 65%). IR (film): υ 2950, 2795, 1591, 1577, 1455, 1353, 1305, 1262, 1118, 1062, 739 cm^{-1}. ^{1}H-NMR ($CDCl_3$): δ 7.65 (t, J = 7.7 Hz, 1H, H4), 7.35 (d, J = 7.7 Hz, 2H, H3, H5), 3.73 (s, 4H, CH_2-pyr), 3.59 (t, J = 6.9 Hz, 4H, CH_2Cl), 2.81 (t, J = 6.9 Hz, 4H, CH_2N), 2.35 (s, 6H, CH_3). ^{13}C-NMR ($CDCl_3$): δ 158.23 (C2, C6), 136.93 (C4), 121.31 (C3, C5), 63.59 (CH_2-pyr), 58.69 (CH_2N), 42.59 (CH_3), 41.56 (CH_2Cl). MS (CI) m/z 290 ($[M+H]^+$, 39%), 254 (100) (calcd $C_{13}H_{21}Cl_2N_3$ 289.1). Anal. Calcd for $C_{13}H_{21}Cl_2N_3$: C, 53.80; H, 7.29; N, 14.48, Cl 24.43. Found: C, 53.94; H, 7.09; N, 14.77.

2,6-Bis{[((6-amino-acridin-3-yl)methoxycarbonylamino)-ethyl]methylaminomethyl} pyridine (**4**). To a solution of (6-amino-3-

acridinyl)carbamic acid methyl ester (**3**) (184 mg, 0.69 mmol) in dry DMF (5 mL), 80% NaH (41 mg, 1.38 mmol) was added. The reaction mixture was stirred under an argon atmosphere for 20 min and then a solution of 2,6-bis[(2-chloroethyl)methylaminomethyl]pyridine (**2**) (100 mg, 0.345 mmol) in dry DMF (6 mL) was added. The reaction mixture was heated at 50 °C for 20 h and then concentrated at reduced pressure. The crude product thus obtained was purified by flash column chromatography on silica gel using ethyl acetate/acetone/triethylamine (5:3:1), affording unreacted carbamate **3**. Continued elution with ethyl acetate/methanol/triethylamine (10:2:1) afforded the desired product as an oil. The product was then dissolved in chloroform and precipitated with diethyl ether affording 81 mg (31%) of an orange solid. Mp: 128-130 °C. IR (KBr): υ 3414, 1702, 1638, 1612, 1459, 1383, 1158 cm^{-1}. ^{1}H-NMR ($CDCl_3$): δ 8.49 (s, 2H, H9), 7.85 (d, J = 2.2 Hz, 2H, H4), 7.80 (d, J = 9.0 Hz, 2H, H1), 7.77 (d, J = 9.0 Hz, 2H, H8), 7.35 (t, J = 7.7 Hz, 1H, H4 pyr), 7.30 (dd, J = 9.0, 2.2 Hz, 2H, H2), 7.19 (d, J = 2.2 Hz, 2H, H5), 7.09 (d, J = 7.7 Hz, 2H, H3, H5 pyr), 7.00 (dd, J = 9.0, 2.2 Hz, 2H, H7), 3.95 (t, J = 6.9 Hz, 4H, CH_2N-acridine), 3.68 (s, 6H, OCH_3), 3.55 (s, 4H, CH_2-pyr), 2.63 (t, J = 6.9 Hz, 4H, CH_2NMe), 2.17 (s, 6H, NCH_3). ^{13}C-NMR ($CDCl_3$): δ 158.40 (C2, C6 pyr), 155.86 (CO), 151.16 (C10a), 149.51 (C4a), 148.65 (C6), 143.57 (C3), 136.57 (C4 pyr), 135.42 (C9), 129.72 (C8), 128.57 (C1), 124.63 (C2), 124.06 (C4), 123.20 (C9a), 121.94 (C8a), 120.82 (C3, C5 pyr), 120.15 (C7), 106.00 (C5), 63.77 (CH_2-pyr), 55.46 (CH_2NMe), 52.96 (OCH_3), 48.31 (CH_2N-acridine), 42.52 (NCH_3). MS (ESI) m/z 752 $[M+H]^+$ (calcd for $C_{43}H_{45}N_9O_4$ 751.36). Anal. Calcd for $C_{43}H_{45}N_9O_4$: C, 68.69; H, 6.03; N, 16.77. Found: C, 68.81; H, 6.13; N, 16.49. A stock solution of **4** was prepared in dimethyl sulfoxide (purity ≥ 99.9%) and was stored at –20 °C until use.

Viscometric Titrations. UltraPure™ Calf Thymus DNA (Invitrogen Catalog Number 15633-019, average size ≤ 2000 bp, 10 mg/mL in ddH_2O) was used without further purification. Viscosity experiments were conducted in a Cannon-Ubbelohde size 75 capillary viscometer immersed in a thermostated, circulating water bath maintained at 25 ± 0.2 ºC. Compound **4** was titrated in a Buffer A: 6 mM Na_2HPO_4, 2 mM NaH_2PO_4, 1 mM Na_2EDTA, and 15 mM NaCl (pH 7.0). Alternatively, Cu(II) and Cu(II):**4** (ligand to metal ratio of 1:1) were titrated in Buffer B: 20 mM sodium phosphate (pH 7.0). In three separate titrations, a total of five 10 μL aliquots of each of the following three stock solutions were sequentially added to 1000 μL of the appropriate buffer in the viscometer containing 200 μM bp calf thymus (CT) DNA: (i) **4** (400 μM in Buffer A); (ii) Cu(II):**4** (400 μM each, in Buffer B), and Cu(II) (400 μM in Buffer B). After each sequential addition, the resulting solution was allowed to equilibrate for 15 min before the flow time was recorded with a stopwatch. (The final concentrations of **4**, Cu(II):**4**, and Cu(II) ranged from 4 to 20 μM in each of the three titrations.) The flow times of the buffer and then of the DNA in buffer were also recorded. All measurements were averaged over four trials to an accuracy of $\pm$ 0.2 s. After subtracting the averaged flow time of the buffer, DNA (η_0) and dye-DNA (η) averaged flow times were plotted as $(\eta/\eta_o)^{1/3}$ versus the molar ratio ***r*** of dye to DNA bp *(43)*. Slopes were generated by conducting linear least square fits to these data (KaleidaGraph version 3.6.4 software).

Competition Dialysis Assay. Calf thymus (CT), *Clostridium perfringens* (CP), and *Micrococcus lysodeikticus* (ML) DNAs and the synthetic polynucleotides poly(dA)-poly(dT), $[poly(dGdC)]_2$ and $[poly(dAdT)]_2$ were purchased from Sigma and were used without further purification. A buffer containing 6 mM Na_2HPO_4, 2 mM NaH_2PO_4, 1 mM

Na_2EDTA, and 185 mM NaCl (pH 7.0) was utilized in the preparation of all nucleic acid stock solutions. The concentrations of the nucleic acid solutions were determined by UV-visible spectrophotometry using the λ_{max} values and extinction coefficients listed in Table 3.S1 (Supporting Information). In a buffer consisting of 6 mM Na_2HPO_4, 2 mM NaH_2PO_4, 1 mM Na_2EDTA, and 15 mM NaCl (pH 7.0), competition dialysis experiments were performed as described by Chaires *(44, 45)*. For each dialysis assay, a 0.5 mL volume of DNA (75 μM bp DNA in buffer; Table 3.S1) was pipetted into one of 6 individual Spectra/Por DispoDialyzer units (S135062, Spectrum Laboratories, Inc.). The 6 dialysis units were then placed in a beaker containing 225 mL of a 1.5 μM solution of **4** in buffer. The beaker was covered with Parafilm and wrapped in foil, and its contents were allowed to equilibrate with continuous stirring for 24 h at room temperature (20-22 ºC). At the end of the equilibration period, the DNA solutions inside the dialysis units were carefully transferred to microcentrifuge tubes and a 10.0% (w/v) stock solution of sodium dodecyl sulfate (SDS) was added to give a final concentration of 1.0% (w/v). The DNA-SDS solutions were allowed to equilibrate for 2 h, after which the total concentration of ligand **4** (C_t) was determined by UV-visible absorbance measurements using the extinction coefficient for free ligand **4** in the presence of 1.0% SDS (ε_{451} = 22,716 M^{-1} cm^{-1}). An appropriate correction for the slight dilution of the sample resulting from the addition of SDS stock solution was made. The concentration of free ligand **4** (C_f; ε_{451}= 12,500 M^{-1} cm^{-1}) was also determined spectrophotometrically using an aliquot of the dialysate solution. The amount of DNA-bound **4** (C_b) was calculated by difference ($C_b = C_t - C_f$).

Thermal Melting Studies. Individual 3 mL solutions containing 15 μM bp of calf thymus DNA (Invitrogen Cat. #15633-019) in 20 mM sodium phosphate buffer pH 7.0 or in 20 mM sodium phosphate buffer pH 7.0, 10 μM **4** and/or 10 μM $CuCl_2$ were placed in 3 mL (1 cm) quartz cuvettes (Starna). The DNA was then denatured by increasing the temperature from 25 °C to 100 °C at a rate of 0.5 °C min^{-1} while absorbance was monitored at 260 nm. KaleidaGraph™ Version 3.5 software was used to approximate the first derivative of $\Delta A_{260}/\Delta T$ vs temperature, where the T_m value for each melting transition was marked by the maximum of the first derivative plot.

Photocleavage of Supercoiled Plasmid DNA. Concentration profile reactions were conducted in a volume of 20 μL as follows. A total of 38 μM bp of pUC19 plasmid DNA in 20 mM sodium phosphate buffer pH 7.0 or in 20 mM sodium phosphate buffer pH 7.0, 50 μM, 30 μM, 20 μM, 10 μM, 5 μM, or 2 mM of $CuCl_2$ and/or one mol equiv (50 μM, 30 μM, 20 μM, 10 μM, 5 μM, or 2 μM) of **4** was irradiated for 50 min at 419 nm and 22 °C. A parallel control reaction consisting of 20 mM sodium phosphate buffer pH 7.0, 38 μM bp of pUC19, 50 μM of $CuCl_2$, and 50 μM of **4** was kept in the dark for 50 min.

Individual time course reactions were conducted in a volume of 20 μL. A total of 38 μM bp of pUC19 plasmid DNA in 20 mM sodium phosphate buffer pH 7.0 or in 20 mM sodium phosphate buffer pH 7.0, 50 μM $CuCl_2$ and/or 50 μM **4** was irradiated at 419 nm and 22 °C. The 20 μL reactions were removed from the Rayonet Photochemical Reactor at 10, 20, 30, 40 or 50 min time intervals. Parallel controls consisting of 20 mM sodium phosphate buffer pH 7.0, 38 μM bp of pUC19 plasmid, 50 μM of $CuCl_2$, and/or 50 μM of **4** were kept in the dark for 50 min. After the addition of 3 μL of electrophoresis

loading buffer to the photocleavage reactions (15.0% (w/v) Ficoll, 0.025% (w/v) bromophenol blue), cleavage products were separated on a 1.0% non-denaturing agarose gel stained with ethidium bromide (0.5 μg/mL). To determine the percent conversion of supercoiled plasmid DNA to nicked and linear forms, the gel was visualized on a transilluminator set at 302 nm, photographed, and then quantitated using ImageQuant v. 5.2 software (Amersham Biosciences).

Colorimetric Detection of Copper(I). A series of 500 μL reactions was prepared in which each contained 20 mM sodium phosphate buffer pH 7.0 and one or more of the following reagents: 50 μM of **4**, 50 μM of $CuCl_2$, and 38 μM bp of pUC19 plasmid DNA. The samples were irradiated at 419 nm in the absence and presence of 100 μM of bathocuproinedisulfonic acid disodium salt hydrate, while a parallel set of reactions was kept in the dark. After 50 min, the solutions were visually examined for color change, placed in 500 μL quartz cuvettes, and monitored between 200 nm and 600 nm for evidence of Cu(I)–bathocuproine complex formation. As a positive control, 500 μL samples containing 20 mM sodium phosphate buffer pH 7.0 and 100 μM bathocuproinedisulfonic acid disodium salt hydrate in the presence of 50 μM $CuCl_2$ or 50 μM $CuCl_2$ and 50 μM L-ascorbic acid were reacted at 22 °C for 1 min, after which UV-visible spectra were recorded.

Inhibition of DNA Photocleavage. Twenty μL reactions containing 20 mM sodium phosphate buffer pH 7.0, 38 μM bp pUC19 plasmid DNA, 50 μM of **4**, and 50 μM of $CuCl_2$ were irradiated at 419 nm for 50 min in the presence of either 100 mM sodium azide, 100 mM D-mannitol, 100 U superoxide dismutase, 100 U catalase, or 100 μM bathocuproinedisulfonic acid disodium salt hydrate. Reaction products were then

resolved on a 1.0% non-denaturing agarose gel and quantitated as described above. The percent inhibition of DNA photocleavage was calculated based on a comparison to parallel reactions run in the absence of scavenger or chelator.

DNA Photocleavage at Nucleotide Resolution. *Eco*RI linearized pUC19 plasmid was 3'-end-labeled using Sequenase™ Version 2.0 and [^{35}S]dATPαS according to an established laboratory protocol *(46)*. Unincorporated nucleotides were removed with a G-50 Sephadex spun column. The DNA was then digested with *Fsp*I to produce a restriction fragment 138 bp in length, and resolved on a 2.0% agarose gel. The fragment was excised and DNA was isolated using a QIAquick Gel Extraction Kit purchased from Qiagen. The purified DNA was stored in a total volume of 400 μL of deionized, distilled water at -78 °C.

Typical photocleavage reactions contained 15 μM bp of the 138 bp DNA fragment in 20 mM sodium phosphate buffer pH 7.0 or in 20 mM sodium phosphate buffer pH 7.0, 5 μM **4** and 5 μM $CuCl_2$ (50 μL total volume). The samples were irradiated for 2 h at 419 nm, after which DNA was precipitated with 40 μg glycogen/2.5 volumes EtOH, and washed with 70.0% EtOH. A duplicate set of reactions was precipitated, dissolved in 100 mL of 1.0% piperidine, heated at 90 °C for 30 min, and then lyophilized to dryness. Cleavage products without and with piperidine treatment were dissolved in 4 μL of Sequenase™ Stop Solution (95.0% (v/v) deionized formamide, 10 mM EDTA, 0.1% (w/v) xylene cyanol and 0.1% (w/v) bromophenol blue), denatured for 3 min at 95 °C, and resolved on a 10.0% denaturing polyacrylamide gel adjacent to G, G+A, and T chemical sequencing reactions. To determine yields, the gel was scanned with a FujiFilm Image Reader v. 2.01 Gel Imaging System. The resulting storage-

phosphor autoradiogram was quantitated using FujiFilm ImageGauge v. 3.41 software. The DNA sequencing reactions were performed as previously described *(46)*.

Results and Discussion

Our approach to the design of ligand **4** combines a 2,6-bis(aminomethyl)pyridine-based copper binding moiety and two photochemically active 3,6-acridinediamine groups as DNA recognition elements. The ligand 2,6-bis(aminomethyl)pyridine and its amino-*N*-substituted analogs form stable 1:1 complexes with Cu(II) ($\log Q_{Cu(II)}$ = 15.2-15.7, equilibrium quotient Q = [ML]/[M][L]; *47, 48*). Alternatively, acridine orange, proflavin, and other 3,6-acridinediamines intercalate into DNA and, upon irradiation with visible light, efficiently effect DNA photocleavage *(16, 49-51)*. Therefore, the acridine rings of **4** were intended to increase DNA binding and to initiate DNA photocleavage. We also took into account that cleavage levels might be enhanced by acridine sensitized photoreduction of pyridine-bound copper(II).

Synthesis of Ligand 4. Compound **4** was obtained from 2,6-bis[(2-hydroxyethyl)methylaminomethyl]pyridine (**1**) *(40)*, which upon treatment with thionyl chloride at room temperature for 24 h, followed by basification with sodium carbonate afforded 2,6-bis[(2-chloroethyl)methylaminomethyl]pyridine (**2**) as a brown oil in 65% yield. Compound **2** was reacted with (6-amino-3-acridinyl)carbamic acid methyl ester (**3**) *(41)* in anhydrous DMF with 80% NaH as base at 50 °C for 20 h (Scheme 3.1). Purification of the crude product afforded **4** in 31% yield.

Scheme 3.1. Synthesis of Ligand 4

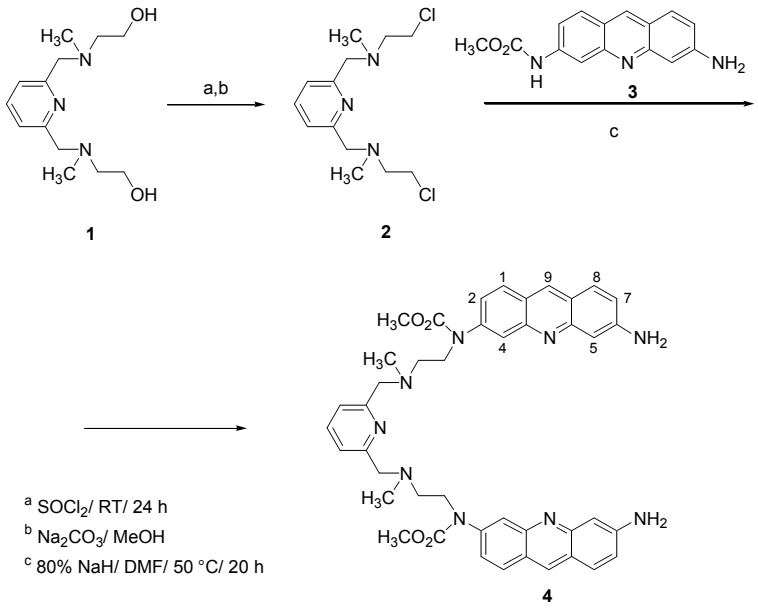

Viscometric Analysis. In order to test for the intercalating ability of **4** and to further examine its behaviour as a groove binder or as a mono- or bis-intercalator, DNA viscosity measurements were conducted. In the process of intercalation, helical DNA unwinds to accommodate planar aromatic ring systems that become inserted in between DNA base pairs. This process is accompanied by an effective increase in contour length that adds to the intrinsic viscosity of the DNA polymer. Because groove binding compounds do not markedly lengthen helical DNA, there is no significant change in viscosity *(52)*. Consequently, viscometric titrations represent a highly reliable method for establishing the binding modes of DNA interacting ligands *(52)*.

The viscometry data for compound **4** and copper(II) are presented as plots of $(\eta/\eta_o)^{1/3}$ (the relative increase in DNA contour length) versus ***r*** (the molar ratio of added compound to DNA base pairs). The contour lengths in the presence (η) and absence (η_o)

of these reagents were calculated by the method of Cohen and Eisenberg *(43)*. Figure 3.1 shows that compound **4** increases the relative contour length of calf thymus DNA as a function of increasing ***r*** and that the slope (0.82) obtained from the $(\eta/\eta_o)^{1/3}$ versus ***r*** plot falls within the range expected for monofunctional intercalators *(53)*. It is conceivable that the lowest energy conformation of **4** is incompatible with the neighbor exclusion principle and therefore permits the intercalation of only one acridine ring. In contrast, the viscometric data of copper(II) with CT DNA yield slopes of -0.12 and 0.41 in the absence and presence of one mol equiv of **4**, respectively. The observed reduction in slope from 0.82 to 0.41 may indicate that interaction of the compound's 2,6-bis(aminomethyl)pyridine linker with copper(II) induces a conformational change that introduces a competing, non-intercalative DNA binding mode, most likely groove binding. Notwithstanding, the increase in the apparent DNA contour length by the copper(II) complex of **4** is still substantial, suggesting some degree of intercalative binding *(54)*.

Electrospray Ionization Mass Spectrometry. Our next goal was to obtain direct evidence of copper(II) complex formation. Ligand **4** was reacted with $CuCl_2$ in HPLC grade methanol at a ligand to metal ratio of 1:1 (90 min, 22 °C), after which a positive-ion electrospray (ESI) mass spectrum was recorded (Figure 3.S1 in Supporting Information). Isotopic distributions of molecular ions corresponding to the following 1:1 metallic complexes were observed: (i) $[\mathbf{4}HCuCl]^{2+}$ between 425 and 428 *m/z* (calcd for $[C_{43}H_{46}N_9O_4CuCl]^{2+}$ 425.13); (ii) $[\mathbf{4}CuCl]^{1+}$ between 849 and 855 *m/z* (calcd for $[C_{43}H_{45}N_9O_4CuCl]^{1+}$ 849.26); and (iii) $[\mathbf{4}HCuCl_2]^{1+}$ between 885 and 892 *m/z* (calcd for $[C_{43}H_{46}N_9O_4CuCl_2]^{1+}$ 885.24).

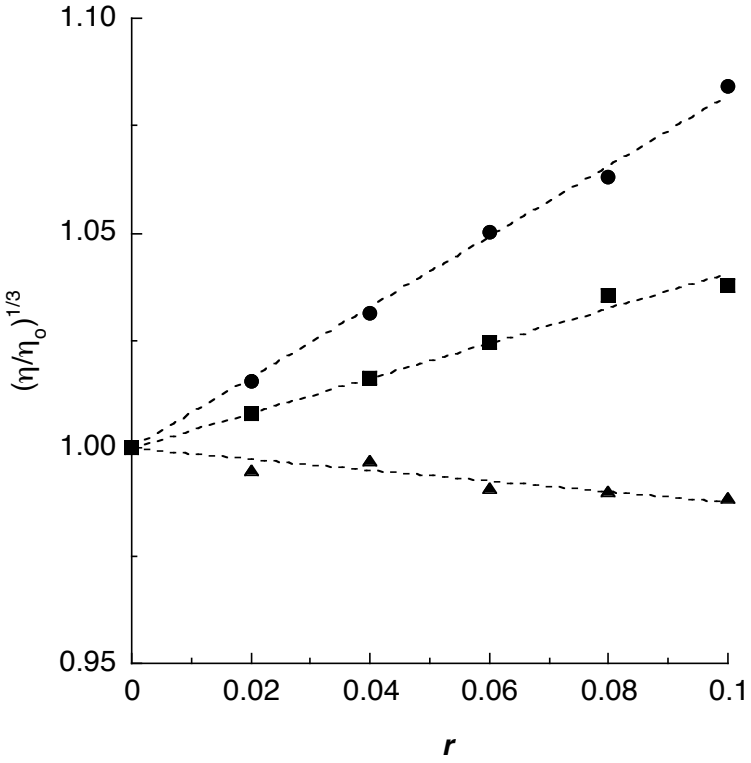

Figure 3.1. Change in relative DNA contour length $(\eta/\eta_o)^{1/3}$ of CT DNA as a function of ***r***, the molar ratio of compound to DNA base pairs. Viscometric titrations were conducted in the presence of: (i) compound **4** (circles; slope = 0.82; 6 mM Na_2HPO_4, 2 mM NaH_2PO_4, 1 mM Na_2EDTA and 15 mM NaCl buffer pH 7.0); (ii) compound **4** and copper(II) at a ligand to metal ratio of 1:1 (squares; slope = 0.41; 20 mM sodium phosphate buffer pH 7.0); (iii) copper(II) (triangles; slope = -0.12; 20 mM sodium phosphate buffer pH 7.0).

Competition Dialysis. The results of dialysis experiments are depicted in a bar graph which shows the concentrations of ligand **4** bound to calf thymus, *Clostridium perfringens,* and *Micrococcus lysodeikticus* DNAs and to the synthetic, double-helical polynucleotides poly(dA)-poly(dT), $[poly(dGdC)]_2$ and $[poly(dAdT)]_2$ (Table 3.S1, Figure 3.2). The data were obtained after equilibrating 1.5 μM of **4** (in the dialysate solution) and 75 μM bp of nucleic acid (in each sample dialysis unit) for 24 h. At the end

of the equilibration period, UV-visible spectra were recorded in order to determine the concentrations of free ligand **4** and DNA-bound **4**. The amount of the DNA-bound ligand was averaged over three trials and the estimated error was between 5-10% for each nucleic acid structure tested. The competition dialysis data were then used to calculate the apparent association constants of ligand **4**, given by $K_{app} = C_b / C_f$ [DNA], where C_b and C_f are the DNA-bound and free ligand concentrations, respectively, and [DNA] is the concentration of DNA in molar base pairs (Table 1).[1] Clearly, the data in Figure 3.2 and Table 3.1 indicate that ligand **4** shows a preference for GC base pairs as exemplified by an increase in levels of binding to ML DNA (71% GC, $K_{app} = 1.26 \times 10^5\ M^{-1}$) relative to CP DNA (31% GC; $K_{app} = 0.85 \times 10^5\ M^{-1}$).

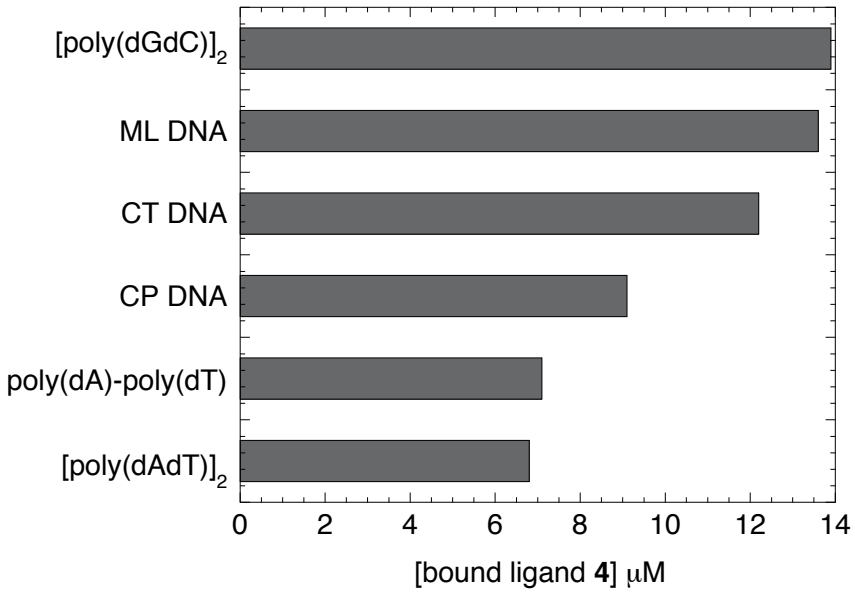

Figure 3.2. The bar graph indicates the concentrations of DNA-bound ligand **4** detected after a 24 h equilibration in competition binding dialysis studies of six DNA sequences.

Table 3.1. Apparent Association Constants Obtained by Competition Dialysis[a]

Deoxyribo Nucleic Acid	K_{app} x10^5 M^{-1}
$[poly(dGdC)]_2$ (100% GC)	1.30
ML DNA (72% GC)	1.26
CT DNA (42% GC)	1.13
CP DNA (31% GC)	0.85
poly(dA)-poly(dT) (0% GC)	0.66
$[poly(dAdT)]_2$ (0% GC)	0.63

[a] The abbreviations ML DNA, CT DNA, and CP DNA correspond to *Micrococcus lysodeikticus,* Calf thymus, and *Clostridium perfringens* DNAs, respectively.

Thermal Melting Studies. The majority of DNA intercalators bind to double-helical DNA through a combination of π-π stacking and electrostatic interactions. As a consequence, double-helical DNA is stabilized, and the melting temperature (T_m) of the duplex is increased as a function of the increasing binding affinity of the intercalator *(55).* Melting temperature (T_m) values of 15 μM bp calf thymus DNA in 20 mM sodium phosphate buffer pH 7.0 were derived from thermal melting curves recorded at 260 nm (Figure 3.3). While 10 μM of Cu(II) had no effect in the absence of the ligand, 10 μM of **4** increased the T_m of calf thymus DNA by 4 °C and 10 °C in the absence and presence of 10 μM concentrations of Cu(II), respectively. Taken together, these data indicate that **4** binds to double-helical DNA, thereby increasing its stability. Duplex stability is then further enhanced by the interaction of **4** with copper(II). In light of the above viscometric data, this result would appear to suggest that groove binding and intercalation of **4** in the presence of Cu(II) might stabilize duplex DNA to a greater degree than simple monointercalation. It is conceivable that complex formation with positively copper might

enhance electrostatic interactions between **4** and the negatively charged phosphate backbone of the DNA duplex. Notwithstanding, the increase in T_m observed when Cu(II) is added to **4** indicates that the apparent DNA association constant K_{app} of the Cu(II) complex of **4** is higher than the K_{app} of the free ligand **4**.[1] The small increases in low temperature absorbance produced by compound **4** and its Cu(II) complex probably arise from thermally induced changes in the ratio of DNA-bound ligand to free ligand (Figure 3.3; *56*).

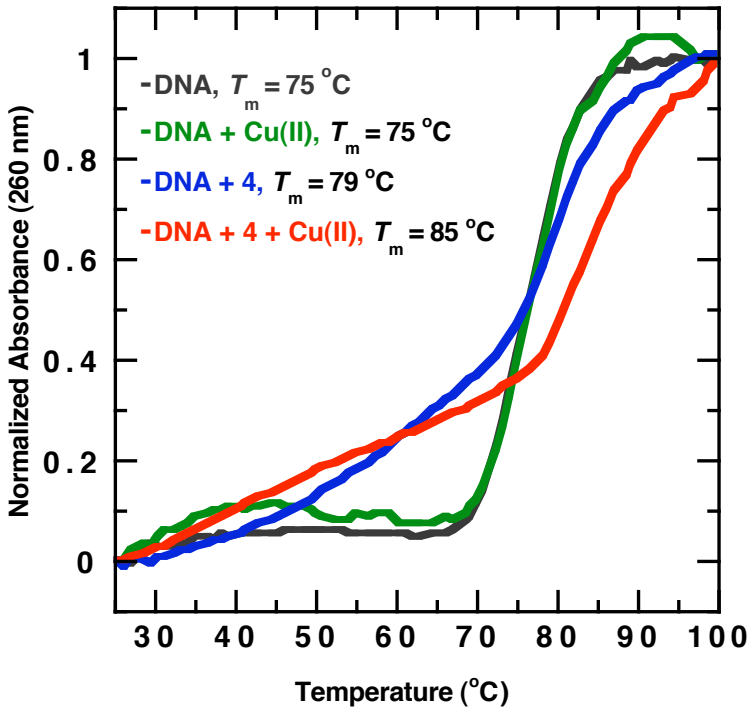

Figure 3.3. Thermal melting curves and T_m values of 15 μM bp calf thymus DNA in the absence and presence of 10 μM **4** and/or 10 μM $CuCl_2$ (20 mM sodium phosphate buffer pH 7.0).

Photocleavage of Supercoiled Plasmid DNA. To detect the formation of DNA frank strand breaks,[2] a preliminary concentration profile was conducted in which individual samples containing 38 μM bp of pUC19 plasmid DNA in 20 mM sodium

phosphate buffer pH 7.0 were equilibrated with 50 μM to 2 μM of **4** in the absence and presence of one mol equiv of $CuCl_2$. The samples were irradiated for 50 min at 419 nm and 22 °C in an aerobically ventilated Rayonet Photochemical Reactor, after which DNA photocleavage products were resolved on a 1.0% non-denaturing agarose gel. The results of the profile showed that one mol equiv of Cu(II) enhanced DNA photocleavage produced by 50 to 20 μM concentrations of compound **4** in a concentration-dependent fashion, with maximum levels of photocleavage occurring in the 50 μM reaction (Figure 3.S2 in Supporting Information).

DNA photocleavage as a function of time was studied next. Reactions consisting of 20 mM sodium phosphate buffer pH 7.0 with 38 μM bp pUC19 plasmid DNA, 50 μM of compound **4**, and 50 μM of $CuCl_2$ were irradiated as described above, except that the reactions were removed at 10 to 50 min time points prior to agarose gel electrophoresis. While 50 μM of intercalator **4** clearly demonstrated time-dependent DNA photocleavage (Figure 3.4, Lanes 1 to 5), reaction yields were markedly enhanced at all time points upon the addition of equivalent concentrations of $CuCl_2$ (Figure 3.4, Lanes 6 to 10). (Virtually no cleavage was observed in parallel control reactions run in the dark; Figure 3.4, Lanes C3 and C4.) Notably, after 50 min of irradiation, supercoiled plasmid was converted into 28% nicked DNA in the presence of Cu(II)/buffer, 55% nicked in **4**/buffer, and 75% nicked plus 18% linear when **4**/Cu(II)/buffer were present in combination (Figure 3.4, Lanes C2, 5, and 10, respectively). Taking into consideration that 15% of photonicked DNA was produced in buffer alone, it is evident that ligand **4** and Cu(II) interact in a synergistic rather than additive fashion. Because photoreduction of Fe(III) is readily effected with visible light by means of electron transfer from the photochemically excited

triplet states of acridine orange and other 3,6-diaminoacridines *(57, 58)*, we hypothesized that a potential source of synergism might involve acridine sensitized photoreduction of pyridine-bound Cu(II). Subsequent reaction of Cu(I) with O_2 would be expected to generate DNA cleaving, reactive oxygen species *(59-61)*.

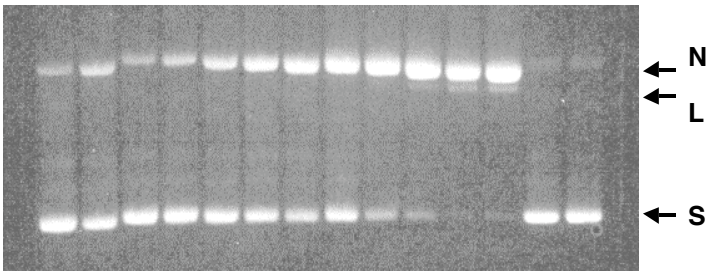

Lane:	C1	C2	1	2	3	4	5	6	7	8	9	10	C3	C4
Irr. (min)	50	50	10	20	30	40	50	10	20	30	40	50	0	0
4	-	-	+	+	+	+	+	+	+	+	+	+	+	+
$CuCl_2$	-	+	-	-	-	-	-	+	+	+	+	+	-	+
% N	15	28	21	26	37	46	55	61	65	70	78	75	11	12
% L	0	0	0	0	0	0	0	0	3	9	12	18	0	0
% S	85	72	79	74	63	54	45	39	32	21	10	8	89	88

Figure 3.4. A photograph of a 1.0% non-denaturing agarose gel showing photocleavage of pUC19 plasmid DNA in the presence of 50 μM of **4** without and with 50 μM of $CuCl_2$ (22 °C, pH 7.0). **C1** and **C2** correspond to DNA irradiated at 419 nm, without and with $CuCl_2$, respectively (no **4**). **C3** and **C4** correspond to DNA treated for 50 min with **4,** without and with $CuCl_2$, respectively (no hν). **Lanes 1-10** correspond to DNA irradiated at 419 nm for 10, 20, 30, 40, and 50 min in the presence of **4**, without and with $CuCl_2$. The above yields corresponding to **C1**, **C2**, **Lane 5,** and **Lane 10** were averaged over three trials with standard deviations of ± 3%, ± 5%, ± 3%, and ± 2%, respectively. S, L, and N designate supercoiled, linear, and nicked forms of pUC19 plasmid DNA.

Colorimetric Detection of Copper(I). Our next goal was to obtain experimental evidence that would substantiate photoreduction of Cu(II) by ligand **4**. We utilized a colorimetric assay based on bathocuproinedisulfonic acid disodium salt hydrate (BCS),

which forms a 2:1 stable, brightly colored orange complex with Cu(I) (λ_{max} = 480 nm; ε = 13,500 M^{-1} cm^{-1}; *62)*. Photolysis reactions in 20 mM sodium phosphate buffer pH 7.0 were irradiated at 419 nm and 22 °C for 50 min in the presence of one or more of the following reagents: 50 μM **4**, 50 μM $CuCl_2$, 38 μM bp pUC19 plasmid DNA, 100 μM BCS, after which UV-visible spectra were immediately recorded (Figure 3.5). Parallel reactions run in the dark were used as negative controls (Figure 3.5 B, D). As a control for BCS-Cu(I) complex formation, 100 μM BCS was reacted with 50 μM $CuCl_2$ in the absence and presence of 50 μM of the reducing agent L-ascorbic acid (Figure 3.5 F).

As expected, the addition of BCS to Cu(II) produced a bright orange color and signature 480 nm absorption in the L-ascorbic acid control reaction (Figure 3.5 F), but not in any of the dark DNA reactions (even those containing **4** and/or Cu(II); Figure 3.5 B, D), and not in any reactions in which BCS was omitted (Figure 3.5 A, B). However, the DNA reaction irradiated in the presence of ligand **4**, Cu(II), and BCS produced a significant orange color change. In addition, a strong hyperchromic absorption band indicative of the formation of a BCS-Cu(I) complex was observed at 472 nm (Figure 3.5 C: DNA + **4** + Cu(II) + BCS). (Spectral overlap with **4** and/or one of its photoproducts most likely accounts for the 8 nm blue shift relative to 480 nm: Figure 3.5 C compared to Figure 3.5 E, F.) Importantly, there was no evidence of BCS-Cu(I) complex formation when **4** was omitted from the photocleavage reaction (Figure 3.5C: DNA + Cu(II) + BCS). When DNA was left out, significant absorption and color were still produced (Figure 3.5 E: **4** + Cu(II) + BCS). Therefore, the BCS data collectively indicate that bis-acridine ligand **4** sensitizes photoreduction of Cu(II) to Cu(I) and that DNA is not required for photoreduction.

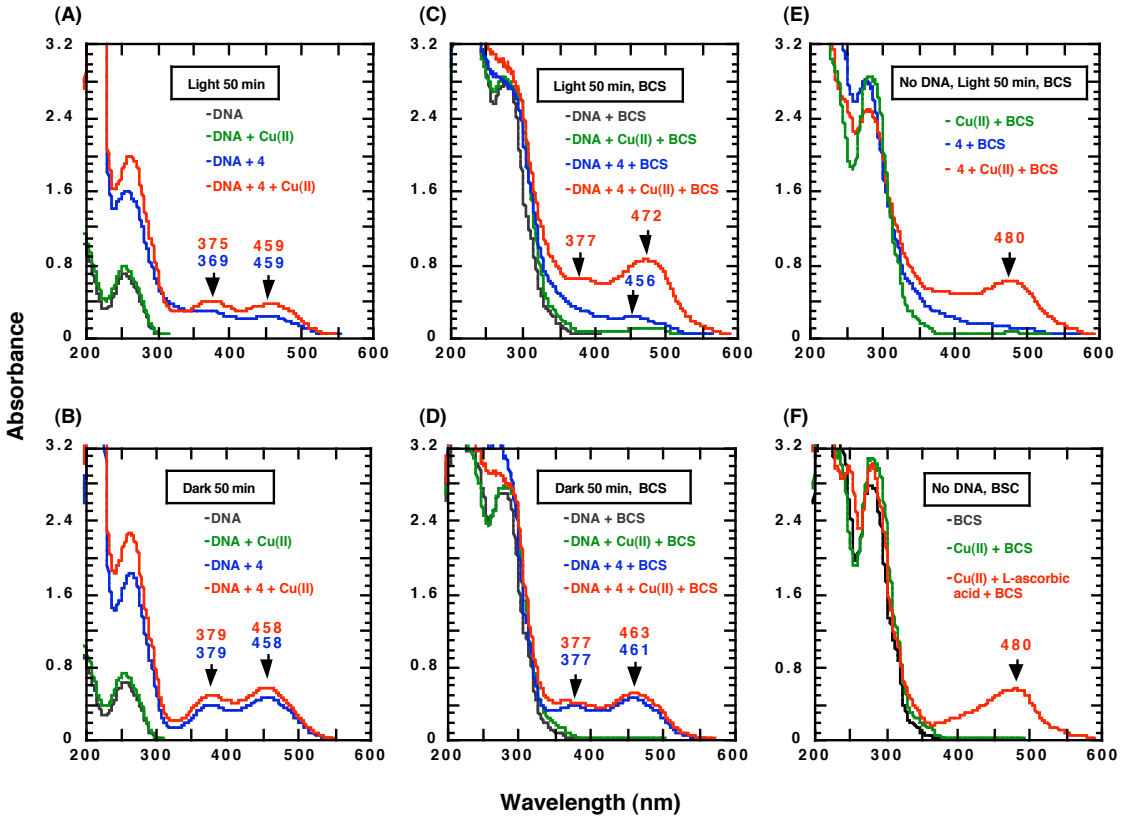

Figure 3.5. UV-visible spectra to assay for Cu(I)-BCS complex formation in 20 mM sodium phosphate buffer pH 7.0, 22 °C.

Inhibition of DNA Photocleavage. To further investigate mechanism(s) underlying the Cu(II)-assisted formation of DNA frank strand breaks, we conducted the following inhibition experiments. Individual photocleavage reactions consisted of 38 μM bp of pUC19 plasmid DNA, 50 μM of **4** and 50 μM of $CuCl_2$ pre-equilibrated with one of the following reagents: the singlet oxygen ($^1O_2$) scavenger sodium azide, the hydroxyl radical (•OH) scavenger D-mannitol, the hydrogen peroxide (H_2O_2) scavenger catalase, the superoxide (O_2•$^-$) scavenger superoxide dismutase (SOD), and the Cu(I)-specific chelating agent BCS. From examination of the data in Table 3.2, it is evident that sodium azide, catalase, and BCS blocked frank stand break formation to a significant degree,

while D-mannitol was almost completely ineffective. Intermediate levels of inhibition were produced by SOD, indicating that superoxide contributes to photocleavage. (SOD produces H_2O_2, which can itself play a part in cleavage and thereby lower inhibition by this enzyme.) Although the piperidine labile lesion 8-hydroxyguanosine is the primary form of DNA damaged produced by singlet oxygen, the relative efficiency of sodium azide implies that singlet oxygen may play a major role: singlet oxygen is capable of cleaving DNA directly by producing frank strand breaks at guanine bases *(63)*. However, because frank strand breaks account for no more than 5% of total DNA damage produced by $^1O_2$ *(64)*, it is conceivable that cleavage inhibition by sodium azide involves a copper-peroxide type complex *(60)* of ligand **4**. The relatively strongly inhibitory effects of catalase and of the Cu(I)-specific chelating agent BCS clearly indicate that hydrogen peroxide and Cu(I) participate in DNA photocleavage. Alternatively, the ineffectiveness of the hydroxyl radical scavenger D-mannitol suggests that freely diffusible hydroxyl radicals do not make a significant contribution. This latter result is consistent with the majority of literature reports in which copper-peroxide type complexes rather than hydroxyl radicals were found to be the principal reactive species involved in DNA cleavage by Cu(II)/Cu(I) redox cycling systems *(59-61, 65)*. A mechanism consistent with the above photocleavage inhibition data is shown in Figure 3.6 *(61)*. It is conceivable that Cu(II) bound to the pyridine linker of ligand **4** is photoreduced to Cu(I), which in turn reacts with hydrogen peroxide to produce a DNA damaging Cu(I)-peroxide complex. Because the colorimetric BCS assay detected Cu(I) only when **4** was present, it can also be inferred that DNA photocleavage involves acridine-sensitized photoreduction of Cu(II) to Cu(I).

Table 3.2. Average % Inhibition of DNA Photocleavage by Scavengers and BCS[a]

Scavenger/chelator	Species Targeted	Percent Inhibition
D-mannitol (100 mM)	•OH	5±1
superoxide dismutase (100 U)	O_2•$^-$	29±1
BCS (100 mM)	Cu(I)	51±2 [b]
catalase (100 U)	H_2O_2	56±2
sodium azide (100 mM)	$^1O_2$	61±3

[a] Individual reactions consisting of 38 μM bp of pUC19 plasmid DNA equilibrated with 50 μM of **4**, 50 μM of $CuCl_2$, and one of the above reagents were irradiated under aerobic conditions at 419 nm for 50 min at 22 °C. Percent inhibition was averaged over three trials with error reported as standard deviation. Final reagent concentrations are in parenthesis. [b] In control experiments, we observed direct photocleavage of DNA by BCS in the absence of **4** (data not shown). Therefore, the 51% inhibition produced by BCS may be lower than the actual % inhibition value.

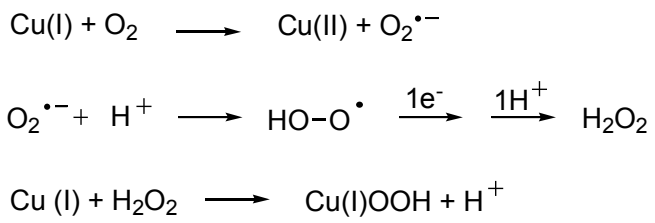

Figure 3.6. A proposed model in which superoxide (O_2•$^-$), hydrogen peroxide (H_2O_2), and Cu(I) contribute to the formation of a Cu(I)-peroxide complex.

DNA Photocleavage at Nucleotide Resolution. In order to map the sequence-specificity of Cu(II)-assisted DNA photocleavage, pUC19 plasmid was linearized with *Eco*RI, 3'-end labeled with [^{35}S]dATPαS, and then cut with *Fsp*I to produce a 138 bp restriction fragment *(58).* Reactions containing 15 μM bp of the radiolabeled DNA fragment in the absence and presence of 5 μM **4** and 5 μM $CuCl_2$ were irradiated at 419 nm for 2 h (20 mM sodium phosphate buffer pH 7.0). Half of the reactions were

subsequently treated with 1.0% piperidine (90 °C, 30 min) in order to produce strand breaks at alkaline labile lesions in the DNA. Products were electrophoresed adjacent to G, G+A, and T chemical sequencing reactions on a 10.0% denaturing polyacrylamide gel, after which cleavage patterns were analyzed. Shown in Figure 3.7 are cleavage plots of a representative 40 bp sequence within the radiolabeled restriction fragment. The top 20 bases producing the highest levels of photocleavage appear in the inset of each plot. In the absence of piperidine, it is evident that the Cu(II) complex of **4** almost always produces frank strand breaks without a marked base preference (Figure 3.7A). This result suggests that photocleavage may involve hydrogen atom abstraction from deoxyribose. Because sugar residues are present in every nucleotide, reagents which function by hydrogen atom abstraction are expected to cleave at all nearby DNA sequences irrespective of base composition *(11)*. Singlet oxygen and direct electron transfer from DNA nucleobases produce DNA damage predominately at guanine bases *(11, 63)*, and are therefore unlikely to have made overriding contributions to the formation of frank strand breaks. Alternatively, the cleavage pattern was changed after the DNA photolysis reactions were treated with piperidine, showing preferential damage at guanine. This result indicates that alkaline labile lesions were formed at guanine bases, either through the production of singlet oxygen and/or by direct electron transfer from DNA (Figure 3.7B).

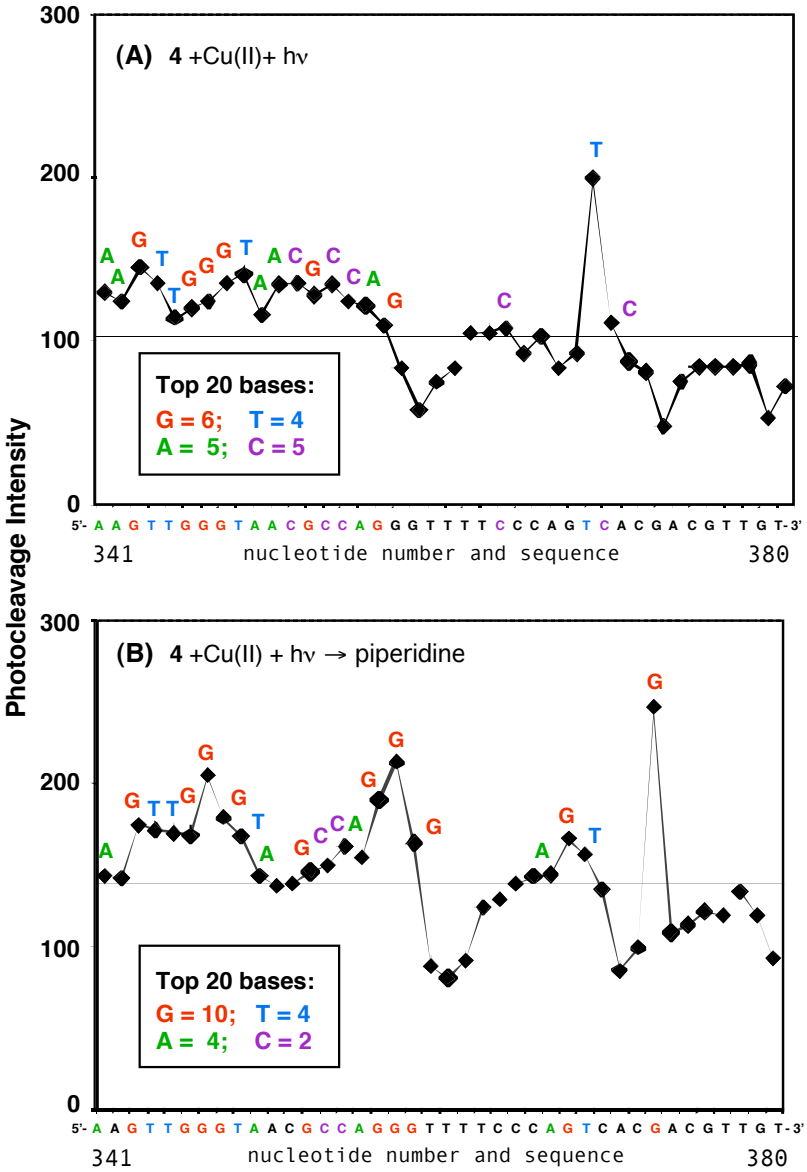

Figure 3.7. Cleavage plots of a representative 40 bp DNA sequence. Photocleavage intensities as a function of DNA base were calculated by quantitating a storage-phosphor autoradiogram of DNA photocleavage products resolved on a 10.0% denaturing polyacrylamide gel (Figure 3.S3 in Supporting Information). A total of 15 μM bp of ^{35}S 3'-end labeled 138 bp restriction fragment was irradiated at 419 nm in the presence of 5 μM **4** and 5 μM $CuCl_2$ without **(A)** and with **(B)** subsequent piperidine treatment. The ordinate is in units of *f*a – *f*c, where *f*a is the fractional cleavage intensity produced in the photocleavage reaction and *f*c is fractional cleavage intensity in a parallel control reaction in which DNA was irradiated in the absence of the Cu(II) complex of compound **4,** without **(A)** and with **(B)** the piperidine treatment. A horizontal line has been drawn through each plot in order to identify the top 20 DNA bases (inset) producing the highest levels of cleavage.

Conclusion

In summary, our data indicate that Cu(II) markedly enhances DNA photocleavage by ligand **4** under near physiological conditions of temperature and pH. Although the precise cleavage mechanism is unknown, at this time we believe that the formation of frank strand breaks may involve acridine sensitized photoreduction of Cu(II) to Cu(I) followed by reaction of **4**/Cu(I) with hydrogen peroxide to form a copper-peroxide complex. Considering the bioavailability of copper at the cellular level, copper-based photonucleases are advantageous in comparison to complexes based on other metals or to chemical nucleases which require an external reducing agent for their activity. To the best of our knowledge, bis-acridine **4** is only the third example of a photonuclease that has been shown to cleave DNA by a process that involves direct photochemical reduction of copper *(14, 15)*. Our future work will focus on mechanistic studies and on synthetic endeavors to develop new copper-based photonucleases for use in chemical and medical applications.

Footnotes

[1] Competition dialysis experiments were conducted at room temperature in sodium phosphate buffer pH 7.0. Under these conditions, the UV-visible spectra of the Cu(II) complex of **4** and of ligand **4** were found to be nearly super imposable. Therefore, the K_{app} of the Cu(II) complex of **4** could not be accurately determined by competition dialysis because the concentration of the Cu(II) complex of **4** versus that of **4** could not be ascertained.

[2] DNA frank strand breaks are defined as single- or double-stranded DNA breaks directly induced by the effects of a cleaving reagent alone, in the absence of subsequent treatment with alkaline or with a secondary amine such as piperidine.

Acknowledgment

We thank Timothy C. Laeger, Prof. Marcus W. Germann, and Prof. W. David Wilson for their assistance (Georgia State University). Support of this research by the CAM-UAH (2005-012; A.L.), the CAM (GR-MAT 2004-0810; M.-M.R.), the National Science Foundation (CHE-9984772; K.B.G.), and the American Chemical Society Petroleum Research Fund (32897-G3; K.B.G.) is gratefully acknowledged.

Literature Cited

(1) Barton, J. K. (1986) Metals and DNA: molecular left-handed complements. *Science 233,* 727-734.

(2) Pyle, A. M., and Barton, J. K. (1990) Probing nucleic acids with transition metal complexes. *Prog. Inorg. Chem. 38,* 413-475.

(3) Erkkila, K. E., Odom, D. T., and Barton J. K. (1999) Recognition and reaction of metallointercalators with DNA. *Chem. Rev. 99,* 2777-2795.

(4) Huber, P. W. (1993) Chemical nucleases: their use in studying RNA structure and RNA-protein interactions. *FASEB J. 7,* 1367-1375.

(5) Pratviel, G., Bernadou, J., and Meunier, B. (1995) Carbon-hydrogen bond of DNA sugar units as targets for chemical nucleases and drugs. *Angew. Chem. Int. Ed. Engl. 34,* 746-769.

(6) Burrows, C. J., and Muller, J. G. (1998) Oxidative nucleobase modifications leading to strand scission. *Chem. Rev. 98,* 1109-1151.

(7) Pratviel, G., Bernadou, J., and Meunier, B. (1998) DNA and RNA cleavage by metal complexes. *Adv. Inorg. Chem. 45,* 251-312.

(8) Cadet, J., and Vigny, P. (1990) The Photochemistry of Nucleic Acids. *Bioorganic Photochemistry* (H. Morrison, Ed.) Vol. 1 pp 1-272, Wiley, New York.

(9) Kochevar, I. E., and Dunn, D. A. (1990) Photosensitized Reactions of DNA: Cleavage and Addition. *Bioorganic Photochemistry* (H. Morrison, Ed.) Vol. 1 pp 273-315, Wiley, New York.

(10) Saito, I., and Nakatani, K. (1996) Design of DNA-cleaving agents. *Bull. Chem. Soc. Jpn. 69,* 3007-3019.

(11) Armitage, B. (1998) Photocleavage of nucleic acids. *Chem. Rev. 98,* 1171-1200.

(12) Barton, J. K., and Raphael, A. L. (1984) Photoactivated stereospecific cleavage of double-helical DNA by cobalt(III) complexes. *J. Am. Chem. Soc. 106,* 2466-2468.

(13) Subramanian, R., and Meares, C. F. (1986) Photosensitization of cobalt bleomycin. *J. Am. Chem. Soc. 108,* 6427-6429.

(14) Kuwahara, J., Suzuki, T., Funakoshi, K., and Sugiura, Y. (1986) Photosensitive DNA cleavage and phage inactivation by copper(II)-camptothecin. *Biochemistry 25,* 1216-1221.

(15) Gude, L., Fernández, M. J., Grant, K. B., and Lorente, A. (2005) Syntheses and copper(II)-dependent DNA photocleavage by acridine and anthracene 1,10-phenanthroline conjugate systems. *Org. Biomol. Chem. 3,* 1856-1862.

(16) Wilson, B., Gude, L., Fernández, M.-J., Lorente, A., and Grant, K. B. (2005) Tunable DNA photocleavage by an imidazole-acridine conjugate. *Inorg. Chem. 44,* 6159-6173.

(17) Spector, W. S. (1956) *Handbook of Biological Data* p 52, W.B. Saunders Company, Philadelphia.

(18) Wacker, W. E. C., and Vallee, B. L. (1959) Nucleic acids and metals. I. Chromium, manganese, nickel, iron, and other metals in ribonucleic acid from diverse biological sources. *J. Biol. Chem. 234,* 3257-3262.

(19) Cantor, K. P., and Hearst, J. E. (1966) Isolation and partial characterization of metaphase chromosomes of a mouse ascites tumor. *Proc. Natl. Acad. Sci. USA 55,* 642–649.

(20) Bryan, S. E., Vizard, D. L., Beary, D. A., LaBiche, R. A., and Hardy, K. J. (1981) Partitioning of zinc and copper within subnuclear nucleoprotein particles. *Nucleic Acids Res. 9,* 5811-5823.

(21) Fürst, P., and Hamer, D. (1989) Cooperative activation of a eukaryotic transcription factor: interaction between Cu(I) and yeast ACE1 protein. *Proc. Natl. Acad. Sci. USA 86*, 5267–5271.

(22) Thiele, D. J. (1992) Metal-regulated transcription in eukaryotes. *Nucleic Acids Res. 20,* 1183–1191.

(23) Mc Millin, D. R., and Mc Nett, K. M. (1998) Photoprocesses of copper complexes that bind to DNA. *Chem. Rev. 98,* 1201-1219.

(24) Eppley, H. J., Lato, S. M., Ellington, A. D., and Zaleski, J. M. (1999) Transition metal kinamycin model as a DNA photocleaver for hypoxic environments: bis(9-diazo-4,5-diazafluorene)copper(II) nitrate. *Chem. Comm.* 2405-2406.

(25) Benites, P. J., Holmberg, R. C., Rawat, D. S., Kraft, B. J., Klein, L. J. Peters, D. G., Thorp, H. H., and Zaleski, J. M. (2003) Metal-ligand charge-transfer-promoted photoelectronic Bergman cyclization of copper metalloenediynes: photochemical DNA cleavage via C-4' H-atom abstraction. *J. Am. Chem. Soc. 125,* 6434-6446.

(26) Dhar, S., and Chakravarty, A. R. (2003) Efficient visible light induced nuclease activity of a ternary mono-1,10-phenanthroline copper(II) complex containing 2-(methylthio)ethylsalicylaldimine. *Inorg. Chem. 42,* 2483-2485.

(27) Dhar, S., Senapati, D, Das, P. K., Chattopadhyay, P., Nethaji, M., and Chakravarty, A. R. (2003) Ternary copper complexes for photocleavage of DNA

by red light: direct evidence for sulfur-to-copper charge transfer and d-d band involvement. *J. Am. Chem. Soc. 125,* 12118-12124.

(28) Dhar, S., Senapati, D., Reddy, P. A., Das, P. K., and Chakravarty, A. R. (2003) Metal-assisted red light-induced efficient DNA cleavage by dipyridoquinoxaline-copper(II) complex. *Chem. Comm.* 2452-2453.

(29) Vaidyanathan, V. G., and Nair, B. N. (2003) Oxidative cleavage of DNA by tridentate copper (II) complex. *J. Inorg. Biochem. 93,* 271-276.

(30) Gupta, T., Dhar, S., Nethaji, M., and Chakravarty, A. R. (2004) Bis(dipyridophenazine)copper(II) complex as major groove directing synthetic hydrolase. *Dalton Trans.* 1896-1900.

(31) Reddy, P. A., Santra, B. K., Nethaji, M., and Chakravarty, A. R. (2004) Metal-assisted light-induced DNA cleavage activity of 2-(methylthio)phenylsalicylaldimine Schiff base copper(II) complexes having planar heterocyclic bases. *J. Inorg. Biochem. 98,* 377-386.

(32) Dhar, S, and Chakravarty, A. R. (2005) Photosensitizer in a molecular bowl: steric protection enhancing the photonuclease activity of copper(II) scorpionates. *Inorg. Chem. 44,* 2582-2584.

(33) Dhar, S., Nethaji, M., and Chakravarty, A. R. (2005) Effect of charge transfer bands on the photo-induced DNA cleavage activity of [1-(2-thiazolylazo)-2-naphtholato]copper(II) complexes. *J. Inorg. Biochem. 99,* 805-812.

(34) Patra, A. K., Dhar, S., Nethaji, M., and Chakravarty, A. R. (2005) Metal-assisted red light-induced DNA cleavage by ternary L-methionine copper(II) complexes of planar heterocyclic bases. *Dalton Trans.* 896-902.

(35) Patra, A. K., Nethaji, M., and Chakravarty, A. R. (2005) Red-light photosensitized cleavage of DNA by (L-lysine)(phenanthroline base)copper(II) complexes. *Dalton Trans*. 2798-2804.

(36) Halliwell, B., and Gutteridge, J. M. C. (1984) Oxygen toxicity, oxygen radicals, transition metals and disease. *Biochem. J. 219,* 1-14.

(37) Linder, M. C. (1991) *Biochemistry of Copper,* Plenium Press, New York.

(38) Peña, M. M., Lee, J., and Thiele, D. J. (1999) A delicate balance: homeostatic control of copper uptake and distribution. *J. Nutr. 129*, 1251-1260.

(39) Chevion, M. (1988) A site-specific mechanism for free radical induced biological damage: the essential role of redox-active transition metals. *Free Radical Bio. Med. 5,* 27-37.

(40) Kady, I. O., and Tan, B. (1995) Metal-catalyzed intramolecular hydrolysis of phosphate esters. *Tetrahedron Lett. 36,* 4031-4034.

(41) Lorente, A., Fernández-Saiz, M., Espinosa, J.-F., Jaime, C., Lehn, J.-M., and Vigneron, J.-P. (1995) Cyclo-bis-intercalands with acridine subunits linked by rigid spacers. *Tetrahedron Lett. 36,* 5261-5264.

(42) Sambrook, J., Fritsch, E. F., and Maniatis, T. (1989) *Molecular Cloning: A Laboratory Manual 2nd ed.,* Cold Spring Harbor Laboratory, Cold Spring Harbor, NY.

(43) Cohen, G., and Eisenberg, H. (1966) Conformation studies on the sodium and cesium salts of calf thymus deoxyribonucleic acid (DNA). *Biopolymers 4*, 429-440.

(44) Ren, J., and Chaires, J. B. (2001) Rapid screening of structurally selective ligand binding to nucleic acids. *Methods Enzymol. 340,* 99-108.

(45) Chaires, J. B. (2002) A competition dialysis assay for the study of structure-selective ligand binding to nucleic acids. *Current Protocols in Nucleic Acid Chemistry,* John Wiley & Sons, New York, p 8.8.1-8.3.8.

(46) Yang, X., and Grant, K. B. (2002) Chemical sequencing of restriction fragments 3'-end-labeled with [^{35}S]dATPαS. *J. Biochem. Biophys. Methods 50,* 123-128.

(47) Couturier, Y., and Petitfaux, C. (1978) Composition and stability of copper complexes and pyridine amine-copper complexes. XI. Comparison of monopyridine mono- and diamines. *Bull. Soc. Chim. France 11-12, Pt. 1*, 435-441.

(48) Garcia Basallote, M., and Martell, A. E. (1988) New multidentate ligands. 29. Stabilities of metal complexes of the binucleating macrocyclic ligand BISBAMP and dioxygen affinity of its dinuclear cobalt(II) complex. *Inorg. Chem. 27*, 4219-4224.

(49) Freifelder, D., Davison, P. F., and Geiduschek, E. P. (1961) Damage by visible light to the acridine orange--DNA complex. *Biophys. J. 1,* 389-400.

(50) Piette, J., López, M., Calberg-Bacq, C. M., and Van de Vorst, A. (1981) Mechanism for strand-break induction in DNA-proflavine complexes exposed to visible light. *Int. J. Radiat. Biol. 40*, 427-433.

(51) Espinosa, J.-F., Fernández, M.-J., Grant, K. B., Gude, L., Rodrigo, M.-M., and Lorente, A. (2004) Synthesis, DNA intercalation and europium(III)-triggered

DNA photocleavage by a bis-proflavine succinamide conjugate. *Tetrahedron Lett. 45,* 4017-4020.

(52) Suh, D. and Chaires, J. B. (1995) Criteria for the mode of binding of DNA binding agents. *Bioorg. Med. Chem. 3,* 723-728.

(53) Chaires, J. B., Leng, F., Przewloka, T., Fokt, I., Ling, Y-H., Pérez-Soler, R., and Priebe, W. (1997) Structure-based design of a new bisintercalating anthracycline antibiotic. *J. Med. Chem. 40*, 261-266.

(54) Pilch, D. S., Kirolos, M. A., Liu, X., Plum, G. E., and Breslauer, K. J. (1995) Berenil [1,3-bis(4'-amidinophenyl)triazene] binding to DNA duplexes and to a RNA duplex: evidence for both intercalative and minor groove binding properties. *Biochemistry 34,* 9962-9976.

(55) Wilson, W. D., Tanious, F. A., and Fernández-Saiz, M. (1997) Evaluation of Drug-Nucleic Acid Interactions by Thermal Melting Curves. in *Drug-DNA Interaction Protocols* (K. R. Fox, Ed.) Humana Press, New Jersey.

(56) Satyanarayana, S., Dabrowiak, J. C., and Chaires, J. B. (1993) Tris(phenanthroline)ruthenium(II) enantiomer interactions with DNA: mode and specificity of binding. *Biochemistry 32*, 2573-2584.

(57) Oster, G. K., and Oster, G. (1959) Photoreduction of metal ions by visible light. *J. Am. Chem. Soc. 81,* 5543-5545.

(58) Kellmann, A. (1974) Primary photochemical processes of cationic acridine orange in aqueous solution studied by flash photolysis. *Photochem. Photobiol. 20,* 103-108.

(59) Yamamoto, K., and Kawanishi. S. (1989) Hydroxyl free radical is not the main active species in site-specific DNA damage induce by copper(II) ion and hydrogen peroxide. *J. Biol. Chem. 264,* 15435-15440.

(60) Li, Y., and Trush, M. A. (1993) DNA damage resulting from the oxidation of hydroquinone by copper: role for a Cu(II)/Cu(I) redox cycle and reactive oxygen generation. *Carcinogenesis* 1303-1311.

(61) Oikawa, S., and Kawanishi, S. (1998) Distinct mechanisms of site-specific DNA damage induced by endogenous reductants in the presence of iron(III) and copper(II*). Biochim. Biophys. Acta 1399,* 19-30.

(62) Wong, A., Huang, H.-C., and Crooke, S. T. (1984) Mechanism of deoxyribonucleic acid breakage induced by 4'-(9-acridinylamino)methanesulfon-m-anisidide and copper: role for cuprous ion and oxygen free radicals. *Biochemistry 23,* 2946-2952.

(63) Devasagayam, T. P., Steenken, S., Obendorf, M. S., Schulz, W. A., and Sies, H. (1991) Formation of 8-hydroxy(deoxy)guanosine and generation of strand breaks at guanine residues in DNA by singlet oxygen. *Biochemistry 30,* 6283-6289.

(64) Di Mascio, P., Wefers, H., Do-Thi, H. P., Lafleur, M. V., and Sies, H. (1989) Singlet molecular oxygen causes loss of biological activity in plasmid and bacteriophage DNA and induces single-strand breaks. *Biochim. Biophys. Acta. 1007,* 151-157.

(65) Masarwa, M., Cohen, H., Meyerstein, D., Hickman, D. L., Bakac, A., and Espenson, J. H. (1988) Reactions of low-valent transition-metal complexes with

hydrogen peroxide. Are they “Fenton-like” or not? 1. The case of Cu^{+} aq and Cr^{2+} aq. *J. Am. Chem. Soc. 110,* 4293-4297.

Supporting Information

Table 3.S1. Nucleic Acid Samples Used in Competition Dialysis Experiments[a]

Deoxyribo Nucleic Acid	λ (nm)	ε (M^{-1}(bp) cm^{-1})
$[poly(dGdC)]_2$ (100% GC)	254	16,800
ML DNA (72% GC)	260	13,846
CT DNA (42% GC)	260	12,824
CP DNA (31% GC)	260	12,476
poly(dA)-poly(dT) (0%GC)	260	12,000
$[poly(dAdT)]_2$ (0% GC)	262	13,200

[a] ε is the molar extinction coefficient at the wavelength l, expressed in terms of DNA base pairs.

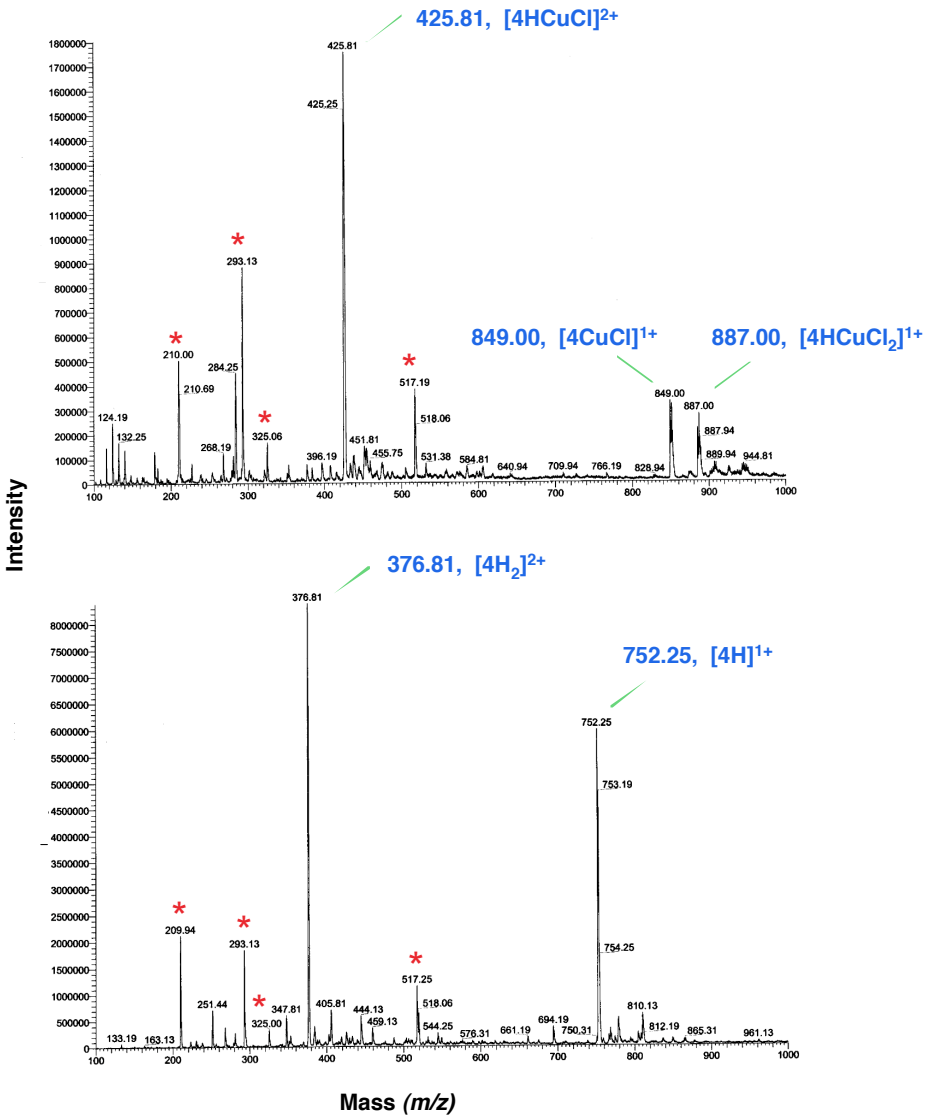

Figure 3.S1. **(A)** Positive ion ESI mass spectrum showing complexes formed between ligand **4** and $CuCl_2$ in HPLC grade methanol at a ligand to metal ratio of 1:1. Isotopic distributions of molecular ions corresponding to the following 1:1 metallic complexes are observed: (i) $[\mathbf{4}HCuCl]^{2+}$ between 425 and 428 *m/z* (calcd for $[C_{43}H_{46}N_9O_4CuCl]^{2+}$ 425.13); (ii) $[\mathbf{4}CuCl]^{1+}$ between 849 and 855 *m/z* (calcd for $[C_{43}H_{45}N_9O_4CuCl]^{1+}$ 849.26); (iii) $[\mathbf{4}HCuCl_2]^{1+}$ between 885 and 892 *m/z* (calcd for $[C_{43}H_{46}N_9O_4CuCl_2]^{1+}$ 885.24). **(B)** Positive ion ESI mass spectrum of ligand **4** in HPLC grade methanol (no $CuCl_2$). The following isotopic distributions of molecular ions corresponding to ligand **4** are observed: (i) $[\mathbf{4}H_2]^{2+}$ between 377 and 378 *m/z* (calcd for $[C_{43}H_{47}N_9O_4]^{2+}$ 376.69); (ii) $[\mathbf{4}H]^{1+}$ between 752 and 755 *m/z* (calcd for $[C_{43}H_{46}N_9O_4]^{1+}$ 752.37). A comparison of the spectra shows that there is no evidence of free ligand **4** in **(A)**. The asterisk identifies peaks in common to both spectra.

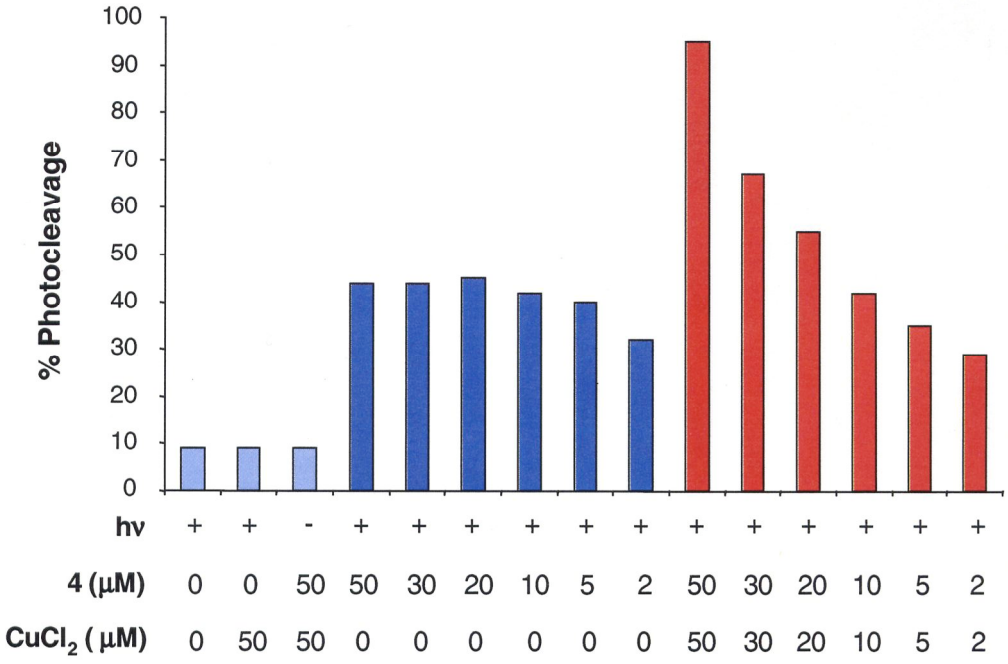

Figure 3.S2. Concentration profile: percent photocleavage of pUC19 plasmid DNA. Reactions contained 20 mM sodium phosphate buffer pH 7.0 and 38 μM bp DNA without and with 50 μM to 2 μM concentrations of $CuCl_2$ and/or compound **4**. The samples were aerobically irradiated at 419 nm for 50 min at 22 ºC. The results showed that nicked DNA was the exclusive cleavage product, with the exception of the reaction irradiated in the presence of 50 μM of $CuCl_2$ and 50 μM of compound **4**. (In this reaction, nicked and linear DNA forms were produced in 87% and 8% yield, respectively.)

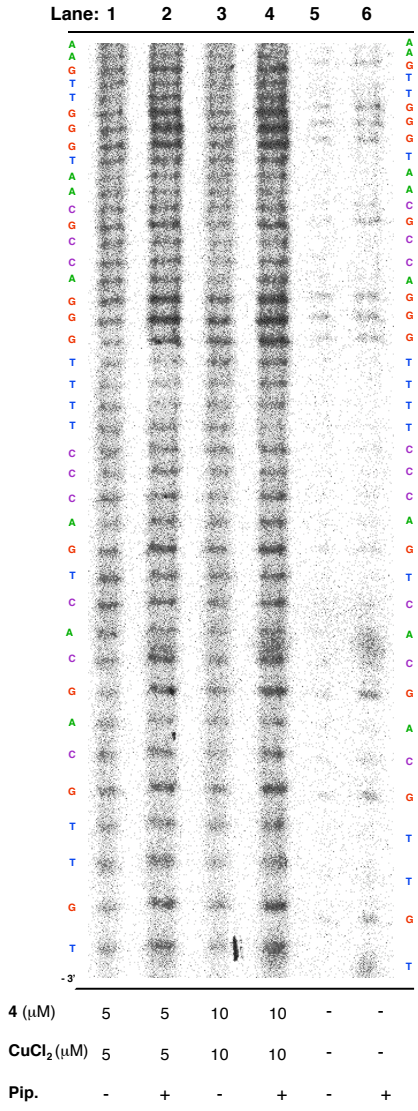

Figure 3.S3. A storage-phosphor autoradiogram of DNA photocleavage products resolved on a 10.0% denaturing polyacrylamide gel. Shown in the gel is a representative 40 bp sequence within an ^{35}S 3'-end labeled 138 bp restriction fragment from pUC19. **Lanes 1, 2:** 15 μM bp the restriction fragment irradiated at 419 nm, in the presence of 5 μM **4** and 5 μM $CuCl_2$, without and with subsequent piperidine treatment. **Lanes 3, 4:** 15 μM bp of the restriction fragment irradiated in the presence of 10 μM **4** and 10 μM $CuCl_2$, without and with subsequent piperidine treatment. **Lanes 5, 6:** 15 μM bp of the restriction fragment irradiated without and with subsequent piperidine treatment (no **4,** no $CuCl_2$). DNA bases are identified to the right and left of the gel. To produce the cleavage plot shown in **Figure 7A** of the accompanying manuscript, **Lane 5** (*f*c) was subtracted from **Lane 1** (*f*a). To produce the cleavage plot shown in **Figure 7B** of the accompanying manuscript, **Lane 6** (*f*c) was subtracted from **Lane 2** (*f*a).

CHAPTER IV

Synthesis and DNA Interactions of a Bis-Phenothiazinium Photosensitizer

(The content of this chapter will be submitted by Wilson, B.; Fernández, M.-J.; Lorente, A.; Grant, K. B. an American Chemical Society journal. The contributions to this project by the author of this dissertation were as follows: design and synthesis of the photosensitizer **3**; conception and execution of all biological, biophysical, and photochemical experiments; and authorship of the original manuscript. Drs. Fernández and Lorente were instrumental in directing the strategies developed for the synthesis of compound **3** as well as made minor revisions to the manuscript. Dr. Grant made extensive revisions to the final manuscript.)

Abstract

We report the synthesis and characterization of *N*,*N*'-bis[(7-dimethylamino)phenothiazin-5-ium-3-yl]-4,4'-ethylenedipiperidine diiodide (**3**), consisting of two photosensitizing phenothiazinium rings attached to a central ethylenedipiperidine linker. At all time points (10, 30, 60 min) and all wavelengths (676, 700, 710 nm) tested, photocleavage of pUC19 plasmid DNA (22 °C and pH 7.0) was markedly enhanced by 1 μM of **3** in comparison to 1 μM of the parent phenothiazine methylene blue (**MB**). In addition, the photocleavage levels produced by 5 to 0.5 μM concentrations of compound **3** were consistently higher than the cleavage levels produced using approximately twice as much **MB** (10 to 1.0 μM). (As an example, 710 nm irradiation of 5 μM of **3** and 10 μM of **MB** cleaved the plasmid DNA in 93% and 71% yields, respectively). Scavenger assays provided evidence for the involvement of DNA damaging singlet oxygen and hydroxyl radicals, whereas analysis of photocleavage products at nucleotide resolution revealed that DNA damage (i.e., frank strand breaks and alkaline-labile lesions) occurred predominantly at guanine bases. While compound **3** and **MB** both appeared to increase duplex stability, the T_m values of calf thymus (CT) and *C.*

perfringens DNAs were increased by 13 ºC and 18 ºC in the presence of compound **3**, in comparison to only 4 ºC and 6 ºC in the presence of **MB**. Finally, viscometric data indicated that CT DNA can interact with compound **3** and **MB** by a combination of groove binding and monofunctional intercalation, and with compound **3** by a third, bisintercalative binding mode.

Introduction

In photodynamic therapy (PDT), photosensitizing drugs are employed to effectively treat a variety of malignant tumors and non-cancerous diseases.[1] PDT offers the advantage of selective localization and light activation of the photosensitizer in diseased tissue, thereby minimizing damage to healthy cells. Notwithstanding, only a few drugs, mostly first and second generation porphyrin derivatives, have been approved clinically.[1a,b] There is now a great interest in the development of alternative photosensitizing agents for use in PDT. An important requirement of PDT is strong absorption of light within a therapeutic window of 600 - 800 nm.[1b] These longer wavelengths reduce light scattering and are more readily transmitted by biological constituents, thereby providing maximal light penetration.

The phenothiazine dye methylene blue (**MB**; Scheme 1) strongly absorbs light at 664 nm (ε = 6.40 x 10^4 M^{-1} cm^{-1} in H_2O). With regards to PDT, **MB** has demonstrated efficient photodynamic activity in several malignant cell lines,[2] murine tumor models,[3] and in the palliation of human esophageal cancer.[4] Additionally, **MB** has exhibited photoinactivation of nosocomial bacterial pathogens[5] and is utilized as a photodecontamining agent in donated blood products.[6b] Specifically, **MB** has been shown to photoinactivate the human immunodeficiency virus in culture media[6a] and in human

plasma.[6b] Recent, preliminary studies have indicated that cell cultures phototreated in the presence of **MB** significantly reduce the infectivity of West Nile virus.[6b]

Methylene blue meets a second important criterion of PDT: low levels of cytotoxicity in the absence of irradiation.[1d] Due to its low toxicity in human cells, **MB** has been employed in histopathology as a tumor delineating agent[7a] and as a radioactive diagnostic tracer for breast cancer.[7b] Low toxicity levels have permitted other non-PDT clinical applications, which include the administration of **MB** as an antidote for nitrate poisoning and as effective treatments for methemoglobinemia and for ifosfamide-induced encephalopathy.[8]

While methylene blue has been reported to accumulate in mitochondria and lysosomes,[9] Rück and co-workers have demonstrated that irradiation triggers the re-localization of **MB** from lysosomes to the cell nucleus.[9a] **MB** is positively charged at physiological pH (pK_a = 12.0),[10] rendering DNA an attractive biological target. In fact, it has been well established that **MB** can non-covalently bind to DNA (K_a = 7-10 x 10^5 M^{-1}), by exhibiting one of two different binding modes (intercalation or groove binding), as a function of DNA sequence.[11] Its close association with DNA is the basis for effective oxidative photodamage by **MB**.[12]

In spite of the many advantages of **MB**, the use of phenothiazine-based chromophores in PDT has remained relatively unexplored. Herein we report the synthesis and characterization of photosensitizer **3** in which two phenothiazine intercalating units are attached by an electron donating ethylenedipiperidine linker. Our goal was to design a reagent capable of photocleaving DNA more efficiently and at longer wavelengths than **MB**.

Results and Discussion

Synthesis. Bis-(phenothiazinium)ethylenedipiperidine salt **3** was synthesized according to Scheme 4.1. The precursors **1** and **2** are both known compounds,[13] and **2** was prepared by making a minor modification to the published literature procedure (chloroform was utilized as solvent instead of methanol). While the syntheses of other 3,7-disubstituted phenothiazin-5-ium salts have been reported,[13,14] the nucleophilic attachment of a linker chain to two equivalents of **2** to form dicationic **3** required the exploration of a number of different solvents (e.g., methanol, chloroform, DMSO) and counterions (e.g, hexafluorophosphate). The synthesis of the iodide salt of **3** was finally achieved in DMF using cesium carbonate as base.

Scheme 4.1[a]

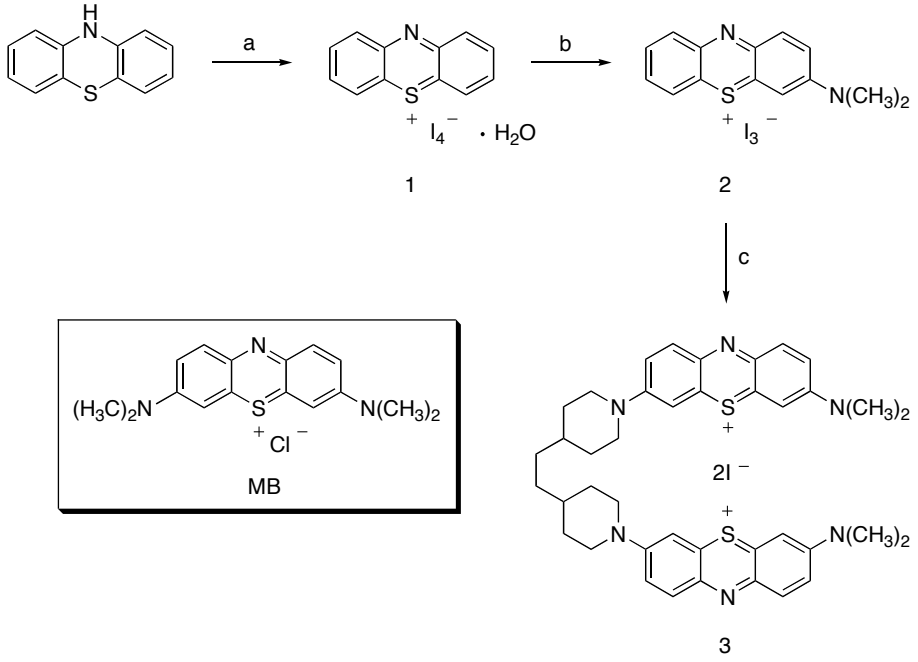

[a] Reagents and conditions: a) I_2, $CHCl_3$, 5 ºC, 2 h, 80%; b) $HN(CH_3)_2$ in CH_3OH, $CHCl_3$, RT, 4 h, 55%; c) 4,4'-ethylenedipiperidine dihydrochloride, Cs_2CO_3, DMF, RT, 48 h, 54%.

UV-Visible Spectrophotometry. In our first set of experiments, we recorded UV/vis absorption spectra of compound **3** and **MB** in the presence and absence of calf thymus (CT) DNA (10 μM phenothiazine, 380 μM bp CT DNA, 10 mM sodium phosphate buffer pH 7.0; Figure 4.1, Table 4.1). The negatively charged surfactant sodium dodecyl sulfate (SDS) was added to samples with no DNA in order to disrupt intermolecular aggregation of **3** and **MB**. Under our experimental conditions, compound **3** exhibited maxima at 676 nm (ε = 1.45 x 10^5 M^{-1} cm^{-1}) and 680 nm (ε = 7.78 x 10^4 M^{-1} (bp) cm^{-1}) in the presence of 1% SDS and DNA, respectively. Alternatively, λ_{max} values for **MB** were 661 nm (ε = 7.84 x 10^4 M^{-1} cm^{-1}) in the presence of 1% SDS and 674 nm (ε = 5.80 x 10^4 M^{-1} (bp) cm^{-1}) in the presence of DNA. It is evident that DNA-bound compound **3** absorbs light more strongly and at longer wavelengths in comparison to **MB** (Figure 4.1, Table 4.S1 in Supporting Infromation).

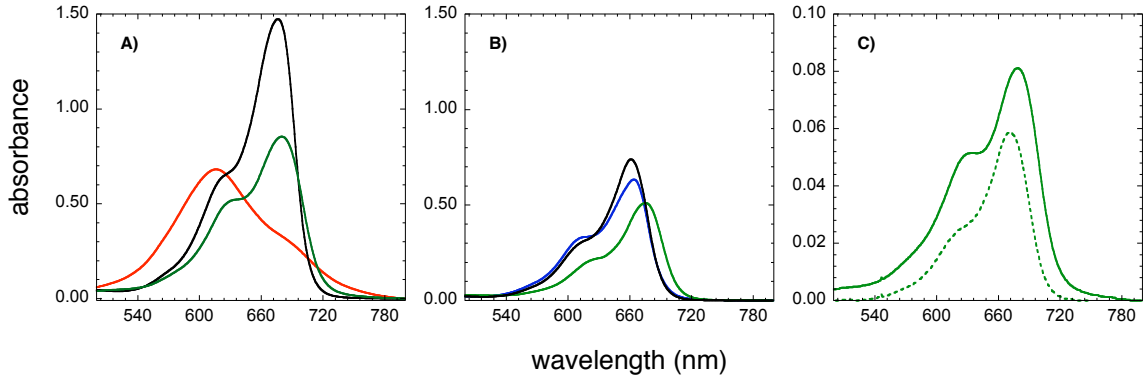

Figure 4.1. UV-visible spectra recorded at 22 ºC in 10 mM sodium phosphate buffer pH 7.0 of **A**) 10 μM compound **3** (red) or of **B**) 10 μM **MB** (blue) in the presence of 380 μM bp calf thymus DNA (green) or 1% sodium dodecyl sulfate (w/v) (black). **C**) 1 μM compound **3** (solid green line) or 1 μM MB (dashed green line) with 38 μM bp calf thymus DNA in 10 mM sodium phosphate buffer pH 7.0. The samples containing DNA were pre-equilibrated for 12 h in the dark at 22 ºC.

Table 4.1. Absorbance Data[a]

compound	λ_{max} (nm)	ε x 10^4 (M^{-1} cm^{-1})	ε x 10^4 (M^{-1}(bp) cm^{-1})
3	615	*nd*	*na*
3 + 1% SDS	676	14.5	*na*
3 + DNA	680	*na*	7.78
MB	664	6.43	*na*
MB + 1% SDS	661	7.84	*na*
MB + DNA	674	*na*	5.80

[a] Extinction coefficients for compound **3** and **MB** were determined in 10 mM sodium phosphate buffer pH 7.0 using solutions containing 1 to 10 μM of dye in the presence and absence of 1% sodium dodecyl sulfate (w/v) or 38 to 380 μM bp calf thymus DNA. The samples containing DNA were pre-equilibrated for 12 h in the dark at 22 ºC. *na* = not applicable; *nd* = not determined due to aggregation in buffer.

Photocleavage Experiments. DNA photocleavage as a function of wavelength (676, 700 and 710 nm) and time (10, 30, 60 min) was studied next. Reactions were carried out in 10 mM sodium phosphate buffer pH 7.0 with 38 μM bp pUC19 plasmid DNA and 1 μM of **3** or **MB**. The samples were aerobically irradiated using a Photon Technology light supply fitted with a 75 W xenon lamp and a monochromator. DNA photocleavage products were then visualized on a 1.0% non-denaturing agarose gel. While both phenothiazines showed time-dependant photocleavage that continued to increase even after 30 min of irradiation, compound **3** exhibited markedly higher levels of cleavage at all time points and all wavelengths tested (Figure 4.2). In Figure 4.1C, the absorbance spectra of 1 μM compound **3** and **MB** in the presence of 38 μM bp calf thymus DNA are shown. The absorption of DNA-bound compound **3** is stronger and more red-shifted than **MB** at the three wavelengths examined (Figure 4.1C, Table 4.S2 in

Supporting Information). The absorbance data (Table 4.S2) are in agreement with the higher levels of photocleavage produced by 1 μM compound **3** in comparison to **MB**. We then used the longest wavelength to compare DNA photocleavage as function of dye concentration. Reactions consisting of 38 μM bp pUC19 plasmid DNA and 10 to 0.25 μM of compound **3** or **MB** were irradiated at 710 nm for 60 min. Compound **3** consistently generated higher levels of DNA photocleavage at all of the six concentrations (Figure 4.3). Notably, irradiation of only 5 μM of dye at 710 nm produced cleavage yields of 93% and 59% for **3** and **MB**, respectively. In addition, the cleavage levels produced by 5 to 0.5 μM concentrations of compound **3** were consistently higher than the cleavage produced using approximately twice the amount of **MB** (10 to 1.0 μM).

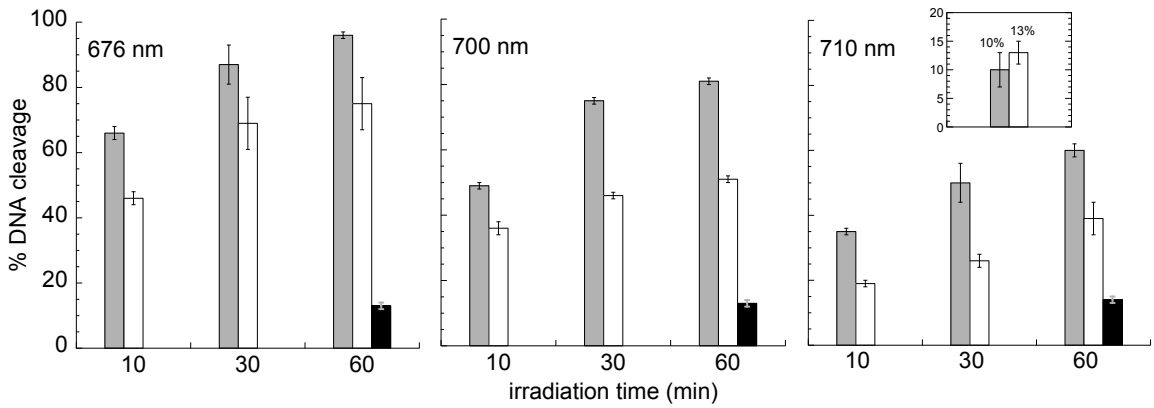

Figure 4.2. DNA photocleavage % of 38 μM bp pUC19 plasmid DNA in the presence of 1 μM compound **3** (gray bars) or 1 μM **MB** (white bars) in 10 mM sodium phosphate buffer pH 7.0 at 22 ºC. The samples were irradiated at: 676, 700, or 710 nm with a 75 W xenon lamp connected to a monochromator. The black bars represent DNA that was irradiated for 60 min in 10 mM sodium phosphate buffer pH 7.0 in the absence of dye. In the inset are dark controls in which 1 μM of **3** and 1 μM of **MB** were reacted with 38 μM bp pUC19 plasmid for 60 min (22 ºC, no hν). DNA cleavage % (% nicked + % linear DNA) was averaged over three trials with error bars representing standard deviation.

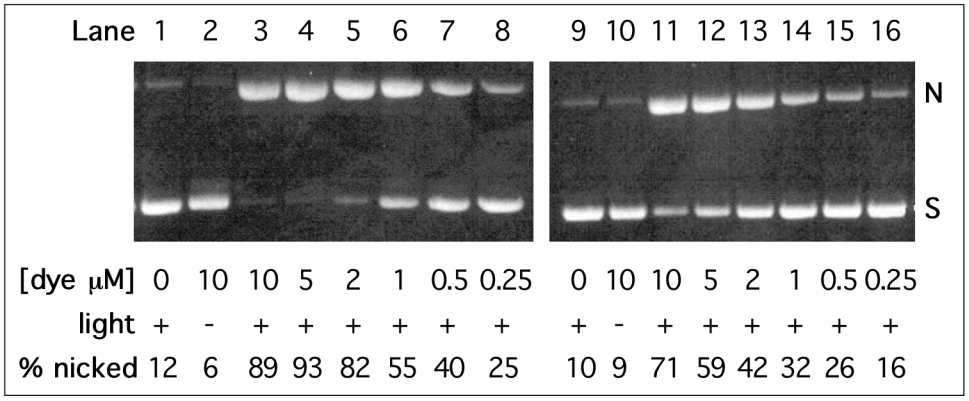

Figure 4.3. Photograph of a 1% nondenaturing agarose gel showing photocleavage of pUC19 plasmid DNA. Samples contained 10 mM sodium phosphate buffer pH 7.0 and 38 μM bp DNA in presence and absence of dye. After being equilibrated for 12 h in the dark at 22 ºC, the samples were aerobically irradiated at 710 nm for 60 min at 22 ºC. Lanes 1 and 9: DNA controls (no dye). Lanes 3 to 8: 10 to 0.25 μM compound **3**. Lanes 11 to 16: 10 to 0.25 μM **MB**. Lanes 2 and 10: 10 μM **3** and 10 μM **MB** (no hν). Abbreviations: **N** = nicked; **S** = supercoiled. It is evident that DNA photocleavage yields increase as a function of increasing dye concentration with one exception, we attribute the slight decrease in photocleavage observed in the presence of 10 μM of compound **3** to DNA precipitation.

Inhibition of DNA Photocleavage. DNA photodamage by **MB** proceeds through Type I (electron transfer) and Type II (energy transfer) pathways.[12] We therefore conducted scavenger experiments to test for DNA damaging Type I hydroxyl radicals (•OH) and DNA damaging Type II singlet oxygen ($^1O_2$). A total of 50 mM of the •OH scavenger D-mannitol or of the $^1O_2$ scavenger sodium azide was added to photolysis reactions containing 1 μM compound **3** or 1 μM **MB** and 38 μM bp plasmid DNA (10 mM sodium phosphate pH 7.0). DNA photocleavage yields in the presence of D-mannitol and sodium azide were reduced by approximately 20% and 48% in reactions containing compound **3** and by 20% and 40% in reactions with **MB** (Table 4.2). These data confirm that Type I and Type II photochemical pathways contribute to phenothiazine-induced DNA photocleavage.

Table 4.2. Percent Inhibition of DNA Photocleavage by Compound **3** and **MB**[a]

compound	D-mannitol	sodium azide
3	20 ± 1	48 ± 2
MB	20 ± 7	40 ± 1

[a] Individual reactions consisted of 38 μM bp pUC19 plasmid DNA, 1 μM compound **3** or 1 μM **MB**, and 50 mM of each of the above reagents in 10 mM sodium phosphate buffer pH 7.0 were aerobically irradiated at 710 nm for 60 min, 22 ºC. Percent inhibition was averaged over three trials with errors reported as standard deviation.

DNA Photocleavage at Nucleotide Resolution. To further investigate mechanism(s) underlying photocleavage, pUC19 plasmid DNA was linearized with *Eco*RI, 3'-end labeled with [^{35}S]dATPαS, and then cut with *Fsp*I to generate a 138 bp restriction fragment. Duplicate sets of reactions containing 15 μM bp of the radiolabeled DNA in 10 mM sodium phosphate buffer pH 7.0 without and with 5 μM of **3** and 5 μM of **MB** were irradiated for 60 min in a ventilated Rayonet Photochemical Reactor fitted with twelve 575 nm lamps (spectral output 400-650 nm). In order to produce DNA strand breaks at alkaline labile lesions, half of the reactions were treated with 1.0% piperidine (90 °C, 30 min) immediately after the 60 min irradiation period. Products were resolved adjacent to G, G+A, and T chemical sequencing reactions on a 10.0% denaturing polyacrylamide gel. Shown in Figure 4.4 are photocleavage plots generated from a representative 40 bp sequence within the 138 bp radiolabeled DNA fragment. In the absence of piperidine, it is evident that the majority of pronounced frank strand breaks produced by compound **3** and **MB** are at guanine bases (Figure 4.4A). This result points to a photocleavage mechanism that involves either singlet oxygen and/or direct electron transfer from DNA nucleobases, as both produce preferential DNA damage at

guanines.[15,16] Figure 4.4A also indicates that hydroxyl radicals are less likely to have made a major contribution to the formation of frank strand breaks. These reactive oxygen species cleave DNA by abstracting hydrogen atoms from deoxyribose. Because sugar residues are present at every nucleotide position, hydroxyl radicals and other reagents which function by hydrogen atom abstraction tend to cleave at all nearby DNA sequences irrespective of the base.[15] (It is interesting to note that the cleavage patterns produced by compound **3** and **MB** are in agreement with the results scavenger experiments summarized in Table 4.2: the higher levels of cleavage inhibition exhibited by sodium azide in comparison to D-mannitol indicate that singlet oxygen, rather than hydroxyl radicals, makes the more significant contribution to the formation of DNA frank strand breaks.) Figure 4.4B shows that levels of damage at guanine bases are dramatically increased after the DNA photolysis reactions are treated with piperidine. This result indicates that **3** and **MB** formed alkaline labile lesions at guanine bases, either through the production of singlet oxygen and/or by direct electron transfer from DNA.

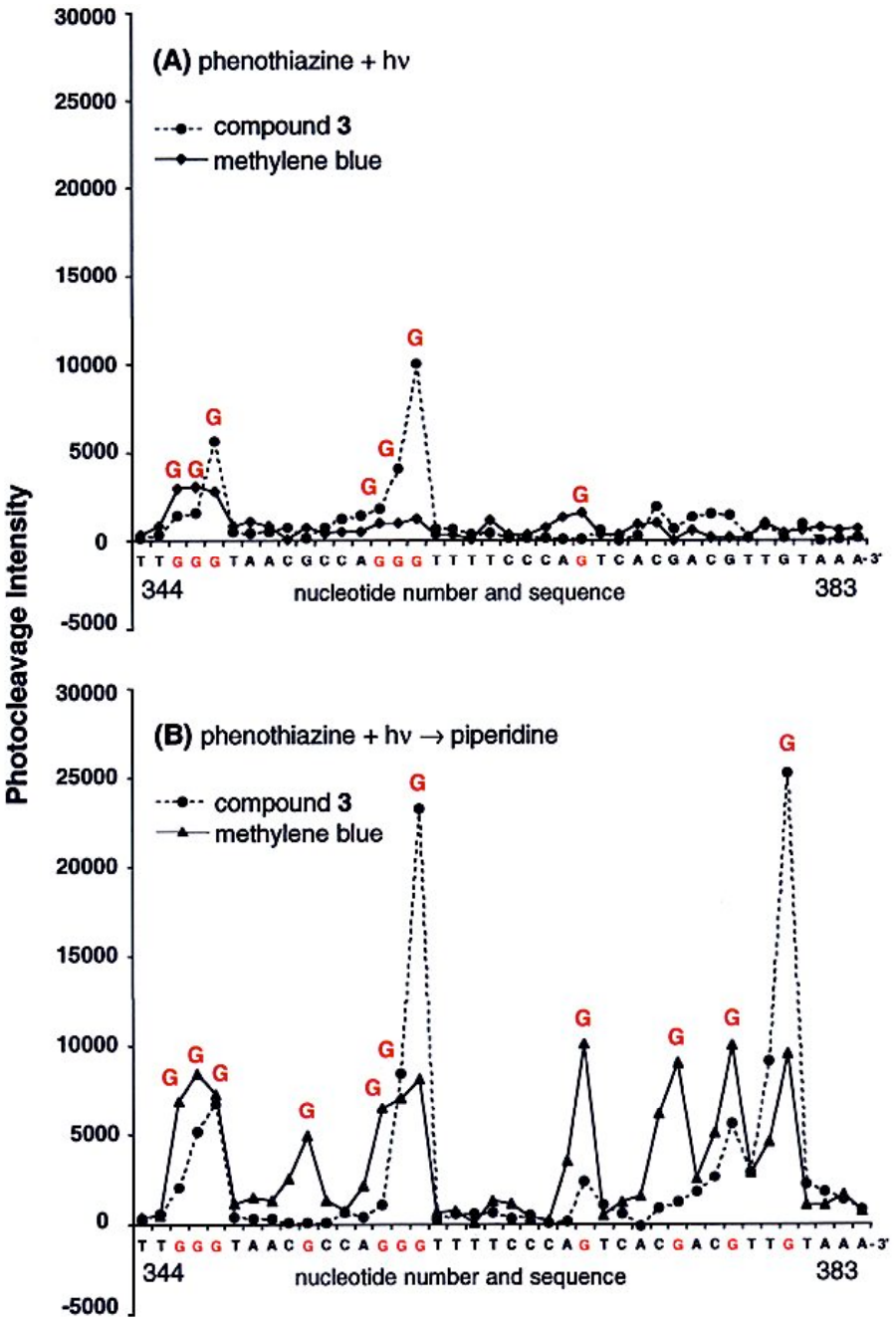

Figure 4.4. Cleavage plots of a representative 40 bp DNA sequence. Photocleavage intensities as a function of DNA base were calculated by quantitating a storage-phosphor autoradiogram of DNA cleavage products resolved on a 10.0% denaturing polyacrylamide gel. A total of 15 μM bp of ^{35}S 3'-end labeled 138 bp restriction fragment was irradiated at 575 nm in the presence of 5 μM **3** and 5 μM **MB** without (**A**) and with (**B**) post-irradiation piperidine treatment.

Thermal Denaturation Studies. Thermal melting studies offer a reliable method for ranking the relative binding affinities of ligands that stabilize duplex DNA. In the process of intercalation and/or groove binding, free energy contributions from π-π, van der Waals, electrostatic and hydrogen bonding interactions stabilize helical DNA. As a result, these forces increase the DNA binding affinity, thereby increasing the melting temperature of the DNA-ligand complex. The melting curves shown in Figure 4.5A were generated at dye to DNA bp molar ratios (**r** = [dye]/[DNA bp]) of 0.0 and 0.3. Under these conditions, the melting temperature (T_m) obtained for 12.5 μM bp CT DNA was 65 ºC, while the addition of compound **3** or **MB** produced T_m values of 78 ºC (ΔT_m = 13 ºC) and 69 ºC (ΔT_m = 4 ºC), respectively. We then recorded thermal melting curves at **r** values ranging from 0.05 to 0.6 (Figure 4.5B). At **r** ≥ 0.3, the ΔT_m values produced by compound **3** (Figure 4.5B) did not change. In the case of **MB**, a plateau in ΔT_m values was not observed by raising the **r** value from 0.3 to 0.6 (Figure 4.5B). The corresponding T_m for **MB** was 69 ºC (ΔT_m = 4 ºC), which is still significantly lower than the T_m of 78 ºC (ΔT_m = 13 ºC), recorded for compound **3** at **r** = 0.3. These data show that compound **3** saturates the DNA binding sites at a lower concentration in comparison to **MB**. Even at the lowest ratio tested (**r** = 0.05), the addition of **3** raised the T_m of CT DNA from 65 ºC to 70 ºC compared to only 66 ºC for **MB**.

In order to further examine the relative DNA binding affinities of compound **3** and **MB**, parallel melting isotherms were generated employing *C. perfringens* DNA (CP) DNA. In comparison to CT DNA (58% AT), CP DNA possesses a slightly higher AT content (69% AT). As shown in Figure 4.6, the T_m of 12.5 μM bp CP DNA is 60 ºC while the addition of **3** or **MB** (**r** = 0.3) raises the T_m by 78 ºC (ΔT_m = 18 ºC) and 66 ºC (ΔT_m = 6

ºC), respectively. Collectively, the melting data indicate that compound **3** effects a 3-fold higher level of duplex stabilization than **MB** with either CT DNA (Figure 4.5A) or CP DNA (Figure 4.6). These results show that higher DNA binding affinity in addition to stronger light absorption exhibited by compound **3** may account for its more efficient DNA photocleaving ability as compared to **MB**.

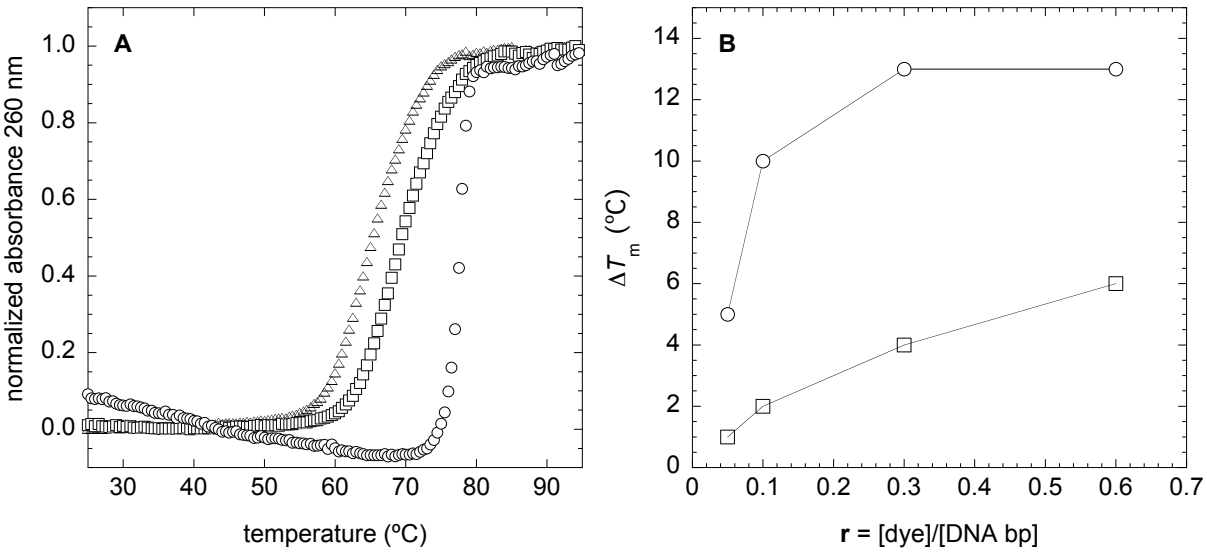

Figure 4.5. Melting curves of: (**A**) 12.5 μM bp CT DNA (Δ, T_m = 65 ºC); 12.5 μM bp CT DNA with 3.75 μM of **MB** (□, T_m = 69 ºC) or with 3.75 μM of **3** (○, T_m = 78 ºC) in 10 mM sodium phosphate buffer pH 7.0 and (**B**) ΔT_m of 12.5 μM bp calf thymus DNA as a function of increasing dye concentration. ○: [compound **3**] = 0.625, 1.25, 3.75, or 7.50 μM. □: [**MB**] = 0.625, 1.25, 3.75, or 7.50 μM.

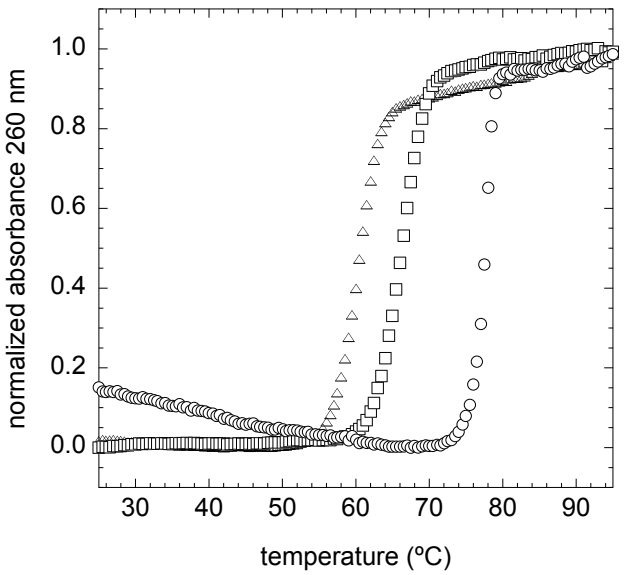

Figure 4.6. Melting curves of: 12.5 μM bp *C. perfringens* (CP) DNA (Δ, T_m = 60 ºC); 12.5 μM bp CP DNA with 3.75 μM of **MB** (□, T_m = 66 ºC) or with 3.75 μM of **3** (○, T_m = 78 ºC) in 10 mM sodium phosphate buffer pH 7.0.

Viscosity Assays. When an intercalator binds to duplex DNA, the helix unwinds and lengthens to accommodate the ligand in between base pairs. This increase in length results in an increase in DNA viscosity. (Groove binding compounds do not lengthen helical DNA and viscosity is not significantly changed.[17]) In the case of classical monointercalators, the slopes observed from plots of the cubed root of the relative viscosity $((\eta/\eta_o)^{1/3})$ versus **r** (molar ratio of bound ligand to DNA bp) range from 0.80 to 1.50.[18] Alternatively, for bisintercalators typical slopes are from 1.3 to 2.3.[18c,19] Figure 4.7 shows that viscometric data of **MB** with CT DNA (42% GC) yields a slope of 0.962 ± 0.002, clearly consistent with monofunctional intercalation, while the slope for compound **3** is 1.50 ± 0.13 and is within the ranges expected for both mono- and bisintercalators. Notwithstanding, **3** increases the viscosity of CT DNA to a significantly greater extent than **MB** (Figure 4.7), leading us to hypothesize that the association of

compound **3** with DNA might involve the existence of multiple binding modes (e.g., concomitant monointercalation, bisintercalation, and/or groove binding). In fact, combinations of these modes are thought to account for DNA viscosity enhancements produced by a number of bifunctional agents with non-ideal slopes (usually lower than twice the slope of the corresponding monointercalator).[20]

To test our hypothesis, we performed viscometric measurements of **3** and **MB** in the presence of additional double-helical sequences. Plots of $(\eta/\eta_o)^{1/3}$ versus **r** for poly(dA)•poly(dT) and alternating poly[(dA-dT)]$_2$ DNAs yielded slopes of 0.22 and 1.18 for compound **3**, and 0.17 and 1.11 for **MB**, respectively (Figure 4.S4 in the Supporting Information). These data indicate the existence of different binding modes as a function of DNA sequence: groove binding for poly(dA)•poly(dT) and monointercalation for poly[(dA-dT)]$_2$. However, taking into consideration the minimal effect of compound **3** on poly(dA)•poly(dT) viscosity, we recorded the circular dichroism (CD) spectra shown in Figure 4.8. The strong, positive induced CD signal at 690 nm confirms the formation of a complex in which **3** associates with the duplex via DNA groove binding.

Our viscosity data are also consistent with a published CD study in which **MB** was shown to bind to poly(dA)•poly(dT) and alternating poly[(dA-dT)]$_2$ via groove binding and intercalation, respectively.[21] We next attempted to measure the viscosity of poly(dG)•poly(dC) and *M. lysodeikticus* (28% AT) DNA, but were unsuccessful due to DNA precipitation in the presence of high concentrations of **3**. Notwithstanding, when the poly(dA)•poly(dT), alternating poly[(dA-dT)]$_2$, and CT DNA (58% AT) slopes are compared side by side, it can be inferred that CT DNA interacts with **MB**

monofunctional intercalation, and with compound **3** by a combination of three modes: groove binding, and mono- and bisintercalation.

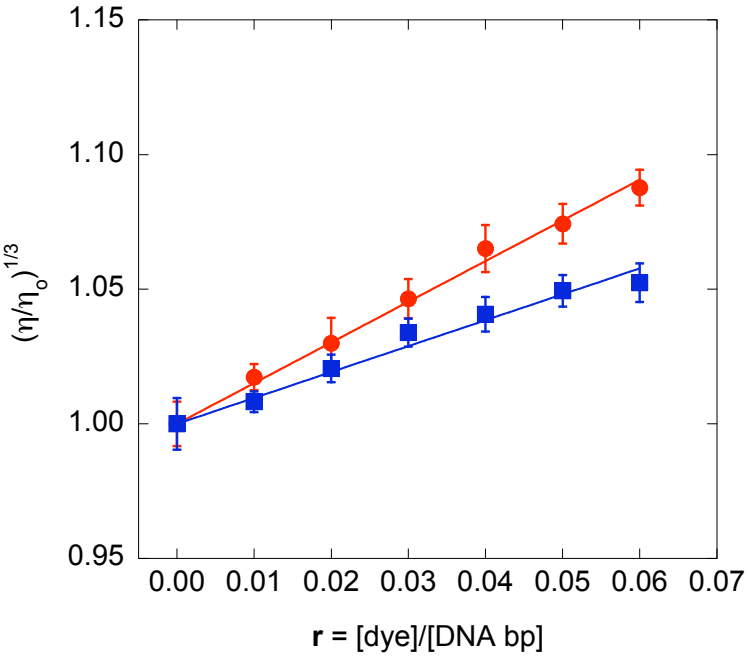

Figure 4.7. Viscometric measurements of CT DNA in the presence of compound **3** (●, slope = 1.50 ± 0.130, R = 0.997) and **MB** (■, slope = 0.962 ± 0.002, R = 0.987). The values were averaged at least over three trials. Error bars represent standard deviation.

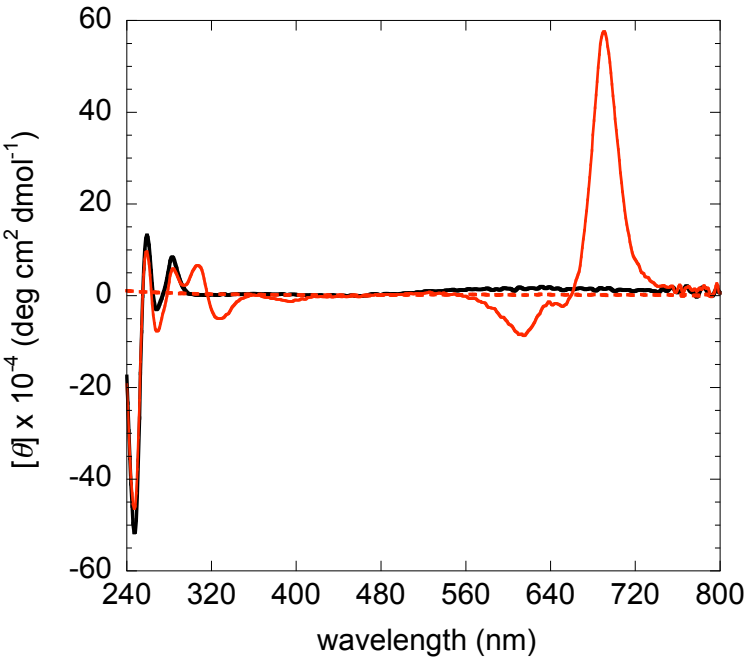

Figure 4.8. CD spectra recorded at 22 ºC of 10 mM sodium phosphate buffer pH 7.0 in the presence and absence of 50 μM bp poly(dA)•poly(dT) DNA or 12 μM of compound **3**. Red dashed line: compound **3**. Red solid line: poly(dA)•poly(dT) DNA. Black Solid line: compound **3** + poly(dA)•poly(dT) DNA.

Conclusion

In summary, we have synthesized a new DNA photocleaving agent (**3**) in which two phenothiazine units are attached by an ethylenedipiperidine linker. In comparison to the phenothiazine methylene blue, this compound absorbs light more strongly at longer wavelengths, exhibits higher levels of photocleavage under near physiological conditions of temperature and pH, and, as indicated by T_m data, associates more strongly with double-helical DNA. Finally, to the best of our knowledge, compound **3** represents the first example of a phenothiazine that binds to DNA through bisintercalation. Our future research efforts will focus on obtaining high-resolution structural data that will aid in the design of new and effective DNA intercalators. We envisage that phenothiazine-based

compounds will represent attractive alternatives to porphyrins for use in phototherapeutic applications.

Experimental Section

General Methods. Melting points were determined in a Stuart Scientific model SMP10 apparatus. Infrared spectra were taken on an FT-IR Perkin Elmer Spectrum One spectrophotometer. ^{1}H and ^{13}C NMR spectra were recorded at 300 and 75 MHz, respectively, on a Varian Unity One instrument. Carbon and proton assignments for compound **3** were based on HMQC experiments. Tetramethyl silane was utilized as an internal reference. Elemental analyses (CHNS) were conducted on a Leco CHNS-932 automatic analyzer while iodine composition was performed by oxygen flask combustion and by ion chromatography (Atlantic Microlabs, Inc. Norcross, GA). Electrospray ionization (ESI) mass spectra were generated on a Micromass Q-Tof hybrid mass spectrometer. Merck silica gel 60 (230-400 ASTM mesh) was employed for flash column chromatography. UV-visible and CD spectra were recorded with a UV-1601 Shimadzu spectrophotometer and a JASCO J-810 spectropolarimeter, respectively. Thermal melting curves were generated using a Cary Bio 300 UV-Vis spectrophotometer .

Distilled, deionized water was utilized in the preparation of all buffers and aqueous reactions. Chemicals were of the highest available purity and were used without further purification. Methylene blue chloride (99.99% purity) was purchased from Fluka. Allyl alcohol, Cesium carbonate, chloroform, dimethylamine (2 M solution in methanol), DMF, dimethyl sulfate, ethidium bromide, 4,4'-ethylenedipiperidine dihydrochloride, formic acid, iodine, 10*H*-phenothiazine, piperidine, potassium permanganate, sodium azide, D-mannitol, sodium phosphate dibasic, and sodium phosphate monobasic were

obtained from the Aldrich Chemical Co. Transformation of *Escherichia coli* competent cells (Stratagene, XL-blue) with pUC19 plasmid (Sigma) and growth of bacterial cultures in Lauria-Bertani broth were performed according to standard laboratory procedures.[22] The plasmid DNA was purified with a Qiagen Plasmid Mega Kit. The restriction enzymes *Eco*RI and *Fsp*I were purchased from New England BioLabs. Ultra Pure™ calf thymus (Invitrogen Lot No. 15633-019, 10 mg/mL, average size ≤ 2000 bp) and *C. perfringens* DNA (Sigma, Lot No. 024K4065, purity ratio A_{260}/A_{280} = 1.9) were used without purification. The DNA polymers poly(dA)•poly(dT) (average size ~6000 bp, Lot No. GD0276), and poly[(dA-dT)]$_2$ (average size ~5183 bp, Lot No. GF0106) were obtained as lyophilized powders from Amersham Biosciences. They were dissolved in 10 mM sodium phosphate pH 7.0 and were used without further purification. The concentrations of all DNA solutions were determined by UV-Vis spectrophotometry using the following extinction coefficients in units of M^{-1} (bp) cm^{-1}: calf thymus DNA, ε_{260} = 12,824; *C. perfringens* DNA, ε_{260} = 12,476; poly(dA)•poly(dT), ε_{260} = 12,000; and poly[(dA-dT)]$_2$, ε_{262} = 13,200.

Phenothiazin-5-ium tetraiodide hydrate (**1**). A solution of 10*H*-phenothiazine (0.566 g, 2.84 mmol) in 20 mL of chloroform was stirred at 5 ºC and iodine (2.16 g, 8.51 mmol) dissolved in 50 mL of chloroform was added drop-wise over 1 h. The reaction mixture was stirred at 5 ºC for an additional h and the progress was monitored by silica gel TLC using chloroform as the solvent. The precipitate from the reaction was then filtered, washed with a copious amount of chloroform and was dried under high vacuum overnight to afford 1.63 g (80% yield) of dark-blue solid **1**; R_f = 0.09 (chloroform); M.p. 170 ºC (decomp.); ^{1}H NMR (300 MHz, Acetone-d_6): δ = 8.01 (m, 2H), 7.92 (m, 2H), 7.64

ppm (m, 4H); ^{13}C NMR (75 MHz, Acetone-d_6): δ = 153.58, 130.67, 129.47, 128.64, 125.50, 123.52 ppm; IR (film): n = 2967, 1558, 1467, 1440, 1311, 1233, 1131, 1067, 1023, 841, 705 cm^{-1}. LRMS (ESI): calcd for $C_{12}H_8NS$ [M$^+$]: 198.0; found: 199.0 [M+H$^+$]$^+$.

3-(Dimethylamino)phenothiazin-5-ium triiodide (**2**). To a solution of phenothiazin-5-ium tetraiodide hydrate (0.400 g, 0.553 mmol) in 20 mL of chloroform was added a 2 M solution of dimethylamine in methanol (0.553 mL, 1.106 mmol) drop-wise over 4 h. The reaction progress was monitored by silica gel TLC (3:7 10% aqueous ammonium acetate/methanol, v/v). The resultant precipitate was filtered, washed with chloroform and allowed to air dry. Product **2** (189 mg, 55% yield) was obtained as a dark-blue solid; R_f = 0.28 (3:7 10% aqueous ammonium acetate/methanol, v/v); M.p. 144 – 145 ºC; ^{1}H NMR (300 MHz, DMSO-d_6): δ = 8.22 (dd, J = 8.0 Hz, J = 1.6 Hz, 1H, H-9), 8.17 (dd, J = 8.0 Hz, J = 1.6 Hz, 1H, H-6), 8.10 (d, J = 10 Hz, 1H, H-1), 8.04 (dd, J = 10 Hz, 1H, H-2), 8.00 (d, J = 2.4 Hz, 1H, H-4), 7.85 (m, 2H, H-7 and H-8), 3.64 and 3.60 ppm (2s, 6H, N(CH$_3$)$_2$); ^{13}C NMR (75 MHz, DMSO-d_6): δ = 156.09, 144.13, 139.81, 139.56, 138.03, 134.55, 133.22, 129.81, 126.27, 126.06, 125.84, 109.66, 43.35, 42.88 ppm; IR (film): ν = 2800, 1617, 1559, 1489, 1429, 1411, 1252, 1118, 1411, 1078, 887, 835, 772 cm^{-1}; LRMS (ESI): calcd for $C_{14}H_{13}N_2S$ [M$^+$]: 241; found: 241. Anal. Calcd for $C_{14}H_{13}N_2SI_3$: C, 27.03; H, 2.11; N, 4.50; S, 5.15; I, 61.20. Found: C, 27.12; H, 1.97; N, 4.46; S, 5.23; I, 60.94.

***N*,*N*'-Bis[(7-dimethylamino)phenothiazin-5-ium-3-yl]-4,4'-ethylenedipiperidine diiodide** (**3**)**.** To a solution of **2** (0.200 g, 0.322 mmol) in 20 mL of DMF were added 4,4'-ethylenedipiperidine dihydrochloride (0.044 g, 0.161mmol) and cesium carbonate (0.629 g, 1.931 mmol). The reaction was vigorously stirred at RT for

48 h and then concentrated under reduced pressure. The progress of the reaction was monitored by silica gel TLC (9.5:0.5 dichloromethane/methanol, v/v). The resultant solid was purified by flash column chromatography (3 cm column, 39 g silica gel) using (9.5:0.5 dichloromethane/methanol, v/v) as the eluent. Then, two successive recrystallizations from methanol afforded 81 mg (54% yield) of dark-blue solid **3**; R_f = 0.2 (9.5:0.5 dichloromethane/methanol, v/v); M.p. > 300 ºC; ^{1}H NMR (300 MHz, $CDCl_3$:CD_3OD): δ = 7.95 (d, *J* = 9.6 Hz , 2H, H-1), 7.94 (d, *J* = 9.6 Hz , 2H, H-9), 7.48 (m, 4H, H-6 and H-8), 7.33 (dd, *J* = 9.6, 2.7 Hz, 2H, H-2), 7.26 (d, *J* = 2.7 Hz, 2H, H-4), 4.42 (d, *J* = 13.5 Hz, 4H, CH_2-α), 3.43 (s, 12H, NCH_3), 3.38 (m, overlap with CH_3OH, 4H, CH_2-α), 2.06 (d, *J* = 11.7 Hz, 4H, CH_2-β), 1.81 (broad, 2H, CH), 1.37 ppm (m, 8H, CH_2-CH_2 and CH_2-β); ^{13}C NMR (75 MHz, $CDCl_3$:CD_3OD): δ = 154.26 and 153.35 (C-3, C-7), 139.16 and 138.66 (C-1, C-9), 136.41, 135.90, 135.79, and 134.78 (C4a, C5a, C9a and C10a), 119.32 and 118.61 (C-2, C-8), 107.12 and 106.39 (C-4, C-6), 49.25 (C-α), 41.61 (NCH_3), 35.82 (CH), 33.02 and 32.85 ppm (C-β, CH_2-CH_2); IR (film): ν = 2907, 1592, 1487, 1389, 1330, 1232, 1133, 1038, 969, 883, 825, 779 cm^{-1}; HRMS (ESI): *m*/*z* calcd for $C_{40}H_{46}N_6S_2$ [M^+]: 674.3225; found: 337.1612 [M^+/2].

UV-Visible Spectrophotometry. Extinction coefficients for compound **3** and **MB** were determined using 500 μL solutions containing 1 to 10 μM of dye in the presence and absence of 38 to 380 μM bp calf thymus DNA in 10 mM sodium phosphate buffer pH 7.0. The solutions were pre-equilibrated for 12 h in the dark, after which spectra were recorded in 1 cm quartz cuvettes at 22 ºC. The absorbance was then plotted as a function of concentration and linear least square fits to these data yielded slopes (KaleidaGraph version 3.6.4 software) that were averaged over three trials. Using the

procedure described above, extinction coefficients in the absence of calf thymus DNA were also recorded in the presence of a final concentration of 1% sodium dodecyl sulfate (w/v).

Photocleavage Experiments. Individual samples consisted of 38 μM bp pUC19 plasmid DNA and 1 μM of compound **3** or **MB** in 10 mM sodium phosphate buffer pH 7.0 (total volume 20 μL). The samples were pre-equilibrated in the dark for 12 h at 22 ºC, after which they were kept in the dark or aerobically irradiated at 676, 700 or 710 nm for 10, 30, or 60 min at 22 ºC using a Photon Technology Inc. Model A1010 light supply fitted with a 75 W xenon lamp and a monochromator with a grating (blazed at 500 nm, 1200 lines/mm, 20 nm slit width). After irradiation, cleavage products were electrophoresed on a 1% nondenaturing agarose gel stained with ethidium bromide (0.5 μg/mL), visualized on a transilluminator set at 302 nm, photographed and scanned. The amounts of supercoiled, nicked, and linear plasmid DNA were quantitated by densitometry using ImageQuant version 5.2 software (Amersham Biosciences). In DNA photocleavage as a function of concentration, reactions consisted of 10 to 0.0 μM compound **3** or **MB** with 38 μM bp pUC19 plasmid DNA in 10 mM sodium phosphate buffer pH 7.0 (total volume 20 μL). The samples were pre-equilibrated in the dark for 12 h at 22 ºC, after which they were kept in the dark or aerobically irradiated at 710 nm for 60 min. Photocleavage yields were calculated using the formula [(nicked DNA + linear DNA)/total DNA] x 100. The density of supercoiled DNA was multiplied by a correction factor of 1.22 to account for the decreased binding affinity of ethidium bromide to supercoiled DNA as compared to the nicked and linear forms.

Inhibition of DNA Photocleavage. Immediately prior to irradiation, a final concentration of 50 mM of sodium azide or of D-mannitol was added to individual 20 μL reactions. Each consisted of 38 μM bp pUC19 plasmid DNA pre-equilibrated with 1 μM of compound **3** or **MB** in 10 mM sodium phosphate buffer pH 7.0 in the dark for 12 h at 22 ºC. Control reactions containing 1 μM of compound **3** or **MB**, 38 μM bp pUC19 plasmid, and 10 mM sodium phosphate buffer pH 7.0 were run in the absence of scavenger. The samples were then aerobically irradiated at 710 nm using a Photon Technology Inc. light supply (Model A1010) fitted with a 75 W xenon lamp and monochromator with a grating (blazed at 500 nm, 1200 lines/mm, 20 nm slit width) for 60 min at 22 ºC. Reaction products were resolved on a 1.0% nondenaturing agarose gel and quantitated as described above. The percent inhibition of DNA photocleavage was calculated as follows: [((% cleavage without scavenger) - (% cleavage with scavenger))/(% cleavage without scavenger)] x 100.

DNA Photocleavage at Nucleotide Resolution. *Eco*RI linearized pUC19 plasmid was 3'-end-labeled using Sequenase™ Version 2.0 (USB Scientific) and [^{35}S]dATPαS (GE Healthcare) according to an established laboratory protocol.[23] Unincorporated nucleotides were removed with a G-50 Sephadex spun column (Roche Diagnostics). The DNA was then digested with *Fsp*I to produce a restriction fragment 138 bp in length, and resolved on a 2% agarose gel. The fragment was excised and DNA was isolated using a QIAquick Gel Extraction Kit purchased from Qiagen. The purified DNA was stored in a total volume of 400 μL of deionized, distilled water at -78 °C.

Typical photocleavage reactions contained 15 μM bp of the 138 bp DNA fragment in 10 mM sodium phosphate buffer pH 7.0 or in 10 mM sodium phosphate

buffer pH 7.0, 5 μM **3** and **MB** (50 μL total volume). The reaction samples were pre-equilibrated in the dark, 22 ºC for 2 hours and then were aerobically irradiated in a ventilated Rayonet Photochemical Reactor (Southern New England Ultraviolet Co.) fitted with twelve 575 nm lamps (spectral output 400-650 nm) for 60 min. The photolyzed DNA was precipitated with 40 μg glycogen/2.5 volumes neat EtOH, and washed with 70% EtOH. A duplicate set of reactions was precipitated, dissolved in 100 μL of 1.0% piperidine, heated at 90 °C for 30 min, and then lyophilized to dryness. Cleavage products without and with piperidine treatment were dissolved in 4 μL of Sequenase™ Stop Solution (95% (v/v) deionized formamide, 10 mM EDTA, 0.1% (w/v) xylene cyanol and 0.1% (w/v) bromophenol blue), denatured for 3 min at 95 °C, and resolved on a 10.0% denaturing polyacrylamide gel adjacent to G, G+A, and T chemical sequencing reactions. To determine yields, the gel was scanned with a Storm 860 PhosphoImager (Molecular Dynamics). The resulting storage-phosphor autoradiogram was quantitated using ImageQuant 5.2 software (Molecular Dynamics). The DNA sequencing reactions were performed as previously described.[23]

Thermal Denaturation Studies. Individual 3 mL solutions containing 10 mM sodium phosphate buffer pH 7.0 and 12.5 μM bp calf thymus DNA in the presence and absence of 0.625 to 7.50 μM of compound **3** or **MB** in were placed in 3 mL (1 cm) quartz cuvettes (Starna). Similarly, 12.5 μM bp *C. perfringes* DNA was utilized in the absence and presence of 3.75 μM compound **3** or 3.75 μM **MB**. After the samples were equilibrated in the dark for 12 h and 22 ºC, absorbance was monitored at 260 nm while the DNA was denatured using a Peltier heat block programmed to increase the temperature from 25 to 95 ºC at a rate of 0.5 ºC min^{-1}. KaleidaGraph version 3.6.4

software was then used to approximate the first derivative of $\Delta A_{260}/\Delta T$ versus temperature, where the T_m value corresponded to the maximum of each first derivative plot.

Viscosity Assays. In a total volume of 1 mL, individual solutions containing 10 mM sodium phosphate buffer pH 7.0 and 200 μM bp of calf thymus DNA (average length ≤ 2000 bp) in the absence and presence of 2 to 12 μM of compound **3** or **MB** were pre-equilibrated for 12 h in the dark at 22 ºC. DNA viscosity was then measured in a Cannon-Ubbelohde size 75 capillary viscometer immersed in a thermostated water bath maintained at 25 ± 0.1 ºC. The flow times of the buffer, DNA in buffer, and dye-DNA in buffer were measured with a stopwatch. The measurements were averaged over four trials to an accuracy of ± 0.2 s. After subtracting the averaged flow time of the buffer, DNA (η_0) and dye-DNA (η) averaged flow times were plotted as $(\eta/\eta_o)^{1/3}$ versus the molar ratio of dye to DNA bp.[24] Slopes were generated by conducting linear least square fits to these data (KaleidaGraph version 3.6.4 software). The viscosity measurements containing poly(dA)•poly(dT) (average length ~6000 bp) and poly[(dA-dT)]$_2$ (average length ~5183 bp) were conducted exactly as described for calf thymus DNA except that DNA concentrations were decreased to account for the longer average lengths of these polymers as compared to calf thymus DNA. Accordingly, measurements were conducted with 50 μM bp of each polymer and 0.5 to 3 μM of compound **3** or **MB** such that dye to DNA bp molar ratios were consistent with the calf thymus DNA measurements. While the conventional method for performing viscosity assays involves titration of the ligand into a DNA solution inside the viscometer, here we report an alternative and efficient technique that may be particularly useful for **3** as well as for other phenothiazines (e.g.,

1,9-dimethyl methylene blue and methylene blue) where pre-equilibration with DNA is required to reduce ligand stacking associations in solution.[25]

Circular Dichroism Analysis. Samples consisted of 10 mM sodium phosphate buffer pH 7.0 and 12 μM of compound **3** in the presence and absence of 50 μM bp poly(dA)•poly(dT) DNA in a total volume of 500 μL. After equilibration in the dark for 12 h at 22 ºC, spectra were recorded from 800 to 200 nm at 22 ºC in a 0.5 cm quartz cuvette using a scan rate of 100 nm/min and a time constant of 1 s. The spectra were averaged over 4 acquisitions and were baseline-corrected to remove signals generated by the buffer.

References

(1) (a) Dolmans, D. E. J. G. J.; Fukumura, D.; Jain, R. K. *Nat. Rev. Cancer* **2003**, *3*, 380-387; (b) Vrouenraets, M. B.; Visser, G. W. M.; Snow, G. B.; van Dongen, G. A. M. S. *Anticancer Res.* **2003**, *23,* 505-522; (c) Huang, Z. *Technol. Cancer Res. Treat.* **2005**, *4*, 283-293; (d) Nowis, D.; Makowski, M.; Stoklosa, T.; Legat, M.; Issat, T.; Golab, J. *Acta Biochim. Pol.* **2005**, *52*, 339-352.

(2) (a) Boehncke, W-H.; Rück, A.; Naumann, J.; Sterry, W.; Kaufmann, R. *Laser. Surg. Med.* **1996**, *19*, 451-457; (b) Stockert, J. C.; Juarranz, A.; Villanueva, A.; Cañete, M. *Cancer Chemother. Pharmacol.* **1996**, *39*, 167-169; (c) Wainwright, M.; Phoenix, D. A.; Burrow, S. M.; Waring, J. *J. Chemother.* **1999**, *11*, 61-68; (d) Rice, L.; Wainwright, M.; Phoenix, D. A. *J. Chemther.* **2000**, *12*, 94-104.

(3) (a) Orth, K.; Russ, D.; Beck, G.; Rück, A.; Beger, H. G. *Langenbeck. Arch. Surg.* **1998**, *383*, 276-281; (b) Orth, K.; Beck, G.; Genze, F.; Rück, A. *J. Photochem. Photobiol. B.* **2000**, *57*, 186-192.

(4) Orth, K.; Rück, A.; Stanescu, A.; Beger, H. G. *Lancet* **1995**, *345*, 519-520.

(5) (a) Wainwright, M.; Phoenix, D. A.; Laycock, S. L.; Wareing, D. R. A.; Wright, P. A. *FEMS Microbiol. Lett.* **1998**, *160*, 177-181; (b) Wainwright, M.; Phoenix, D. A.; Gaskell, M.; Marshall, B. *J. Antimicrob. Chemother.* **1999**, *44*, 823-825.

(6) (a) Owada, T.; Yamada, Y.; Abe, H.; Hirayama, J.; Ikeda, H.; Sekguchi, S.; Ikebushi, K. *J. Med. Virol.* **2000**, *62*, 421-425; (b) Floyd, R. A.; Schneider, J. E. Jr.; Dittmer, D. P. *Antiviral Res.* **2004**, *61*, 141-151.

(7) (a) Fukui, Y.; Yamakawa, T.; Taniki, T.; Numoto, S.; Miki, H.; Monden, Y. *Cancer* **2001**, *92,* 2868-2874; (b) Eldrageely, K.; Vargas, M. P.; Khalkhali, I.;

Venegas, R.; Burla, M.; Gonzalez, K. D.; Vargas, H. I. *Am. Surg.* **2004**, *70*, 872-875.

(8) Harris, F.; Chatfield, L. K.; Phoenix, D. A. *Curr. Drug Targets* **2005**, *6*, 615-627.

(9) (a) Rück, A.; Köllner, T.; Dietrich, W. S.; Schneckenburger, H. *J. Photochem. Photobiol. B.* **1992**, *12*, 403-412; (b) Noodt, B. B.; Rodal, G. H.; Wainwright, M.; Peng, Q.; Horobin, R.; Nesland, J. M.; Berg, K. *Int. J. Cancer* **1998**, *75*, 941-948.

(10) Harris, R. G.; Wells, J. D.; Johnson, B. B. *Colloids Surf. A Physiochem. Eng. Asp.* **2001**, *180*, 131-140.

(11) Tuite, E. M.; Kelly, J. M. *Biopolymers* **1995**, *35*, 419-433.

(12) Tuite, E. M.; Kelly, J. M. *J. Photochem. Photobiol. B.* **1993**, *21*, 103-124.

(13) Strekowski, L.; Hou, D-F.; Wydra, R. L. *J. Heterocyclic Chem.* **1993**, *30*, 1693-1695.

(14) (a) Leventis, N.; Chen, M.; Sotiriou-Leventis, C. *Tetrahedron* **1997**, *53*, 10083-10092; (b) Mellish, K. J.; Cox, R. D.; Vernon, D. I.; Griffiths, J.; Brown, S. B. *Photochem. Photobiol.* **2002**, *75*, 392-397.

(15) Armitage, B. *Chem. Rev.* **1998**, *98,* 1171-1200.

(16) Devasagayam, T. P.; Steenken, S.; Obendorf, M. S.; Schulz, W. A.; Sies, H. *Biochemistry* **1991**, *30,* 6283-6289.

(17) Suh, D.; Chaires, J. B. *Bioorg. Med. Chem.* **1995**, *3*, 723-728.

(18) (a) Drummond, D. S.; Pritchard, N. J.; Simpson-Gildemeister, V. F. W.; Peacocke, A. R. *Biopolymers* **1966**, *4*, 971-987; (b) Kubota, Y.; Hashimoto, K.; Fujita, K.; Wakita, M.; Miyanohana, E.; Fujisaki, Y. *Biochim. Biophys. Acta*

1977, *478*, 23-32; (c) Chaires, J. B.; Leng, F.; Przewloka, T.; Fokt, I.; Ling, Y-H.; Perez-Soler, R.; Priebe, W. *J. Med Chem.* **1997**, *40*, 261-266.

(19) (a) Huang, C-H.; Mong, S.; Crooke, S.T. *Biochemistry* **1980**, *19*, 5537-5542; (b) Wilson, W. D.; Keel, R. A.; Jones, R. L.; Mosher, C. W. *Nucleic Acids Res.* **1982**, *10*, 4093-4106; (c) Léon, P.; Garbay-Jaureguiberry, C.; Lambert, B.; Le Pecq, J. B.; Roques, B. P. *J. Med. Chem.* **1988**, *31*, 1021-1026; (d) Bordelon, J. A.; Feirabend, K. J.; Siddiqui, S. A.; Wright, L. L.; Petty, J. T. *J. Phys. Chem. B* **2002**, *106*, 4838-4843; (e) Chan, H-L.; Ma, D-K.; Yang, M.; Che, C-M. *J. Biol. Inorg. Chem.* **2003**, *8*, 761-769.

(20) Gaugain, B.; Barbet, J.; Capelle, N.; Roques, B. P.; Le Pecq, J. B. *Biochemistry* **1978**, *17*, 5078-5088; (b) Wakelin, L. P. G.; Romanos, M.; Chen, T. K.; Glaubiger, D.; Canellakis, E. S.; Waring, M. J. *Biochemistry* **1978**, *17*, 5057-5063; (c) Pelaprat, D.; Delbarre, A.; Le Guen, I.; Roques, I.; Le Pecq, J. B. *J. Med. Chem.* **1980**, *23*, 1336-1343; (d) Denny, W. A.; Atwell, G. J.; Willmott, G. A.; Wakelin, L. P. G. *Biophys. Chem.* **1985**, *22*, 17-26; (e) McFayden, N. W.; Sortirellis, D.; Denny, W. A.; Wakelin, L. P. G. *Biochim. Biophys. Acta* **1990**, *1048*, 50-58.

(21) Tuite, E.; Nordén, B. *J. Am. Chem. Soc.* **1994**, *116*, 7548-7556.

(22) Sambrook, J.; Fritsch, E. F.; Maniatis, T. In *Molecular Cloning A Laboratory Manual,* 2nd ed.; Cold Spring Harbor Press: New York, 1989.

(23) Yang, X.; Grant, K. B. *J. Biochem, Biophys. Methods* **2002**, *50*, 123-128.

(24) Cohen, G.; Eisenberg, H.; *Biopolymers* **1969**, *8*, 45-55.

(25) (a) Jockusch, S.; Lee, D.; Turro, N. J.; Leonard, E. F. *Proc. Natl. Acad. Sci. USA* **1996**, *93*, 7446-7451; (b) Mohammad, T.; Morrison, H. *Bioorg. Med. Chem. Lett.* **1999**, *9*, 2249-2254.

Acknowledgment. This work was supported by the NSF (CHE-9984772; K.B.G), the CICYT (Project BQU 2002-02576; A.L.) and the US Department of Education (GAANN Fellowship; B.W.). We are grateful for assistance from Profs. M.W. Germann, T.L., Netzel, L., Strekowski, W.D. Wilson, and Dr. C. Sekar (GSU); and from Dr. M.V. Galakhov (UAH).

Supporting Information Available: Absorbance data of compound **3** and **MB** at irradiating wavelengths. ^{1}H NMR spectrum of compound **3**. Four sets of sequential viscosity measurements of: 50 μM bp alternating poly[(dA-dT)]$_2$ and 50 μM bp poly(dA)•poly(dT) pre-equilibrated with 0.0 to 3.0 μM of compound **3** and with 0.0 to 3.0 μM of **MB**. This material is free of charge via the Internet at http://pubs.acs.org.

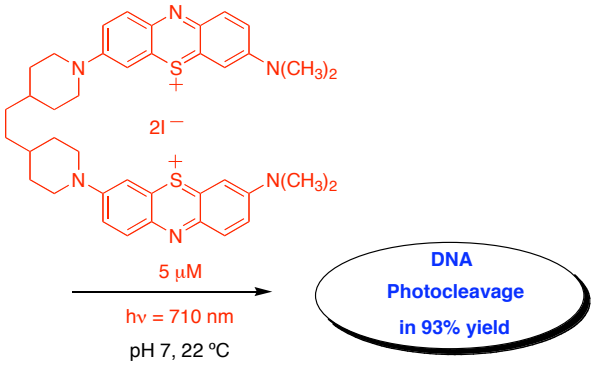

Figure 4.9. Table of content graphic depicting photocleavage by 5 μM of compound **3** irradiated at 710 nm under near physiological conditions of pH and temperature.

Supporting Information

Table 4.S1. Absorbance Data at 10 μM of Dye[a]

	compound **3**	**MB**	Ratio
λ_{max} (nm)	680	674	NA
$Abs_{676\ nm}$	0.8131	0.5091	1.6
$Abs_{700\ nm}$	0.5182	0.1490	3.5
$Abs_{710\ nm}$	0.2498	0.0515	5.0

[a] UV-visible absorbance of 10 μM of dye pre-equilibrated with 380 μM bp of calf thymus DNA in 10 mM sodium phosphate buffer pH 7.0 for 12 h at 22 ºC. Ratio = Abs **3**/Abs **MB**. NA = not applicable.

Table 4.S2. Absorbance Data at 1 μM of Dye[a]

	compound **3**	**MB**	Ratio
λ_{max} (nm)	680	672	NA
$Abs_{676\ nm}$	0.0806	0.0522	1.5
$Abs_{700\ nm}$	0.0472	0.0144	3.3
$Abs_{710\ nm}$	0.0232	0.0046	5.0

[a] UV-visible absorbance data of 1 μM of dye pre-equilibrated with 38 μM bp of calf thymus DNA in 10 mM sodium phosphate buffer pH 7.0 for 12 h at 22 ºC. Ratio = Abs **3**/Abs **MB**. NA = not applicable.

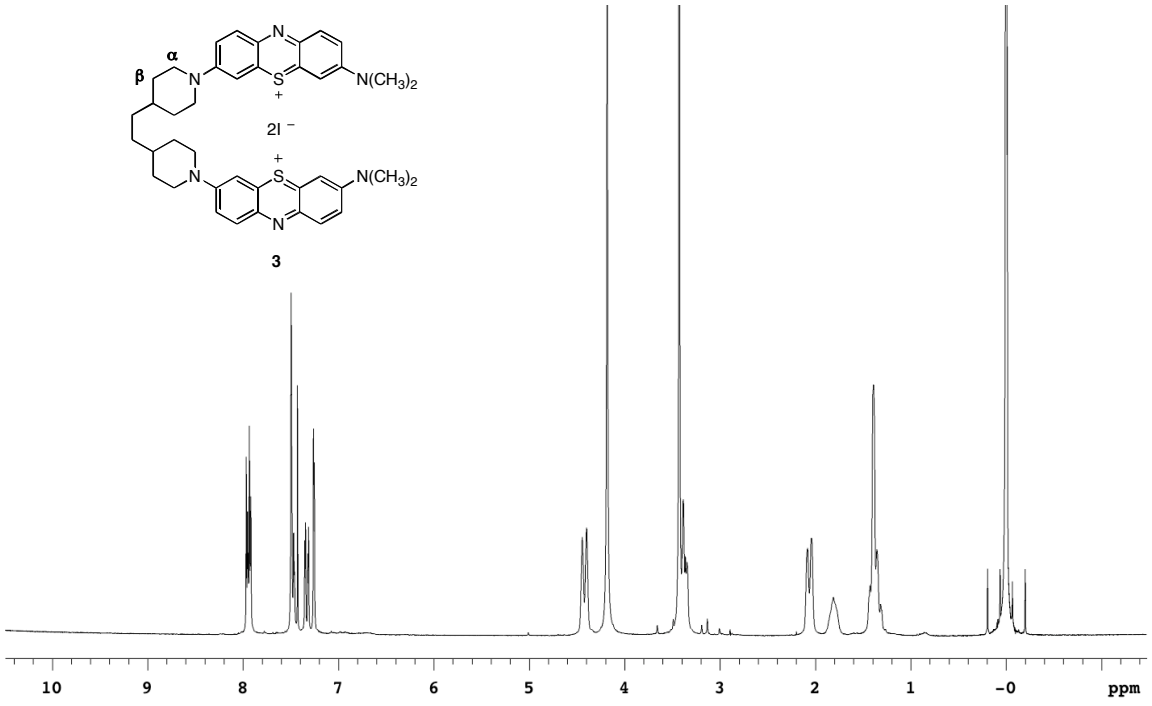

Figure 4.S1. Proton NMR of compound **3**, (300 MHz, $CDCl_3$:CD_3OD): δ = 7.95 (d, *J* = 9.6 Hz , 2H, H-1), 7.94 (d, *J* = 9.6 Hz , 2H, H-9), 7.48 (m, 4H, H-6 and H-8), 7.33 (dd, *J* = 9.6, 2.7 Hz, 2H, H-2), 7.26 (d, *J* = 2.7 Hz, 2H, H-4), 4.42 (d, *J* = 13.5 Hz, 4H, CH_2-α), 3.43 (s, 12H, NCH_3), 3.38 (m, overlap with CH_3OH, 4H, CH_2-α), 2.06 (d, *J* = 11.7 Hz, 4H, CH_2-β), 1.81 (broad, 2H, CH), 1.37 ppm (m, 8H, CH_2-CH_2 and CH_2-β).

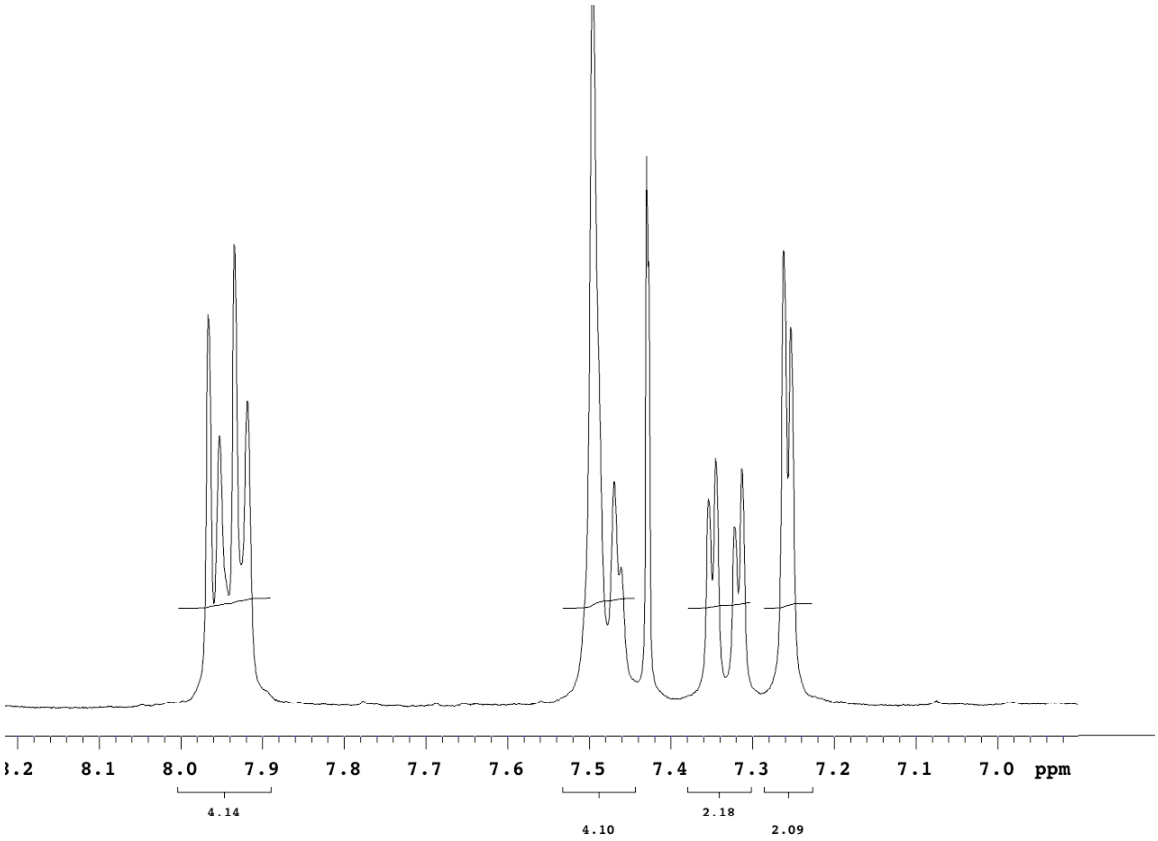

Figure 4.S2. Aromatic region with integration of compound **3** enlarged from Figure 4.S1. δ = 7.95 (d, *J* = 9.6 Hz , 2H, H-1), 7.94 (d, *J* = 9.6 Hz , 2H, H-9), 7.48 (m, 4H, H-6 and H-8), 7.33 (dd, *J* = 9.6, 2.7 Hz, 2H, H-2), 7.26 (d, *J* = 2.7 Hz, 2H, H-4). Note: Resonance at 7.45 ppm is a residual solvent peak of $CHCl_3$.

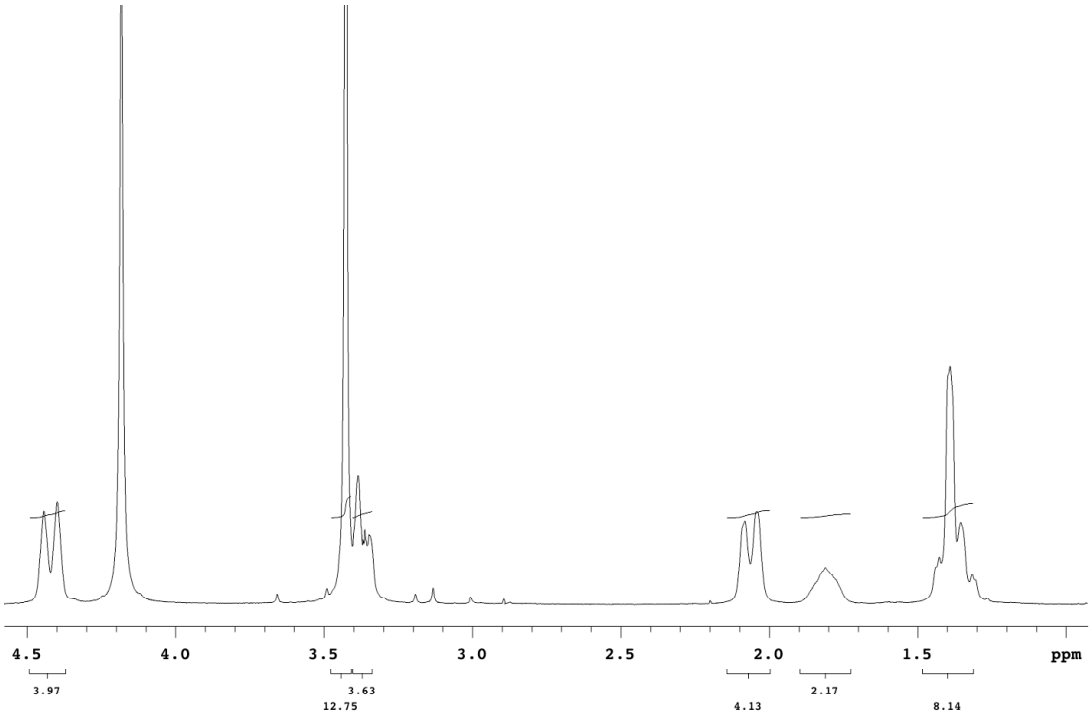

Figure 4.S3. Aliphatic region with integration of compound **3** enlarged from Figure 4.S1. Note: there is overlap with CH_3OH resonances and CH_2-α at 3.38 ppm. δ = 4.42 (d, *J* = 13.5 Hz, 4H, CH_2-α), 3.43 (s, 12H, NCH_3), 3.38 (m, overlap with CH_3OH, 4H, CH_2-α), 2.06 (d, *J* = 11.7 Hz, 4H, CH_2-β), 1.81 (broad, 2H, CH), 1.37 ppm (m, 8H, CH_2-CH_2 and CH_2-β).

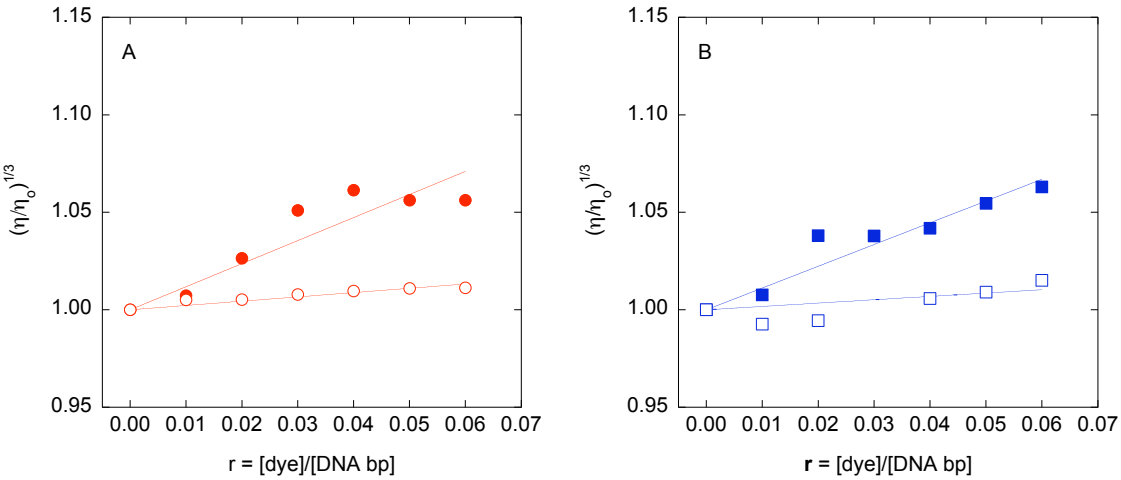

Figure 4.S4. Viscometric measurements as described in the accompanying manuscript were conducted at 25 ± 0.1 ºC in 10 mM sodium phosphate buffer pH 7.0 with 50 μM bp alternating poly[(dA-dT)]$_2$ or 50 μM bp poly(dA)•poly(dT) DNA pre-equilibrated for 12 h in the dark at 22 ºC in the presence of 0.0 to 3 μM of the dyes **A**) compound **3** and **B**) **MB**. Red filled circles: compound **3** with alternating poly[(dA-dT)]$_2$, slope = 1.18, R = 0.9066. Red open circles: compound **3** with poly(dA)•poly(dT), slope = 0.22, R = 0.9202. Blue filled circles: **MB** with alternating poly[(dA-dT)]$_2$, slope = 1.11, R = 0.9518. Blue open circles: **MB** with poly(dA)•poly(dT), slope = 0.17, R = 0.7111.

CHAPTER V

Syntheses and DNA Photocleavage by Phenothiazinium-Piperazinexylene Intercalators

(The data presented in this chapter will be submitted by Wilson, B.; Fernández, M.-J.; Lorente, A.; Grant, K. B. to a peer-reviewed chemistry journal. The contributions to this project by the author of this dissertation were as follows: design and synthesis of photonucleases **5** and **6**; conception and execution of all biological, biophysical, and photochemical experiments; and authorship of the original manuscript. Drs. Fernández and Lorente were instrumental in directing the strategies developed for the synthesis of compounds **5** and **6**.)

Abstract

Two photonucleases incorporating one phenothiazinium ring with a bis-piperazinexylene substituent (compound **5**) or the same bis-piperazinexylene as a linker centrally attached to two phenothiazinium rings (compound **6**) were designed, synthesized and evaluated as DNA photocleaving agents. In reactions employing 10 μM to 0.25 μM of compound **5** or **6**, irradiation with visible light (400-650 nm) produced enhanced cleavage yields of plasmid DNA in a concentration dependent manner under near physiological conditions of pH and temperature (pH 7.0, 22 ºC). Thermal melting assays showed that compounds **5** and **6** increased the T_m of calf thymus DNA by 17 ºC and 19 ºC, respectively. Viscosity measurements revealed that both compounds were bound to DNA as monofunctional intercalators.

Introduction

Phenothiazines are basic dyes that possess redox properties and have been investigated as both potential electrophore probes in supramolecular assemblies[1] and as components in photogalvanic systems for potential solar energy conversion.[2] In

biological systems, this chromophore has been shown to interact with DNA primarily through intercalation. Additionally, phenothiazines are involved in photosensitization reactions and have demonstrated efficient photooxidative damage to DNA as well as to other biomolecules.[3] In this regard, the phenothiazines have been attracting considerable attention as potential photodynamic therapy agents due to their absorption of light within the therapeutic window for PDT (600-800 nm)[4a] and to the low toxicity of the chromophore in human cells.[4b,c] Accordingly, 1,9-dimethyl methylene blue (λ_{max} = 648 nm, methanol)[5b] and 2,8-dimethyl methylene blue (λ_{max} = 630 nm, methanol)[5b] have demonstrated efficient photoactivity against several tumor cell lines.[4b, 5] Moreover, phenothiazines have also exhibited the *in vitro* photoinactivation of nosocomial bacterial[6] and viral[7] pathogens.

In the present study, we describe the syntheses and characterization of 7-dimethylamino-3-(1,1'-[1,4-phenylenebis(methylene)bispiperazine])phenothiazin-5-ium iodide (**5**) and *N*,*N*'-bis[(7-dimethylamino)phenothiazin-5-ium-3-yl]-1,1'-[1,4-phenylenebis(methylene)bispiperazine] diiodide (**6**). Additionally, we evaluate the DNA photocleavage efficiencies, access the DNA binding affinity, and determine the DNA binding modes of the two compounds.

We exploited several design elements in the development of compounds **5** and **6**. The phenothiazine chromophore was selected due to its intercalative DNA binding association and absorption of light at longer wavelengths (> 600 nm). We reasoned that by incorporating this chromophore, DNA photocleavage might be effectively enhanced at longer wavelengths. In addition, bis-piperazinexylene (**4**) was employed as a substituent or as a linker to effect light absorption properties (electron-donating species) and to

potentially enhance DNA binding and duplex stability. DNA intercalating chromophores that possess xylene motifs and/or six member rings (e.g., piperidines, sugars) have been shown to impart additional duplex stability through van der Waals contacts within the grooves and hydrogen bonding.[8] Furthermore, the structural composition (one intercalating ring and a potential groove binding substituent versus two intercalating molecules) was intentionally included in the design rationale to evaluate DNA photocleavage and binding affinity as function of binding mode.

Results and Discussion

Synthesis. Precursor phenothiazin-5-ium tetraiodide hydrate (**1**) and 3-(dimethylamino)phenothiazin-5-ium triodide (**2**) salts (Scheme 5.1) were prepared according to a published literature protocol.[9] In the case of compound **2**, chloroform was employed as the solvent in the reaction instead of methanol. Then, compound **3** was prepared as described by McConnaghie et al. (Scheme 5.2).[10] Although compound **3** was previously hydrolyzed under acidic conditions to afford **4**,[10] we found that bis-piperazinexylene **4** was obtained more efficiently under basic conditions (Scheme 5.2). Under acidic conditions, we obtained mixtures of starting material and product even after employing longer refluxing times (48 h).

After preparing the precursor chromophore **2** and bis-piperazinexylene **4**, our first goal was to synthesize compound **6**. We envisioned that this transformation might require more effort, since two aromatic nucleophilic additions (compound **6**) versus one aromatic nucleophilic addition (compound **5**) would be needed. Moreover, several syntheses of 3,7-disubstituted phenothiazin-5-ium salts have appeared in the literature,[9, 11] while to the

best of our knowledge, no synthetic accounts of bis-phenothiazinium salts (incorporating our design features) have been reported.

Accordingly, in our first attempts methanol, and chloroform were utilized as solvents and various mol equiv of **2** and **4** were explored. Ultimately, we found that reacting 1 mol equiv of each reagent (**2** and **4**) in methanol afforded compound **5** in 34% yield after purification (Scheme 5.3). A small quantity (10%) of impure compound **6** was also recovered. Because yields of compound **6** under the above conditions were not optimal, we explored other strategies. After employing several alternative solvents (e.g., DMSO, DMF) and reaction conditions (e.g., room temperature, refluxing), the synthesis of compound **6** was achieved by using cesium carbonate as base and DMF as solvent, affording compound **6** in 41% yield (Scheme 5.3).

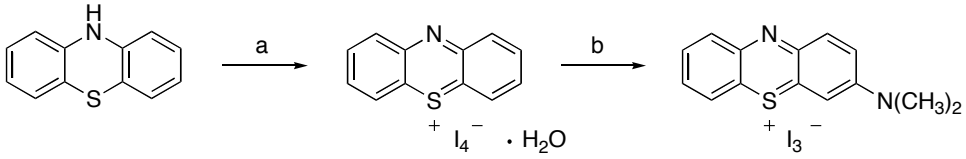

1 **2**

Scheme 5.1. Preparation of precursors **1** and **2**. (a) I_2, $CHCl_3$, 5 ºC, 2 h, 80% yield; (b) $HN(CH_3)_2$ in CH_3OH-$CHCl_3$, RT, 4 h, 55% yield.

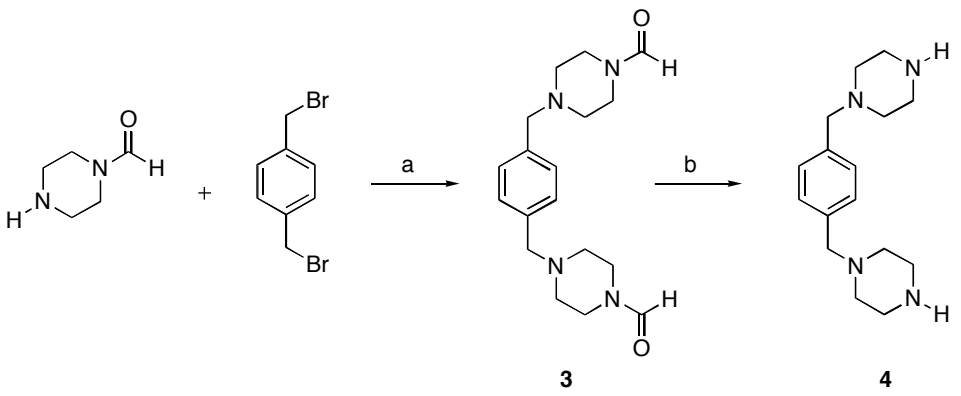

Scheme 5.2. Preparation of **3** and **4**. (a) K_2CO_3, CH_3OH, reflux, 24 h, 75% yield; (b) KOH, EtOH, H_2O, reflux, 24 h, 78% yield.

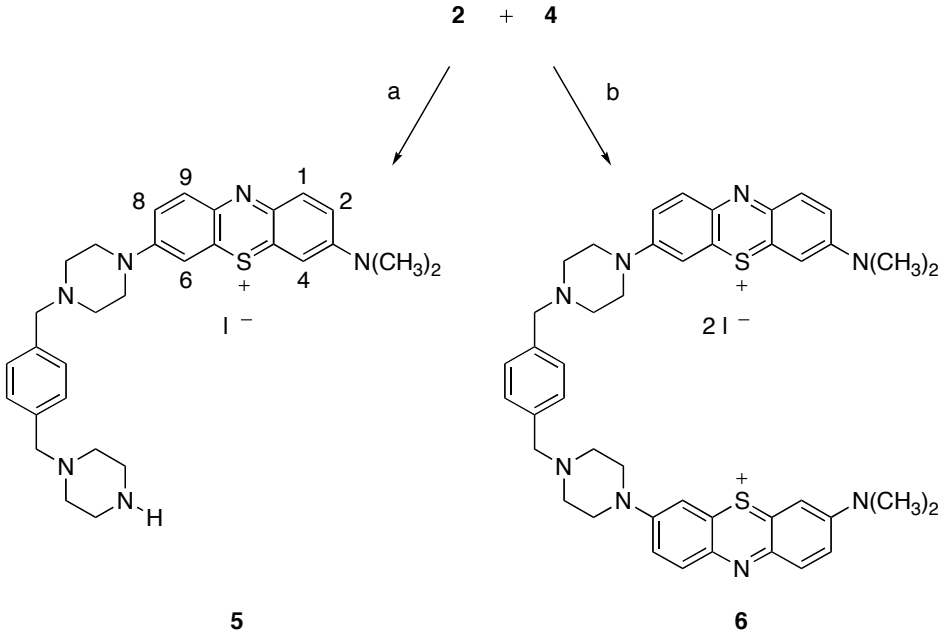

Scheme 5.3. Synthesis of new compounds **5** and **6**. (a) CH_3OH, RT, 72 h, 34% yield; (b) Cs_2CO_3, DMF, RT, 48 h, 41% yield.

UV-Visible Spectrophotometry. The absorption spectra of 10 μM compound **5** and **6** (Fig. 5.1) were recorded in 10 mM sodium phosphate buffer pH 7.0 at 22 ºC. Under these conditions, the λ_{max} observed for **5** and **6** were 662 nm and 580 nm, respectively. Because phenothiazines are known to self-associate in aqueous solutions,[12] the spectra of **5** and **6** were recorded after the addition of 1.0% (w/v) sodium dodecyl sulfate (SDS) as well as after the addition of 380 μM bp calf thymus DNA (10 mM sodium phosphate buffer pH 7.0 at 22 ºC). In the case of DNA, the solutions were allowed to pre-equilibrate for 12 h in the dark at 22 ºC prior to the measurements.

The absorbance spectra of compounds **5** and **6** in the presence of SDS and calf thymus DNA are shown in Figure 5.1. In the presence of 1.0% SDS, the maximal absorbances for 10 μM **5** and **6** are 660 nm ($\varepsilon = 5.81 \times 10^4$ M^{-1} cm^{-1}) and 662 nm ($\varepsilon = 1.46 \times 10^5$ M^{-1} cm^{-1}), respectively. Upon the addition of calf thymus DNA, the respective λ_{max} values for compounds **5** and **6** are 665 nm ($\varepsilon = 3.66 \times 10^4$ M^{-1} (bp) cm^{-1}) and 665 nm (7.80×10^4 M^{-1} (bp) cm^{-1}). It is evident from the data that compound **5** exhibits bathochromicity and hypochromicity in the presence of DNA. In the case of compound **6**, we observe significant disruption of intramolecular self-association upon the addition of DNA as well as bathochromicity. These observations indicate that both compounds interact with DNA. Additionally, the DNA-bound phenothiazines exhibit maximal absorbances greater than 600 nm.

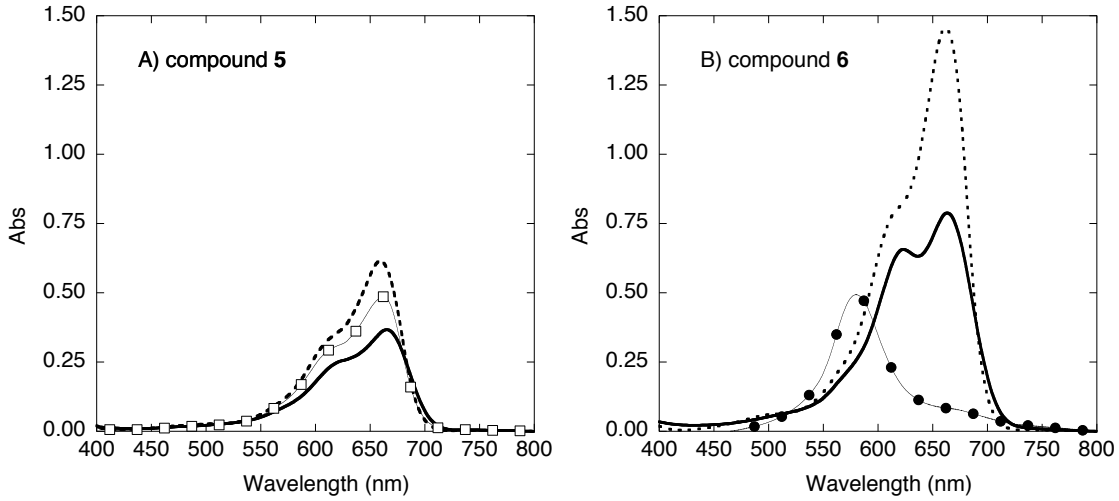

Figure 5.1. UV-visible spectra of **A**) compound **5** and **B**) compound **6** recorded at 22 ºC in 10 mM sodium phosphate buffer pH 7.0 with 10 μM compound **5** (line with squares) or with **6** (line with filled circles) and in the presence of 380 μM bp calf thymus DNA (solid line) or 1.0% sodium dodecyl sulfate (w/v) (dashed line). The samples containing DNA were pre-equilibrated for 12 h in the dark at 22 ºC. ND = not determined due to aggregation in buffer.

Table 5.1. Absorbance Data[a]

compound	λ_{max} (nm)	ε x 10^4 (M^{-1} cm^{-1})	ε x 10^4 (M^{-1}(bp) cm^{-1})
5	662	4.56	*na*
5 + 1% SDS	660	5.81	*na*
5 + DNA	665	*na*	3.66
6	580	*nd*	*na*
6 + 1% SDS	662	14.6	*na*
6 + DNA	665	*na*	7.80

[a] Extinction coefficients for compound **5** and **6** were determined in 10 mM sodium phosphate buffer pH 7.0 using solutions containing 1 to 10 μM of dye in the presence and absence of 1% sodium dodecyl sulfate (w/v) or 38 to 380 μM bp calf thymus DNA. The samples containing DNA were pre-equilibrated for 12 h in the dark at 22 ºC. *na* = not applicable; *nd* = not determined due to aggregation in buffer.

DNA Photocleavage. In the next set of experiments, DNA photocleavage was evaluated as a function of dye concentration and irradiation time. Reaction samples were carried out with 10 to 0.25 μM compound **5** or **6** equilibrated with 38 μM bp pUC19 plasmid DNA in 10 mM sodium phosphate buffer pH 7.0 for 12 h in the dark at 22 ºC. The samples were then aerobically irradiated in a Rayonet Photochemical Reactor fitted with twelve 575 nm lamps for 60 min (spectral output, 400-650 nm). The photolysis reaction products were then resolved on a 1.0% non-denaturing agarose gel. As shown in Figure 5.2, both compounds produced enhanced levels of DNA damage in a concentration dependent manner. The highest photocleavage yields (conversion of supercoiled to nicked form) were 96% (Fig. 5.2, Lane 3) and 93% (Fig. 5.2, Lane 11) for samples irradiated with 10 μM **5** and **6**, respectively.

We then employed 10 μM of compound **5** or **6** equilibrated with 38 μM bp pUC19 plasmid DNA in 10 mM sodium phosphate buffer pH 7.0 to examine the irradiation time dependence on DNA photocleavage (Fig. 5.3). Individual samples were irradiated as described above at time-points ranging from 10 to 60 min. As shown in Figure 5.3, DNA photocleavage by compounds **5** and **6** increased as a function of increasing irradiation time, generating maximal cleavage yields of 93% and 95% at the 60 min time-point.

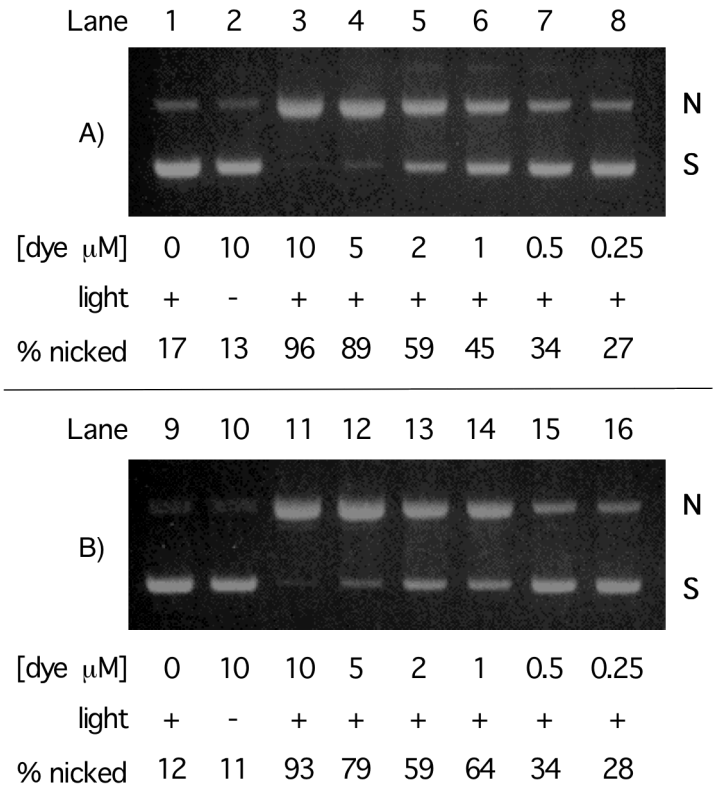

Figure 5.2. Photograph of a 1.0% non-denaturing agarose gel showing photocleavage of pUC19 plasmid DNA. Samples contained 10 mM sodium phosphate buffer pH 7.0 and 38 μM bp DNA in the presence and absence of dye. **A**) compound **5** and **B**) compound **6**. After pre-equilibrated for 12 h in the dark at 22 ºC, the samples were aerobically irradiated in a Rayonet Photochemical reactor fitted with twelve 575 nm lamps for 60 min at 22 ºC. Lanes 1 and 9: DNA controls (no dye). Lanes 3 to 8: 10 to 0.25 μM compound **5**. Lanes 11 to 16: 10 to 0.25 μM compound **6**. Lanes 2 and 10: 10 μM **5** and 10 μM **6** (no hν). Abbreviations: **N** = nicked; **S** = supercoiled.

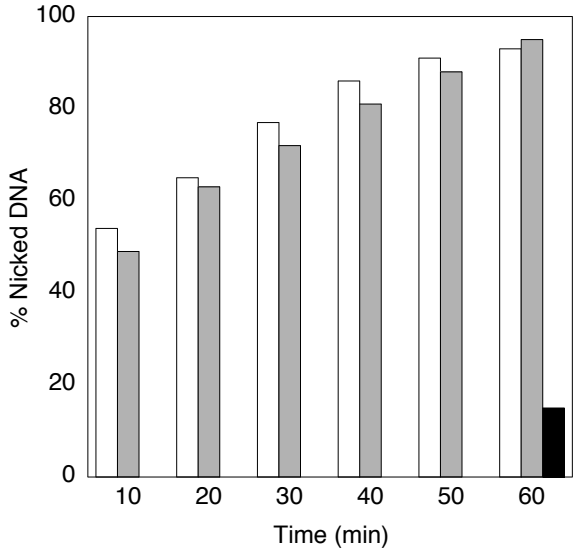

Figure 5.3. DNA photocleavage of 38 μM bp pUC19 plasmid DNA in 10 mM sodium phosphate buffer pH 7.0 by 10 μM compound **5** (white bars) and 10 μM compound **6** (gray bars) as a function of irradiation time. After pre-equilibrated for 12 h in the dark at 22 ºC, the samples were aerobically irradiated in a Rayonet Photochemical reactor fitted with twelve 575 nm lamps for 10-60 min at 22 ºC. The black bar represents DNA that was irradiated for 60 min in 10 mM sodium phosphate buffer pH 7.0 in the absence of dye.

DNA Thermal Denaturation. Melting assays provide a straightforward method to access the relative DNA binding affinities of compounds that associate with double-helical DNA. In the process of intercalation and/or groove binding, free energy contributions from π-π, van der Waals, electrostatic and hydrogen bonding interactions stabilize helical DNA. As a result, these interactions increase the DNA binding affinity, thereby increasing the melting temperature of the DNA-ligand complex.[13]

The melting isotherms shown in Figure 5.4 were generated by employing 12.5 μM bp calf thymus DNA equilibrated in the absence or presence of 7.5 μM **5** or **6** (10 mM sodium phosphate pH 7.0). As compared to calf thymus DNA (T_m = 69 ºC),

compound **5** exhibited a T_m of 86 ºC (ΔT_m = 17 ºC) while compound **6** produced a T_m of 88 ºC (ΔT_m = 19 ºC). Clearly, the T_m values produced by compounds **5** and **6** were significant, thereby indicating significant levels of duplex stabilization interactions.

The above results are consistent with the dicationic nature of both dyes under the experimental conditions employed. At pH 7.0, basic phenothiazine dyes have pK_a values of approximately 12.[14] In the case of compound **5**, the bis-piperazinexylene substituent would be expected to bear one positive charge (secondary amino group of piperazine) as the piperazine tertiary amino group would not be protonated due a reduction in charge density by the withdrawing effects of the xylene as previously described.[10]

Therefore, the positive charge density of compound **6** is imparted by the two phenothiazines, while in compound **5** the bis-piperazinexylene substituent is expected to furnish one and the phenothiazine provide the other positve charge.

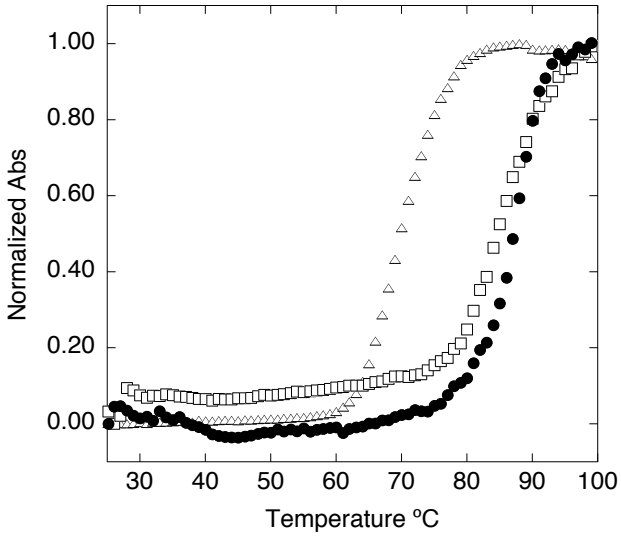

Figure 5.4. Melting isotherms of: 12.5 μM bp CT DNA (Δ, T_m = 69 ºC); 12.5 μM bp CT DNA with 7.50 μM of **5** (□, T_m = 86 ºC) or with 7.50 μM of **6** (●, T_m = 88 ºC) in 10 mM sodium phosphate buffer pH 7.0. The ordinate represents normalized absorbance monitored at 260 nm.

Viscosity Measurements. In order for intercalation to occur, the DNA base pairs separate to form a cavity for the incoming chromophore through localized unwinding of the duplex. Consequently, the contour length of DNA is increased. Because groove binding agents do not unwind helical DNA, hydrodynamic assays (e.g., viscosity) sensitive to the change in DNA length can be employed to distinguish between binding modes.[15] According to the theory of Cohen and Eisenberg, plots of the cubed root of the relative viscosity $(\eta/\eta_o)^{1/3}$ versus **r** the molar ratio of bound ligand to DNA bp (**r**) should result in a slope close to 1.0 for a monointercalator.[16.] The slope of a bisintercalator is then expected to be twice that observed for the monointercalative binding.

Our next goal was to determine the DNA binding mode of compounds **5** and **6**. Viscosity measurements were carried out with individual solutions equilibrated with 10 mM sodium phosphate buffer pH 7.0 and 200 μM bp of calf thymus DNA in the presence (η) and absence (η_o) of dye. The viscosity data (Fig. 5.5) was plotted as $(\eta/\eta_o)^{1/3}$ versus dye to DNA bp molar ratios (**r**) ranging from 0.01 to 0.06. The slopes obtained from these plots were 0.99 and 1.2 for compounds **5** and **6**, respectively. Clearly, both compounds interacted with calf thymus DNA as monofunctional intercalators.

In order to prevent violation of the nearest-neighbor exclusion theory, bisintercalators should possess a linker ≥10 Å in length.[17] While compound **6** meets this requirement,[18] it is conceivable that conformation constraints lower the free energy of binding[19] or that self-association of the dye in the buffer solution prevent the insertion of the second ring.

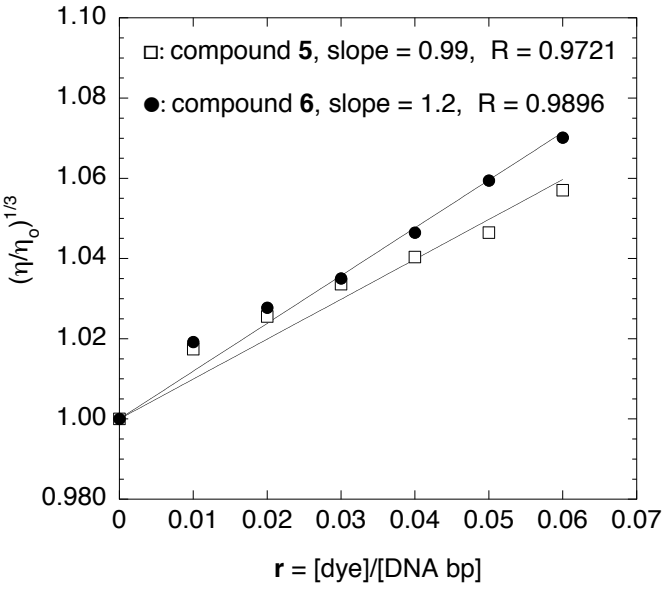

Figure 5.5. Viscosity measurements conducted with 200 μM bp calf thymus DNA in 10 mM sodium phosphate buffer pH 7.0 pre-equilibrated with 0, 2, 4, 6, 8, 10, 12 μM of compound **5** or of compound **6** for 12 h at 22 ºC.

Conclusions

Two cationic and photoactive intercalators incorporating one phenothiazinium ring with a bis-piperazinexylene substituent (compound **5**) or the same bis-piperazinexylene as a linker centrally attached to two phenothiazinium rings (compound **6**) have been synthesized and characterized. In the presence of DNA, both compounds exhibit maximal absorbance at 665 nm in 10 mM sodium phosphate pH 7.0. Moreover, irradiation (400-650 nm) of pUC19 plasmid DNA in the presence of 10 μM **5** or of **6** produces photocleavage yields of 96% and 93%, respectively. DNA melting assays show that significant increases in T_m values were produced by **5** (ΔT_m =17 ºC) and **6** (ΔT_m =19 ºC) relative to calf thymus DNA (in the absence of dye). Lastly, viscosity measurements indicate that both compounds bind to DNA as monofuntional intercalators.

Considering the great interest in developing non-porphyrin based phototherapeutics that strongly absorb light at wavelengths greater than 600 nm and possess low toxicity in human cells, our future research efforts will involve the synthesis of second-generation bis-phenothiazine dyes with improved intercalating abilities.

Experimental

General Methods. Melting points were determined in a Stuart Scientific model SMP10 apparatus. Infrared spectra were taken on an FT-IR Perkin Elmer Spectrum One spectrophotometer. ^{1}H and ^{13}C NMR spectra were recorded at 300 MHz and 75 MHz, respectively, in either Varian Unity One or Varian Mercury-VX-300 spectrometers. Elemental analyses (CHNS) were conducted on a Leco CHNS-932 automatic analyzer while iodine composition was performed by oxygen flask combustion and by ion chromatography (Atlantic Microlabs, Inc. Norcross, GA). Electrospray ionization (ESI) mass spectra were generated on a Micromass Q-Tof hybrid mass spectrometer. Merck silica gel 60 (230-400 ASTM mesh) was employed for flash column chromatography. UV-visible and CD spectra were recorded with a UV-1601 Shimadzu spectrophotometer, while thermal melting curves were generated using a Cary Bio 100 UV-Vis spectrophotometer.

Distilled, deionized water was utilized in the preparation of all buffers and aqueous reactions. Chemicals were of the highest available purity and were used without further purification. Anhydrous magnesium sulfate, cesium carbonate, chloroform, α,α'-dibromo-*p*-xylene, dichloromethane, dimethylamine (2 M solution in methanol), dimethylformamide, ethidium bromide, iodine, methanol, 10*H*-phenothiazine, 1-piperazinecarboxaldehyde, potassium hydroxide, potassium carbonate, sodium phosphate

dibasic, and sodium phosphate monobasic were obtained from the Aldrich Chemical Co. Transformation of *Escherichia coli* competent cells (Stratagene, XL-blue) with pUC19 plasmid (Sigma) and growth of bacterial cultures in Lauria-Bertani broth were performed according to standard laboratory procedures.[20] The plasmid DNA was purified with a Qiagen Plasmid Mega Kit. Ultra Pure™ calf thymus DNA (Invitrogen Lot No. 15633-019, 10 mg/mL, average size ≤ 2000 bp) was used without purification. The concentration of calf thymus DNA solutions were determined by UV-visible spectrophotometry using the following extinction coefficient in units of M^{-1} (bp) cm^{-1}: ε_{260} = 12,824.

Phenothiazin-5-ium tetraiodide hydrate (**1**). A solution of 10*H*-phenothiazine (0.566 g, 2.84 mmol) in 20 mL of chloroform was stirred at 5 ºC and iodine (2.16 g, 8.51 mmol) dissolved in 50 mL of chloroform was added drop-wise over 1 h. The reaction mixture was stirred at 5 ºC for an additional h, while the progress was monitored by silica gel TLC using chloroform as the solvent. The precipitate from the reaction was then filtered, washed with a copious amount of chloroform and was dried under high vacuum overnight to afford 1.63 g (80% yield) of dark-blue solid **1**; R_f = 0.09 (chloroform); M.p. 170 ºC (decomp.); ^{1}H NMR (300 MHz, Acetone-d_6): δ = 8.01 (m, 2H), 7.92 (m, 2H), 7.64 ppm (m, 4H); ^{13}C NMR (75 MHz, Acetone-d_6): δ = 153.58, 130.67, 129.47, 128.64, 125.50, 123.52 ppm; IR (film): ν = 2967, 1558, 1467, 1440, 1311, 1233, 1131, 1067, 1023, 841, 705 cm^{-1}. LRMS (ESI): calcd for $C_{12}H_8NS$ [M^+]: 198.0; found: 199.0 [$M+H^+$]$^+$.

3-(Dimethylamino)phenothiazin-5-ium triiodide (**2**). To a solution of phenothiazin-5-ium tetraiodide hydrate (0.400 g, 0.553 mmol) in 20 mL of chloroform was added dimethylamine in methanol (0.553 mL, 1.11 mmol) drop-wise over 4 h. The

reaction was monitored by silica gel TLC (3:7 10% aqueous ammonium acetate/methanol, v/v). The resultant precipitate was filtered, washed with chloroform and allowed to air dry. Product **2** (189 mg, 55% yield) was obtained as a dark-blue solid; R_f = 0.28 (3:7 10% aqueous ammonium acetate/methanol, v/v); M.p. 144-145 ºC; ^{1}H NMR (300 MHz, DMSO-d_6): δ = 8.22 (dd, J = 8.0 Hz, J = 1.6 Hz, 1H, H-9), 8.17 (dd, J = 8.0 Hz, J = 1.6 Hz, 1H, H-6), 8.10 (d, J = 10 Hz, 1H, H-1), 8.04 (dd, J = 10 Hz, 1H, H-2), 8.00 (d, J = 2.4 Hz, 1H, H-4), 7.85 (m, 2H, H-7 and H-8), 3.64 and 3.60 ppm (2s, 6H, $N(CH_3)_2$); ^{13}C NMR (75 MHz, DMSO-d_6): δ = 156.09, 144.13, 139.81, 139.56, 138.03, 134.55, 133.22, 129.81, 126.27, 126.06, 125.84, 109.66, 43.35, 42.88 ppm; IR (film): ν = 2800, 1617, 1559, 1489, 1429, 1411, 1252, 1118, 1411, 1078, 887, 835, 772 cm^{-1}; LRMS (ESI): calcd for $C_{14}H_{13}N_2S$ [M^+]: 241; found: 241. Anal. Calcd for $C_{14}H_{13}N_2SI_3$: C, 27.03; H, 2.11; N, 4.50; S, 5.15; I, 61.20. Found: C, 27.12; H, 1.97; N, 4.46; S, 5.23; I, 60.94.

1,1'-[1,4-Phenylenebis(methylene)]bis(4-piperazinecarboxaldehyde) (**3**). A solution containing α, α'-dibromo-*p*-xylene (2.60 g, 0.010 mol), 1-piperazine carboxaldehyde (2.30 mL, 0.022 mol) and potassium carbonate (1.40 g, 0.010 mol) in 40 mL of methanol was refluxed under an open atmosphere for 24 h. Reaction progress was monitored by silica gel TLC (44:8:1 chloroform-methanol-ammonium hydroxide, v/v/v). After the starting materials were consumed, the reaction was concentrated to dryness under reduced pressure. The resulting solid was then dissolved in 25 mL of water and extracted with dichloromethane (50 mL) three times. The organic layer was dried over anhydrous magnesium sulfate, filtered and concentrated under reduced pressure to yield 2.47 g (75%) of white solid **3**; R_f = 0.69 (44:8:1 chloroform-methanol-ammonium hydroxide, v/v/v); M.p. 140 – 142 ºC; ^{1}H NMR (300 MHz, DMSO-d_6): δ 2.29 and 2.35 (t,

J = 4.8 Hz, 4H, C<u>H$_2$</u>-NCH$_2$Ph), 3.35 and 3.37 (tt, *J* = 4.8 and 5.2 Hz, 8H, C<u>H$_2$</u>-NCHO), 3.48 (s, 4H, CH$_2$-Ph), 7.27 (s, 4H, Ph-H), 7.99 ppm (s, 2H, NCOH); ^{13}C NMR (75 MHz, DMSO-d_6): δ 39.11 and 44.77 (<u>C</u>H$_2$-NCHO), 51.89 and 53.11 (<u>C</u>H$_2$- NCH$_2$Ph), 61.62 (<u>C</u>H$_2$-Ph), 128.73 (Ph-H), 136.55 (C$_{ipso}$ Ph) 160.68 ppm (CHO); IR (film): ν = 770, 821, 841, 998, 1017, 1125, 1226, 1400, 1431, 1489, 1514, 1668, 2805, 2870 cm^{-1}; LRMS (ESI): calcd for $C_{18}H_{26}N_4O_2$ [M$^+$] 330; found: 331 [M+H$^+$]$^+$.

1,1'-[1,4-Phenylenebis(methylene)]bispiperazine (**4**). A solution of **3** (0.500 g, 1.50 mmol) in 3 mL of ethanol and 2 mL of water was treated with potassium hydroxide (0.421 g, 7.50 mmol) and refluxed under an open atmosphere for 24 h. Reaction progress was monitored by silica gel TLC (44:8:1 chloroform-methanol-ammonium hydroxide, v/v/v). After the starting material was consumed, the reaction mixture was allowed to cool and was then extracted with dichloromethane (10 mL) three times. The organic layer was dried over anhydrous magnesium sulfate, filtered and concentrated under reduced pressure to yield 0.321 g (78%) of white solid **4**; R_f = 0.45 (44:8:1 chloroform-methanol-ammonium hydroxide, v/v/v); M.p. 146 – 148 ºC; ^{1}H NMR (300 MHz, DMSO-d_6): δ 2.23 (t, *J* = 4.6 Hz, 8H, C<u>H$_2$</u>-NCH$_2$Ph), 2.64 (t, *J* = 4.6 Hz, 8H, C<u>H$_2$</u>-NH), 3.36 (s, 4H, CH$_2$-Ph), 7.19 ppm (s, 4H, Ph-H); ^{13}C NMR (75 MHz, DMSO-d_6): δ 45.55 (<u>C</u>H$_2$-NH), 54.07 (<u>C</u>H$_2$- NCH$_2$Ph), 62.62 (<u>C</u>H$_2$-Ph), 128.5 (Ph-H), 136.7 (C$_{ipso}$ Ph); IR (film): ν = 765, 830, 858, 1008, 1134, 1249, 1335, 1360, 1453, 1514, 2804, 2880, 3244 cm^{-1}; LRMS (ESI): calcd for $C_{16}H_{26}N_4$ [M$^+$]: 274; found: 275 [M+H$^+$]$^+$, 138 [M+H$^+$]$^{+2}$.

7-Dimethylamino-3-(1,1'-[1,4-phenylenebis(methylene)bispiperazine]) phenothiazin-5-ium iodide (**5**). A solution of **2** (0.507 g, 0.815 mmol) and **4** (0.224 g, 0.815 mmol) in 25 mL of methanol was vigorously stirred for 72 h. The progress of the

reaction was monitored by silica gel TLC (9.5:0.5 dichloromethane-methanol, v/v). The reaction was concentrated under reduced pressure and the resultant solid was purified by flash column chromatography (4 cm column, 70 g silica gel) using 9.5:0.5 dichloromethane-methanol, v/v as the eluent to afford 170 mg (34%) of dark-blue solid **5**; R_f = 0.2 (9.5:0.5 dichloromethane-methanol, v/v); M.p. > 300 ºC; ^{1}H NMR (300 MHz, DMSO-d_6): δ 2.55 (b, 8H,$\underline{CH_2}$-β, β') 3.09 (t, J = 5 Hz, 4H, $\underline{CH_2}$-α'), 3.37 (s, 6H, NCH_3), 3.54 (s, 4H, $\underline{CH_2}$-Ph) 3.85 (s, broad, 4H, $\underline{CH_2}$-α), 7.30 (m, 4H, Ph-H), 7.51-7.68 (m, 4H, H-2, H-4, H-6 and H-8) 7.90 ppm (m, 2H, H-1 and H-9); ^{13}C NMR (75 MHz, DMSO-d_6): δ 40.66 (NCH_3), 42.48 (C-α'), 46.74 (C-α), 48.38 (C-β), 51.65 (C-β'), 60.36 and 60.53 (CH_2-Ph), 106.41 and 106.52 (C-4 or C-6), 118.22 and 119.01 (C-2 or C-8), 128.27 (C-Ph), 133.04 and 133.36 (C-9a or C-10), 134.33 (C_{ipso}-Ph), 135.10 and 135.94 (C4a or C-5a), 137.25 and 137.39 (C-1 or C-9), 152.25 (C-7) and 153.45 ppm (C-3); IR (film): ν = 779, 825, 882 , 990, 1042, 1136, 1229, 1352, 1386, 1487, 1593, 1743 cm^{-1}; HRMS (ESI): calcd for $C_{30}H_{37}N_6S$ 513.2800, found 513.2815 [M^+] and 257.1462 [M^+/2].

***N*,*N*'-Bis[(7-dimethylamino)phenothiazin-5-ium-3-yl]-1,1'-[1,4-phenylenebis(methylene)bispiperazine] diiodide** (**6**). To a solution of **2** (0.200 g, 0.322 mmol) in 20 mL of dimethylformamide were added **4** (0.044 g, 0.160 mmol) and cesium carbonate (0.156 g, 0.480 mmol). The reaction was vigorously stirred at RT for 48 h and then concentrated under reduced pressure. The progress of the reaction was monitored by TLC (9.5:0.5 dichloromethane-methanol, v/v). The resultant solid was purified via flash column chromatography (3 cm column, 39 g silica gel) using 9.5:0.5 dichloromethane-methanol, v/v as the eluent to afford 66 mg (41%) of dark-blue solid **6**; R_f = 0.3 (9.5:0.5 dichloromethane-methanol, v/v) M.p. > 300 ºC; ^{1}H NMR (300 MHz,

DMSO-d_6): δ 2.55 (s, 8H,$\underline{CH_2}$-β), 3.38 (s, 12H, NCH_3), 3.55 (s, 4H, $\underline{CH_2}$-Ph) 3.85 (s, broad, 8H, $\underline{CH_2}$-α) 7.31 (s, 4H, Ph-H), 7.55-7.69 (m, 8H, H-2, H-4, H-6 and H-8) 7.93 ppm (m, 4H, H-1 and H-9); ^{13}C NMR (75 MHz, DMSO-d_6): δ 41.91 (NCH_3), 47.99 (C-α), 53.01 (C-β), 61.76 (CH_2-Ph), 107.77 (C-4, C-6), 119.53 and 120.39 (C-2, C-8), 129.59 (C-Ph), 137.16 and 138.75 (C-1, C-9), 153.45 ppm (C-3 or C-7); IR (film): ν = 778, 830, 881, 1001, 1035, 1140, 1228, 1347, 1385, 1488, 1590, 2834, 2884, 2954 cm^{-1}; HRMS (ESI): calcd for $C_{44}H_{48}N_8S_2$ 752.3443, found 376.1725 [M^+/2].

UV-Visible Spectrophotometry. Extinction coefficients for compound **5** and **6** were determined using 500 μL solutions containing 1 to 10 μM of dye in the presence and absence of 38 to 380 μM bp calf thymus DNA in 10 mM sodium phosphate buffer pH 7.0. After a 12 h pre-equilibration period in the dark, UV-visible spectra were recorded in 1 cm quartz cuvettes at 22 ºC. The absorbance was then plotted as a function of concentration and linear least square fits to these data yielded slopes (KaleidaGraph version 3.6.4 software) that were averaged over three trials. Using the procedure described above, extinction coefficients in the absence of calf thymus DNA were also recorded in the presence of a final concentration of 1% sodium dodecyl sulfate (w/v).

DNA Photocleavage. Individual samples consisted of 38 μM bp pUC19 plasmid DNA and 10 to 0.0 μM of compound **5** or **6** in 10 mM sodium phosphate buffer pH 7.0 (total volume 20 μL). The samples were pre-equilibrated in the dark for 12 h at 22 ºC, after which they were kept in the dark or were aerobically irradiated in a Rayonet Photochemical reactor fitted with twelve 575 nm lamps (Southern New England Ultraviolet Co.) for 60 min. In time course experiments, individual 20 μL reactions contained 10 μM **5** or **6** and 38 μM bp pUC19 plasmid DNA in 10 mM sodium

phosphate buffer pH 7.0. The samples were pre-equilibrated in the dark for 12 h at 22 ºC, after which they aerobically irradiated as described above for 10 to 60 min. The resulting cleavage products were electrophoresed on a 1% nondenaturing agarose gel stained with ethidium bromide (0.5 μg/mL), visualized on a transilluminator set at 302 nm, photographed and scanned. The amounts of supercoiled and nicked plasmid DNA were quantitated by densitometry using ImageQuant version 5.2 software (Amersham Biosciences). Photocleavage yields were calculated using the formula [(nicked DNA)/total DNA] x 100. The density of supercoiled DNA was multiplied by a correction factor of 1.22 to account for the decreased binding affinity of ethidium bromide to supercoiled DNA as compared to the nicked and linear forms.

Thermal Melting Studies. Individual 3 mL solutions containing 10 mM sodium phosphate buffer pH 7.0 and 12.5 μM bp calf thymus DNA in the presence and absence of 7.50 μM of compound **5** or **6** in were placed in 3 mL (1 cm) quartz cuvettes (Starna). After the samples were equilibrated in the dark for 12 h and 22 ºC, absorbance was monitored at 260 nm while the DNA was denatured using a Peltier heat block programmed to increase the temperature from 25 to 100 ºC at a rate of 0.5 ºC min^{-1}. KaleidaGraph version 3.6.4 software was then used to approximate the first derivative of $\Delta A_{260}/\Delta T$ versus temperature, where the T_m value corresponded to the maximum of each first derivative plot.

Viscosity Measurements. In a total volume of 1000 μL, individual solutions containing 10 mM sodium phosphate buffer pH 7.0 and 200 μM bp of calf thymus DNA (average length ≤ 2000 bp) in the absence and presence of 2 to 12 μM of compound **5** or **6** were pre-equilibrated for 12 h in the dark at 22 ºC. DNA viscosity was then measured

in a Cannon-Ubbelohde size 75 capillary viscometer immersed in a thermostated water bath maintained at 25 ± 0.2 ºC. The flow times of the buffer, DNA in buffer, and dye-DNA in buffer were measured with a stopwatch. The measurements were averaged over four trials to an accuracy of $\pm$ 0.2 s. After subtracting the averaged flow time of the buffer, DNA (η_0) and dye-DNA (η) averaged flow times were plotted as $(\eta/\eta_o)^{1/3}$ versus the molar ratio of dye to DNA bp. Slopes were generated by conducting linear least square fits to these data (KaleidaGraph version 3.6.4 software). While the conventional method for performing viscosity assays involves titration of the ligand into a DNA solution inside the viscometer, here we report an alternative and efficient technique that may be particularly useful for **5** and **6** as well as for other phenothiazines (e.g., 1,9-dimethyl methylene blue and methylene blue), where pre-equilibration with DNA is required to reduce ligand stacking associations in solution.[12]

Acknowlegments. This work was supported by the NSF (CHE-9984772; K.B.G), the CICYT (Project BQU 2002-02576; A.L.) and the US Department of Education (GAANN Fellowship; B.W.). We are grateful for assistance from Profs. M.W. Germann, T.L., Netzel, L., Strekowski, W.D. Wilson (GSU) and from Dr. M.V. Galakhov (UAH).

References

1. Müller, T. J. J. *Tetrahedron Lett*. **1999**, *40*, 6563.

2. Genwa, K. R.; Chouhan, A. *J. Chem. Sci*. **2004**, *116*, 339.

3. Tuite, E. M.; Kelly, J. M. *J. Photochem. Photobiol. B: Biol*. **1993**, *21*, 103.

4. (a) Detty, M. R.; Gibson, S. L.; Wagner, S. J. *J. Med. Chem*. **2004**, *47*, 3897. (b) Harris, F.; Sayed, Z.; Hussain, S.; Phoenix, D. A. *Photodiag. Photodyn. Ther*. **2004**, *1*, 231. (c) Harris, F.; Chatfield, L.K.; Phoenix, D. A. *Curr. Drug Targets* **2005**, *6*, 615.

5. (a) Wainwrigth, M.; Phoenix, D. A.; Rice, L.; Burrow, S. M.; Waring, J. *J. Photochem. Photobiol. B*. **1997**, *40*, 233. (b) Rice, L.; Wainwright, M.; Phoenix, D. A. *J. Chemother*. **2000**, *12*, 94.

6. (a) Wainwright, M.; Phoenix, D. A.; Laycock, S. L.; Wareing, D. R. A.; Wright, P. A. *FEMS Microbiol. Letts*. **1998**, *160*, 177. (b) Wainwright, M.; Phoenix, D. A.; Gaskell, M.; Marshall, B. *J. Antimicrob. Chemother*. **1999**, *44*, 823.

7. (a) Owada, T.; Yamada, Y.; Abe, H.; Hirayama, J. Ikeda, H. Sekguchi, S.; Ikebushi, K. *J. Med. Virol*. **2000**, *62*, 421. (b) Floyd, R. A.; Schneider, J. E. Jr.; Dittmer, D. P. *Antiviral Res*. **2004**, *61*, 141.

8. (a) Gao, Q.; Williams, L. D.; Egli, M.; Rabinovich, D.; Chen, S-L.; Quigley, G. J.; Rich, A. *Proc. Natl. Acad. Sci. USA* **1991**, *88*, 2422. (b) Krugh, T. R. *Curr. Opin. Struct. Biol*. **1994**, *4*, 351. (c) Chaires, J. B. *Curr. Opin. Struct. Biol*. **1998**, *8*, 314.

9. Strekowski, L.; Hou, D-F.; Wydra, R. L. *J. Heterocyclic Chem*. **1993**, *30*, 1693.

10. McConnaughie, A. W.; Spychala, J.; Zhao, M.; Boykin, D.; Wilson, W. D. *J. Med. Chem*. **1994**, *37*, 1063.

11. (a) Leventis, N.; Chen, M.; Sotiriou-Leventis, C. *Tetrahedron* **1997**, *53*, 10083. (b) Mellish, K. J.; R. D.; Cox, Vernon, D. I.; Griffiths, J.; Brown, S. B. *Photochem. Photobiol.* **2002**, *75*, 392.

12. (a) Jockusch, S.; Lee, D.; Turro, N. J.; Leonard, E. F. *Proc. Natl. Acad. Sci. USA* **1996**, *93*, 7446. (b) Mohammad, T.; Morrison, H. *Bioorg. Med. Chem. Lett.* **1999**, *9*, 2249.

13. Wilson, W. D.; Tanious, F. A.; Fernández-Saiz, M. In *Drug-DNA Interaction Protocols*; Fox, K. R., Ed.; Humana Press: New Jersey, 1997; pp 219-240.

14. Harris, R. G.; Wells, J. D.; Johnson, B. B. *Colloids Surf. A Physiochem. Eng. Asp.* **2001**, *180*, 131.

15. Suh, D.; Chaires, J. B. *Bioorg. Med. Chem.* **1995**, *3*, 723.

16. Cohen, G.; Eisenberg, H.; *Biopolymers* **1969**, *8*, 45.

17. Wilson, W. D. In *Nucleic Acids in Chemistry and Biology*; Blackburn, G. M.; Gait, M. J., Eds.; Oxford University Press: New York, 1996; pp 331-370.

18. The linker length (11 Å) of compound **6** was determined by measuring the bond distances in between the two phenothiazines rings of a three-dimensional structure produced by CambridgeSoft Corporation Chem 3D Pro software version 5.0 (the energy was not minimized).

19. Wilson, W. D. *Compr. Nat. Prod. Chem.* **1999**, *7*, 427.

20. Sambrook, J.; Fritsch, E. F.; Maniatis, T. In *Molecular Cloning A Laboratory Manual*; 2nd ed.; Cold Spring Harbor Press: New York, 1989.

CHAPTER VI

Allele-Specific PCR-Based Genotyping of a Normal Variation in Human Color Vision

(This chapter is verbatim as it appears in Wilson, B.; Lubin, I. M.; Grant, K. B. *Journal of Chemical Education* **2003**, *80*, 1289-1291. The contributions to the project from the author of this dissertation were as follows: collection and extraction of DNA from volunteer subjects, allele-specific amplification of the DNA, and authorship of the original manuscript. Dr. Lubin's contribution was the conception of designing a laboratory exercise based on the extraction of DNA from buccal cells. Additionally, Dr. Lubin made helpful suggestions regarding the content of the manuscript. Dr. Grant's contributions were conception of amplifying the SNP involved in human color vision, PCR primer design, minor revisions to the manuscript as well as revisions to the supplemental material section.

Abstract

This laboratory exercise offers undergraduate biochemistry students the opportunity to gain experience in a variety of techniques employed in modern molecular biology and biochemistry laboratories. Students utilize microcentrifugation and silica-gel column chromatography to extract DNA from their own buccal (cheek) epithelial cells. The polymerase chain reaction (PCR) and agarose gel electrophoresis are then employed to identify a single nucleotide polymorphism (SNP) that is responsible for a commonly encountered variation in human red color vision.

Introduction

The tremendous impact of the Human Genome Project on the life sciences, both in basic research and in education, has given rise to a need for new laboratory experiments in undergraduate biochemistry. Two main goals of the Human Genome Project are to sequence the entire 3.2 billion base pair human genome and to identify an estimated 100,000 human genes by the year 2003 (*1*). Although 99% of human DNA

sequences are identical across populations, most genetic variation can be traced to single nucleotide polymorphisms (SNPs) (*1, 2*). An SNP is a base substitution found at a single nucleotide position (*3*). Approximately 1.4 million SNPs have been mapped within the human genome (*2*). Chakravarti and others anticipate that SNP analyses will lead to the development of new therapeutic drugs by uncovering genetic differences that influence human disease susceptibility (*1-4*). SNP analysis also makes important contributions towards the study of normal human physiology by providing clues that elucidate gene function and evolutionary development (*3*). Nevertheless, there are few if any undergraduate laboratory experiments that provide students with training in this important area of human genetics research. We have therefore designed a new exercise with the aim of providing direct "hands-on" experience and knowledge beyond what is obtained through routine laboratory instruction.

The following experiment entails the identification of a single nucleotide polymorphism responsible for a normal variation in human red color vision. In the course of this exercise, students will extract their own DNA from buccal (cheek) epithelial cells using a safe and non-invasive procedure. An allele-specific polymerase chain reaction (PCR) will then be employed to amplify a fragment of the gene encoding human red cone opsin. Finally, visualization of the amplified DNA by agarose gel electrophoresis will serve to identify the SNP.

Molecular Basis for Human Color Vision. Human color vision is mediated by red, blue, and green membrane bound proteins (opsins) each residing in different cone cells within the retina. Although the three cone opsins contain the same chromophore, 11-*cis* retinal, their absorption maxima vary greatly, from 426 nm for human blue cone

opsin to 557 nm for human red cone opsin (*5, 6*). Within the human red cone opsin gene, a thymine to guanine single nucleotide polymorphism results in a serine to alanine amino acid substitution at position 180 of the red opsin (*7*, *8*). The wavelength of maximal absorbance (λ_{max}) is shifted from 557 nm for the serine wild type opsin to 552 nm for the alanine variant (*6*). This difference is due to the close proximity of amino acid position 180 to the 11-*cis* retinal chromophore. Because the red cone opsin gene is located on the long arm of the X chromosome (*9*), males can be homozygous for either the serine or alanine allele, while females are either homozygous or heterozygous. In any case, individuals with one or more serine alleles of the opsin have a greater sensitivity to red light (*6* - *8*). Although this difference in perception is only slight, it is significant in practical terms. If an individual were to coordinate a shirt with a tie, someone else with the alternate allele might say that the colors were a bad match.

DNA Extraction from Buccal Cells. Several traditional methods of DNA extraction for PCR analysis, such as fractionation of white cells from whole blood, yield large quantities of quality DNA. However, these methods are often impractical in classroom, diagnostic, and research settings due to the inconvenience of drawing blood, risk of exposure to blood-borne pathogens, and/or complicated extraction procedures (*10*). DNA isolation from buccal cells has been successfully employed in PCR-based human genetics research (*10*, *11*). The procedure is safe, non-invasive, reproducible, fast, and inexpensive. Herein, undergraduate biochemistry students remove a small sample of their own buccal cells by performing a brief oral swab with a soft-bristled, sterile cytobrush. (Because the cytobrush is similar in texture to a toothbrush, there is no discomfort associated with this procedure, no loss of blood, and no risk of infection.) The

students then extract approximately 2 to 5 μg of genomic DNA from the buccal cells using a commercially available QIAamp™ DNA Mini Kit in which cell lysates are microcentrifuged through a silica-gel membrane spin column.

Allele Specific PCR. Allele-specific PCR (AS-PCR) is a well-established method affording facile detection of single nucleotide polymorphisms in genomic DNA (*12*). AS-PCR provides reliable SNP detection, requires no post-PCR processing, and avoids radioactive or fluorescent labeling of primers, thereby reducing cost and labor time (*13*). In this approach, two separate PCR reactions are conducted for each genomic DNA sample. In the first PCR reaction, the 3'-base of one PCR primer will anneal to only one out of two alleles, while the opposing PCR primer hybridizes to both alleles. The second PCR reaction is carried out using the opposing primer and a primer with a 3'-base that is specific for the second allele. The two PCR reactions are then resolved on a nondenaturing agarose gel, upon which the presence or absence of a band in each of two adjacent gel lanes indicates the genotype.

Shown in Figure 6.1 is a schematic of the allele-specific PCR strategy employed in our laboratory exercise. The primer pair F<u>T</u>/R amplifies the serine allele of the human red cone opsin gene, while the primer pair F<u>G</u>/R amplifies the alanine allele.

Experimental Procedure

A biochemistry laboratory equipped with standard pipetters, a PCR thermal cycler, an electrophoresis gel box and power supply, a microcentrifuge, vortexers, and a UV transilluminator will be required to conduct this laboratory experiment. In large classroom settings, students may work in teams designated by one buccal cell donor per team. Two cytobrushes are collected per donor (one from each cheek).

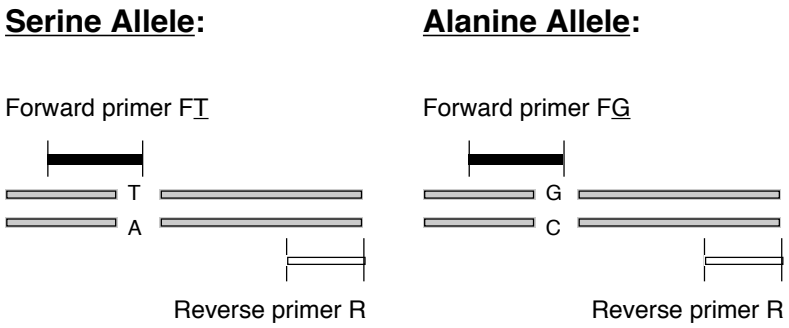

Figure 6.1. Allele-specific PCR amplification of two human red cone opsin polymorphic variants using forward primer FT (5'-TGCCTTCTCCTGGATCTGGT-3'), forward primer FG (5'-TGCCTTCTCCTGGATCTGGG-3'), and reverse primer R (5'-ATGATGATAGCGAGTGGGATG-3').

Each brush is placed in the inner cheek and is gently twirled for 1 min to collect dead buccal cells. The subsequent DNA extraction procedure is completed in ~ 2 h at a cost of approximately 2 dollars per extraction. (Most materials and reagents are included in the QIAamp™ DNA Mini Kit.) The most time-consuming component of the laboratory exercise entails the polymerase chain reaction, which requires approximately 1/2 h to set-up and 4 h to run. The cost of each PCR reaction is approximately 2 dollars, based on reagents purchased from Roche Molecular Biochemicals. Buccal cell collection, DNA extraction, and PCR set-up are carried out during an initial 3 1/2 h laboratory period, at which time the PCR thermal cycler is programmed to run overnight. In a subsequent 3 1/2 h laboratory period, a 1% agarose gel is cast and stained with ethidium bromide, after which the allele-specific PCR products are electrophoresed and then visualized at 302 nm on a UV transilluminator. Detailed notes, laboratory protocols, and buffer recipes, along with a list of equipment, supplies, and chemicals, appear in the supplemental material section of *JCE online*.[ω]

Hazards. Students should wear splash proof goggles and latex gloves at all times. Ethidium bromide is a known mutagen and should therefore be reacted with bleach prior to disposal. Spent cytobrushes, pipette tips, collection tubes, and spin columns should be washed with EtOH and buccal waste solutions should be reacted with bleach.

Results and Discussion

Buccal DNA samples were isolated from 7 female and 7 male Caucasian volunteers and were screened for the red cone opsin SNP. Shown in Figure 6.2 are the corresponding allele-specific PCR reactions resolved on two 1% agarose gels. It is evident that 3 of the 7 females (43%) are heterozygous for the serine (thymine) and alanine (guanine) alleles, while the remaining four females (57%) are homozygous for serine. Of the 7 male volunteers, six (86%) are homozygous for serine and one (14%) is homozygous for the alanine allele.

In a population distribution study, Windericks et al. screened 50 Caucasian males for the red cone polymorphism and found that 62% carried the serine allele while 38% were homozygous for alanine (*8*). In a recent survey of 9 females by Neitz et al., 56% were found to be heterozygous, while 33% and 11% were homozygous for serine and alanine respectively (*14*). Together with our results, the above data indicate that serine is the predominant allele associated with the red cone opsin SNP.

A) Female Donors:

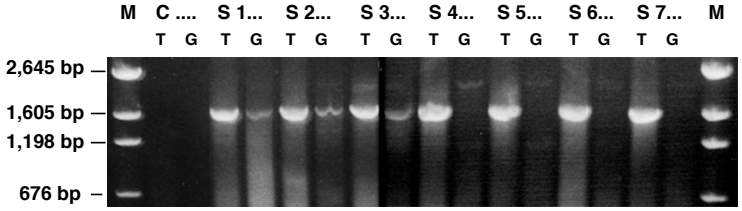

B) Male Donors:

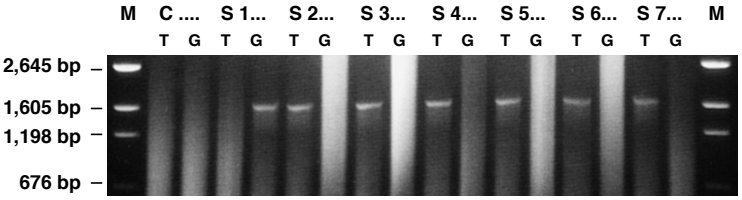

Figure 6.2. Human red cone opsin allele-specific PCR reactions resolved on 1% nondenaturing agarose gels. Serine and alanine reactions were run with primer pairs FT/R and FG/R respectively, for A) seven female and B) seven male buccal cell donors. M: pGEM DNA size marker. C: control PCR reaction, without template DNA. S: PCR reaction, with template DNA. T: serine (thymine) PCR reaction. G: alanine (guanine) PCR reaction.

Conclusion

We have presented a new undergraduate biochemistry laboratory exercise in which students extract DNA from their own buccal cells and employ allele-specific PCR to identify a single nucleotide polymorphism that is responsible for a normal variation in red color vision. This exercise has substantial educational merit in that the techniques presented are widely employed in industrial, academic, and government research institutions. Therefore, the exercise is likely to be of great benefit to undergraduate chemistry students, particularly those seeking careers in biochemistry, forensics, medicinal chemistry, medicine, and related fields.

Acknowledgments

We thank Xia Yang and Miki Kassai for assistance and the National Science Foundation for financial support under grant DUE-0089417 (Professor Jerry C. Smith, Georgia State University).

Supplemental Material

Detailed information for students and instructors is available in this issue of *JCE Online.*

Notes

1. Dr. Lubin's participation in this work was undertaken in his private capacity. No official support or endorsement by the Centers for Disease Control and Prevention is intended or should be inferred.
2. The sequence variation determined in this exercise should not be construed to indicate the presence or absence of any medical condition including those related to color vision. This exercise was developed to teach principles of PCR and its application in molecular genetics. Pipetting and other experimental errors can occur that result in absence of PCR products or incorrect determination of the sequence variation. Since it is not feasible to access or critically control for all such errors in the context of this exercise, results should not be taken as definitive assignment of sequence variations to specific individuals.

Literature Cited

(1) Human Genome Program, U.S. Department of Energy, *Genomics and Its Impact on Medicine and Society: A 2001 Primer* **2001**.

(2) The International SNP Map Working Group. *Nature* **2001**, *409*, 928-933.

(3) Stoneking, M. *Nature* **2001**, *409*, 821-822.

(4) Chakravarti, A. *Nature* **2001**, *409*, 822-823.

(5) Oprian, D. D.; Asenjo, A. B.; Lee, N.; Pelletier, S. L. *Biochemistry* **1991**, *30,* 11367-11372.

(6) Merbs S. L.; Nathans J. *Nature* **1992**, *356,* 433-435.

(7) Neitz, M.; Neitz, J.; Jacobs, G. H. *Science* **1991**, *252*, 971-974.

(8) Winderickx, J.; Lindsey, D. T.; Sanocki, E.; Teller, D.Y.; Motulsky, A. G.; Deeb, S. S. *Nature* **1992**, *356*, 431-433.

(9) Nathans, J.; Thomas, D.; Hogness D. S. *Science* **1986,** *232,* 193-202.

(10) Richards, B.; Skoletsky, J.; Shuber, A. P.; Balfour, R.; Stern, R. C.; Dorkin, H. L.; Parad, R. B.; Witt, D.; Klinger, K. W. *Hum. Mol. Genet.* **1993**, *2,* 159-163.

(11) Crawford, D. C.; Meadows, K. L.; Newman, J. L.; Taft, L. F.; Pettay, D. L.; Gold, L. B.; Hersey, S. J.; Hinkle, E. F.; Stanfield, M. L.; Holmgreen, P.; Yeargin-Allsopp, M.; Boyle, C.; Sherman, S. L. *Am. J. Hum. Genet.* **1999**, *64*, 495-507.

(12) Thompson, M. W.; McInnes, R. R.; Willard, H. F. *Genetic in Medicine*, 5th ed; W. B. Saunders Company: Philadelphia, **1991**; p.108.

(13) Wilson, R. C.; Wei, J. Q.; Cheng, K. C.; Mercado, A. B.; New, M. I. *J. Clin. Endocrinol. Metab.* **1995**, *80*, 1635-1640.

(14) Neitz, M.; Kraft, T. W.; Neitz, J. *Vision Res.* **1998**, *38*, 3221-3225.

Supplemental Material

<u>Part 1</u>: DNA Extraction from Buccal Cell Samples using a QIAamp™ DNA Mini Kit

Experimental Procedure

1. Two cytobrushes will be used, one brush for each of your cheeks (left and right).

2. Place a sterile cytobrush in between your gums and cheek. Gently twirl each brush both in the upper and bottom cheeks, 1 min per brush.

3. Place each brush into a separate 1.7 mL microcentrifuge tube and clip off the brush handle with a pair of scissors.

4. Add 500 μL of **phosphate buffered saline** (PBS) to each of the two tubes. Vortex the tubes vigorously for 1 min. Scrape the bristles against the walls of the tube. Remove the brushes with a pair of forceps and discard into a solid waste container containing 70% ethanol.

5. Decant the contents of one tube into the other to obtain a total volume of 1000 μL. (After decanting, transfer any residual liquid with a pipette tip. Discard the used pipette tip into the solid waste container.)

6. Centrifuge at 8,000 RPM for 5 min. Decant the supernatant into a liquid waste container containing a 5% bleach solution.

7. Add 200 μL of **PBS** to the microfuge tube and resuspend the cell pellet by vortexing vigorously for 1 min.

8. Add 20 μL of **Proteinase K** and mix by pulse-vortexing for 15 s. (Use of the **QIAamp Kit** begins here.)

9. Add 200 μL of lysis **Buffer AL** to the sample and mix by pulse-vortexing for 15 s.

10. Incubate at 56 °C for 10 min, then centrifuge at 8,000 RPM for 15 s.

11. Add 200 μL of **100% ethanol** to the sample and mix by pulse-vortexing for 15 s. Centrifuge for 2 - 3 s.

12. Transfer 500 μL of the total solution (~ 700 μL) from **step 11** to the **QIAamp spin column** (placed in a 2 mL collection tube) without wetting the rim of the column. Centrifuge at 8,000 RPM for 2 min and decant the filtrate into the liquid waste container.

13. Repeat **step 12** once more with the remaining solution from **step 11**.

14. Discard the used collection tube into the solid waste container. Place the **QIAamp column** into a clean 2 mL collection tube.

15. Add 500 μL of **Buffer AW1**, centrifuge at 8,000 RPM for 1 min, and decant the filtrate into the liquid waste container.

16. Add 500 μL of **Buffer AW2** and centrifuge at 14,000 RPM for 3 min.

17. Examine the column to ensure that there is no residual liquid adhering to the silica-gel membrane. If found, continue to centrifuge until all of the liquid has been transferred to the collection tube.

18. Decant the filtrate into the liquid waste container. Discard the used collection tube into the solid waste container.

19. Place the **QIAamp spin column** into a clean 1.7 mL microcentrifuge tube and add 100 μL of **ddH_2O** to the column. Close the column's cap, leaving the cap of the outer 1.7 mL centrifuge tube open. Incubate at room temperature for 5 min. To elute DNA, centrifuge at 8,000 RPM for 2 min.

20. Discard the spin column into the solid waste container. Close the cap on the 1.7 mL centrifuge tube containing the DNA. The approximate yield of DNA will be 10 - 40 ng/μL.

Commentary

In this section of the laboratory, you will perform an oral swab with a soft-bristled, sterile cytobrush (Fisher Scientific). This procedure will remove a small quantity of your buccal (cheek) cells, which are dislodged from the brush by vortexing in **PBS**. You will then use a **QIAamp™ DNA Mini Kit** to isolate a sample of your own genomic DNA from the resulting cell suspension. DNA purification using the **QIAamp™ Kit** is based on a simple bind-wash-elute procedure. Nucleic acids are adsorbed onto a silica-gel membrane in the presence of high concentrations of chaotropic salts, which remove water from hydrated molecules in solution. Polysaccharides and proteins do not adsorb onto the silica and are removed. After two wash steps, pure nucleic acids are eluted under low-salt conditions in small volumes.

Isolation Procedure. The precise chemical compositions, concentrations, and pH values of the buffers contained in the **QIAamp™ DNA Mini Kit** are proprietary and are not described by the manufacturer. The buccal cell pellet is resuspended in **PBS** to which **Proteinase K** and **Buffer AL** are added. Lysis **Buffer AL** contains a chaotropic, guanidinium-based salt that degrades cell membrane and denatures proteins, while **Proteinase K** enzymatically hydrolyzes accessible peptide amide bonds. The lysate is then applied to the **QIAamp spin column** containing an unmodified silica-gel membrane which retains the DNA. (It has been determined empirically that nucleic acids bind to silica at pH ≤7.5, in the presence of ethanol and high concentrations of salt (*1*). The

precise mechanism through which DNA is adsorbed onto the silica is unknown.) After brief centrifugation, proteins and cellular debris are eluted in the filtrate. The first wash **Buffer AW1** contains a different chaotropic salt which serves to further denature proteins and elute residual protein contamination from the membrane. The ethanol-based wash **Buffer AW2** is then utilized to remove any residual salts. Finally, **ddH_2O** is used to elute the purified DNA from the membrane.

Instructor's Notes

All procedures in Parts 1 and 2 of this exercise can be conducted in a single 3 1/2 h laboratory period.

All buffer solutions, proteinase K, spin columns, and collection tubes are included in the QIAamp™ DNA Mini Kit (with the exception of PBS and 100% ethanol). Although the QIAamp Kit contains an eluting buffer (Buffer AE), its use is not recommended for applications that involve subsequent PCR amplification of genomic DNA, as Buffer AE contains salts that may interfere with PCR. Also note that the QIAamp Kit includes a Handbook with step by step instructions for the extraction of DNA from many different types of tissue. The buccal extraction protocol described here was adapted from the "Blood and Body Fluid Spin Protocol" on pp. 22-24 of the January 1999 QIAamp Handbook. Before beginning this laboratory exercise, you should read the Handbook included in your particular Kit to determine if any instructions have been updated or changed.

Literature Cited

1. Vogelstein, B; Gillespie, D. *Proc. Natl. Acad. Sci. USA* **1979**, *76,* 615-619.

Part 2: PCR Protocol, Genotyping a Serine/Alanine Polymorphism of the Long-Wavelength Cone Opsin in Normal Human Color Vision

Experimental Procedure

1. You will prepare two separate PCR reactions which will be used to identify wild type and polymorphic alleles of the human red cone opsin gene. The first reaction will utilize primer pair **FT/R** while the second will utilize primer pair **FG/R**.

FT: Forward Primer 5'-ATTGCCTTCTCCTGGATCTGG**T**-3'

FG: Forward Primer 5'-ATTGCCTTCTCCTGGATCTGG**G**-3'

R: Reverse Primer 5'- AGCATGATGATAGCGAGTGGGA-3'

2. Add 10 μL of genomic DNA (10 - 40 ng/μL, in **ddH_20**) to each of two pre-labeled PCR tubes (one for primer pair **FT/R** and one for primer pair **FG/R**).

3. To each tube, add 40 μL of a **PCR cocktail mix*** prepared by the Laboratory Instructor. The resulting 50 μL PCR reaction will contain:

	1X	Final Concentration
DNA Template (10 - 40 ng/μL)	10.0 μL	(2.0 – 8.0 ng/μL)
dNTP's (10 mM each nucleotide)	1.0 μL *	200 μM
10X PCR buffer w/Mg^{++}	5.0 μL *	1X
Forward primer (10 μM)	5.0 μL *	1 μM
Reverse primer (10 μM)	5.0 μL *	1 μM
Taq polymerase (5 Units /μL)	0.5 μL *	0.05 Units/μL
Deionized water	23.5 μL*	
Total Volume	50 μL	

4. Vortex and centrifuge each tube briefly.

5. Add three drops of mineral oil to each tube with a Pasteur pipette. This will prevent the mixture from evaporating during PCR amplification.

6. Centrifuge briefly.

7. Load the samples into a **Perkin-Elmer Model 480 Thermal Cycler** programmed with the following cycling parameters:

94 °C	5 min	1 cycle	Initial Denaturation
94 °C	50 s	45 cycles	Denaturation
64 °C	1 min	45 cycles	Annealing
72 °C	2 min	45 cycles	Elongation
72 °C	10 min	1 cycle	Final Extension

Note: because PCR is an extremely sensitive technique, the Instructor will prepare and run two additional reactions (one for primer pair **FT/R** and a second for primer pair **FG/R**) containing all reagents with the exception of template DNA, which will be substituted by equivalent volumes of water. These two reactions will serve as negative controls to rule out the presence of trace levels of contaminating DNA in buffer, primers, dNTP's, enzyme, and in any other reagents you utilized to prepare your PCR reactions.

Commentary

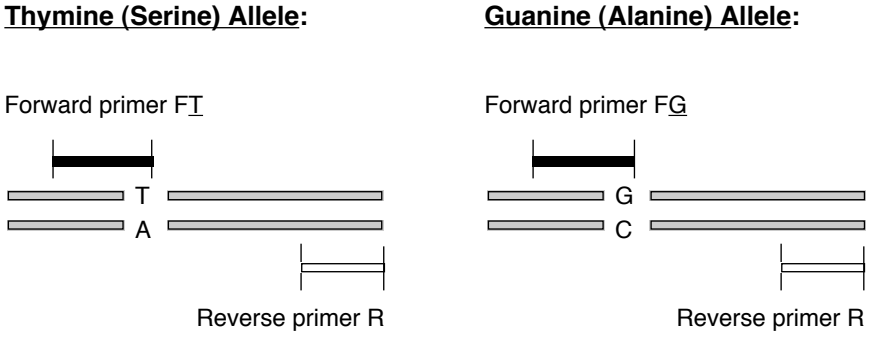

"Allele-specific PCR amplification of two human red cone opsin variants."

In this section of the laboratory, you will utilize the polymerase chain reaction (PCR) to screen your genomic DNA sample. The purpose of this exercise will be to identify a common genetic polymorphism that accounts for a normal variation in human color vision. This polymorphism involves a **thymine** to **guanine** base substitution in the gene encoding human red cone opsin. Shown above, the primer pair **FT/R** will amplify the thymine allele of the opsin, while the primer pair **FG/R** will amplify the guanine allele.

As light enters the eye, it hits the retina, where cone cells containing blue, green, and red opsins mediate color vision. The opsins bind tightly to the chromophore 11-*cis* retinal. This chromophore absorbs light differently, depending upon how it is held by the opsin. The above thymine to guanine base substitution produces a corresponding serine to alanine amino acid substitution at position 180 of human red cone opsin. Because position 180 is near 11-*cis* retinal, the wavelength of maximal absorbance (λ_{max}) of the red cone opsin is shifted from 557 nm (for the serine variant) to 552 nm (for the alanine variant; *1,2).* As a result, individuals with serine alleles of the opsin have a greater

sensitivity to red light. Although the difference between the two types of color vision is only slight, it is significant in practical terms: if an individual were to buy a shirt and tie that he or she believed to be a good color match, someone else with the alternate allele might say that they are not.

Because the human red cone opsin gene is X-linked, males will be homozygous for either the serine or the alanine allele, while females will be either homozygous or heterozygous (serine and alanine alleles, each on separate X chromosomes).

Instructor's Notes

All procedures in Parts 1 and 2 of this laboratory exercise can be conducted in a single 3 1/2 h laboratory period. At this time, the PCR reactions should be set-up to run overnight. (The PCR reactions will require approximately 1/2 h to set-up and 5 h to run.)

As a time-saving measure, you should prepare a PCR "cocktail" mix which the students will use to set-up their PCR reactions. For multiple reactions, use of a cocktail minimizes pipetting errors. As described in the experimental procedure, this cocktail includes all asterisked PCR reagents minus template DNA. To make the cocktail, simply multiply each 1X volume times the total number of PCR reactions plus one. Remember to prepare separate cocktails for each primer pair and to keep all PCR reagents on ice. (The 10X PCR buffer w/Mg^{++} is provided with Taq polymerase purchased from Roche Molecular Biochemicals under catalog # 1146165.)

You should also utilize the procedures in Part 2 to prepare two negative control PCR reactions (one for primer pair F<u>T</u>/R and a second for primer pair F<u>G</u>/R) in which template DNA is substituted by equivalent volumes of water. Prior to running the PCR

reactions, add ~ 2 drops of mineral oil to each well of the thermal cycler heating block. This will ensure uniform heating and cooling of all PCR reaction tubes.

PCR Troubleshooting. In this laboratory exercise, we have designed PCR primers and have optimized cycling parameters, reagent concentrations, and other experimental variables to avoid errors commonly encountered in PCR experiments. These errors can result in the absence of PCR product, nonspecific priming, primer-dimer formation, and/or the production of faint or smeared PCR bands. Although we have advised the use of a PCR cocktail, inaccurate pipetting may still be a problem in the context of an undergraduate laboratory setting.

We suggest that you perform the FT/R and FG/R PCR reactions in advance of the laboratory exercise in order to verify the integrity of the PCR reagents that you have purchased. We would also like to point out that the PCR cycling parameters described here have been optimized for a Perkin-Elmer Model 480 DNA thermal cycler. Thermal cyclers from other manufactures should work well, but the cycling parameters may need to be adjusted in advance to optimize sensitivity and specificity of the PCR reactions. It is also advisable to set aside approximately 10 min of the initial laboratory period in order to allow students to become familiar with laboratory equipment and to practice pipetting water into microcentrifuge tubes. Finally, there are several excellent literature references that provide additional information on PCR optimization and troubleshooting strategies *(3-5)*.

Literature Cited

1. Winderickx, J.; Lindsey, D. T.; Sanocki, E.; Teller, D.Y.; Motulsky, A. G.; Deeb, S. S. *Nature* **1992**, *356*, 431-433.

1. Merbs S. L.; Nathans J. *Nature* **1992**, *356,* 433-435.
2. Sambrook, J.; Fritsch, E.F.; Maniatis, T. *Molecular Cloning: A Laboratory Manual*; Cold Spring Harbor Laboratory Press: Cold Spring Harbor, New York, 1989.
3. Ausubel, F.M.; Brent, R.; Kingston, R.E.; Moore, D.D.; Seidman, J.G.; Smith, J.A.; Struhl, K. *Current Protocols in Molecular Biology*; John Wiley & Sons, Inc.: New York, 1998.
4. McPherson, M.J.; Moller, S.G. *PCR: the Basics from Background to Bench*; Springer-Verlag New York Inc.: New York, 2000.

<u>Part 3</u>: Agarose Gel Electrophoresis, Genotyping A Serine/Alanine Polymorphism of the Long-Wavelength Cone Opsin in Normal Human Color Vision

Experimental Procedure: Gel Pouring Demonstration (to be conducted by the Laboratory Instructor)

1. The ends of a 10 x 15 cm agarose gel casting tray are sealed with tape to form a mold. Electrophoresis combs are placed in the tray.
2. A 2% agarose gel is cast as follows:

   BioRad Mini Sub Gel apparatus: A total of 105 mL of **1X Tris-acetate EDTA Buffer** (TAE) is transferred to a 250 mL Erlenmeyer flask and 2.1 g of **agarose** are added. The neck of the flask is loosely sealed with saran wrap, and a magic marker is used to annotate the fluid level on the side of the flask. The agarose mixture is then boiled for ~3 min using a microwave oven set at high power. An oven mitt is utilized to swirl the contents of the flask intermittently. The solution should be visually inspected to ensure that all agarose has completely dissolved. If any buffer

has evaporated, the flask should be filled to the mark with **ddH_2O** and its contents swirled.

3. The agarose solution is cooled to ~60 °C. A total of 10.5 μL of **ethidium bromide** (5 mg/mL) is added and the flask is swirled to mix.
4. To cast the gel, the agarose solution is poured into the gel tray. Air bubbles are aspirated from the poured gel using a Pasteur pipette. The gel is then allowed to solidify undisturbed (~40 min at room temperature).
5. A few mL of **1X TAE** are poured onto the tray. The tape is gently removed and the gel tray is transferred to an electrophoresis tank.
6. Approximately 700 mL of **1X TAE** are added to the tank. The gel combs are gently removed and a total of 70 μL of **ethidium bromide** (5 mg/mL) is added to the **1X TAE**.

Experimental Procedure: Loading and Running the Gel Demonstration (to be conducted by the Instructor and Students)

1. In order to separate the PCR products from the mineral oil layer, insert a pipette tip through the mineral oil and transfer 20 μL of the **FT/R** PCR reaction from the lower (aqueous) layer to a new 1.7 mL microfuge tube. In a similar fashion, transfer 20 μL of the **FG/R** reaction into a second 1.7 mL microfuge tube. Add 3 μL of **6X loading buffer** to each, briefly spin the microfuge tubes, vortex, and spin again.

2. The Instructor will add 3 μL of **6X loading buffer** to 20 μL of a 1:20 dilution of **pGEM DNA size marker.** He or she will load the resulting solution into two outside wells of the 2% agarose gel (11 μL per well). The Instructor will also load

two control PCR reactions in which the template DNA has been substituted by equivalent volumes of water.

3. Load 20 μL of the **FT/R** PCR reaction followed by 20 μL of the **FG/R** reaction into interior wells of the gel, from left to right, in the order indicated below.

Loading ⟶

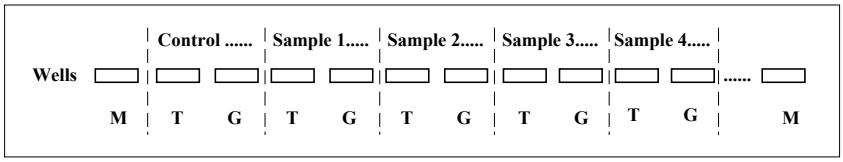

M = pGEM DNA size marker (2645 bp - 36 bp).
Control = PCR reactions, without template DNA.
Sample = PCR reactions, with template DNA.
T = FT/R PCR reaction.
G = FG/R PCR reaction.

"Agarose gel loading scheme."

4. The Instructor will close the lid of the gel tank and will attach the leads so that the DNA will migrate towards the anode (red lead).

5. The Instructor will apply a voltage of 1-5 V/cm (measured as the distance between electrodes). If the leads have been attached correctly, the bromophenol blue in the loading buffer will migrate from the wells into the body of the gel (towards the anode). He or she will run the gel (~1 h) until the bromophenol blue has migrated an appropriate distance.

6. After turning off the electric current and removing the leads and the lid from the gel tank, the Instructor will (i) transfer the gel tray from the tank to a UV transilluminator set at 302 nm, (ii) remove the tray, (iii) and photograph the gel (optional).

7. Draw a sketch of the gel in your laboratory notebook. Discard all unused genomic DNA and PCR amplified DNA into the liquid waste container containing 5% bleach solution.

Commentary

In the final section of this laboratory, you will run your individual PCR reactions on a 2% agarose gel adjacent to a **pGEM DNA size marker** (Promega). The **pGEM marker** is comprised of DNA fragments that are 2645, 1605, 1198, 676, 517, 460, 396, 350, 222, 179, 126, 75, 65, 51, and 36 bp in size. The relative mobilities of these fragments will enable you to identify your PCR products as follows. The primer pairs **FT/R** and **FG/R** will each produce a DNA fragment 1661 bp in size in the case of heterozygous females (both serine-**T** and alanine-**G** alleles are present, each on a separate X chromosome). For homozygous males and females carrying the serine allele, only the **FT/R** primer pair will produce a 1661 bp PCR product. Alternatively, only the **FG/R** primer pair will produce a 1661 bp fragment in males and females that are homozygous for the alanine allele.

Agarose Gel Electrophoresis. Agarose gel electrophoresis is a routinely used method for the separation and identification DNA fragments ranging from 200 bp to 50 kbp in length *(1,2)*. Agarose, which is extracted from seaweed, in a linear polysaccharide consisting of repeating D-galactose and 3,6-anhydro L-galactose subunits. When voltage is applied across an agarose gel, negatively charged DNA will migrate through the agarose pores towards the positively charged anode. The rate of migration is (i) inversely proportional to the $\log_{10}$ of the number of base pairs in the DNA fragment and is (ii) unaffected by base composition. The locations of bands containing as little as 1 ng – 10

ng DNA can be determined by treating the agarose gel with the fluorescent intercalating dye ethidium bromide. **(Ethidium bromide is a mutagen and should be handled with extreme care.)** Finally, the size of the DNA fragments which can be accurately resolved is a function of the amount of agarose used to pour the gel (% [w/v]).

Instructor's Notes

All procedures in Part 3 of this laboratory exercise should be conducted in a second 3 1/2 h laboratory period. As part of a gel pouring demonstration, you should cast and then run the 2% agarose gel that the students will use to resolve their PCR reactions. In this way, it will only be necessary to use a single gel electrophoresis apparatus and power supply to conduct this laboratory exercise. In addition, you should prepare and load the pGEM DNA size marker and the negative PCR control reactions into appropriate wells of the 2% agarose gel.

It may be necessary to optimize the volume of molten agarose used to cast the gel, if an alternative to the recommended gel apparatus is employed. It is also important to note that the robustness of the PCR reactions will depend on the yields of DNA obtained in the extraction step of this laboratory exercise. Relatively low yields of genomic DNA may produce faint PCR bands on the agarose gel. Finally, you should stress to your students that their PCR data should not be taken as a definitive assignment of sequence variation as it is not feasible to rule out the possibility of pipetting and other experimental errors in the context of the laboratory exercise.

Literature Cited

1. Sambrook, J.; Fritsch, E.F.; Maniatis, T. *Molecular Cloning: A Laboratory Manual*; Cold Spring Harbor Laboratory Press: Cold Spring Harbor, New York, 1989.
2. Ausubel, F.M.; Brent, R.; Kingston, R.E.; Moore, D.D.; Seidman, J.G.; Smith, J.A.; Struhl, K. *Current Protocols in Molecular Biology*; John Wiley & Sons, Inc.: New York, 1998.

Hazards

Students should wear splash proof goggles and latex gloves at all times. Ethidium bromide is a known mutagen and should therefore be reacted with bleach prior to disposal. Spent cytobrushes, pipette tips, collection tubes, and spin columns should be washed with 70 % EtOH and buccal waste solutions should be reacted with bleach prior to disposal.

Product Information

Chemicals, Supplies, and Equipment

Product	**Manufacturer**	**Catalog #**	**CAS#**
Agarose	Invitrogen	15510019	-
Bromophenol blue	Aldrich	114405	[62625-28-9]
Cyto-Soft cytobrushes	Fisher	2226357	-
DNA thermal cycler	Perkin-Elmer	Model 480	-
dNTP mix (10 mM each)	Roche	1581295	-
EDTA	Aldrich	106321	[85715-60-2]
Electrophoresis power supply	Invitrogen	Model 250	-
Ethanol (100%)	Aldrich	245119	[64-17-5]
Ethidium bromide tablets	Sigma	E2515	[1239-45-8]
Ficoll (20% aqueous solution)	Sigma	F5415	[26873-85-8]
Gel electrophoresis apparatus (large)	Owl Scientific	Model A1	-
Gel electrophoresis apparatus (small)	Bio-Rad	Wide Mini Sub	-
Glacial acetic acid	Aldrich	338826	[64-19-7]
KCl	Aldrich	208000	[7442-40-7]
KH_2PO_4	Sigma	P5379	[7778-77-0]
Microcentrifuge tubes (1.7 mL)	VWR	20170-650	-
Mineral Oil	Fisher	O121-1	-
Na_2HPO_4	Sigma	S9390	[7782-85-6]

NaCl	Aldrich	223514	[7647-14-5]
PCR primers	BioSource	Custom Order	-
PCR reaction tubes (0.6 mL)	Costar	29442-340	-
pGEM DNA size marker	Promega	G1741	-
Polaroid camera*	Fisher	FBPDC34	-
Polaroid B&W film 3000 ISO*	Fisher	617538	-
QIAamp DNA Mini Kit	Qiagen	51304	-
Taq polymerase Kit	Roche	1146165	-
Tris base	Aldrich	154563	[77-86-1]
UV Transilluminator	VWR	21475-464	-
Vortexer	VWR	58816-121	-

* These items are optional. They are not required to conduct this laboratory exercise.

Manufacturers

Aldrich	1-800-558 9160
Bio-Rad Laboratories	1-800-424-6723
BioSource International	1-800-788-4362
Fisher Scientific	1-800-766-7000
Invitrogen Life Technologies	1-800-828-6686
Owl Scientific Inc.	1-800-242-5560
Perkin-Elmer Biosystems	1-800-327-3002
Promega Corporation	1-800-356-9526
Qiagen	1-800-426-8157
Roche Molecular Biochemicals	1-800-262-1640
Sigma	1-800-325-3010

VWR Scientific Products 1-800-932-5000

Buffer Preparation

Ethidium Bromide (5 mg/ml):

Dissolve one 100 mg ethidium bromide tablet (Sigma) in 20 mL of ddH_2O. Protect the solution from light in an amber bottle or with aluminum foil. Store at room temperature.

PBS:

Dissolve 8 g of NaCl, 0.2 g of KCl, 1.44 g of Na_2HPO_4 and 0.24 g of KH_2PO_4 in 800 mL of ddH_2O. Adjust pH to 7.4 with HCl, add ddH_2O to 1000 mL. Sterilize by autoclaving. Store at room temperature.

6X Loading Buffer (0.25% Bromophenol Blue, 15% Ficoll):

Dissolve 2.5 mg of bromophenol blue in 25 mL of ddH_2O. Add 75 mL of 20% Ficoll. Store at room temperature.

50X TAE Buffer:

Dissolve 242 g of Tris base in 600 mL of ddH_2O, add 57.1 mL of glacial acetic acid and 100 mL of 0.5M EDTA (pH 8.0). Adjust final volume to 1 liter with ddH_2O. (1X TAE is made from this stock solution by diluting with ddH_2O.) Store at room temperature.

SUMMARY

In Chapter II the syntheses of two acridine chromophores incorporating two or four metal binding imidazole rings were described. DNA photocleavage assays were conducted with compound **7** (four imidazole rings) and compound **10** (two imidazole rings) in the absence and presence of 16 metals salts in sodium phosphate buffer pH 7.0. Irradiation of pUC19 plasmid DNA employing a low-intensity broad spectrum fluorescent lamp for 50 min (under aerobic conditions) revealed that photocleavage yields by compound **7** were significantly enhanced in the presence of Hg(II), Fe(III), Cd(II), Zn(II), V(V), and Pb(II). Moreover, compound **7** consistently produced higher levels of metal-assisted DNA photocleavage in comparison to compound **10**. DNA cleavage yields by compound **7** irradiated without metal or run in the dark exhibited low levels of cleavage.

To further examine DNA photocleavage and to gain insight on the factors effecting metal-assisted photodamage, nicking assays were conducted by employing different buffers and by varying the pH. These experiments indicated that at pH 5.0 compound **7** demonstrated efficient levels of DNA photocleavage. However, as the pH was increased cleavage levels were dramatically reduced. At pH values ranging from 6.0-8.0 and in the presence of Hg(II), Fe(III), Cd(II), Zn(II), V(V), and Pb(II), DNA photocleavage yields were markedly enhanced. DNA thermal denaturation studies were then conducted with calf thymus DNA in the presence of compound **7** and $ZnCl_2$ as a function of pH. At pH 5.0, the T_m value produced by compound **7** (no metal) was 96 ºC while the value at pH 7.0 was 84 ºC. Upon the addition of $ZnCl_2$, the T_m exhibited by compound **7** at pH 7.0 was 90 ºC. Collectively, these studies indicated that both buffer

and pH could be utilized to effect metal-assisted DNA photocleavage. Moreover, the metals might be compensating for the loss in positive charge density in compound **7** as the pH was increased thereby increasing duplex stabilization and consequently enhancing DNA photocleavage yields.

Scavenger assays with the six photoactive metal ions were employed to provide insights into the photosensitization mechanism(s) underlying DNA damage. In the case of Fe(III), metal-assisted photocleavage predominantly proceeded through a type I (hydroxyl radical) mechanism. Metal-assisted DNA photocleavage by Hg(II), Cd(II), Zn(II), V(V), and Pb(II) proceeded via type I and type II mechanisms. Additionally, DNA photocleavage yields were dramatically reduced in photolysis reactions containing the metal chelator EDTA, further establishing the necessary requirement for the presence of Hg(II), Fe(III), Cd(II), Zn(II), V(V), and Pb(II) in DNA photodamage mediated by compound **7**.

The next studies explored the photochemical (absorbance and emission) properties and DNA binding affinity (T_m) of compound **7** in the presence of the 16 metals salts and calf thymus DNA. Based on the Hard-Soft Acid-Base theory, imidazole is a borderline base which would be expected to form stable complexes with borderline and soft acid metals. In the case of the borderline or soft acids, two trends emerged. First, the photocleavage enhancing metals Zn(II), Cd(II), Hg(II), and Pb(II) exhibited high T_m values and relatively low levels of fluorescence quenching in the presence of DNA. Alternatively, the DNA photocleavage inactive metals Ni(II), Co(II), and Cu(II) produced increased T_m values and the highest levels of fluorescence quenching with DNA. While its conceivable that these three borderline metals interacted with compound **7** and

increased the T_m values of calf thymus DNA, their inability to enhance DNA photocleavage might be attributed to the high levels of fluorescence quenching produced in the presence of these metal ions and DNA. The hard acid metals Sn(IV), Sc(III), Zr(IV), Cr(III), Ca(II), Mg(II), and Mn(II) produced low cleavage, while Fe(III) and V(V) exhibited high levels of DNA photocleavage, respectively. Additionally, these 9 hard acid metals did not significantly effect fluorescence quantum yields or the T_m of calf thymus DNA. In order to test for the one-electron photoreduction of Fe(III) and V(V) by the excited state triplet of compound **7**, a colorimetric assay using 1,10-phenanthroline was developed. Accordingly, the assay revealed the involvement of Fe(II) and V(IV) thereby suggesting that DNA photodamage in the presence of these two metal ions might proceed via a Fenton mechanism generating cytotoxic diffusible hydroxyl radicals.

In Chapter III, the synthesis and characterization of a bisacridine incorporating a copper(II) binding pyridine linker (compound **4**) was reported. In the absence of metal, ligand **4** displayed higher apparent binding constants and preferential binding to GC-rich DNA sequences as determined by employing a competitive equilibrium dialysis experiment. DNA photocleavage studies employing pUC19 plasmid DNA irradiated at 419 nm under aerobic conditions equilibrated with compound **4** and $CuCl_2$ in sodium phosphate buffer pH 7.0 were conducted. These studies indicated that while irradiated ligand **4** exhibited direct single strand breaks, in the presence of copper(II) DNA photodamage produced additional double strand scission thereby markedly enhancing cleavage yields.

To gain insight into the DNA binding affinity of compound **4** in the presence of Cu(II) ions, DNA thermal denaturation experiments with calf thymus DNA were

conducted. DNA equilibrated with only $CuCl_2$ did not exhibit any changes in the T_m values (T_m values for DNA = 75 ºC and with Cu(II) = 75 ºC), while the addition of compound **4** (no metal) produced a T_m value of 79 ºC. In the presence of **4** and Cu(II) ions, the ΔT_m was increased by 6 ºC in comparison to the value obtained for ligand **4** without metal.

With regards to the DNA photosensitization mechanism(s) involved in photodamage, scavenger assays indicated the involvement of a singlet oxygen, hydrogen peroxide and Cu(I). Because photoreduction of Fe(III) and V(V) by the excited state acridine was observed in the previous study, a colorimetric assay employing the Cu(I)-specific chelating agent bathocuproinedisulfonic acid disodium salt was employed. This experiment provided evidence for the one-electron photoreduction of Cu(II) by the excited state acridine chromophore and thus its involvement in mediating efficient DNA photodamage via a Cu(I)-peroxide radical center. Furthermore, analysis of DNA photocleavage at nucleotide resolution assays utilizing a ^{35}S radiolabeled 138 bp from pUC19 plasmid DNA fragment revealed direct DNA strand breaks without any base specificity, thereby suggesting the participation of radicals in hydrogen atom abstraction from deoxyribose at every nucleotide position. In contrast, post-irradiation addition of piperidine base to the reactions containing ligand **4** and $CuCl_2$ ions revealed alkali-labile damage predominantly at guanine bases, most likely produced by singlet oxygen.

Taken together, these studies indicate that incorporating metal binding domains to DNA photosensitizing acridine conjugates, can significantly increase the photoactivity of these agents in the presence of metals. In the case of compound **7**, efficient DNA photodamage is achieved by employing a low-intensity light and can be modulated by

buffer and pH. Additionally, compound **7** demonstrates fluorescence emission tunability in the presence of metals and may serve as a chemical tool to further probe nucleic acid-ligand interactions. With regards to compound **4**, the fact that non-specific DNA damage was observed at every nucleotide position, make it conceivable that this ligand has potential applications as a photofootprinting reagent. Finally, considering that Zn(II), Fe(III) and Cu(II) are biologically important metal ions, photosensitizers that form complexes with or can be effected by these metals may offer enhanced *in vivo* reactivity.

Chapter IV described the syntheses, characterization, and evaluation of a new photosensitizer incorporating two phenothiazine rings (compound **3**) and an electron donating 4,4'-ethylenedipiperidine linker. The phenothiazine chromophore and linker were introduced to potentially effect DNA photosensitization at longer wavelengths and to provide additional DNA stability.

In the presence of DNA, compound **3** exhibited stronger absorption of light at a longer wavelength (ε_{680} = 7.78 x 10^4 M^{-1} (bp) cm^{-1}) in comparison to the archetypal phenothiazine **MB** (ε_{674} = 5.80 x 10^4 M^{-1} (bp) cm^{-1}). DNA photocleavage experiments demonstrated that utilizing only 1 μM of compound **3** effected higher cleavage levels at all wavelengths (676, 700, 710 nm) and time-points (10, 30, 60 min) tested as compared to 1 μM **MB**. Irradiation of DNA at the longest wavelength (710 nm) as a function of concentration also revealed that compound **3** possessed higher DNA cleaving activity. Notably, 5 μM of compound **3** and 5 μM **MB** produced photocleavage yields of 93% and 59%, respectively.

DNA photocleavage inhibition of compound **3** was observed in the presence of sodium azide (type II mechanism, singlet oxygen) and to a lesser extent with D-mannitol

(type I mechanism, hydroxyl radicals). Additionally, the analysis of DNA photodamage at nucleotide resolution indicated the formation of both direct strand breaks and alkali-labile lesions predominantly at guanine bases, pointing to the involvement of singlet oxygen and/or electron transfer from guanine.

In order to investigate binding affinity, DNA melting experiments in the absence and presence of compound **3** or **MB** with calf thymus and *C. perfringens* DNAs were conducted. In each case, the ΔT_m values produced by compound **3** pre-equilibrated with calf thymus or *C. perfringens* DNAs were approximately 3-fold higher than the values exhibited by **MB** under the identical experimental conditions. Furthermore, evaluation of ΔT_m as a function of the molar ratio of dye to calf thymus DNA bp (**r**) demonstrated that the ΔT_m values were consistently higher for compound **3** than **MB** at all the **r** values tested (**r** = 0.05–0.6). Moreover, a plateau in the ΔT_m produced by **3** at a **r** value ≥ 0.3 was observed thereby suggesting the saturation of DNA binding sites. This was not case for **MB**: the ΔT_m values continued to increase as a function of increasing dye concentration (**r** > 0.3). Effectively, compound **3** demonstrated enhanced levels of duplex stabilization compared to **MB**, thereby indicating a stronger association with DNA.

Viscometric measurements were conducted to ascertain the DNA binding mode(s) of compound **3** in comparison to **MB**. The viscosity enhancement of CT DNA (slope = 0.962) produced by **MB** was consistent with monointercalation. However, the viscosity enhancement of CT DNA (slope = 1.50) exhibited by compound **3** indicated the possibility of multiple binding modes. To test this hypothesis, viscometric measurements with poly(dA)•poly(dT) and alternating poly[(dA-dT)]$_2$ DNAs yielded slopes of 0.22 and 1.18 for compound **3**, and 0.17 and 1.11 for **MB**, respectively. Collectively, these assays

revealed that compound **3** is likely to associate with heterogeneous DNA through a combination of binding modes including monointercalation, bisintercalation, and/or groove binding.

The syntheses, characterization, and evaluation of two new photonucleases incorporating one phenothiazinium ring with a bis-piperazinexylene substituent (compound **5**) or the same bis-piperazinexylene as a linker centrally attached to two phenothiazinium rings (compound **6**) were described in Chapter V. In the presence of DNA, both compounds exhibited maximal absorbance at 665 nm in 10 mM sodium phosphate pH 7.0. Moreover, 400-650 nm irradiation of pUC19 plasmid in the presence of 10 μM **5** or **6** produced efficient photocleavage. DNA melting assays showed significant changes in the ΔT_m values produced by **5** (17 ºC) and **6** (19 ºC) relative to calf thymus DNA (in the absence of dye). Lastly, viscosity measurements indicated that both compounds bind to DNA as monointercalators.

The impetus for designing the three new phenothiazine-based photosensitizers was to synthesize putative bisintercalators incorporating a chromophore that might effectively mediate DNA photodamage at longer wavelength within the therapeutic window for photodynamic therapy (600-800 nm). Towards this end, all three compounds exhibited maximal absorption of light in the presence of DNA at wavelengths greater than 650 nm and mediated efficient levels of DNA photocleavage. Moreover, cooperative and stronger associations with DNA as demonstrated by thermal melting studies was indicated for compounds **3**, **5**, and **6** in comparison to the **MB** parent. In the case of compound **3**, irradiation of pUC19 plasmid DNA at 710 nm produced approximately a two-fold increase in cleavage yield in comparison to **MB**. Additionally, viscosity data

indicated that compound **3** associates with DNA through multiple modes including bisintercalation.

Finally, the DNA isolation and amplification procedures presented in Chapter VI constitute a laboratory workshop which provided participants with pratical experience in commonly utilized methods in molecular biology. Moreover, the methods were modified to be appropriate for the use in an undergraduate laboratory setting. While the goal was to examine a single nucleotide polymorphism involved in a normal variation in human color vision, the protocols offer experimental flexibility and can be utilized to investigate other interesting single nucleotide polymorphisms.

With regards to the acridine and phenothiazine photosensitizers, the author of this dissertation and her co-workers hope that the project findings described herein will stimulate a growing interest in the design of new intercalating photosensitizers for the use in non-porphyrin based phototherapeutics.